STUDIES ON SURFACE PLASMON RESONANCE BASED FIBER OPTIC SENSORS

Thesis submitted in fulfillment of the requirements for the Degree of

DOCTOR OF PHILOSOPHY

By

MAHIMA RANI

Department of Physics and Materials Science and Engineering
JAYPEE INSTITUTE OF INFORMATION TECHNOLOGY
(Declared Deemed to be University U/S 3 of UGC Act)
A-10, SECTOR-62, NOIDA, INDIA

July, 2014

Dedicated

To

My Parents

TABLE OF CONTENTS

DECLARATION BY THE SCHOLAR

I hereby declare that the work reported in the Ph.D. thesis entitled **"Studies on surface plasmon resonance based fiber optic sensors"** Submitted at **Jaypee Institute of Information Technology, Noida, India,** is an authentic record of my work carried out under the supervision of **Dr. Navneet Kumar Sharma.** I have not submitted this work elsewhere for any other degree or diploma. I am fully responsible for the contents of my Ph.D. Thesis.

(Mahima Rani)

Department of Physics and Materials Science & Engineering

Jaypee Institute of Information Technology, Noida, India

July 8, 2014

SUPERVISOR'S CERTIFICATE

This is to certify that the work reported in the Ph.D. thesis entitled **"Studies on surface plasmon resonance based fiber optic sensors",** submitted by **Mahima Rani** at **Jaypee Institute of Information Technology, Noida, India,** is a bonafide record of her original work carried out under my supervision. This work has not been submitted elsewhere for any other degree or diploma.

(Dr. Navneet Kumar Sharma)

Assistant Professor (Senior Grade)

Department of Physics and Materials Science & Engineering

Jaypee Institute of Information Technology, Noida, India

July 8, 2014

ACKNOWLEDGEMENTS

I would like to express my sincere thanks to our almighty God for his grace in completion of this thesis.

I greatly thank my learned and respectable supervisor **Dr. Navneet Kumar Sharma,** Department of Physics and Materials Science & Engineering, Jaypee Institute of Information Technology, Noida who supported and guided me unconditionally throughout my research with his patience and encouragement. The outcome of this research would have never happened lacking his encouragement, unreserved support and the freedom in research given to me.

I thank almighty for having given me an opportunity of doing research work under kind guidance of **Dr. Sharma**. There was not only thought-provoking discussion on research problems but also got to learn moral characteristics of life and a rock solid support of him whenever I required. **Dr. Sharma**, more than supervisor, he has been like father figure to me.

Very special thanks to **Prof. K. C. Mathur**, **Prof. D. K. Rai and Prof. Bani Singh**. Their valuable teaching assistance and suggestions on various topics and courses related to my Ph.D. course work have just been incredible which has extensively improved my research completion. Their proficient teaching approach was accountable for making this subject most fascinating in physics.

I thankfully acknowledge Jaypee Institute of Information Technology, Noida for providing me teaching assistantship throughout my Ph.D. work.

I owe my earnest appreciation, love and thankfulness to my family – my dear parents Smt. Sumedha Arya and Dr. Rajpal Singh, my brother-sister Abhinav, Yamini and Vidya. Without their constant support and encouragement I could never have finished my PhD research work. Their blessings and encouragement have shown me the path to pursue goals in my life. I would like to express my gratitude and sincere thanks to all my colleagues and friends including Prateek, Sarika, Swati, Nidhi, Chitra, Vineet, Kanika, Neetima, Kishor, Dinesh, Pradeep and Manoj for maintaining a friendly environment and helping me in several discussions.

Lastly I offer my genuine regards and blessings to all those who helped me in any respect in successfully completion of this dissertation.

(Mahima Rani)

ABSTRACT

Over the past few decades, researchers have shown immense interest in a new technology, named Surface plasmon resonance (SPR) which utilizes the fascinating light-matter interaction involved at a metal-dielectric interface. This technology is employed for fast and accurate measurement of various physical, chemical and biochemical parameters. The present thesis is focused on the theoretical studies of SPR based fiber optic sensors with different materials for sensitivity enhancement. First study presents the theoretical analysis of SPR based fiber optic sensor with bi layers of ITO-Au. The SPR sensor shows high sensitivity with two resonance dips, one in the visible and other in the near infrared region of spectrum. Besides it, increase in ITO layer thickness decreases the sensitivity of both left and right resonance dips for all thicknesses of Au layer. In another study, the theoretical analysis has been extended to SPR based fiber optic sensor with indium oxide (In_2O_3). In_2O_3 layer based SPR sensor is found to possess high sensitivity with resonance dip in near infrared region of spectrum. The sensitivity of SPR sensor decreases with increase in thickness of In_2O_3 layer. Next study discusses the theoretical investigations of LSPR based fiber optic sensor with nanoparticles. Nanoparticles of four materials: ITO, Au, Ag and Cu are considered. The sensitivity of sensor increases with increase in thickness of nanoparticles layer for all four materials. Also, for a fixed thickness of nanoparticles layer, the sensitivity of sensor further increases as the particle size of nanoparticles increases. Another important study analyzes a SPR based fiber optic sensor with nanocomposites theoretically. Several nanocomposites comprising nanoparticles of Au, Ag and Cu with their varying volume fractions embedded in host dielectric matrices of titanium oxide (TiO_2) and indium nitride (InN) are considered. The sensitivity of Au/Ag/Cu-InN nanocomposites based SPR sensor for all thicknesses of nanocomposites with any volume fraction of nanoparticles is higher than that of Au/Ag/Cu-TiO_2 nanocomposites. Further, the sensitivity of SPR sensor increases with increase in both thickness of nanocomposites and volume fraction of metal nanoparticles. Last study reports a SPR based fiber optic sensor with InN theoretically. Depending upon various parameter values of InN, two SPR sensors viz “Sensor A” and “Sensor B” have been considered. Both sensors A and B reveal their SPR resonance dips in near IR region of spectrum. InN layer based fiber optic SPR sensor with Sensor A parameter values displays high sensitivity.

LIST OF ACRONYMS & ABBREVIATIONS

ATR	Attenuated total internal reflection
ITO	Indium tin oxide
LSPR	Localized surface plasmon resonance
PCS	Plastic clad silica
RIU	Refractive index unit
SPR	Surface plasmon resonance
TCO	Transparent conducting oxide
TIR	Total internal reflection
TM	Transverse magnetic

LIST OF FIGURES

LIST OF TABLES

CHAPTER 1

INTRODUCTION

1.1 Background

The optoelectronics and fiber optic communication industries have witnessed the exponential growth during past three decades. The optoelectronics industry has enriched numerous advantageous products such as compact disc (CD) players, laser printers, bar code scanners, optical switching devices, organic light emitting diodes and laser pointers [1]. On the other hand, fiber optics has revolutionized the telecommunication industry by providing high performance and extremely reliable telecommunication links. In parallel with these developments, fiber optic sensor technology is also emerging with equal pace [2-5]. The remarkable interest in optical fibers for their use in sensing applications can be attributed to numerous magical advantages such as: they are flexible, light weighted and small in size (therefore miniaturization can be attained). They are purely dielectric and hence they can be easily used in hazardous areas. They are immune to electromagnetic interference. Further, remote sensing as well as distributed sensing can be achieved by using them. In addition, optical fibers are highly sensitive, environmental resistant, explosion proof as well as have large bandwidth and very short response time. Because of these advantages, fiber optic sensors have been finding variety of applications in electrical power industry, industrial process control, medical sciences, automobiles, defense sector and research. Besides it, fiber optic sensors are significantly advantageous over traditional sensors in many ways such as cost difference and improved quality. Their applications in these fields allow the measurement of various physical and chemical parameters such as rotation, acceleration, electric field, magnetic field, temperature, refractive index, concentration, pressure, acoustics, vibration, linear and angular positions, strain, humidity, viscosity and pH [6-52]. Basically, a fiber optic sensor requires a light source, sensor geometry, detection system and referencing scheme. A typical fiber optic sensor utilizes launching of light at one end of the fiber which is guided

through the fiber using the phenomenon of total internal reflection. The measurand (sample) is placed in contact with the core of the optical fiber. This measurand modulates some property of the guided light such as wavelength, phase, intensity, polarization etc. At the output end of the fiber, the change in the light property is measured to obtain the information about the change in the measurand. The fiber optic sensors are mainly classified in following three categories:

(i) External sensors: External sensors are those in which, the optical fiber used is bare ended and it only collects and guides the light rays. For example, laser Doppler velocimeter and non contact displacement sensor etc.

(ii) Intrinsic sensors: Intrinsic sensors are those in which, optical fiber becomes the main and key element. The optical fiber is used to transmit the light from source to the probe attached at the other end of the fiber. Further this light signal is sent to the detector.

(iii) Extrinsic sensors: Extrinsic sensors are those in which, optical fiber does not play any role in sensing. It is used just for the transmission and receiving of light.

Numerous techniques have been used for sensing such as doppler effect, interferometry, photolumnisense, evanescent wave absorption spectroscopy and surface plasmon resonance (SPR). Apart from all other sensing techniques, SPR has achieved much attention during last thirty years. Starting with the first application of SPR [53], several other research groups [54-87] have used the phenomenon of surface plasmon resonance for sensing various physical and chemical parameters. Apart from sensing, SPR technique is also suitable for microscopic imaging [88], miniaturized plasmonic waveguides [89], polarizers [90] and surface enhanced Raman scattering (SERS) spectroscopy [91].

Surface plasmon resonance has a wide history of around 100 years. Recently it has attracted a good interest due to variety of reasons. First observation about surface plasmon was made by Wood in 1902 [92]. As per his observation, when polarized light was shone on a mirror with the diffraction grating on its surface, an anomalous pattern of dark and bright bands was observed in the reflected light. In 1907, Zenneck theoretically demonstrated that the radio frequency surface electromagnetic waves occur at the boundary of two media when one medium is a lossy dielectric or metal and the other is a loss free medium [93]. He concluded that the lossy part of the dielectric constant is responsible for binding the electromagnetic waves to the interface. In 1909, Somerfield observed that the field amplitudes

of the surface waves present on the metal dielectric interface vary inversely as the square root of the distance from the source dipole [94]. In 1941, Fano concluded theoretically that the anomalies reported by Wood (in 1902) were because of the excitation of surface waves on the surface of diffraction grating [95]. In 1957, Ritchie theoretically revealed the excitation of the surface plasmons on the metal surface [96]. In 1959, a large drop in reflectivity was observed by Thurbadar when thin metal films were illuminated on a substrate but this phenomenon was not linked with the surface plasmons [97]. Powell and Swan in 1960 observed that electrons could excite surface plasmons at the metal dielectric interface [98]. Stern and Ferrell revealed that the electromagnetic waves at the metallic surface involved electromagnetic radiation coupled to the surface plasmons [99]. Later in 1968, Otto explained Thurbadar's results and explained that the drop in the intensity of reflected light in attenuated total internal reflection is because of the excitation of surface plasmons [100]. However, due to a finite gap between the metal layer and the prism base, the Otto configuration is not very much suitable for the practical point of view rather it is more suited for the study of single crystal surface. Kretschmann, in 1971 modified Otto configuration by directly depositing a thin metallic layer on to the base of a coupling prism and the dielectric medium (sample) whose refractive index is to be measured, is kept in contact with the metallic layer [101]. If a p-polarized i.e. transverse magnetic (TM) polarized light is incident on the metal-prism interface and the reflectance is measured as a function of angle of incidence, a sharp dip is obtained at a particular angle called the resonance angle. By measuring this resonance angle, the value of dielectric constant of the sample can be determined. This method is known as angular interrogation method. However, the prism based SPR sensor has a number of shortcomings. Bulky size of the prism and the presence of various optical and mechanical moving parts are some of the drawbacks which make it difficult in optimization and commercialization on a large scale. In addition, remote sensing can not be realized by the prism based SPR sensing device. After the introduction of the phenomenon of SPR in sensing by Kretschmann, various efforts were made towards the development of optical fiber SPR sensors. The miniaturization of SPR probe is achieved by the use of optical fiber due to its small core diameter.

Further, fiber optic SPR sensing offers simplified optical design and the capability for remote sensing. In a fiber optic SPR sensor, the metal layer is directly deposited on to the core of the optical fiber. The SPR sensing method of fixed range of angle of incidence and modulated wavelength is generally used in a SPR based fiber optic sensor. This method is called as wavelength interrogation method. This is because of the reason that spectral

distribution of light may be preserved in an optical fiber, whereas the angular intensity distribution of light will be indistinguishable due to mode mixing (as a consequence of inherent bending) of the multimode optical fiber in practical sensing applications. Also, the sensor is normally fabricated on a multimode optical fiber, where there is not a fixed angle of incidence rather a range of incident angles are allowed to propagate in the fiber.

The metals used for the SPR excitations are generally gold and silver. Though, they have their own limitations. Silver has a small value of the imaginary part of the dielectric constant, which gives a sharp resonance dip leading to a better detection accuracy. On the other hand, silver is chemically very reactive and it gets oxidized very quickly when comes in contact with air or water. However, gold is chemically very stable and the gold coated SPR sensor offers high sensitivity than that of silver. Since, any SPR sensor should have high value of sensitivity as well as detection accuracy, a single metallic layer having the properties of both silver and gold can be extremely advantageous. Zynio et al. proposed an idea of using a combination of gold and silver layers as a bimetallic one for the prism based sensors [102]. Later this bimetallic combination was utilized for SPR based fiber optic sensor [103]. For further improvement in sensitivity of the SPR sensors, several modifications were carried out in the SPR probe. For example, the use of tapering the SPR probe with symmetric [104] and asymmetric metallic coatings [105] was presented. There was observation of multiple SPR dips in case of asymmetric metallic coating. Along with these, dual-tapered and tetra-tapered fiber optic SPR probes for gas and liquid sensing [106], asymmetric double layer covered tapered fiber optic sensor [107] and a truncated tapered fiber optic SPR sensor for detection of refractive index [108] have also been reported. In continuation to this, with time a large number of theoretical and experimental research investigations have been carried out to improve the performance of SPR based fiber optic sensor [122,123,73,74,77,79,83-86].

1.2 Plasmons and surface plasmons

Band theory of solids can explain almost all properties of the solid state. However, plasma model is also a quite different approach which can explain various properties of the solid state. The free electrons in the metal are like electron gas with high density of about 10^{23} cm^{-3}. The positive ions have infinitely large mass compared to the mass of the free electrons. According to jellium model [109], these positive ions can be replaced by a positive constant

background charge. Still, the total charge density in the conductor remains zero. If the density of the free electrons is now locally reduced by applying an external electric field on the conductor so that the movement of the free electrons may occur, the negatively charged free electrons are no longer screened by the background rather they begin to get attracted by the positive ion background. Hence, free electrons start moving towards the positive region and get accumulated with a density higher than required for the local charge neutrality. Now, at this point the Coulomb repulsion among the moving free electrons acts as a restoring force and generates motion in opposite direction. The resultant of these two forces (attractive driving force and repulsive restoring force) set up the longitudinal oscillations among the free electrons. These longitudinal density fluctuations known as plasma oscillations propagate through the entire volume of the metal. Frequency of these plasma oscillations is given by,

$$\omega_p = \sqrt{\frac{4\pi n e^2}{m_0}} \tag{1.1}$$

Where n is the density of free electrons, e is the electronic charge and m_0 is the mass of electron [110].

The coherent oscillations of free electrons on metal-dielectric interface are called as surface plasmons. Surface plasmons are the propagating electron density waves occurring at the metal-dielectric interface and can also be viewed as the electromagnetic waves strongly bound to the interface. They are transverse magnetically (TM) polarized in nature and therefore can be excited only by the TM polarized light. Let us consider a metal and a dielectric layer to be stacked along the *z*-axis and the direction of propagation of the surface plasmon wave along x-axis.

The field associated with the surface plasmon wave is given as,

$$E = E_0 \exp[\, i(k_x x \pm k_z z - \omega t)] \tag{1.2}$$

+ and – signs are for $z \geq 0$ and $z \leq 0$ respectively. The propagation constant k_z is imaginary which makes the exponential decay of the field. The wave vector k_x is parallel to the x-axis and is give as, $k_x = \frac{2\pi}{\lambda_p}$; λ_p is called as plasma wavelength [110]. By applying the boundary

conditions at the metal-dielectric interface, the dispersion relation for surface plasmon wave can be obtained to be,

$$k_{sp} = k_x = \frac{\omega}{c}\left(\frac{\varepsilon_m \varepsilon_d}{\varepsilon_m + \varepsilon_d}\right)^{1/2} \tag{1.3}$$

Where ε_m and ε_d are the dielectric constants of metal and dielectric respectively. ω is the frequency of incident light and c is the speed of light in vacuum.

The variation of electric field associated with surface plasmon wave across the interface is shown in Fig. 1.1.

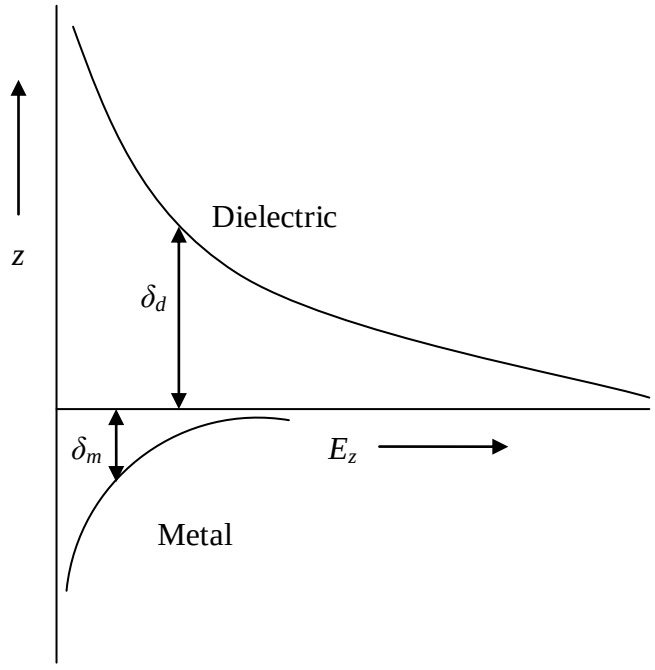

Figure 1.1: Exponential decay of field intensity of surface plasmon wave at the metal-dielectric interface. δ_d and δ_m are the penetration depths of the surface plasmon wave in dielectric and metal respectively

Some useful parameters related to surface plasmon waves are defined below:

1.2.1 Propagation length

Surface plasmon wave is an exponentially decaying wave both in metal as well as in dielectric medium. The dielectric constant of metal ε_m is a complex number and hence from Eq. (1.3), the propagation constant of the surface plasmon wave k_{sp} will also be a complex number.

$$k_{sp} = k_x = k_x' + ik_x'' \tag{1.4}$$

$$k_x' = \frac{\omega}{c}\left(\frac{\varepsilon_m' \varepsilon_d}{\varepsilon_m' + \varepsilon_d}\right)^{1/2} \tag{1.5}$$

$$k_x'' = \frac{\omega}{c}\left(\frac{\varepsilon_m' \varepsilon_d}{\varepsilon_m' + \varepsilon_d}\right)^{1/2} \frac{\varepsilon_m''}{2(\varepsilon_m')^2} \tag{1.6}$$

Where $\varepsilon_m = \varepsilon_m' + i\varepsilon_m''$ is the dielectric constant of metal with ε_m' and ε_m'' being the real and imaginary parts [110]. Also k_x' and k_x'' are the real and imaginary parts of propagation constant of surface plasmon wave. The length over which the intensity of the surface plasmon wave decreases to $1/e$ of its maximum value is called as the propagation length and is given as,

$$L_{sp} = (2k_x'')^{-1} \tag{1.7}$$

For silver-air interface at λ = 514.5 nm, L_{sp} = 22 µm. L_{sp} becomes 500 µm at λ = 1060 nm [110].

1.2.2 Penetration depth

The propagation constant of the surface plasmon wave along the z-axis is given as,

$$k_{zi} = \left[\varepsilon_i \left(\frac{\omega}{c} \right)^2 - k_x^2 \right]^{1/2} \tag{1.8}$$

Here, *i* corresponds to 1 and 2 for metal and dielectric medium respectively [110]. The electric field amplitude of surface plasmon wave decreases exponentially perpendicular to the interface. The perpendicular distance over which the field amplitude reduces to $1/e$ of its value at the interface is called as the penetration depth of the surface plasmon wave.
For silver-air interface at λ = 600 nm, δ_m = 24 nm and δ_d = 390 nm. Also for gold-air interface at λ = 600 nm, δ_m = 31 nm and δ_d = 280 nm [110].

1.3 Excitation of surface plasmons

There are several methods to excite surface plasmon waves such as prism coupling, grating coupling, excitation using highly focussed optical beams, excitation upon charged particle impact, near field excitation etc. Initially in 1957 as suggested by Ritchie [96], surface plasmon waves can be excited by low energy electron beam diffraction experiments. The most common technique used for the excitation of surface plasmon wave is the prism coupling. The two different configurations, Otto configuration and Kretschman-Raether configuration are based on prism coupling utilizing attenuated total internal reflection. Another technique used for the excitation of surface plasmon waves is the grating coupling. In this technique, light beam is launched from the dielectric on to the metal grating, which generates a series of diffracted waves. These diffracted waves can couple with the surface plasmon wave provided the propagation constant of the diffracted wave propagating along the grating surface matches with the propagation constant of the surface plasmon wave [57]. The surface plasmon waves can also be excited by a microscope of high numerical aperture [111]. Near field optical microscopic technique also permits the local excitation of surface plasmon polariton over an area $a << \lambda_0$ (a is the area and λ_0 is the free space wavelength) and hence acts as a point source for surface plasmon waves [112]. The excitation of surface plasmon waves by light is discussed below in detail.

1.3.1 Excitation of surface plasmons by light

As stated above, the surface plasmons can be excited by light. The propagation constant of light wave having frequency ω, in air is given by,

$$k_{inc} = \frac{\omega}{c} \tag{1.9}$$

For the excitation of surface plasmons, the propagation constant of the incident light should be equal to the propagation constant of the surface plasmon wave given by Eq. (1.3). As the surface plasmon wave is TM-polarized, the incident light used for the excitation should be p-polarized. Since the dielectric constant of dielectric medium is positive ($\varepsilon_d > 0$) and that of metal is negative ($\varepsilon_m < 0$), therefore for a given frequency the propagation constant of the surface plasmon wave is always greater than the propagation constant of the incident light. Therefore, surface plasmons can never be excited only by the direct light. Hence, to excite surface plasmon wave at a particular wavelength, an extra amount of momentum (Δk) and so energy is needed to be imparted to the direct light. Numerous techniques were utilized to increase the momentum of the light for the excitation of surface plasmons. Though, the first effort was made by Otto in 1968, which utilizes a prism to produce the evanescent wave for the excitation of surface plasmon wave [100]. However, this method was hard to implement practically and hence was later modified by Kretschmann and Raether [113]. These various techniques are discussed below in detail.

1.3.2 Otto configuration

In 1968, Otto utilized a coupling prism for the excitation of the surface plasmon wave [100]. The idea behind this configuration was the coupling of surface plasmon wave with the evanescent wave. The evanescent wave arises at the base of a coupling prism due to attenuated total reflection when a light beam is incident at an angle greater than the critical angle (θ_{ATR}) of the interface, as shown in Fig. 1.2.

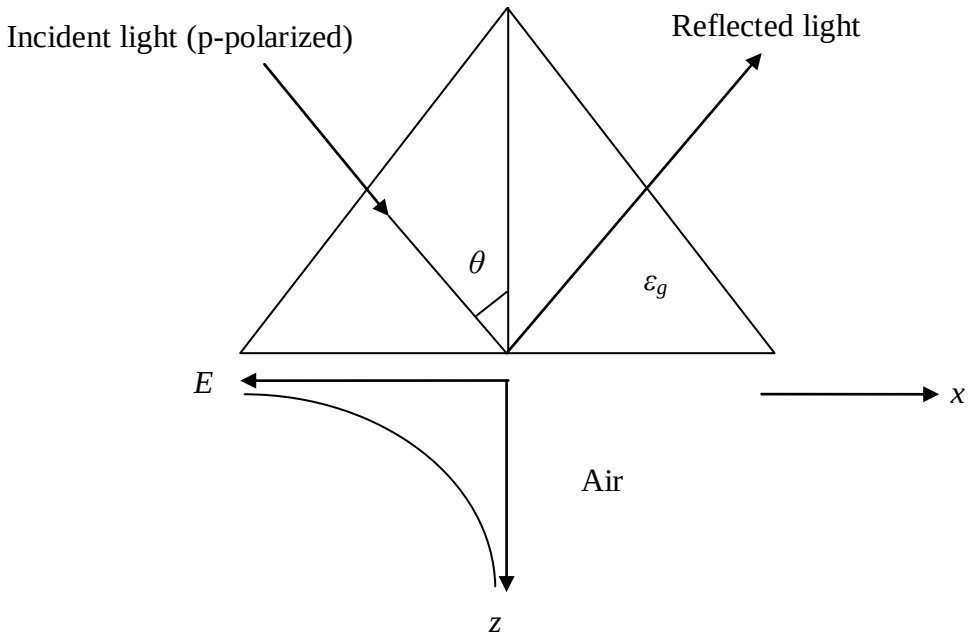

Figure 1.2: Setting up of an evanescent wave at the prism-air interface at an angle $\theta > \theta_{ATR}$

The evanescent wave is decaying in nature and it has the propagation constant along the interface. Both these characteristics of an evanescent wave match to those of a surface plasmon wave and hence there is a strong possibility of interaction between these two waves. The x-component of the propagation constant of the evanescent wave at prism-air interface is given as,

$$k_{ev} = \frac{\omega}{c}\sqrt{\varepsilon_g}\, sin\theta \tag{1.10}$$

Where, ε_g is the dielectric constant of the material of the prism and θ is the angle of incidence of p-polarized light [110].

In Otto configuration, for the excitation of surface plasmon wave, the metal layer is kept underneath the prism base keeping the gap between the two as shown in Fig. 1.3. The gap is filled with the sample liquid having refractive index smaller than that of prism.

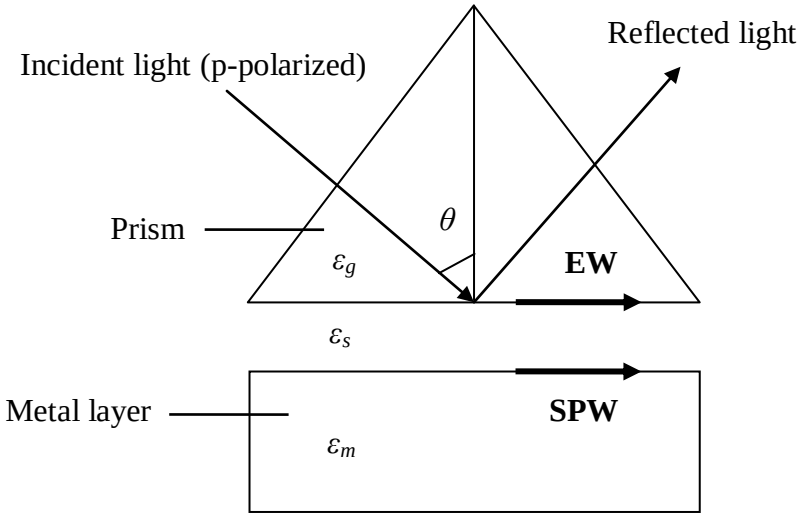

Figure 1.3: Otto configuration for the excitation of surface plasmons at metal-dielectric interface

The evanescent wave at the prism-liquid interface excites the surface plasmon wave at the metal-dielectric interface if the wave vectors of the evanescent wave and surface plasmon wave are same. When the two wave vectors match, the reflected light shows a minimum. Though, this configuration is quite difficult to realize as one has to maintain the finite gap between the base of the prism and metal layer. However, this method has been found very interesting and useful for studying the single crystal metal surfaces and adsorption on them. Later in 1968, this configuration was modified by Kretschmann and Raether [113]. Kretschmann and Raether configuration is one of the most famous techniques to be used for the excitation of surface plasmon wave till date.

1.3.3 Kretschmann-Raether configuration

Improving Otto configuration [100], in which there was an air gap between the prism base and the metal layer, Kretschmann and Raether discovered a new configuration [113,101] for the excitation of surface plasmons as shown in Fig. 1.4. In this configuration, similar to Otto configuration, evanescent wave excites the surface plasmons. A thin metal film nearly 50 nm thick is coated at the base of a high refractive index glass prism and is kept in direct contact with the dielectric sensing medium of lower refractive index.

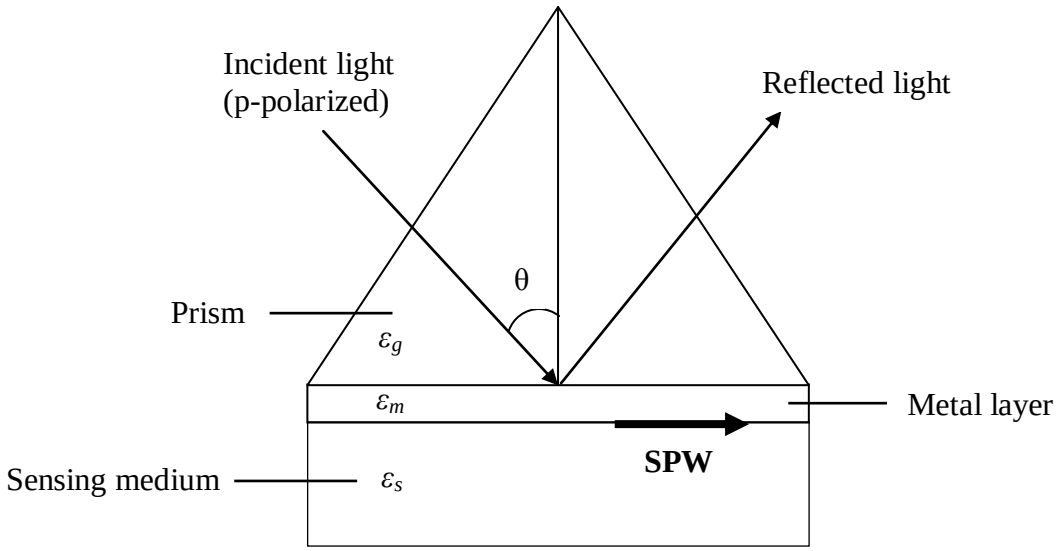

Figure 1.4: Kretschmann configuration for the excitation of surface plasmons at metal-dielectric interface

When a p-polarized light is incident through the prism on the interface of the prism and metal layer at an angle θ equal to or greater than the angle of ATR (θ_{ATR}), the evanescent wave is produced at the prism-metal interface, which propagates along the interface. When the wave vector of the evanescent wave matches with that of the surface plasmon wave, resonance occurs and the energy gets coupled to the surface plasmons. This resonance condition appears in form of minima in the reflected light intensity. Fig. 1.5 depicts the dispersion curves of both evanescent wave and the surface plasmon wave.

The wave vector k_{ev} of the evanescent wave is equal to the lateral component of the incident light wave vector (k_g) travelling in the prism [110]. Therefore,

$$k_{ev} = k_g \sin\theta = \frac{\omega}{c}\sqrt{\varepsilon_g}\sin\theta \tag{1.11}$$

The wave vector of the surface plasmon wave is given by Eq. (1.3). As discussed earlier, the excitation of surface plasmons takes place only when the wave vector of the evanescent wave matches exactly with that of the surface plasmon wave of same frequency and state of polarization. This occurs at a particular angle of incidence θ_{res}, known as the resonance angle. Hence the resonance condition for surface plasmons is given as,

$$\frac{\omega}{c}\sqrt{\varepsilon_g}\,\sin\theta_{res} = \frac{\omega}{c}\sqrt{\frac{\varepsilon_m \varepsilon_s}{\varepsilon_m + \varepsilon_s}} \tag{1.12}$$

Where ε_s is the dielectric constant of the sensing medium.

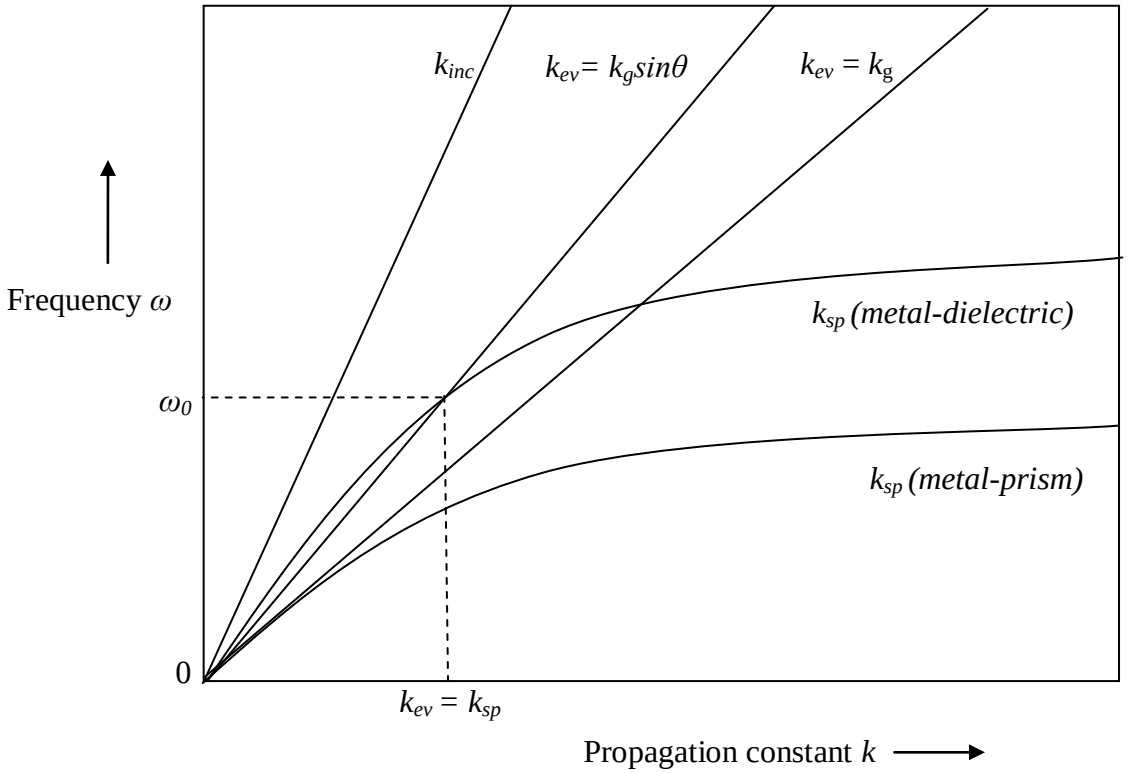

Figure 1.5: Dispersion curves for direct light wave in dielectric (k_{inc}), evanescent wave (k_{ev}) for $\theta = \theta_{ATR}$ and $\theta = \frac{\pi}{2}$, surface plasmon wave k_{sp} at metal-dielectric interface and at metal-prism interface

Fig. 1.5 reveals that the propagation constant curves for surface plasmon wave and evanescent wave cross each other at many points lying between $k_{ev} = k_g \sin\theta$ *and* $k_{ev} = k_g$ (at a particular frequency for different angles of incidence). It means that the propagation constant of the evanescent wave (k_{ev}) may coincide with that of the surface plasmon wave (at the metal-dielectric interface) at a particular frequency and angle of incidence of light beam. An important thing to be noticed here is that the propagation constant of surface plasmon wave at the metal-prism interface lies right to the maximum propagation constant of evanescent wave

(k_{ev} = k_g) and the two curves never cross each other. This confirms that surface plasmons at metal-prism interface can never be excited.

1.4 Sensing principle of SPR

The excitation of surface plasmons at the metal-dielectric interface, results in the transfer of energy from incident light to surface plasmons. This reduces the reflected light intensity (reflectance) at some particular angle of incidence known as the resonance angle. If the output signal i.e. reflectance (R) is measured as a function of incident angle θ, a sharp dip is observed at resonance angle θ_{res} due to the transfer of energy to surface plasmons as shown in Fig. 1.6. Knowing this resonance angle θ_{res}, the dielectric constant of the sensing medium can be determined using Eq. (1.12). The resonance angle is very sensitive to the variations in the refractive index or the dielectric constant of the sensing medium. Even a minute change in the refractive index of the sensing medium alters the resonance condition significantly. Increase in the refractive index of the sensing medium enhances the corresponding resonance angle. Thus, by knowing the change in the resonance angle, the change in the refractive index of the sensing medium can be determined. The method, in which the dielectric constant of the sensing medium is obtained by changing the incidence angle of the incident light and keeping the wavelength of the light fixed, is known as the angular interrogation method.

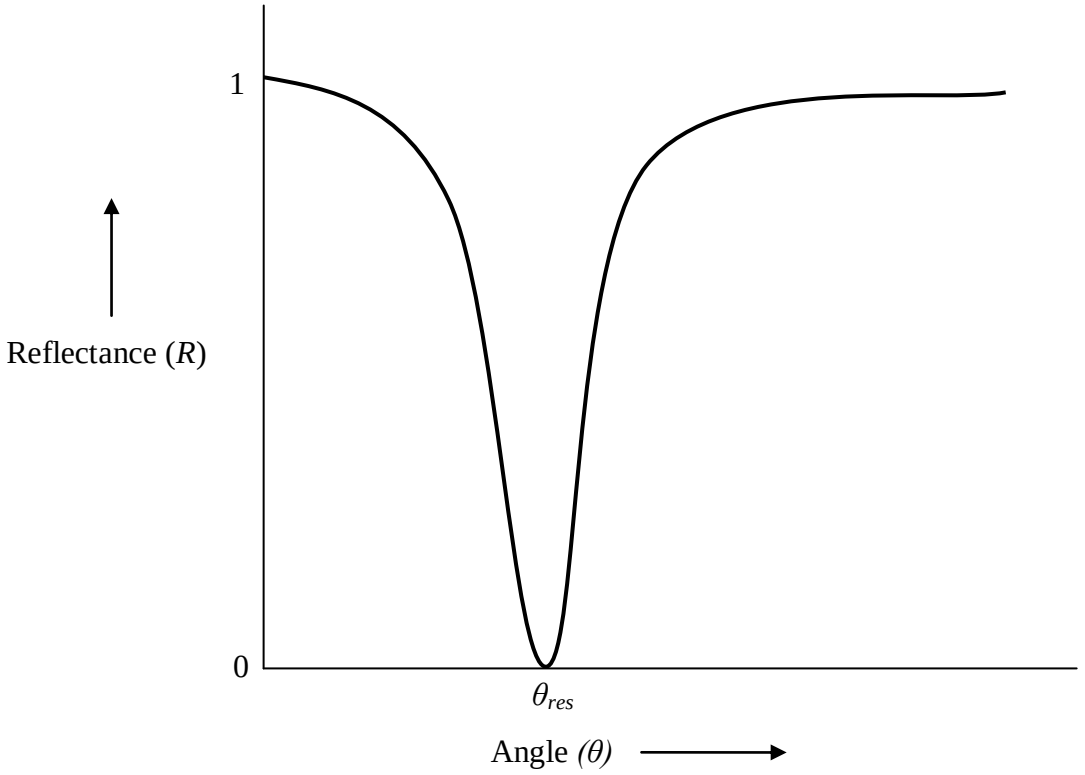

Figure 1.6: Reflectance (R) as a function of angle of incidence (θ) at the prism-metal interface. A sharp dip in reflected signal is observed at an angle θ_{res}

However, there is another method called as the spectral interrogation (wavelength interrogation) method, in which the wavelength of the light beam is varied by keeping the angle of incidence fixed. In spectral interrogation method, white light from a polychromatic source is launched on the metal layer through the prism at a particular angle of incidence greater than the critical angle. The evanescent field so produced extends through the metal layer. The wave vector of the evanescent wave given by Eq. (1.11) and the wave vector of the surface plasmon wave given by Eq. (1.3) are wavelength dependent because the dielectric constant of metal, material of the prism and sensing medium are wavelength dependent. For a surface plasmon wave to be excited, the two wave vectors must be same. This happens at a particular wavelength of the incident light, which results in transfer of energy from the incident wave to the surface plasmon wave and hence large attenuation in the reflected light intensity takes place. The SPR curve obtained in this case is same as one shown in Fig. 1.6 except that instead of angle, wavelength is taken on the x-axis and the resonance angle is replaced by the resonance wavelength and as a result, the complete resonance curve is

determined. Hence, one can determine the refractive index of the sensing medium by monitoring the resonance wavelength (λ_{res}) from the reflected light intensity spectrum. To cover a greater range of the refractive index of the sensing medium, the spectral interrogation method is much better.

1.5 Kretschmann-Raether configuration in optical fiber

As mentioned earlier, Kretschmann configuration used for the excitation of surface plasmons comprises a dielectric prism and a thin metal layer coated on to the base of the prism. The total internal reflection phenomena and therefore the generation of evanescent waves is the basis behind the excitation of surface plasmons. In a typical optical fiber, guidance of light takes place through total internal reflection phenomena at the core-cladding interface. An evanescent wave is generated in the cladding of the fiber, which propagates along the core-cladding interface. This evanescent field decays exponentially in the cladding region. Because of these properties, the bulky prism in the Kretschmann configuration can be replaced by the core of the optical fiber. In an optical fiber based SPR sensor, a small length of cladding is removed from the middle portion of the fiber and a thin metal layer such as gold or silver is coated on to the bare core. The medium which is needed to be sensed is placed in contact with the metal layer as shown in Fig. 1.7. As the wavelength-intensity distribution is preserved in an optical fiber, the wavelength interrogation method is used in this case.

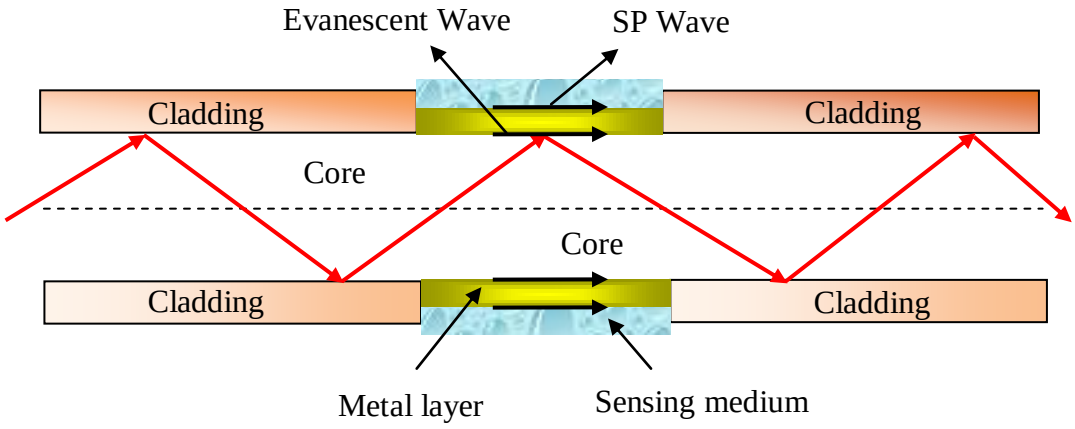

Figure 1.7: Kretschmann configuration for the excitation of surface plasmons at metal-dielectric interface realized in a multimoded optical fiber

Hence, the light from a polychromatic source is launched at one of the ends of the fiber and the transmitted light is received at the other end of the fiber. As the sensor uses a multimode fiber, a range of angles corresponding to guided rays are launched in the fiber and corresponding to each angle of incidence, resonance occurs at one particular wavelength. By measuring the resultant resonance wavelength, the refractive index and hence the dielectric constant of the sensing medium can be determined. Also, a minute change in the refractive index of the sensing medium alters the resonance condition. The shift in the resonance wavelength is a measure of the change in the refractive index of the sensing medium.

1.6 Performance parameters of the SPR sensor

In angular interrogation based SPR sensor, the resonance angle (θ_{res}) is determined corresponding to refractive index of the sensing medium (n_s). A small change in the refractive index of the sensing medium δn_s shifts the resonance angle by $\delta\theta_{res}$. While in case of wavelength interrogation method, instead of shift in resonance angle, a shift in resonance wavelength $\delta\lambda_{res}$, takes place. Sensitivity is the main performance parameter, which determines the performance of a fiber optic SPR sensor. For a typical SPR based fiber optic sensor, the sensitivity should be as high as possible.

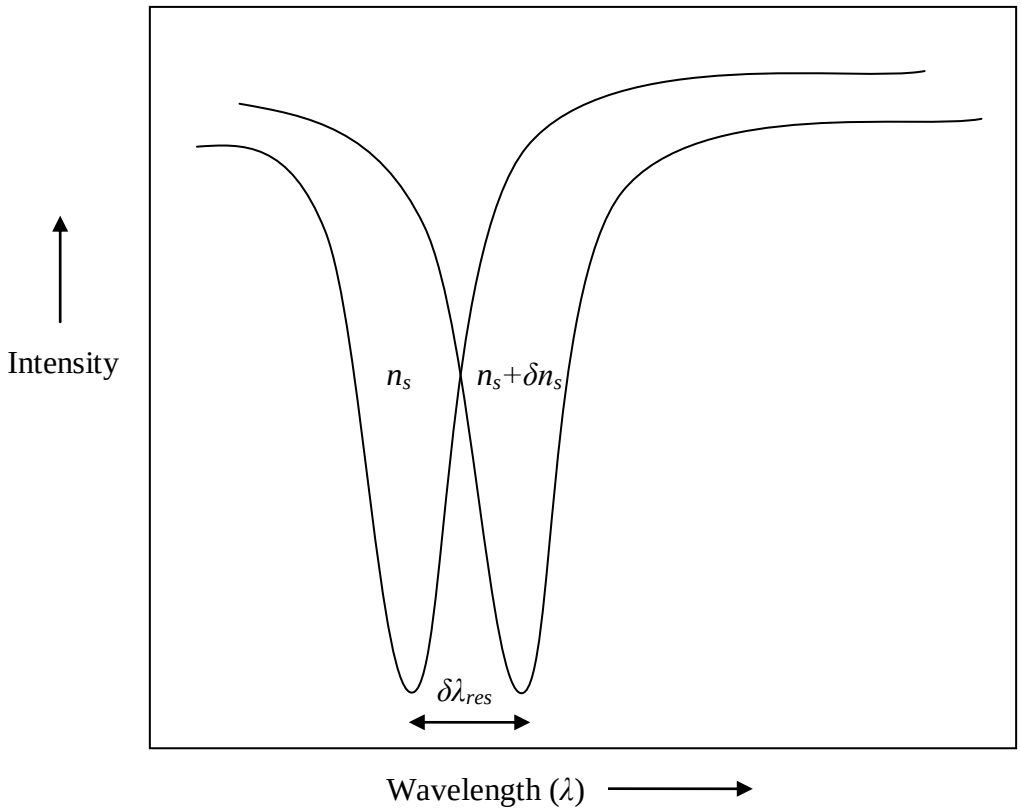

Figure 1.8: The shift in resonance wavelength ($\delta\lambda_{res}$) with a change in refractive index of the sensing medium

Thus, the sensitivity of a SPR sensor depends on the shift in resonance angle (angular interrogation) or the resonance wavelength (wavelength interrogation) with a change in the refractive index of the sensing medium. Larger is the shift, better will be the sensitivity of the SPR sensor. To define the sensitivity of a SPR based sensor, two SPR curves are plotted for two different values of the refractive index of the sensing medium as shown in Fig. 1.8. On increasing the refractive index of the sensing medium by an amount δn_s, the resonance wavelength also shifts by an amount $\delta\lambda_{res}$. Hence, the sensitivity of a SPR based fiber optic sensor is defined as [66],

$$S_n = \frac{\delta\lambda_{res}}{\delta n_s} \tag{1.13}$$

1.7 Thesis formation

As mentioned earlier, for observing SPR, Kretschmann configuration is most widely used. In Kretschmann configuration, a high refractive index prism is coated with a thin metal layer touching the sample (sensing medium). Surface plasmon waves are excited by evanescent wave from the prism at the total reflection condition. The SPR phenomenon using Kretschmann configuration was first time demonstrated for biosensing by Liedberg et al. in 1983 [54]. Their experiment released numerous opportunities in the area of SPR based sensors for chemical and biological applications. However, in the fiber optic SPR sensor, the prism is replaced by the core of the optical fiber and a thin metal layer is directly deposited on to the core of the optical fiber. For SPR sensing, the method of fixed angle of incidence and modulated wavelength i.e. wavelength interrogation method is chosen. The utilization of optical fiber along with surface plasmon resonance for sensing applications was first time done by Jorgenson and Yee [55]. Since then fiber optic SPR sensor has been an interesting research subject and a number of devices have been reported on fiber optic SPR sensors [114-117]. However with time, a large number of theoretical and experimental research investigations have been carried out to improve the performance of the fiber optic SPR sensor [58,62,118-123,73-87]. Now a days, some new types of fiber optic sensors such as micro and nano structured fiber sensors are attracting a number of researchers due to outstanding progress in the fields of surface plasmon resonance and photonic crystal fiber technology. In continuation to this, we have carried out the theoretical analysis of different materials based fiber optic SPR sensors to enhance the sensitivity of the fiber optic sensor.

Chapter 1 of the thesis gives general introduction about fiber optic sensors. As the surface plasmon resonance (SPR) forms the subject of the thesis, this chapter covers SPR based fiber optic sensors in greater detail. It reviews various fiber optic sensors for the measurement of different physical and chemical parameters as well as discusses the phenomenon of surface plasmon resonance. A section of this chapter is also dedicated to the recent SPR based fiber optic sensors for various sensing applications.

Gold (Au) and silver (Ag) metals are mainly utilized for SPR sensor. However, Ag based SPR sensor is not chemically much stable because Ag is very prone to oxidation. The problem of oxidation of Ag is automatically eliminated by coating another metal on it. Zynio et al. reported a SPR sensor based on resonant bimetallic layers of Ag-Au (Ag as an inner layer and Au as an outer layer) [102]. In addition of protecting Ag against oxidation by the outer Au

layer, this SPR sensor based on bimetallic layers showed high values of both sensitivity and detection accuracy. However, both of these metals have various significant disadvantages like occurrence of band to band transitions in the visible spectral region for Au films and very thin films of deposited Au and Ag are not continuous but agglomerate as islands [71]. Apart from this, the SPR sensors with a single metallic layer/bimetallic layers have their SPR wavelength in the visible range and therefore not permitting the sensing in the infrared spectral region, which needs attention to many environmental and security applications. It has been possible to obtain the surface plasmon resonance with transparent conducting metal oxide thin films. Recently, Indium tin oxide (ITO) has been reported to be a better substitute of noble metals (Au and Ag) for producing surface plasmons [124,125]. Highest available transmissivity for visible light combined with the lowest electrical resistivity, reflection spectra in IR region and wide band gap semiconductor makes ITO as most widely used transparent conducting metal oxide. In addition to this, ITO thin films are continuous (i.e. no agglomeration as islands) and no involvement of band to band transitions. Villar et al. have shown that surface plasmon resonances can be produced with ITO coated optical fibers [126]. In order to enhance the sensitivity of ITO based SPR sensor further, **Chapter 2** presents the theoretical analysis of SPR based fiber optic sensor with bi layers of ITO (as an inner layer)-Au (as an outer layer). In the SPR based fiber optic sensor, the sensing system consisting of a fiber core-ITO-Au-sensing medium is considered. The plastic cladding around the core from the middle portion of a step index multimode plastic clad silica (PCS) fiber is removed and is then coated with a thin ITO layer, which is then further coated with Au layer. These bi layers of ITO-Au are finally surrounded by the sensing medium. Liquids of different refractive indices are assumed as the sensing mediums. The light from a broadband source is launched into one of the ends of the optical fiber with proper optics and the transmitted light is detected at the other end of the optical fiber. The surface plasmon resonance produced by coupling of evanescent light to surface plasmons is used as the sensing mechanism. The wavelength interrogation method is used for the analysis of SPR based fiber optic sensor. In this method, the wavelength of the light from the broadband source is varied and the corresponding transmitted power through the optical fiber is measured. The proposed SPR based fiber optic sensor with bi layers of ITO-Au is shown to possess high sensitivity with two resonance dips, one in the visible and other in the near infrared region of spectrum, opposite to the single metal layer based SPR sensor with one and only resonance dip. The reason of occurrence of two resonance dips can be understood by the double character of ITO. In the region of high reflectance (wavelengths

higher than 1500 nm), the imaginary part of refractive index of ITO is higher while it is lower for the low reflectance region (wavelengths lower than 1500 nm) [126]. This low reflectance region i.e. low imaginary part of refractive index of ITO is responsible for the generation of double resonance dips. Moreover, these two differentiated SPR dips have been obtained from the same device within 510 nm to 870 nm spectrum. Besides it, increase in ITO layer thickness decreases the sensitivity of both left and right resonance dips for all values of thickness of Au layer. This happens because the thick ITO layer permits less interaction between surface plasmon mode and fiber mode, resulting in little absorption of light power by the sensing medium around resonance wavelength. This forms the ground of increase in normalized transmitted power and as a result decreases the sensitivity of the sensor. Furthermore, for a fixed thickness value of ITO layer, the sensitivity of left resonance dip increases with the increase in Au layer thickness while that of right resonance dip decreases with the increase in Au layer thickness. The optimized values of thicknesses of ITO and Au layers of SPR based fiber optic sensor are found to be 100 nm and 35 nm respectively. The 100 nm ITO-35 nm Au layers based SPR sensor has been shown to possess 1929 nm/RIU and 929 nm/RIU sensitivities for left and right resonance dips respectively.

Among various transparent conducting oxides, Indium oxide (In_2O_3) is a potential material for sensing applications due to its highest available transmissivity for visible light combined with the lowest electrical resistivity, reflection spectra in IR region and wide band gap semiconductor, making it one of the most widely used transparent conducting oxides [127]. Recently, In_2O_3 has been reported to be a better replacement of noble metals for producing surface plasmons [128]. **Chapter 3** describes the SPR based fiber optic sensor with Indium oxide (In_2O_3) theoretically. In the sensor, the sensing system comprising of a fiber core-In_2O_3-sensing medium is considered. The sensitivity of the sensor is studied for various thickness values of In_2O_3 layer. The In_2O_3 layer based sensor possesses high sensitivity with resonance dip in the near infrared region of spectrum allowing the sensing in the infrared spectral region, which needs attention to many environmental and security related applications. The sensitivity of the sensor decreases with the increase in the thickness of In_2O_3 layer. The 170 nm thick In_2O_3 layer based fiber optic SPR sensor comprises high sensitivity of 4600 nm/RIU.

The metal nanoparticles (much smaller than the wavelength of light) are supposed to have better sensing performances than materials in the micro or larger scales and reveal tremendous optical properties because of the collective excitation of conduction electrons [129]. A metal-

dielectric interface on the nanoparticles produce significant changes in the optical properties, which make them size and shape dependent. Localized surface plasmon resonance (LSPR) refers to metallic nanoparticles and takes place when the frequency of incident light is equal to the frequency of collective oscillations of conduction electrons in metallic nanoparticles [130]. The LSPR wavelength is reliant on nanoparticle material, size, shape and surrounding medium refractive index [131,132]. Therefore, the sensitivity of LSPR sensor is controlled/optimized by the change of the sizes and shapes of nanoparticles. **Chapter 4** discusses the theoretical investigations of LSPR based fiber optic sensor with nanoparticles. Nanoparticles of four materials: Indiums tin oxide (ITO), gold (Au), silver (Ag) and copper (Cu) have been considered individually and the nanoparticles are assumed to be spherical in shape with various radii. In the LSPR based fiber optic sensor, the sensing system consisting of fiber core-nanoparticles (of one material at a time)-sensing medium is assumed. The sensitivity of LSPR based fiber optic sensor with each nanoparticle layer individually for various thickness values and with different particle sizes is studied. The sensitivity of LSPR based fiber optic sensor increases with the increase in the thickness of nanoparticles layer for all four materials. Also, for a fixed value of thickness of nanoparticles layer, the sensitivity of LSPR based fiber optic sensor further increases as the particle size of nanoparticles increases. This can be explained in terms of the variation in absorption of light due to the change in particle size of the nanoparticles [133]. The decrease in particle size results in decrease in collision wavelength, that in turn increases the imaginary part of the dielectric function of metallic nanoparticles and hence the imaginary part of propagation constant of surface plasmon wave. The optimized values of thickness and particle size of nanoparticles layers for all four materials individually are found to be 60 nm and 20 nm respectively. The sensitivity of LSPR based fiber optic sensor is obtained to be 6240 nm/RIU, 4525 nm/RIU, 3550 nm/RIU and 3340 nm/RIU for 60 nm thick nanoparticles layer with fixed 20 nm particle size of ITO, Au, Ag and Cu nanoparticles respectively. Containing sensitivity of 6240 nm/RIU, the 60 nm thick ITO nanoparticles layer (with 20 nm particle size) based LSPR sensor has been shown to comprise better sensing performance than Au, Ag and Cu nanoparticles based LSPR sensors.

The noble metals are not appropriate for sensing of samples having low refractive indices (such as gases) as the SPR sensors based on these metals offer small sensitivity. Besides, their SPR resonance dips arise in UV region. **Chapter 5** elaborates the theoretical analysis of SPR based fiber optic sensor with nanocomposite. Numerous nanocomposites comprising

nanoparticles of gold (Au), silver (Ag) and copper (Cu) with their varying volume fractions embedded in host dielectric matrices of titanium oxide (TiO_2) and indium nitride (InN) are considered for the study. The sensitivity of Au/Ag/Cu-InN nanocomposites based SPR sensor for all thickness values of nanocomposites with any volume fraction of nanoparticles is higher than that of Au/Ag/Cu-TiO_2 nanocomposites. Further, the sensitivity of the sensor increases with increase in both thickness of nanocomposites and volume fraction of metal nanoparticles. Moreover, for a fixed nanocomposite thickness and fixed volume fraction of metal nanoparticles, the sensitivity of sensor is superior for Au nanoparticles based nanocomposites to that of Ag and Cu nanoparticles. The rationale that Au nanoparticles show higher sensitivity than Ag/Cu nanoparticles is attributed to the large value of real part of dielectric function of Au at all wavelengths [103]. Thus, Au nanoparticles in any nanocomposite enhance the shift between resonance wavelengths for a given change of refractive index of the sensing medium and therefore the sensitivity of the sensor increases. The SPR based fiber optic sensor with 70 nm thick Au-InN nanocomposite containing volume fraction of 0.85 illustrates high sensitivity of 2875 nm/RIU.

In recent times, research on plasmonics has been extended to infrared (IR) spectral region beyond the visible region. This leads to explore some new materials which could satisfy the SPR condition at lower plasma frequencies. Recently, Indium nitride (InN) has been found to be a fascinating semiconducting material having band gap around 0.7-1.1 eV because of its numerous advanced properties over other group-III nitrides, metals and transparent conducting oxides. InN is a potential candidate for plasmonics based sensing applications not only in IR but also in THz regimes because of its smaller magnitudes of real permittivity than metals [135]. Further, InN possesses lower value of plasma frequency compared to that of metals, displaying greater confinement of surface plasmon waves to the interface and greater field enhancement in IR and THz regions. In addition, Lu et al. reported the utilization of InN as a suitable material for biosensing due to its high superficial electron concentration [136]. **Chapter 6** of the thesis reports the theoretical study of surface plasmon resonance based fiber optic sensor with InN. Depending upon various parameters values of InN, two SPR sensors viz “Sensor A” and “Sensor B” have been analyzed theoretically. Sensors A and B are found to display maximum sensitivities of 4493 nm/RIU and 3107 nm/RIU for 70 nm and 55 nm thick InN layers respectively. Both sensors A and B reveal their SPR resonance dips in the near IR region of spectrum permitting the sensing in IR spectral region. The 70 nm thick InN

layer based fiber optic SPR sensor with Sensor A parameters values has been shown to acquire high sensitivity of 4493 nm/RIU.

Chapter 7 summarizes all the results reported in the thesis.

The above work has resulted in the following **publications**:

Journals

[1] Sharma N.K., **Rani M.**, Sajal V., "*Surface plasmon resonance based fiber optic sensor with double resonance dips*", *Sensors and Actuators B*, vol. 188, pp. 326-333, 2013.

[2] **Rani M.**, Sharma N.K., Sajal V., "*Surface plasmon resonance based fiber optic sensor utilizing Indium oxide*", Optik, vol. 124, pp. 5034-5038, 2013.

[3] **Rani M.**, Sharma N.K., Sajal V., "*Localized surface plasmon resonance based fiber optic sensor with nanoparticles*", Optics Communications, vol. 292, pp. 92-100, 2013.

[4] **Rani M.**, Shukla S., Sharma N.K., Sajal V., "*Theoretical study of nanocomposites based fiber optic SPR sensor*", Optics Communications, vol. 313, pp. 303-314, 2014.

[5] **Rani M.**, Shukla S., Sharma N.K., Sajal V., "*Theoretical analysis of surface plasmon resonance based fiber optic sensor using indium nitride*", (accepted in Optik).

Conference Proceedings

[1] **Rani M.**, Sharma N.K., "*ITO based fiber optic SPR sensor*", AIP Conf. Proc., vol. 1536, pp. 1117-1118, 2013.

Conferences

[1] **Rani M.**, Sharma N.K., "*Simulation of Cobalt based fiber optic surface plasmon resonance sensor*", International Conference on Optics & Optoelectronics ICOL-2014, Dehradun, March 05-08, 2014.

CHAPTER 2

SURFACE PLASMON RESONANCE BASED FIBER OPTIC SENSOR WITH DOUBLE RESONANCE DIPS

2.1 Introduction

It is well known that gold (Au)/silver (Ag) metals are mainly used for the fabrication of SPR sensors. However, Ag metal based SPR sensor is not chemically much stable because Ag metal is very prone to oxidation. The problem of oxidation of Ag metal is automatically eliminated by coating another metal on it. Zynio et al. reported a SPR sensor based on resonant bimetallic layers of Ag-Au (Ag as an inner layer and Au as an outer layer) [102]. In addition of protecting Ag against oxidation by the outer Au layer, this SPR sensor based on bimetallic layers showed high values of both sensitivity and detection accuracy (signal to noise ratio). Later, other study reported the theoretical analysis of a step index fiber optic surface plasmon resonance sensor with bimetallic layers (Ag and Au) in terms of sensitivity and signal to noise ratio [64]. However, both of these metals have various significant disadvantages like occurrence of band to band transitions in the visible spectral region for Au films and very thin films of deposited Au and Ag metals are not continuous but agglomerate as islands [71]. Apart from this, the SPR sensors with a single metallic layer/bimetallic layers have their SPR wavelength in the visible range and therefore not permitting the sensing in the infrared spectral region, which needs attention to many environmental and security applications. Enough work has been done on transparent conducting metal oxides. It has been possible to achieve surface plasmon resonance with transparent conducting metal oxide (TCO) thin films. Our first choice for TCO is Sn doped In_2O_3 i.e. indium tin oxide (ITO) because ITO has been recently reported to be a better substitute of noble metals (Au and Ag) for producing surface plasmons [124,125]. ITO is most privileged because it offers highest available transmissivity for visible light combined with lowest electrical resistivity. ITO is an n-type, highly degenerate, most widely used wide band gap semiconductor having reflection spectra in IR region. For this reason, it is also used for energy efficient window coatings

[137]. Physical properties of ITO films are strongly affected by Sn doping concentration. Moreover, the charge carriers in ITO behave like an ideal free electron gas with an effective mass of 0.4 *m* and a Fermi energy of $E_F < 1$ eV, where *m* is the free electron mass. The carrier concentration of highly conductive ITO materials usually falls in the range from 10^{20} to 10^{21} cm^{-3}. In addition, ITO thin films are continuous (i.e. no agglomeration as islands) and no involvement of band to band transitions. Villar et al. have shown that surface plasmon resonances can be produced with ITO coated optical fibers [126]. Recently, a surface plasmon resonance based fiber optic sensor with ITO as a SPR active material is analyzed theoretically and has been shown to have the sensing in the infrared region [75].

In this chapter, to enhance the sensitivity of ITO based SPR sensor further, a SPR based fiber optic sensor with bi layers of metal oxide-metal i.e. bi layers of ITO (as an inner layer)-Au (as an outer layer) has been theoretically analyzed. The surface plasmon resonance produced by coupling of evanescent light to surface plasmons is used as the sensing mechanism. The wavelength interrogation method is utilized for the analysis of SPR based fiber optic sensor. In this method, the wavelength of the light from the polychromatic source is varied and the corresponding transmitted power through the optical fiber is measured. At resonance wavelength, a sharp dip in the transmitted power occurs. The resonance wavelength depends on the refractive index of the sensing medium. The sensitivity of the SPR based fiber optic sensor with bi layers has been evaluated numerically. The proposed SPR based fiber optic sensor with bi layers of ITO-Au is shown to possess high sensitivity with two resonance dips, one in the visible and other in the near infrared region of spectrum, opposite to the single metal layer based SPR sensor with one and only resonance dip. Moreover, these two differentiated SPR dips have been obtained from the same device within 510 nm to 870 nm spectrum. Besides it, increase in ITO layer thickness decreases the sensitivity of both left and right resonance dips for all thicknesses of Au layer. Furthermore, for a fixed thickness of ITO layer, the sensitivity of left resonance dip increases with the increase in Au layer thickness while that of right resonance dip decreases with the increase in Au layer thickness. For the best sensing behaviour of SPR based fiber optic sensor, the thicknesses of ITO and Au layers have also been optimized. The optimized thicknesses of ITO and Au layers of SPR based fiber optic sensor are disclosed to be 100 nm and 35 nm respectively. Furthermore, 100 nm ITO-35 nm Au layers based SPR sensor has been shown to have 1929 nm/RIU and 929 nm/RIU sensitivities for left and right resonance dips respectively.

2.2 Theory

The SPR sensing is based on the principle of attenuated total reflection (ATR) with Kretschmann configuration. In the proposed SPR based fiber optic sensor, the sensing system consisting of a fiber core-ITO-Au-sensing medium is considered as shown in Fig. 2.1.

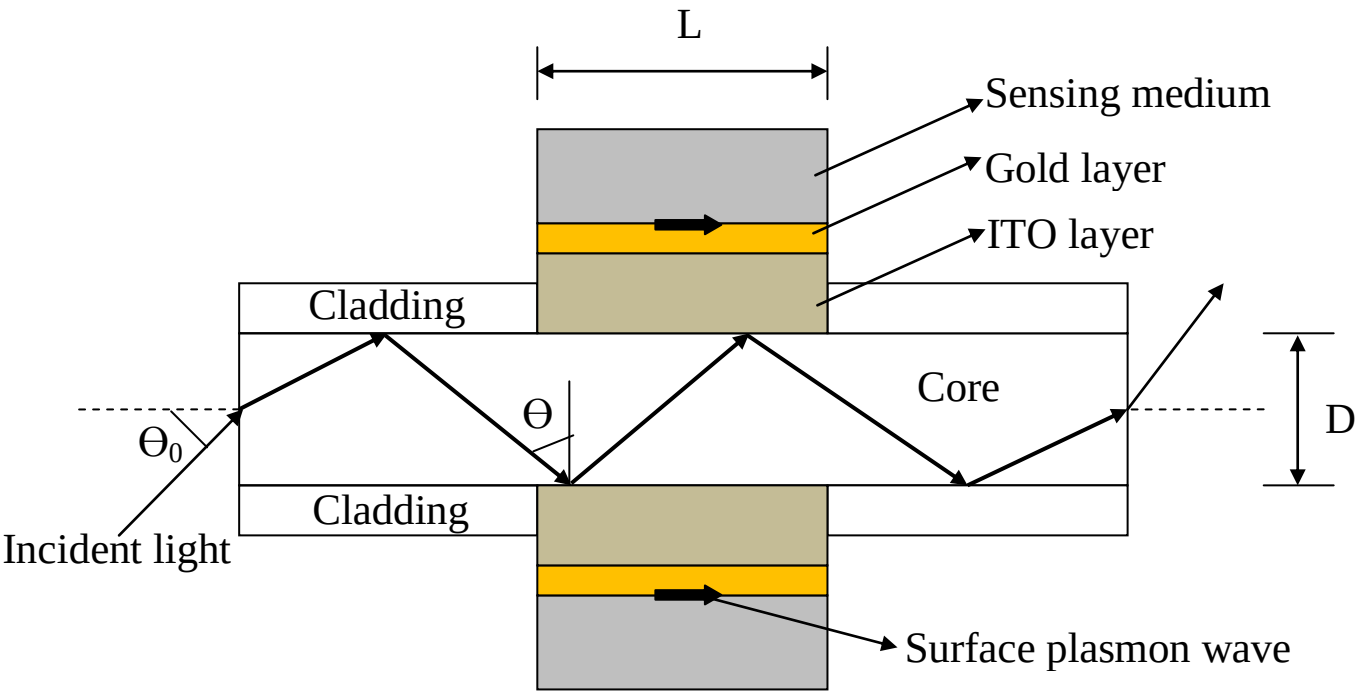

Figure 2.1: Schematic diagram of SPR based fiber optic sensor with bi layers of ITO-Au

The plastic cladding around the core from the middle portion of a step index multimode plastic clad silica (PCS) fiber (Numerical aperture = 0.24 and fiber core diameter = 600 μm) is removed and is then coated with a thin ITO layer, which is then further coated with Au layer. These bi layers of ITO-Au are finally surrounded by the sensing medium. The light from a broadband (polychromatic) source is launched into one of the ends of the optical fiber with proper optics and the transmitted light is detected at the other end of the optical fiber.

In the present study, the surface plasmon resonance produced by coupling of evanescent light to surface plasmons is used as the sensing mechanism and the wavelength interrogation method has been utilized for the analysis of SPR based fiber optic sensor. In this method, the

wavelength of incident light from the white light (polychromatic) source is varied and the corresponding transmitted power through the optical fiber is measured. It is important to notice here that in the present work, a laser source is not used to couple the incident light into the optical fiber rather a white light source has been used. However, if a laser source is assumed to couple the incident light into the optical fiber then the coupling of laser mode into surface plasmons can be realized simply. The mode conversion of TM mode of a laser into surface plasmon wave in a metal coated optical fiber is facilitated by a surface ripple of suitable wave number [138-140]. There is always a wave number mismatch between the TM mode and the surface plasmon wave in an optical fiber. This wave number mismatch corresponds to the required ripple wave number for resonant mode conversion. When a laser beam in TM mode propagates through the optical fiber, it induces oscillatory velocity on the electrons lying at metal surface. This oscillatory velocity beats with the space modulated density to produce a current, driving the surface plasmon wave on the boundary between metal and free space. The field of surface plasmon waves polarizes the metal particles present on metal surface, enhancing local fields at resonance condition. The fields polarize the molecules adsorbed on particles. The scattered field produced by the adsorbed molecules gets enhanced again.

2.2.1 Layer I (Fiber core)

This layer is made of core of optical fiber. The core of the optical fiber is assumed to be made of fused silica. The refractive index of fused silica varies with wavelength according to Sellmeier dispersion relation as,

$$n_1(\lambda) = \sqrt{1 + \frac{a_1\lambda^2}{\lambda^2 - b_1^2} + \frac{a_2\lambda^2}{\lambda^2 - b_2^2} + \frac{a_3\lambda^2}{\lambda^2 - b_3^2}} \tag{2.1}$$

Where, λ is the wavelength in µm and a_1, a_2, a_3, b_1, b_2 and b_3 are Sellmeier coefficients. The values of these coefficients are given as, a_1 = 0.6961663, a_2 = 0.4079426, a_3 = 0.8974794, b_1 = 0.0684043 µm, b_2 = 0.1162414 µm and b_3 = 9.896161 µm [141].

2.2.2 Layer II (ITO layer)

This layer is made of ITO. The dielectric constant of ITO is written according to the Drude model as,

$$\varepsilon_m(\lambda) = \varepsilon_{mr} + i\varepsilon_{mi} = 3.8 - \frac{\lambda^2 \lambda_c}{\lambda_p^2 (\lambda_c + i\lambda)} \tag{2.2}$$

Here, λ_p and λ_c are the plasma wavelength and the collision wavelength respectively. Where, λ_p = 5.649 x 10^{-7} m and λ_c = 11.121 x 10^{-6} m for ITO [71].

2.2.3 Layer III (Au layer)

This layer is made of Au metal. The dielectric constant of any metal can be written according to Drude model as,

$$\varepsilon_m(\lambda) = \varepsilon_{mr} + i\varepsilon_{mi} = 1 - \frac{\lambda^2 \lambda_c}{\lambda_p^2 (\lambda_c + i\lambda)} \tag{2.3}$$

Where, λ_p = 1.6826 x 10^{-7} m and λ_c = 8.9342 x 10^{-6} m for Au [142].

2.2.4 Layer IV (Sensing medium)

This layer is made of sensing medium. The dielectric constant of the sensing medium is ε_s. If n_s is the refractive index of the sensing medium, then $\varepsilon_s = n_s^2$. The resonance condition for excitation of surface plasmon wave is given as,

$$\frac{2\pi}{\lambda} n_1 \sin\theta = \mathrm{Re}\{K_{sp}\} \tag{2.4}$$

Where, $K_{sp} = \frac{\omega}{c}\sqrt{\frac{\varepsilon_m \varepsilon_s}{\varepsilon_m + \varepsilon_s}} = \frac{2\pi}{\lambda}\sqrt{\frac{\varepsilon_m n_s^2}{\varepsilon_m + n_s^2}}$ is the propagation constant of the surface plasmon wave and c is the speed of light in vacuum. The left hand side of Eq. (2.4) denotes the propagation constant of the light incident at an angle θ and the right hand side shows the real part of the propagation constant of the surface plasmon wave. If the refractive index of the sensing medium is changed, the right hand side of the Eq. (2.4) gets modified and therefore the resonance condition will be satisfied at some other value of the wavelength. By observing the shift in the resonance wavelength, a change in the refractive index of the sensing medium can be measured.

2.2.5 Transmitted Power

Meridional rays are the rays that cross the fiber axis between reflections, while the rays that never cross the fiber axis are known as skew rays. Based on the launching condition in an optical fiber, the light source can excite both meridional and skew rays [64]. In the present study, the excitation conditions do not include the contribution of skew rays. However, it has been observed in a research study [143] that, as the skewness parameter increases, the sensitivity of the sensor decreases. Further for short length of optical fiber, the meridional rays can be categorized in to two cases: selected ray launching and all guided rays launching. To simplify the present analysis, only all guided rays launching case of meridional rays have been considered as there is no fixed analytical expression for power distribution if the skew rays are also excited in the optical fiber.

Here, it is essential to note that there is no influence of s-polarization component of incident light on the transmitted power and sensitivity of the sensor as it is well known that the SPR phenomenon does not take place when the incident light has s-polarization [62]. The expression for the reflection coefficient (reflectance) of p-polarized incident light can be obtained by using the matrix method for N-layer model as mentioned in appendix A. Considering that all the guided rays are launched in the fiber using a collimated source and a microscope objective, the angular power distribution of rays guided in the fiber is given as [18],

$$dP \propto \frac{n_1^2 \sin\theta\cos\theta}{(1-n_1^2\cos^2\theta)^2}\,d\theta \tag{2.5}$$

Where, θ is the angle of the ray with the normal to the core-cladding interface. Also, n_1 is the refractive index of the core of the fiber. Further, for launching the incident beam into the optical fiber in order to couple the beam to surface plasmon wave at the metal cladded region, the angle at the core-metal interface in the sensing region should be lying between $\theta = \theta_{cr}$ to $\theta = \frac{\pi}{2}$ [18]. To calculate the effective transmitted power, the reflectance (R_p) for a single reflection is raised to the power of the number of reflections the specific propagating angle undergoes with the sensor interface. Hence, for p-polarized light, the generalized expression for the normalized transmitted power in an optical fiber based SPR sensor will be given as,

$$P_{trans} = \frac{\int_{\theta_{cr}}^{\pi/2} R_p^{N_{ref}(\theta)} \frac{n_1^2 \sin\theta\cos\theta}{(1-n_1^2\cos^2\theta)^2}\,d\theta}{\int_{\theta_{cr}}^{\pi/2} \frac{n_1^2 \sin\theta\cos\theta}{(1-n_1^2\cos^2\theta)^2}\,d\theta} \tag{2.6}$$

Where, $N_{ref}(\theta) = \frac{L}{D\tan\theta}$ (2.7)

And, $\theta_{cr} = \sin^{-1}\left(\frac{n_{cl}}{n_1}\right)$ (2.8)

Here, $N_{ref}(\theta)$ is the total number of reflections performed by a ray making an angle θ with the normal to the core-metal layer interface in the sensing region. L and D are the length of the exposed sensing region and the fiber core diameter respectively. Also, θ_{cr} is the critical angle of the fiber and n_{cl} is the refractive index of the cladding of the fiber.

Here, the power reflection in the metal cladded fiber has not been taken into account due to the small value of intensity reflection coefficient. This can be understood from the fact that in the SPR based fiber optic sensor, when a TM polarized (p-polarized) light enters from the

cladded fiber into the metal coated fiber, it comes across a change in the wave number from k_z' to k_z and a power reflection takes place having intensity reflection coefficient $R \approx \left| \frac{k_z' - k_z}{k_z' + k_z} \right|^2$, where k_z' and k_z are the wave numbers in the cladded fiber and metal coated fiber respectively [138]. The value of R is found to be of the order of only 1%, which is insignificant.

Further, it becomes necessary to discuss here that the light is efficiently coupled back in the optical fiber upon detection of analyte due to the phenomenon of surface enhanced Raman scattering (SERS) [138-140]. SERS is a very useful and sensitive method that allows the detection of organic molecules attached to a rough metal surface. In SERS phenomenon, a laser shines the rough metal surface with metallic particles attached to it. When the laser frequency matches with the natural frequency of plasmon oscillations of particles, the laser induces a vast field in the metallic particles, making them strong dipole oscillators at laser frequency. The molecules adsorbed on the particles thus experience a strong field. The Raman shifted molecular dipoles induce a strong, plasmon enhanced field inside the particles and the particles act as radiating dipoles producing a highly enhanced Raman signal.

2.2.6 Sensitivity

Resonance wavelength (λ_{res}) is determined corresponding to the refractive index of the sensing medium (n_s) in the SPR sensor based on wavelength interrogation. If the refractive index of the sensing medium is altered by δn_s, the resonance wavelength shifts by $\delta\lambda_{res}$. The sensitivity (S_n) of a SPR sensor with wavelength interrogation is defined as [64],

$$S_n = \frac{\delta\lambda_{res}}{\delta n_s} \tag{2.9}$$

2.3 Results and discussion

Various solutions of glycerine in water with different refractive indices are considered as the sensing mediums. For numerical calculations, a range of solutions of glycerine in water with

concentrations that offer refractive indices of 1.30, 1.31, 1.32, 1.33, 1.34 and 1.35 are assumed. The refractive index of the sensing medium is changed from 1.30 to 1.35 in steps of 0.01 and following values of the parameters have been used:

Numerical aperture of the fiber = 0.24, fiber core diameter D = 600 µm, length of the exposed sensing region L = 15 mm.

For the optimization of thicknesses of ITO and Au layers, the transmitted output power of SPR based fiber optic sensor have been calculated for different thickness values (100 nm, 125 nm, 150 nm, 175 nm and 200 nm) of ITO layer for fixed 25 nm, 30 nm, 35 nm and 40 nm thick Au layer. The variations of SPR resonance wavelength of left and right resonance dips with refractive index of sensing medium for various thickness values of ITO layer with 25 nm, 30 nm, 35 nm and 40 nm thick Au layer have been plotted in Figs. 2.2-2.9.

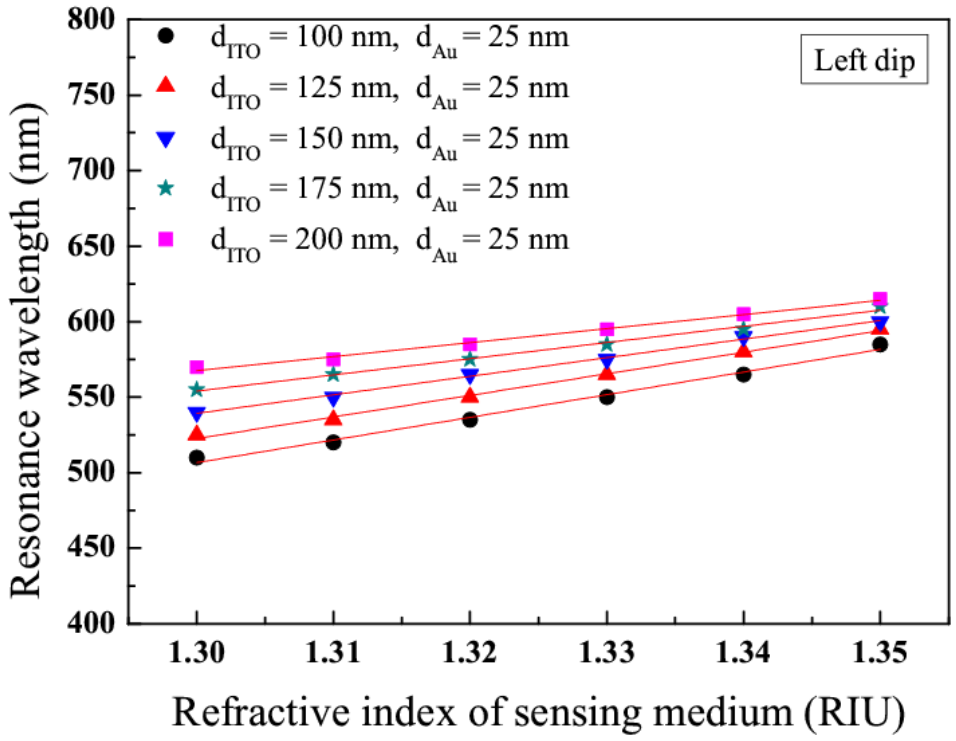

Figure 2.2: Variation of resonance wavelength of left resonance dip with refractive index of sensing medium for different thicknesses of ITO layer with 25 nm thick Au layer

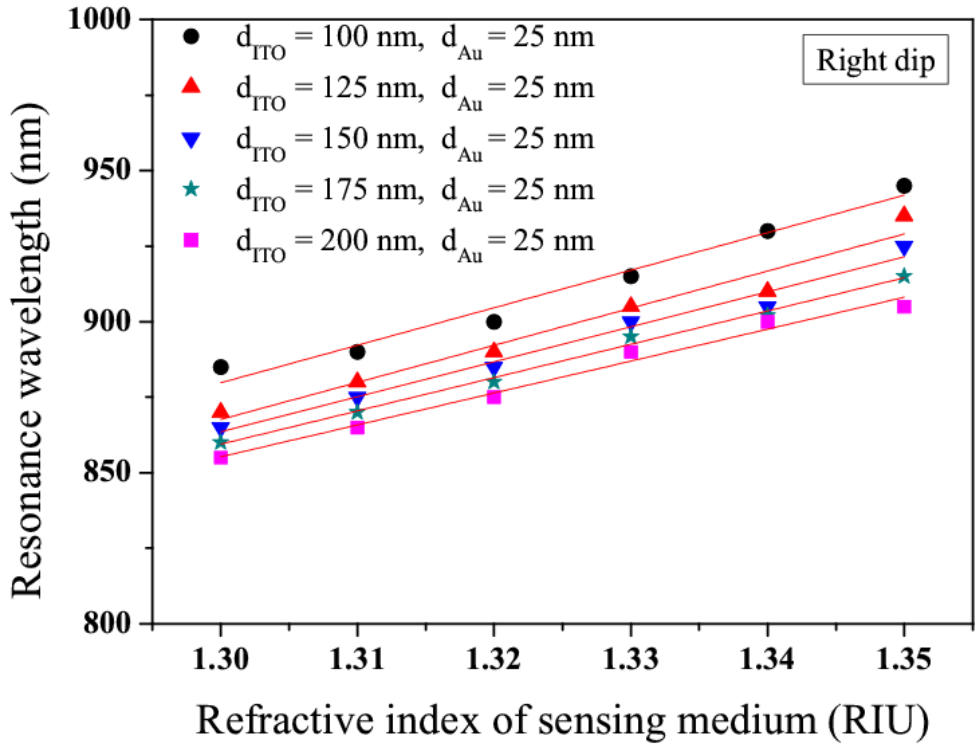

Figure 2.3: Variation of resonance wavelength of right resonance dip with refractive index of sensing medium for different thicknesses of ITO layer with 25 nm thick Au layer

Figs. 2.2 and 2.3 show the plots of resonance wavelength of left and right resonance dips with refractive index of sensing medium for 100 nm ITO-25 nm Au layers, 125 nm ITO-25 nm Au layers, 150 nm ITO-25 nm Au layers, 175 nm ITO-25 nm Au layers and 200 nm ITO-25 nm Au layers respectively.

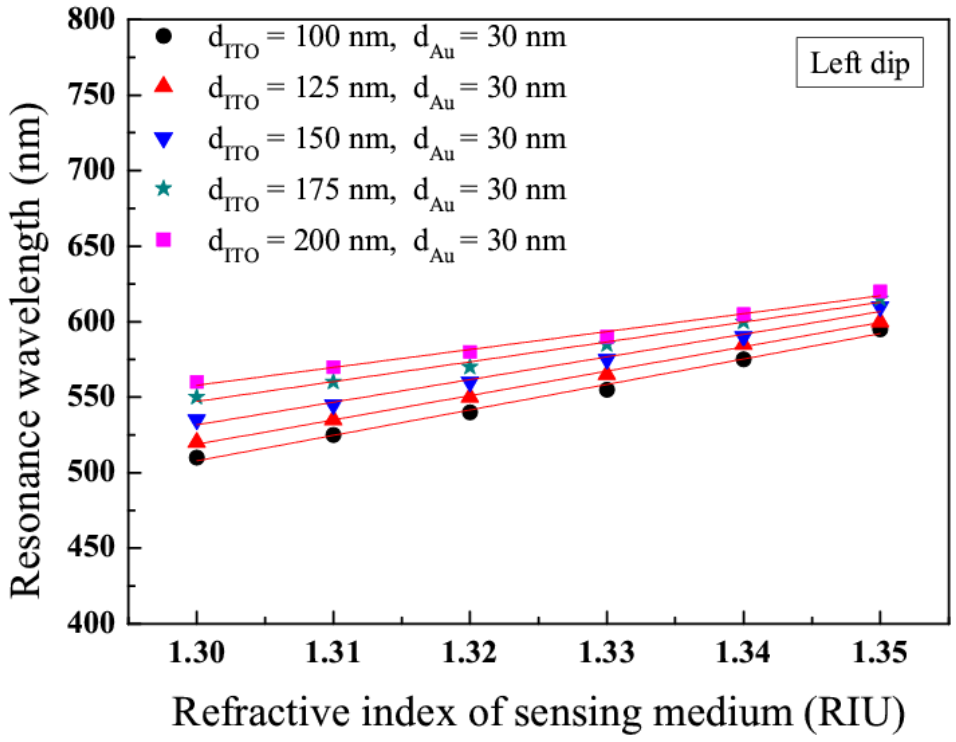

Figure 2.4: Variation of resonance wavelength of left resonance dip with refractive index of sensing medium for different thicknesses of ITO layer with 30 nm thick Au layer

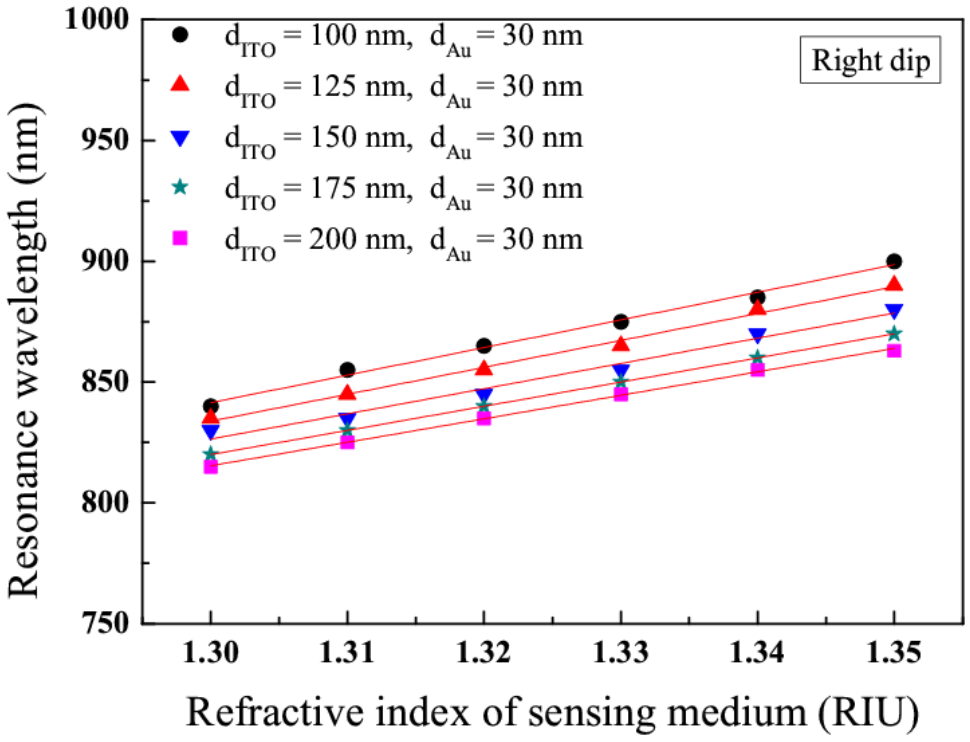

Figure 2.5: Variation of resonance wavelength of right resonance dip with refractive index of sensing medium for different thicknesses of ITO layer with 30 nm thick Au layer

Similarly, Figs. 2.4 and 2.5 illustrate the variations of resonance wavelength of the left and right resonance dips with refractive index of sensing medium for 100 nm ITO-30 nm Au layers, 125 nm ITO-30 nm Au layers, 150 nm ITO-30 nm Au layers, 175 nm ITO-30 nm Au layers and 200 nm ITO-30 nm Au layers respectively.

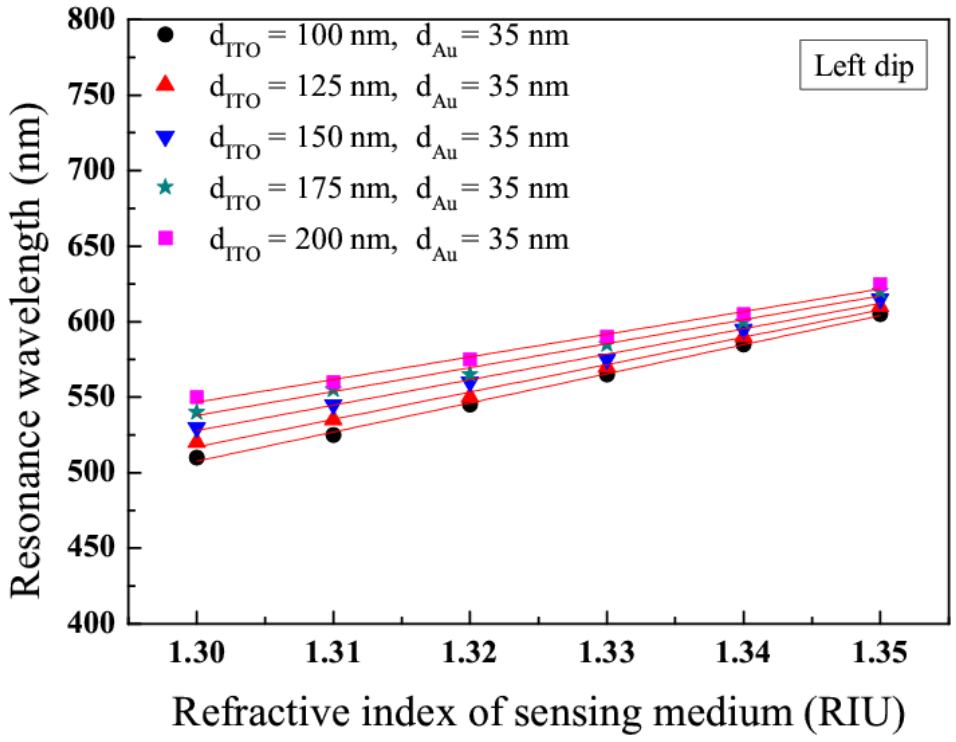

Figure 2.6: Variation of resonance wavelength of left resonance dip with refractive index of sensing medium for different thicknesses of ITO layer with 35 nm thick Au layer

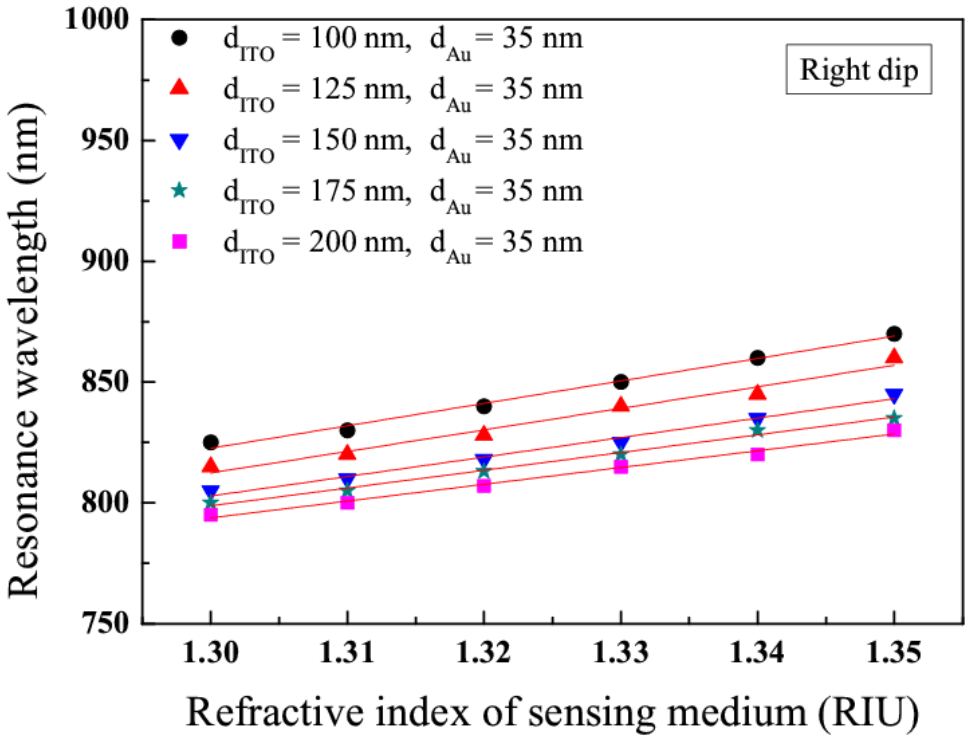

Figure 2.7: Variation of resonance wavelength of right resonance dip with refractive index of sensing medium for different thicknesses of ITO layer with 35 nm thick Au layer

Likewise, Figs. 2.6 and 2.7 demonstrate the variations of resonance wavelength of the left and right resonance dips with refractive index of sensing medium for 100 nm ITO-35 nm Au layers, 125 nm ITO-35 nm Au layers, 150 nm ITO-35 nm Au layers, 175 nm ITO-35 nm Au layers and 200 nm ITO-35 nm Au layers respectively.

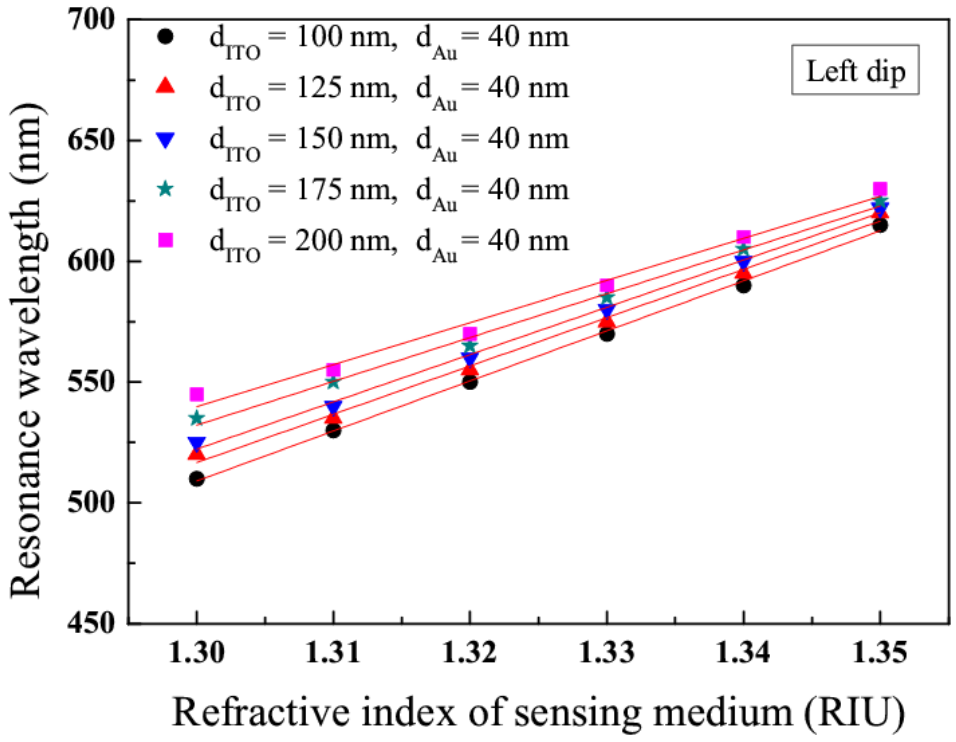

Figure 2.8: Variation of resonance wavelength of left resonance dip with refractive index of sensing medium for different thicknesses of ITO layer with 40 nm thick Au layer

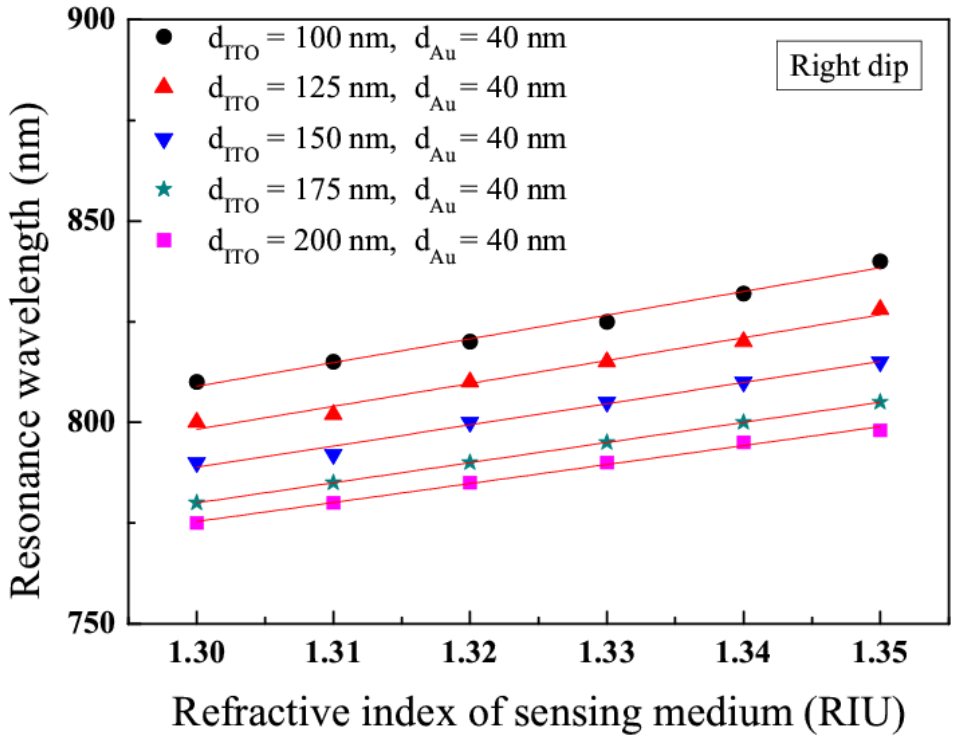

Figure 2.9: Variation of resonance wavelength of right resonance dip with refractive index of sensing medium for different thicknesses of ITO layer with 40 nm thick Au layer

In the same way, Figs. 2.8 and 2.9 display the variations of resonance wavelength of the left and right resonance dips with refractive index of sensing medium for 100 nm ITO-40 nm Au layers, 125 nm ITO-40 nm Au layers, 150 nm ITO-40 nm Au layers, 175 nm ITO-40 nm Au layers and 200 nm ITO-40 nm Au layers respectively. The resonance wavelength of both left and right resonance dips for a variety of thickness values (100 nm to 200 nm) of ITO layer with 25 nm, 30 nm, 35 nm and 40 nm thick Au layer increases in a linear fashion with the increase in refractive index of the sensing medium. The variations of resonance wavelength with the refractive index of the sensing medium for all these cases pursue the same outfit. The slopes of resonance wavelength over the refractive index for left resonance dips are highest for 100 nm ITO-25 nm Au layers, 100 nm ITO-30 nm Au layers, 100 nm ITO-35 nm Au layers and 100 nm ITO-40 nm Au layers while these are least for 200 nm ITO-25 nm Au layers, 200 nm ITO-30 nm Au layers, 200 nm ITO-35 nm Au layers and 200 nm ITO-40 nm Au layers. However, the shifts in resonance wavelength for all these cases are almost linear

over the entire range of refractive indices i.e. 1.30 to 1.35 of the sensing medium. Moreover, the occurrence of two resonance dips can be understood by the double character of ITO. In the region of high reflectance (wavelengths higher than 1500 nm), the imaginary part of refractive index of ITO is higher (of the order of metals) while on the other hand, it is lower for the low reflectance region (wavelengths lower than 1500 nm) [126]. This low reflectance region i.e. low imaginary part of refractive index of ITO is responsible for the generation of double resonance dips.

Further, to see the clear difference between bi layers of ITO-Au with various thickness values and single metal layer of Au (assuming zero thickness of ITO layer), a Fig. 2.10 has also been drawn.

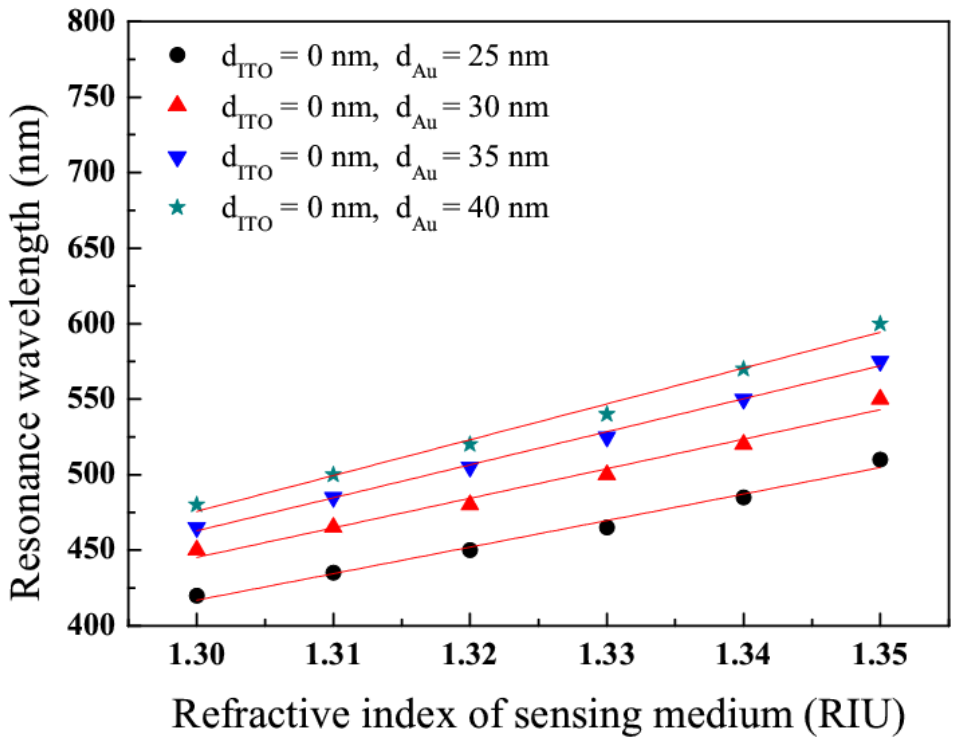

Figure 2.10: Variation of resonance wavelength of single resonance dip with refractive index of sensing medium for fixed zero thickness of ITO layer with different thicknesses of Au layer

Fig. 2.10 shows the variation of resonance wavelength of single resonance dip with refractive index of sensing medium for fixed zero thickness of ITO layer with different thicknesses of Au layer. Fig. 2.10 clearly reveals a single resonance dip due to the presence of only single metal layer, just opposite to the case of bi layers of ITO-Au with a range of thickness values having double resonance dips. In addition, the linear enhancement in resonance wavelengths of both left and right resonance dips for a range of thickness values of bi layers of ITO-Au including single resonance dip for single metal layer of Au (assuming zero thickness of ITO layer) with the increase in refractive index of the sensing medium can be easily seen in all Figs. 2.2–2.10. The explanation for these graphically presented results (shown in Figs. 2.2–2.10) can be ascribed to Eq. (2.4). The change in resonance wavelength with change in refractive index of sensing medium can be explained by the variation of real part of propagation constant (K_{sp}) of surface plasmon wave. It is obvious from Eq. (2.4) that the real part of K_{sp} is responsible for the resonance condition. The real part of K_{sp} will be smaller for small value of refractive index of sensing medium and hence its resonance condition is satisfied at smaller wavelength [103]. Similarly, for the larger value of refractive index of sensing medium, the resonance condition is satisfied at longer wavelength due to having largest real part of K_{sp}.

To clearly observe the left and right resonance dips, Fig. 2.11 is drawn, which shows SPR transmittance curves for various thicknesses of ITO layer and fixed 30 nm thick Au layer at a refractive index of sensing medium = 1.32.

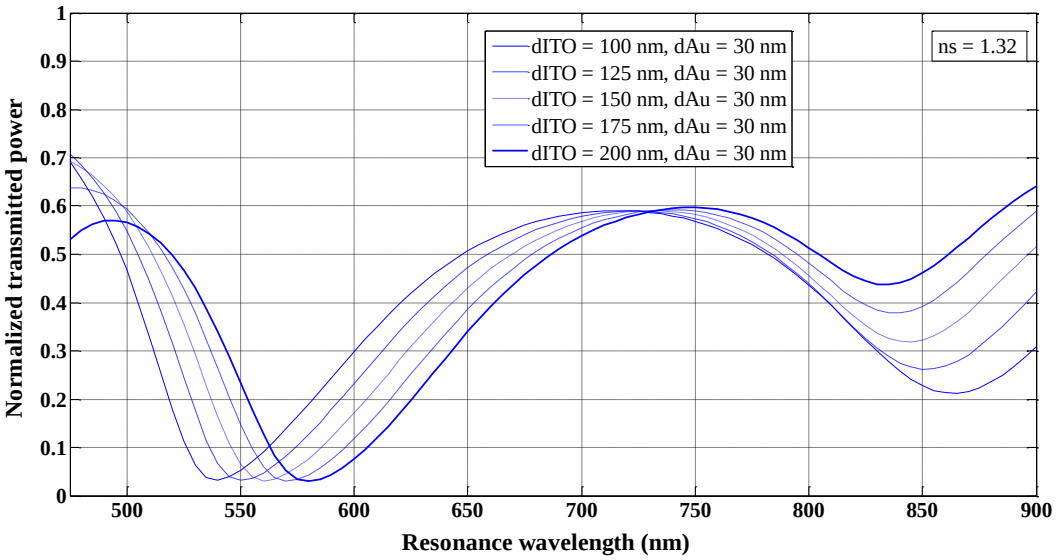

Figure 2.11: SPR transmittance curves for various thicknesses of ITO layer and fixed 30 nm thick Au layer at a refractive index of sensing medium = 1.32

Fig. 2.11 illustrates the SPR transmittance curves for 100 nm ITO-30 nm Au layers, 125 nm ITO-30 nm Au layers, 150 nm ITO-30 nm Au layers, 175 nm ITO-30 nm Au layers and 200 nm ITO-30 nm Au layers at a refractive index of sensing medium = 1.32. In this figure, two dips i.e. left and right resonance dips are clearly noticeable.

To obtain the maximum value of the sensitivity, it will be fine to identify the proper values of thickness of ITO layer and Au layer of SPR based fiber optic sensor. The sensitivities of SPR based fiber optic sensor for various thickness values (100 nm, 125 nm, 150 nm, 175 nm and 200 nm) of ITO layer with fixed 25 nm, 30 nm, 35 nm and 40 nm thick Au layer are compared in table 2.1.

Table 2.1: Comparison of sensitivity of SPR based fiber optic sensor for different thickness values of ITO layer with 25 nm, 30 nm, 35 nm and 40 nm thick Au layer

Thickness of ITO layer (nm)	Sensitivity S_n (nm/RIU)							
	Thickness of Au layer = 25 nm		Thickness of Au layer = 30 nm		Thickness of Au layer = 35 nm		Thickness of Au layer = 40 nm	
	Left resonance dip	Right resonance dip	Left resonance dip	Right resonance dip	Left resonance dip	Right resonance dip	Left resonance dip	Right resonance dip
100	1500	1243	1686	1143	1929	929	2071	589
125	1429	1229	1614	1114	1814	891	2000	569
150	1229	1157	1500	1043	1686	806	1957	526
175	1071	1103	1314	1000	1586	734	1814	500
200	929	1057	1186	971	1500	694	1742	471

It can be seen from table 2.1 that the sensitivity of left resonance dips decreases from 1500 nm/RIU (for 100 nm ITO-25 nm Au layers) to 929 nm/RIU (for 200 nm ITO-25 nm Au layers), 1686 nm/RIU (for 100 nm ITO-30 nm Au layers) to 1186 nm/RIU (for 200 nm ITO-30 nm Au layers), 1929 nm/RIU (for 100 nm ITO-35 nm Au layers) to 1500 nm/RIU (for 200 nm ITO-35 nm Au layers) and 2071 nm/RIU (for 100 nm ITO-40 nm Au layers) to 1742nm/ RIU (for 200 nm ITO-40 nm Au layers). Also, the sensitivity of right resonance dips decreases from 1243 nm/RIU (for 100 nm ITO-25 nm Au layers) to 1057 nm/RIU (for 200 nm ITO-25 nm Au layers), 1143 nm/RIU (for 100 nm ITO-30 nm Au layers) to 971 nm/RIU (for 200 nm ITO-30 nm Au layers), 929 nm/RIU (for 100 nm ITO-35 nm Au layers) to 694 nm/RIU (for 200 nm ITO-35 nm Au layers) and 589 nm/RIU (for 100 nm ITO-40 nm Au layers) to 471 nm/RIU (for 200 nm ITO-40 nm Au layers). Hence, the sensitivity of left resonance dip for 100 nm ITO-40 nm Au layers based SPR sensor is maximum (2071 nm/RIU) and is minimum (929 nm/RIU) for 200 nm ITO-25 nm Au layers based SPR sensor. In addition, the sensitivity of right resonance dip for 100 nm ITO-25 nm Au layers based SPR sensor is highest (1243 nm/RIU) and is lowest (471 nm/RIU) for 200 nm ITO-40 nm Au layers based SPR sensor. The variations of sensitivity of both left and right resonance dips

with thickness of ITO layer for fixed 25 nm, 30 nm, 35 nm and 40 nm thick Au layer have been plotted in Figs. 2.12 and 2.13 respectively.

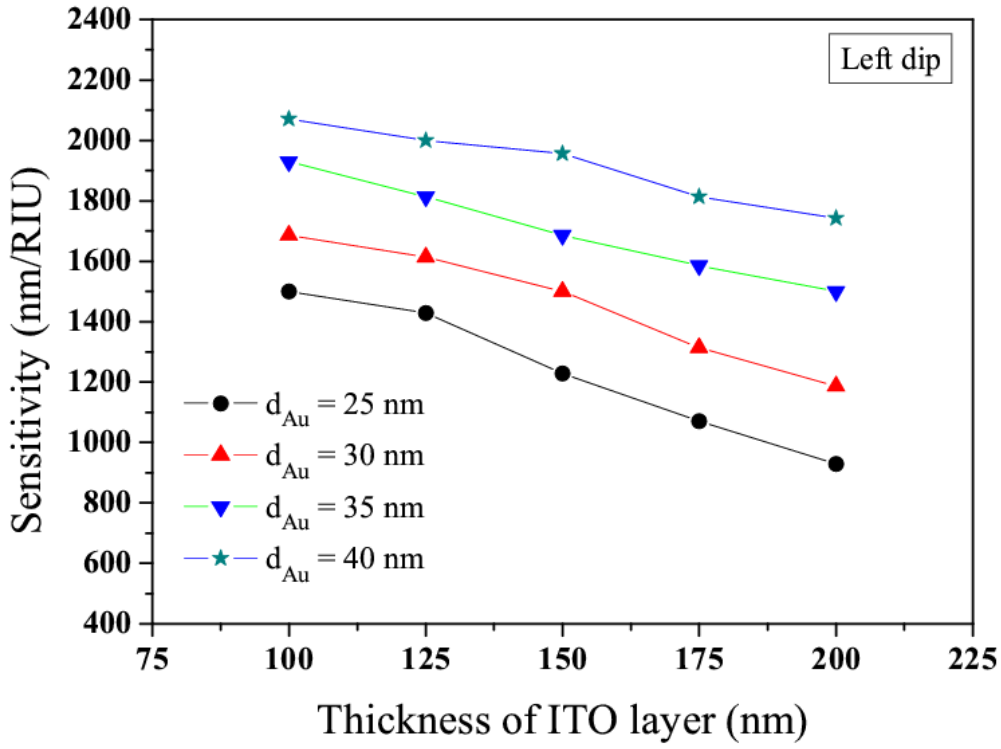

Figure 2.12: Variation of sensitivity of left resonance dip with thickness of ITO layer for fixed 25 nm, 30 nm, 35 nm and 40 nm thick Au layer

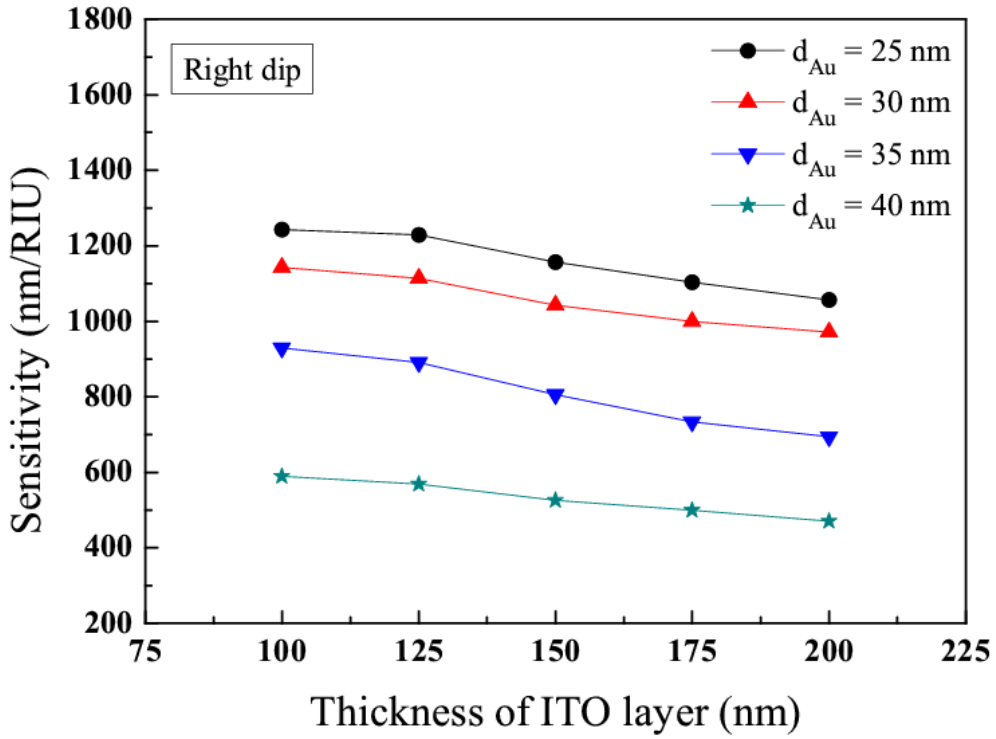

Figure 2.13: Variation of sensitivity of right resonance dip with thickness of ITO layer for fixed 25 nm, 30 nm, 35 nm and 40 nm thick Au layer

Figs. 2.12 and 2.13 depict the variations of sensitivity of both left and right resonance dips with thickness of ITO layer respectively for fixed 25 nm, 30 nm, 35 nm and 40 nm thick Au layer. It is obvious that increase in ITO layer thickness decreases the sensitivity of both left and right resonance dips for all values of thickness of Au layer. This occurs because the thick ITO layer allows less interaction between surface plasmon mode and fiber mode, resulting in little absorption of light power by the sensing medium around resonance wavelength. This forms the basis of increase in normalized transmitted power and as a result decreases the sensitivity of the sensor. In addition, for a fixed thickness of ITO layer, the sensitivity of left resonance dip increases with the increase in Au layer thickness while that of right resonance dip decreases with the increase in Au layer thickness. The reason for this fact can be attributed to the real part of propagation constant (K_{sp}) of surface plasmon wave as it is accountable for the shifting of the resonance condition/wavelength. Au layer exhibits high sensitivity because

Au illustrates large value of real part of its dielectric constant at all wavelengths [103]. Thus, Au layer enhances the shift between resonance wavelengths for a given change of refractive index of the sensing medium and therefore the sensitivity of the left resonance dip increases with the increase in thickness of Au layer for a fixed thickness of ITO layer. Also, the variations of sensitivity of both left and right resonance dips with thickness of Au layer for fixed 100 nm, 125 nm, 150 nm, 175 nm and 200 nm thick ITO layer have been shown in Figs. 2.14 and 2.15 respectively.

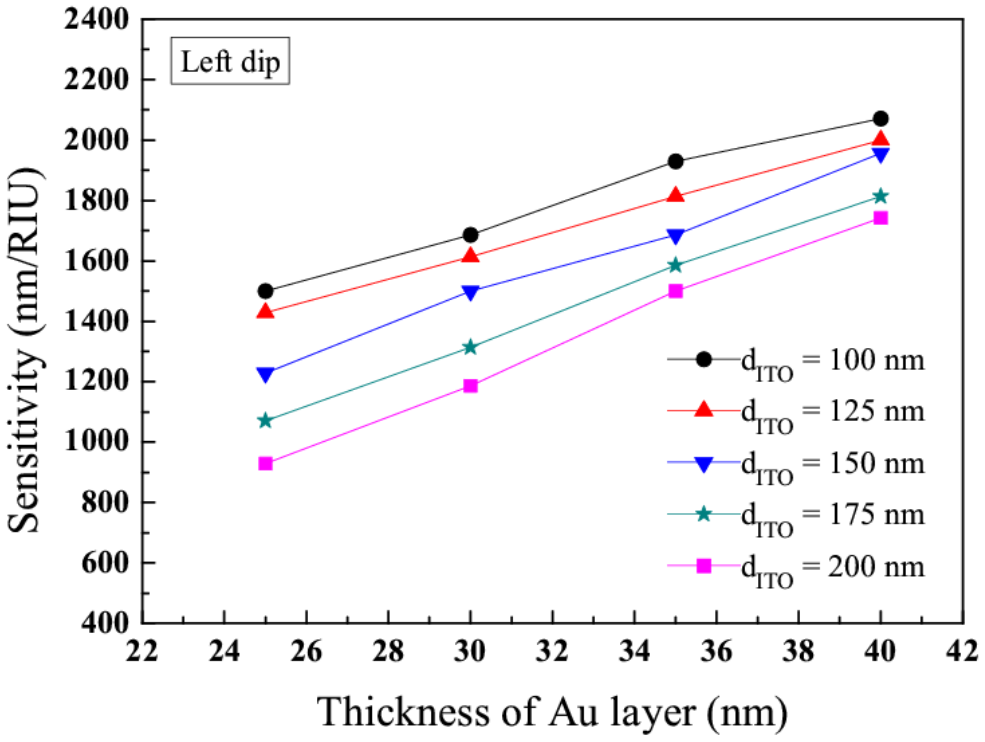

Figure 2.14: Variation of sensitivity of left resonance dip with thickness of Au layer for fixed 100 nm, 125 nm, 150 nm, 175 nm and 200 nm thick ITO layer

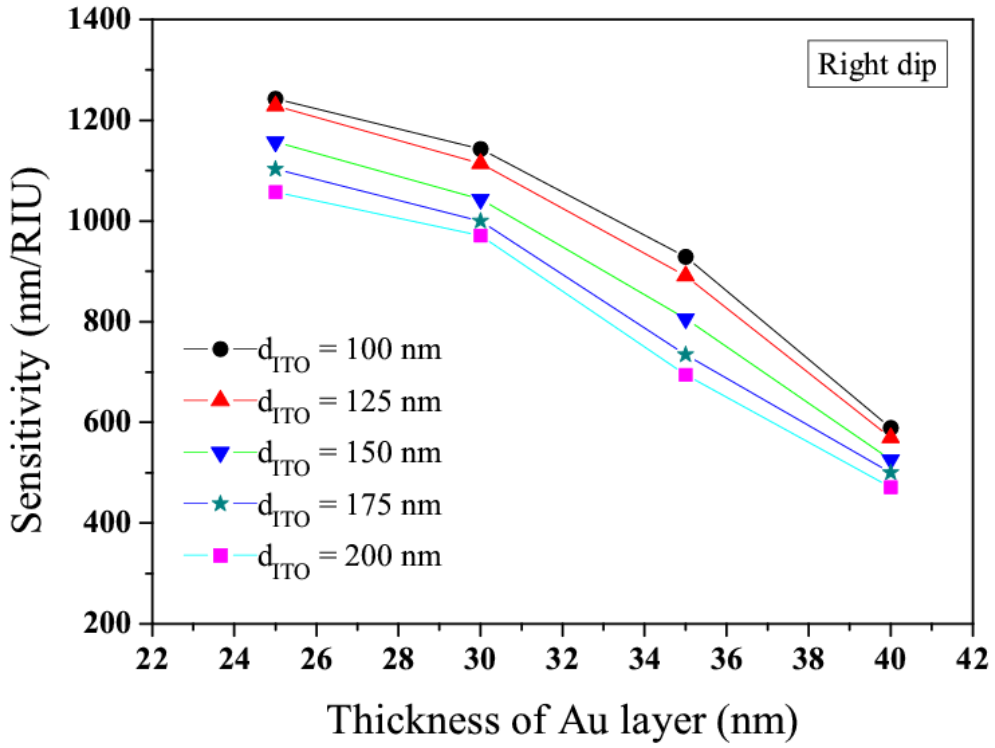

Figure 2.15: Variation of sensitivity of right resonance dip with thickness of Au layer for fixed 100 nm, 125 nm, 150 nm, 175 nm and 200 nm thick ITO layer

Figs. 2.14 and 2.15 represent the variations of sensitivity of both left and right resonance dips with thickness of Au layer respectively for fixed 100 nm, 125 nm, 150 nm, 175 nm and 200 nm thick ITO layer. It is again evident that increase in Au layer thickness increases the sensitivity of left resonance dip and decreases the sensitivity of right resonance dip for all thickness values of ITO layer. Further, for a fixed thickness of Au layer, the sensitivity of both left and right resonance dips decrease with the increase in ITO layer thickness. Once more, to observe the difference between bi layers of ITO-Au with different thickness values and single metal layer of Au (assuming zero thickness of ITO layer), a Fig. 2.16 has been sketched.

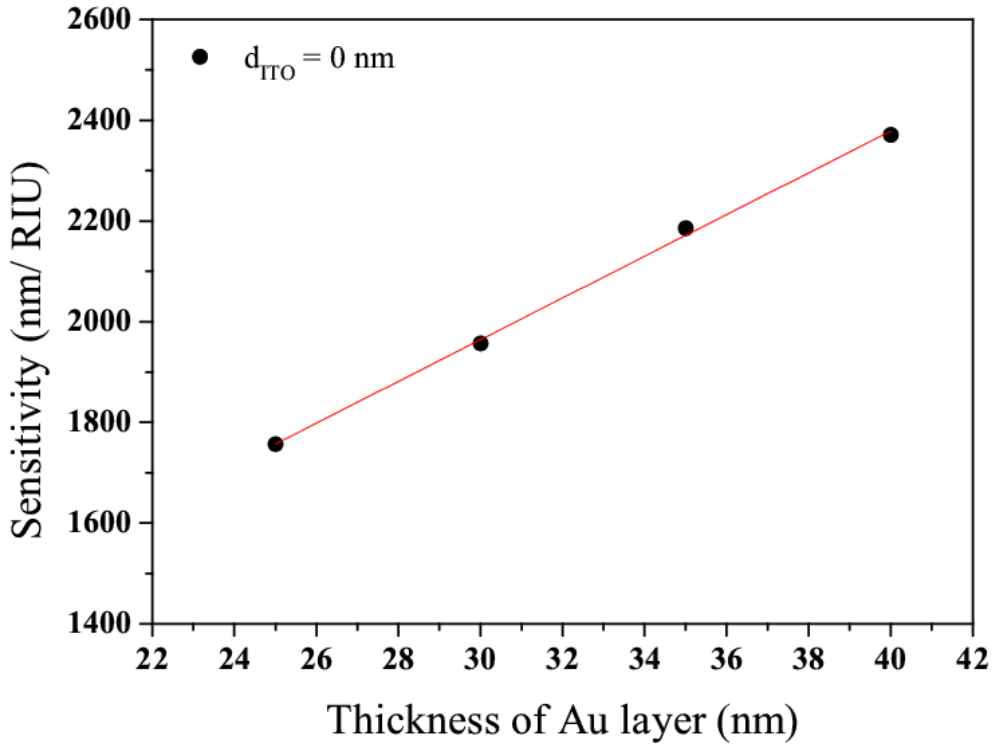

Figure 2.16: Variation of sensitivity of single resonance dip with thickness of Au layer for fixed zero thickness of ITO layer

Fig. 2.16 depicts the variation of sensitivity of single resonance dip with thickness of Au layer for fixed zero thickness of ITO layer. Fig. 2.16 clearly discloses a single resonance dip due to the presence of only single metal layer, just opposite to the case of bi layers of ITO-Au with various thickness values having double resonance dips.

Hence from table 2.1, the sensitivity (shift in resonance wavelength per unit change in refractive index of sensing medium) of left resonance dip is highest (2071 nm/RIU) while the sensitivity of right resonance dip is lowest (589 nm/RIU) for 100 nm ITO-40 nm Au layers based SPR sensor. On the other hand, 100 nm ITO-25 nm Au layers based SPR sensor provides the smaller sensitivity (1500 nm/RIU) for left resonance dip but higher sensitivity (1243 nm/RIU) for right resonance dip. Thus, neither 100 nm ITO-40 nm Au layers nor 100 nm ITO-25 nm Au layers based SPR sensor is capable to provide the highest values of sensitivities for both left and right resonance dips simultaneously. Therefore, in devising SPR based fiber optic sensor, the proper thickness of ITO and Au layers should be chosen

depending upon the left or right resonance dip of interest i.e. either sensitivity of left resonance dip (visible region of spectrum) or the sensitivity of the right resonance dip (near infrared region of spectrum) is required to be the highest. However, it is also obvious from table 2.1 that the average sensitivities (of left and right resonance dips) for fixed 100 nm thick ITO layer with 25 nm, 30 nm, 35 nm and 40 nm thick Au layer are 1372 nm/RIU, 1415 nm/RIU, 1429 nm/RIU and 1330 nm/RIU respectively. Similarly, the average sensitivities for fixed 125 nm thick ITO layer with 25 nm, 30 nm, 35 nm and 40 nm thick Au layer are 1329 nm/RIU, 1364 nm/RIU, 1353 nm/RIU and 1285 nm/RIU respectively. Likewise, the average sensitivities for fixed 150 nm thick ITO layer with 25 nm, 30 nm, 35 nm and 40 nm thick Au layer are 1193 nm/RIU, 1272 nm/RIU, 1246 nm/RIU and 1242 nm/RIU respectively. In the same way, the average sensitivities for fixed 175 nm thick ITO layer with 25 nm, 30 nm, 35 nm and 40 nm thick Au layer are 1087 nm/RIU, 1157 nm/RIU, 1160 nm/RIU and 1157 nm/RIU respectively. Also, the average sensitivities for fixed 200 nm thick ITO layer with 25 nm, 30 nm, 35 nm and 40 nm thick Au layer are 993 nm/RIU, 1079 nm/RIU, 1097 nm/RIU and 1107 nm/RIU respectively. Therefore, it can be easily understood from this discussion that 100 nm ITO-35 nm Au layers based SPR sensor comprises maximum value (1429 nm/RIU) of average sensitivity. However, the sensitivities of left and right resonance dips for 100 nm ITO-35 nm Au layers based SPR sensor are 1929 nm/RIU and 929 nm/RIU respectively, that are not maximum. Now, it is to be cited here that the maximum values of sensitivities of left and right resonance dips are 2071 nm/RIU (for 100 nm ITO-40 nm Au layers based SPR sensor) and 1243 nm/RIU (for 100 nm ITO-25 nm Au layers based SPR sensor) respectively. Thus, it can be concluded that the optimized values of thickness of ITO and Au layers of a SPR based fiber optic sensor are exposed to be 100 nm and 35 nm respectively as 100 nm ITO-35 nm Au layers based SPR sensor possesses maximum value (1429 nm/RIU) of average sensitivity.

So, taking all the above facts in to consideration, it has been found that 100 nm ITO-35 nm Au layers based SPR sensor demonstrates sensitivities of 1929 nm/RIU (in visible region of spectrum) and 929 nm/RIU (in near infrared region of spectrum) for left and right resonance dips respectively.

2.4 Conclusions

The simulation of a SPR based fiber optic sensor with bi layers of metal oxide-metal i.e. bi layers of ITO (as an inner layer)-Au (as an outer layer) has been presented. The sensitivity of SPR sensor for various thickness values (100 nm to 200 nm) of ITO layer with 25 nm, 30 nm, 35 nm and 40 nm thick Au layer is studied theoretically. The proposed SPR sensor with bi layers of ITO-Au possesses high sensitivity with two resonance dips, one in the visible and other in the near infrared region of spectrum, opposite to the single metal layer based SPR sensor with one and only resonance dip. These double resonance dips vary as a function of refractive index of the sensing medium. In addition, two differentiated SPR dips have been obtained from the same device within 510 nm to 870 nm spectrum. Also, increase in ITO layer thickness decreases the sensitivity of both left and right resonance dips for all values of thickness of Au layer. Furthermore, for a fixed thickness of ITO layer, the sensitivity of left resonance dip increases with the increase in Au layer thickness while that of right resonance dip decreases with the increase in Au layer thickness. 100 nm ITO-40 nm Au layers based SPR sensor exhibits high sensitivity (2071 nm/RIU) for left resonance dip in visible region but low sensitivity (589 nm/RIU) for right resonance dip in near infrared region of spectrum. On the other hand, 100 nm ITO-25 nm Au layers based SPR sensor reveals smaller sensitivity (1500 nm/RIU) for left resonance dip in visible region but higher sensitivity (1243 nm/RIU) for right resonance dip in near infrared region of spectrum. Thus, depending upon the region of interest i.e. visible region/near infrared region of spectrum, one should go for 100 nm ITO-40 nm Au layers/100 nm ITO-25 nm Au layers based SPR sensor. However, the optimized thicknesses of ITO and Au layers of SPR based fiber optic sensor are revealed to be 100 nm and 35 nm respectively. Furthermore, 100 nm ITO-35 nm Au layers based SPR sensor demonstrates sensitivities of 1929 nm/RIU and 929 nm/RIU for left and right resonance dips respectively.

CHAPTER 3

SURFACE PLASMON RESONANCE BASED FIBER OPTIC SENSOR UTILIZING INDIUM OXIDE

3.1 Introduction

As discussed in chapter 2, transparent conducting oxides (TCOs) are of immense interest due to their good electrical conductivity, high transparency in the visible region, and high infrared reflectivity. They form vital mechanism in large number of optoelectronic devices such as light emitting diodes, photodetectors, touch panels, flat panel displays, and solar cells [137,144,145]. In addition, it has become possible to obtain surface plasmon resonance with transparent conducting metal oxide thin films [71]. Recently, indium oxide (In_2O_3) has been reported to be a better substitute of noble metals (Au and Ag) for producing surface plasmons [146]. Among various TCOs, In_2O_3 is a potential material for numerous applications such as solar cells and gas sensing due to its highest available transmissivity for visible light combined with lowest electrical resistivity and reflection spectra in IR region [127]. It is an n-type wide band gap semiconductor (band gap ~ 3.7 eV) and has high electrical conductivity. In its stochiometric state, it is insulator and becomes conducting with increasing its oxygen deficiency. Its optical and electrical properties can be considerably modified using suitable doping. Besides it, thin films of In_2O_3 are continuous (i.e. no agglomeration as islands) and no involvement of band to band transitions.

In this chapter, a SPR based fiber optic sensor with In_2O_3 layer has been theoretically discussed. The surface plasmon resonance produced by coupling of evanescent light to surface plasmons is used as the sensing scheme. The wavelength interrogation method is exploited for the analysis of SPR based fiber optic sensor. The SPR sensor with In_2O_3 layer is shown to possess high sensitivity in the near infrared region of spectrum. In addition, the sensitivity of the SPR sensor decreases with increase in the thickness of In_2O_3 layer. 170 nm thick In_2O_3 layer based fiber optic SPR sensor shows high sensitivity of 4600 nm/RIU.

3.2 Theory

The SPR sensing is based on the principle of attenuated total reflection (ATR) with Kretschmann configuration. In the proposed SPR based fiber optic sensor, the sensing system consisting of a fiber core-In_2O_3-sensing medium is considered as shown in Fig. 3.1.

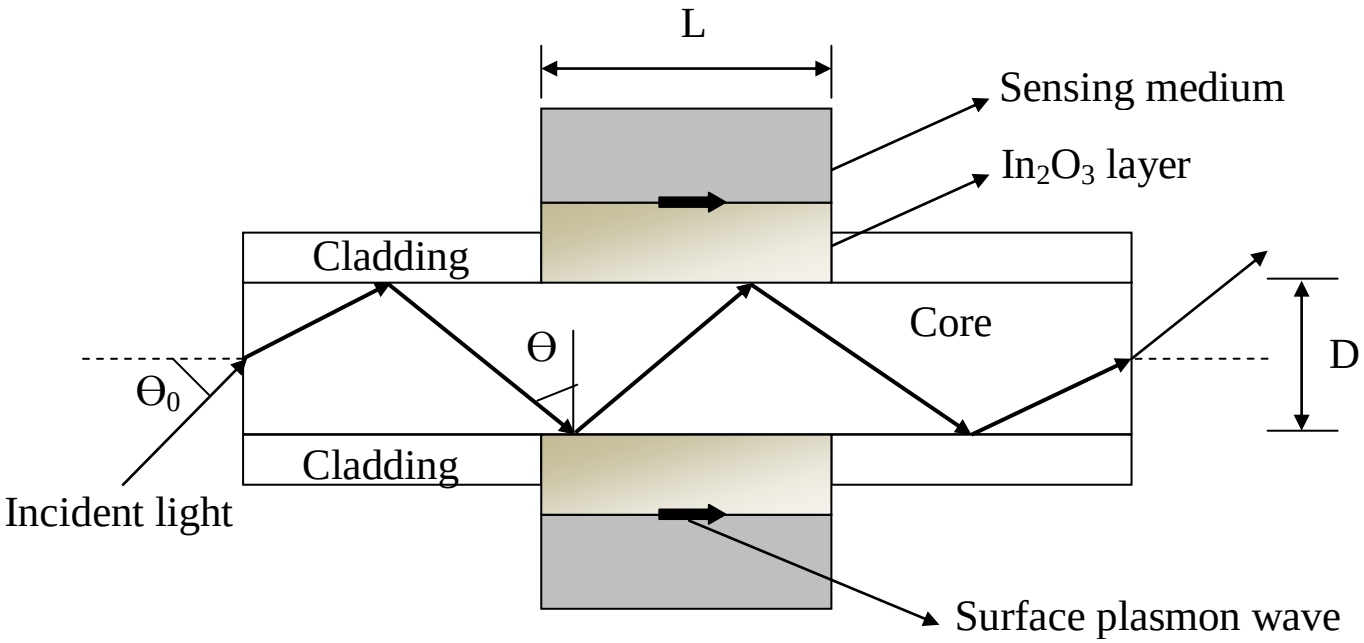

Figure 3.1: Schematic diagram of SPR based fiber optic sensor with In_2O_3 layer

The plastic cladding around the core from the middle portion of a step index multimode PCS fiber is removed and is then coated with a thin In_2O_3 layer. This In_2O_3 layer is finally surrounded by the sensing medium. The light from a broadband (polychromatic) source is launched into one of the ends of the optical fiber with proper optics and the transmitted light is detected at the other end of the optical fiber.

3.2.1 Layer I (Fiber core)

This layer is made of core of optical fiber. The core of the optical fiber is assumed to be made of fused silica. The refractive index of fused silica varies with wavelength according to Sellmeier dispersion relation as,

$$n_1(\lambda) = \sqrt{1 + \frac{a_1\lambda^2}{\lambda^2 - b_1^2} + \frac{a_2\lambda^2}{\lambda^2 - b_2^2} + \frac{a_3\lambda^2}{\lambda^2 - b_3^2}} \tag{3.1}$$

Where, λ is the wavelength in µm and a_1, a_2, a_3, b_1, b_2 and b_3 are Sellmeier coefficients. The values of these coefficients are given as, a_1 = 0.6961663, a_2 = 0.4079426, a_3 = 0.8974794, b_1 = 0.0684043 µm, b_2 = 0.1162414 µm and b_3 = 9.896161 µm [141].

3.2.2 Layer II (In_2O_3 layer)

This layer is made of In_2O_3. The dielectric constant of In_2O_3 is written according to Drude model as [128],

$$\varepsilon(\omega) = \varepsilon_\infty - \frac{\omega_p^2}{\omega^2 + i\frac{\omega}{\tau}} + \frac{s_0\,\omega_0^2}{\omega_0^2 - \omega^2 + i\gamma\,\omega} \tag{3.2}$$

Here, ε_∞ is the high frequency dielectric constant, τ is the electronic scattering time, ω_p is the plasma frequency, s_0 is the oscillator strength, ω_0 is the oscillator resonance frequency and γ is the damping constant. The parameters used for In_2O_3 are: ε_∞ = 3.5, τ = 1.014 x 10^{-14} s rad^{-1}, ω_p = 1.02 x 10^{15} rad s^{-1}, s_0 = 0.7, ω_0 = 7.29 x 10^{15} rad s^{-1} and γ = 7.08 x 10^{14} rad s^{-1} [128].

3.2.3 Layer III (Sensing medium)

This layer is made of sensing medium. The dielectric constant of the sensing medium is ε_s. If n_s is the refractive index of the sensing medium, then $\varepsilon_s = n_s^2$. The resonance condition for excitation of surface plasmon wave is given as,

$$\frac{2\pi}{\lambda} n_1 \sin\theta = \mathrm{Re}\{K_{sp}\} \tag{3.3}$$

Where, $K_{sp} = \frac{\omega}{c}\sqrt{\frac{\varepsilon_m \varepsilon_s}{\varepsilon_m + \varepsilon_s}} = \frac{2\pi}{\lambda}\sqrt{\frac{\varepsilon_m n_s^2}{\varepsilon_m + n_s^2}}$ is the propagation constant of the surface plasmon wave and c is the speed of light in vacuum. The left hand side of Eq. (3.3) denotes the propagation constant of the light incident at an angle θ and the right hand side shows the real part of propagation constant of the surface plasmon wave.

3.2.4 Transmitted Power

The expression for the reflection coefficient (reflectance) of p-polarized incident light can be obtained by using the matrix method for N-layer model as mentioned in appendix A. Considering that all the guided rays are launched in the fiber using a collimated source and a microscope objective, the angular power distribution of rays guided in the fiber is given as [18],

$$dP \propto \frac{n_1^2 \sin\theta\cos\theta}{(1 - n_1^2\cos^2\theta)^2} d\theta \tag{3.4}$$

Where, θ is the angle of the ray with the normal to the core-cladding interface. Also, n_1 is the refractive index of the core of the fiber. To calculate the effective transmitted power, the reflectance (R_p) for a single reflection is raised to the power of the number of reflections the specific propagating angle undergoes with the sensor interface. Hence, for p-polarized light, the generalized expression for the normalized transmitted power in an optical fiber based SPR sensor will be given as,

$$P_{trans} = \frac{\int_{\theta_{cr}}^{\pi/2} R_p^{N_{ref}(\theta)} \frac{n_1^2 \sin\theta\cos\theta}{(1 - n_1^2\cos^2\theta)^2} d\theta}{\int_{\theta_{cr}}^{\pi/2} \frac{n_1^2 \sin\theta\cos\theta}{(1 - n_1^2\cos^2\theta)^2} d\theta} \tag{3.5}$$

Where, $N_{ref}(\theta) = \frac{L}{D\tan\theta}$ (3.6)

And, $\theta_{cr} = \sin^{-1}\left(\frac{n_{cl}}{n_1}\right)$ (3.7)

Here, $N_{ref}(\theta)$ is the total number of reflections performed by a ray making an angle θ with the normal to the core-metal layer interface in the sensing region. *L* and *D* are the length of the exposed sensing region and the fiber core diameter respectively. Also, θ_{cr} is the critical angle of the fiber and n_{cl} is the refractive index of the cladding of the fiber.

3.2.5 Sensitivity

Resonance wavelength (λ_{res}) is determined corresponding to the refractive index of the sensing medium (n_s) in the SPR sensor based on wavelength interrogation. If the refractive index of the sensing medium is altered by δn_s, the resonance wavelength shifts by $\delta\lambda_{res}$. The sensitivity (S_n) of a SPR sensor with wavelength interrogation is defined as [64],

$$S_n = \frac{\delta\lambda_{res}}{\delta n_s} \quad (3.8)$$

3.3 Results and discussion

For numerical calculations, the refractive index of the sensing medium is changed from 1.30 to 1.38 in steps of 0.02 and following values of the parameters have been used:
Numerical aperture of the fiber = 0.24, fiber core diameter D = 600 μm, length of the exposed sensing region L = 15 mm.

To optimize the thickness of In_2O_3 layer, the transmitted output power of SPR based fiber optic sensor have been calculated for various thickness values (170 nm, 220 nm, 270 nm, 320 nm, 370 nm and 420 nm) of In_2O_3 layer. The SPR transmittance curves for different thicknesses of In_2O_3 layer have been plotted in Figs. 3.2 and 3.3.

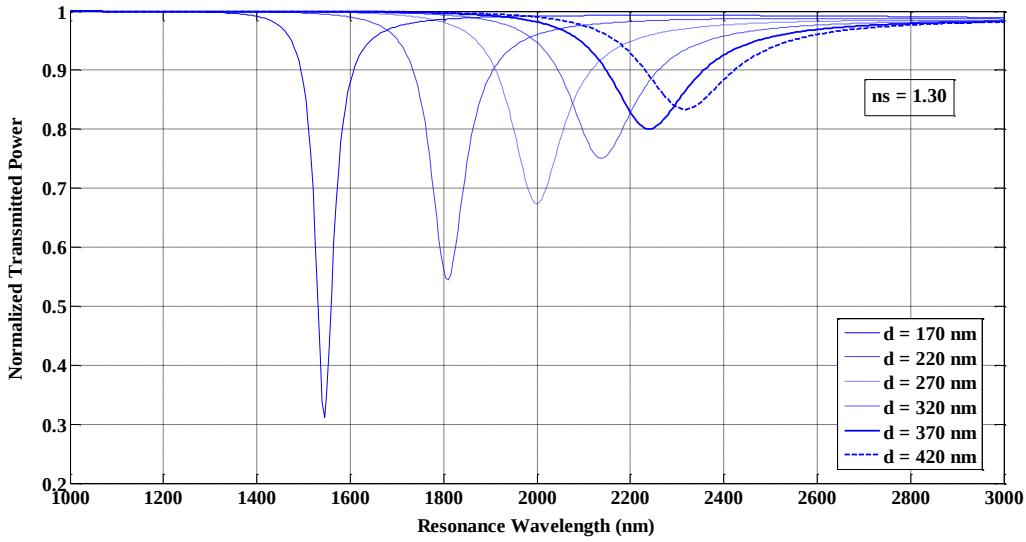

Figure 3.2: Transmittance curves of SPR based fiber optic sensor for different thickness values of In_2O_3 layer for refractive index of sensing medium = 1.30

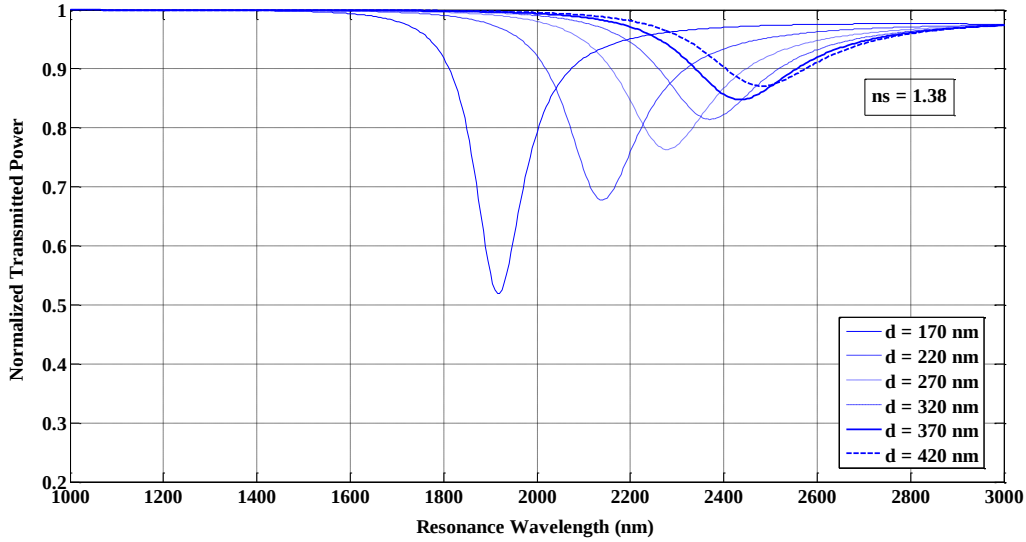

Figure 3.3: Transmittance curves of SPR based fiber optic sensor for different thickness values of In_2O_3 layer for refractive index of sensing medium = 1.38

Figs. 3.2 and 3.3 show the SPR transmittance curves for six different thickness values i.e. 170 nm, 220 nm, 270 nm, 320 nm, 370 nm and 420 nm of In_2O_3 layer as the refractive index

of the sensing medium changes from 1.30 to 1.38 (in steps of 0.02). The corresponding resonance wavelengths of SPR sensor for various thicknesses of In_2O_3 layer are determined and are listed in table 3.1.

Table 3.1: Resonance wavelengths of SPR based fiber optic sensor for different values of thickness of In_2O_3 layer

Thickness of In_2O_3 layer (nm)	Resonance wavelength (nm) for various refractive indices of sensing medium				
	1.30	1.32	1.34	1.36	1.38
170	1545	1610	1690	1790	1915
220	1810	1870	1945	2030	2140
270	2000	2055	2115	2190	2280
320	2140	2185	2240	2300	2370
370	2240	2280	2325	2375	2435
420	2315	2350	2390	2430	2485

From table 3.1, it is clear that the resonance wavelength of SPR sensor shifts from 1545 nm to 1915 nm, 1810 nm to 2140 nm, 2000 nm to 2280 nm, 2140 nm to 2370 nm, 2240 nm to 2435 nm and 2315 nm to 2485 nm for 170 nm, 220 nm, 270 nm, 320 nm, 370 nm and 420 nm thick In_2O_3 layers respectively, as the refractive index of the sensing medium varies from 1.30 to 1.38. Thus, the shift in resonance wavelength of SPR sensor is different for different thicknesses of In_2O_3 layer. The shift in resonance wavelength of the SPR sensor is maximum for 170 nm thick In_2O_3 layer and minimum for 420 nm thick In_2O_3 layer. Also, the shift in resonance wavelength of SPR sensor decreases as the thickness of In_2O_3 layer is increased gradually. The variations of resonance wavelength of SPR sensor with refractive index of sensing medium for different thicknesses of In_2O_3 layer have been plotted in Fig. 3.4.

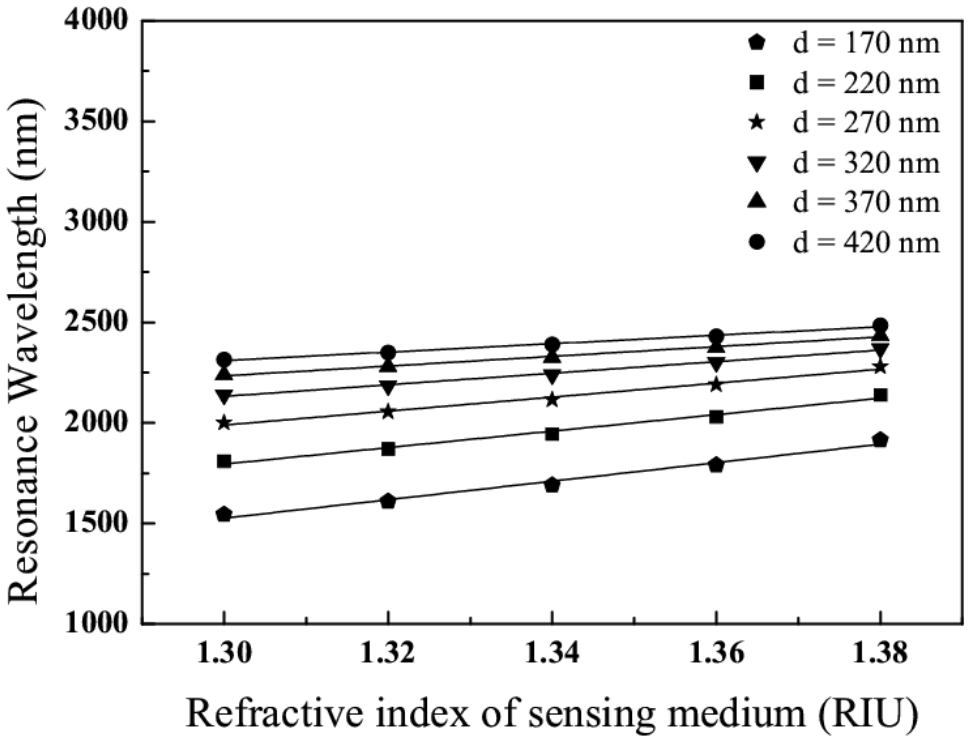

Figure 3.4: Variations of resonance wavelength of the SPR based fiber optic sensor with refractive index of sensing medium for different thickness values of In_2O_3 layer

Fig. 3.4 illustrates the plots of resonance wavelength of SPR sensor with refractive index of sensing medium for various thickness values i.e. 170 nm, 220 nm, 270 nm, 320 nm, 370 nm and 420 nm of In_2O_3 layer. The resonance wavelength of SPR sensor for different thicknesses of In_2O_3 layer increases linearly with increase in refractive index of the sensing medium. The variations of resonance wavelength with refractive index of the sensing medium for all thicknesses of In_2O_3 layer follow the same suit. The slope of resonance wavelength over the refractive index for 170 nm thick In_2O_3 layer is highest while it is least for 420 nm thick In_2O_3 layer. However, the slopes of resonance wavelength over the refractive index for other thickness values (220 nm, 270 nm, 320 nm and 370 nm) of In_2O_3 layer are larger than that of 420 nm thick In_2O_3 layer and are smaller than that of 170 nm thick In_2O_3 layer. Nevertheless, the shifts in resonance wavelength for all these cases are nearly linear over the whole range of refractive indices (i.e. 1.30 to 1.38) of the sensing medium.

To obtain the maximum sensitivity of the SPR sensor, it will be essential to identify the optimized thickness of In_2O_3 layer. The sensitivity of the SPR based fiber optic sensor for various thicknesses of In_2O_3 layer are compared in table 3.2.

Table 3.2: Sensitivity of SPR based fiber optic sensor for different values of thickness of In_2O_3 layer

Thickness of In_2O_3 layer (nm)	Sensitivity S_n (nm/RIU)
170	4600
220	4100
270	3475
320	2875
370	2425
420	2100

It can be seen from table 3.2, that the sensitivity of 170 nm thick In_2O_3 layer based SPR sensor is maximum (4600 nm/RIU) and it is minimum (2100 nm/RIU) for 420 nm thick In_2O_3 layer based SPR sensor. Though, the sensitivities of SPR sensor for other thicknesses (220 nm, 270 nm, 320 nm and 370 nm) of In_2O_3 layer are intermediate between those of 170 nm and 420 nm thick In_2O_3 layers. The variations of sensitivity of the SPR sensor with thickness of In_2O_3 layer have been plotted in Fig. 3.5.

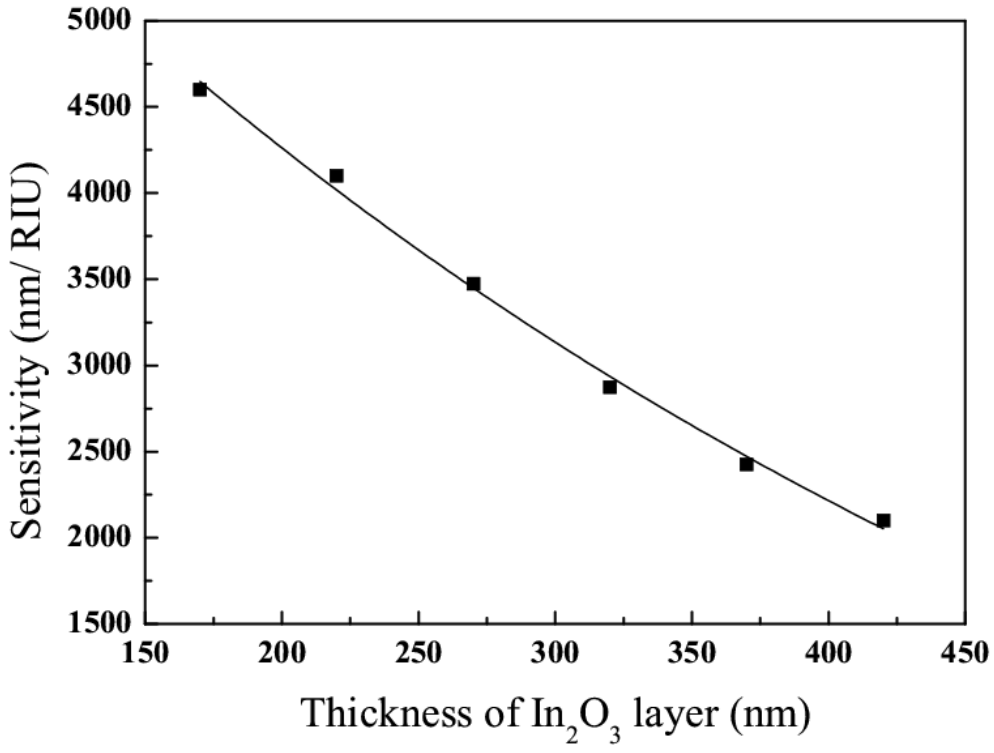

Figure 3.5: Variations of sensitivity of the SPR based fiber optic sensor with thickness of In_2O_3 layer

Fig. 3.5 depicts the variation of sensitivity of the SPR sensor with thickness of In_2O_3 layer. It is noticeable that the sensitivity of the SPR sensor decreases as the thickness of In_2O_3 layer increases. This happens because the thick In_2O_3 layer permits less interaction between surface plasmon mode and the fiber mode, resulting in small absorption of light power by the sensing medium around resonance wavelength. This causes increased normalized transmitted power and hence decreases the sensitivity of the sensor. Further, it can be observed from Fig. 3.5 and table 3.2 that 170 nm thick In_2O_3 layer based SPR sensor has the highest sensitivity (4600 nm/RIU). Therefore, in designing SPR based fiber optic sensor with high sensitivity, the proper thickness of In_2O_3 layer should be chosen. However, the optimized thickness of In_2O_3 layer of the SPR based fiber optic sensor is found to be 170 nm. So, taking all these facts in to consideration, it is concluded that 170 nm thick In_2O_3 layer based fiber optic SPR sensor demonstrates high sensitivity of 4600 nm/RIU.

3.4 Conclusions

The simulation of a SPR based fiber optic sensor with In_2O_3 layer has been presented. The sensitivity of SPR sensor for various thicknesses (170 nm to 420 nm) of In_2O_3 layer is studied theoretically. The proposed In_2O_3 layer based SPR sensor possesses high sensitivity with resonance dip in near infrared region of spectrum allowing the sensing in infrared spectral region, which needs attention to many environmental and security applications. In addition, the sensitivity of the SPR sensor decreases with increase in thickness of In_2O_3 layer. 170 nm thick In_2O_3 layer based fiber optic SPR sensor displays high sensitivity of 4600 nm/RIU.

CHAPTER 4

LOCALIZED SURFACE PLASMON RESONANCE BASED FIBER OPTIC SENSOR USING NANOPARTICLES

4.1 Introduction

In chapters 2 and 3, we have theoretically analyzed SPR based fiber optic sensors utilizing thin layers of transparent conducting oxides. The present chapter deals with the theoretical study of a localized surface plasmon resonance (LSPR) based fiber optic sensor using nanoparticles. It is eminent that the field of nanoparticles has become a wide scientific research area because of their extraordinary nano-scale size dependent properties. Basically, nanoparticles work as a bridge between bulk materials and atomic structures. As the particle size reduces and approaches to nanoscale, the atoms present on the material surface become significant. This interesting behaviour of nanoparticles is due to the large surface area of the material. Their unexpected optical properties to confine their electrons and to produce quantum effects make them unique in research field [147,148]. Metal nanoparticles are also known for their ability to support surface plasmons. The electron plasma oscillations significantly enhance the local electromagnetic field and gives rise to spectrally selective light absorption and scattering. Their optical properties mainly depend on shape, size, metal composition and refractive index of the surrounding medium. Consequently, the surface plasmon properties are directly controlled by the particles geometry. In addition, the metal nanoparticles (much smaller than the wavelength of light) are supposed to have better sensing performance than materials in the micro or larger scales and reveal tremendous optical properties because of the collective excitation of conduction electrons [129]. A metal-dielectric interface on the nanoparticles produce significant changes in the optical properties, which make them size and shape dependent. LSPR normally refers to metallic nanoparticles and takes place when the wave vector and the frequency of the incident light are resonant with that of collective oscillation of conduction electrons in metallic nanoparticles [149]. The LSPR wavelength is reliant on nanoparticle material, size, shape and surrounding medium

refractive index [131,132]. LSPR is found to be more advantageous in sensing applications because the sensitivity of LSPR sensor is controlled/optimized by the change of the sizes and shapes of the nanoparticles [150-158].

In this chapter, a LSPR based fiber optic sensor with nanoparticles layer has been theoretically analyzed. Nanoparticles of four materials: indiums tin oxide (ITO), gold (Au), silver (Ag) and copper (Cu) have been considered. The nanoparticles are assumed to be spherical in shape with various radii. LSPR produced by coupling of evanescent light to surface plasmons is used as the sensing mechanism. The wavelength interrogation method is utilized for the analysis of LSPR sensor. The complete analysis of sensitivity of LSPR sensor with each nanoparticles layer (individually) for various values of thickness and particle size has been done numerically. The present study illustrates that the sensitivity of LSPR sensor increases with increase in thickness of nanoparticles layer for all four materials. In addition, for a fixed thickness of nanoparticles layer, the sensitivity of LSPR sensor further increases as the particle size of nanoparticles increases. The thickness and particle size of nanoparticles layer of LSPR sensor for all four materials are also optimized. The optimized values of thickness and particle size of nanoparticles layers for all four materials are obtained to be 60 nm and 20 nm respectively. 60 nm thick ITO nanoparticles layer (with 20 nm particle size) based LSPR sensor has the highest sensitivity of 6240 nm/RIU and has better sensing performance than that of other three material's nanoparticles.

4.2 Theory

The LSPR sensing is based on the principle of attenuated total reflection (ATR) with Kretschmann configuration. In the proposed LSPR based fiber optic sensor, the sensing system consisting of a fiber core-nanoparticles layer-sensing medium is considered as shown in Fig. 4.1.

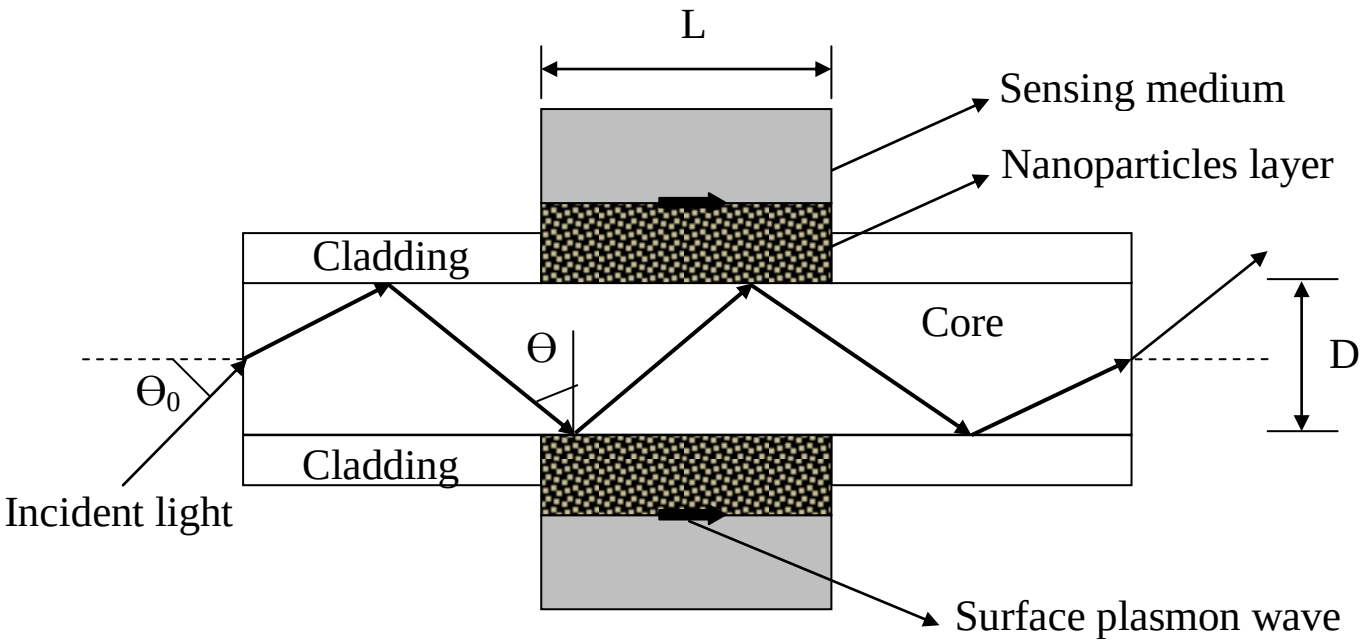

Figure 4.1: Schematic diagram of LSPR based fiber optic sensor with nanoparticles layer

The plastic cladding around the core from the middle portion of a step index multimode PCS fiber is removed and is then coated with a thin layer of nanoparticles of four different materials: ITO, Au, Ag and Cu individually (i.e one layer of nanoparticles of one material at a time), which is then finally surrounded by the sensing medium. The light from a broadband (polychromatic) source is launched into one of the ends of the optical fiber with proper optics and the transmitted light is detected at the other end of the optical fiber.

4.2.1 Layer I (Fiber core)

This layer is made of core of optical fiber. The core of the optical fiber is assumed to be made of fused silica. The refractive index of fused silica varies with wavelength according to Sellmeier dispersion relation as,

$$n_1(\lambda) = \sqrt{1 + \frac{a_1\lambda^2}{\lambda^2 - b_1^2} + \frac{a_2\lambda^2}{\lambda^2 - b_2^2} + \frac{a_3\lambda^2}{\lambda^2 - b_3^2}} \tag{4.1}$$

Where, λ is the wavelength in μm and a_1, a_2, a_3, b_1, b_2 and b_3 are Sellmeier coefficients. The values of these coefficients are given as, a_1 = 0.6961663, a_2 = 0.4079426, a_3 = 0.8974794, b_1 = 0.0684043 μm, b_2 = 0.1162414 μm and b_3 = 9.896161 μm [141].

4.2.2 Layer II (Nanoparticles layer)

This layer is made of nanoparticles of four different materials: ITO, Au, Ag and Cu individually (i.e one layer of nanoparticles of one material at a time). The nanoparticles are considered to be spherical in shape having radius (R) 5 nm, 10 nm, 15 nm, 20 nm, 25 nm and 30 nm. In a metal, when the metal nanoparticle size becomes smaller than the mean free path of the conduction electrons, the surface scattering plays vital role in the dynamics of free electrons, which is very much responsible for LSPR. The mean free path of Drude electrons is reduced by the finite size of the spherical nanoparticles and the size-dependent damping constant of Drude electrons of the metals is given as [159],

$$\Gamma = \Gamma_{Bulk} + \frac{A v_f}{R} \tag{4.2}$$

Where, Γ_{Bulk} is the damping constant of the bulk material, A is a constant having value nearly unity, v_f is the Fermi velocity and R is the radius of the spherical nanoparticle.

Bulk collision wavelength (λ_{cBulk}) corresponds to the damping of electron density oscillations due to collisions among the electrons in the bulk metal. In terms of bulk collision wavelength, the above Eq. (4.2) takes the final form as follows to give the size-dependence of the collision wavelength (λ_c),

$$\frac{c}{\lambda_c} = \frac{c}{\lambda_{cBulk}} + \frac{A v_f}{R} \tag{4.3}$$

Here, c is the speed of light in vacuum.

According to Drude model, the complex dielectric constant (ε_m) of any metal can be written in terms of its plasma wavelength (λ_p) and collision wavelength (λ_c) as,

$$\varepsilon_m(\lambda) = \varepsilon_{mr} + i\varepsilon_{mi} = \varepsilon_\infty - \frac{\lambda^2 \lambda_c}{\lambda_p^2(\lambda_c + i\lambda)} \tag{4.4}$$

Where, ε_∞ is the infrared dielectric constant. ε_∞ = 3.8 for ITO and 1 for Au, Ag and Cu. The values of λ_p, λ_{cBulk} and v_f for ITO, Au, Ag and Cu are given in table 4.1 [142,71].

Table 4.1: Plasma wavelength, Bulk collision wavelength and Fermi velocity for ITO, Au, Ag and Cu

Parameter	ITO	Au	Ag	Cu
Plasma wavelength (λ_p)	5.649 x 10^{-7} m	1.6826 x 10^{-7} m	1.4541 x 10^{-7} m	1.3617 x 10^{-7} m
Bulk collision wavelength (λ_{cBulk})	11.121 x 10^{-6} m	8.9342 x 10^{-6} m	1.7614 x 10^{-5} m	4.0852 x 10^{-5} m
Fermi velocity (v_f)	0.563 x 10^6 m/s	1.40 x 10^6 m/s	1.40 x 10^6 m/s	1.57 x 10^6 m/s

4.2.3 Layer III (Sensing medium)

This layer is made of sensing medium. The dielectric constant of the sensing medium is ε_s. If n_s is the refractive index of the sensing medium, then $\varepsilon_s = n_s^2$. The resonance condition for excitation of surface plasmon wave is given as,

$$\frac{2\pi}{\lambda} n_1 \sin\theta = \mathrm{Re}\{K_{sp}\} \tag{4.5}$$

Where, $K_{sp} = \frac{\omega}{c}\sqrt{\frac{\varepsilon_m \varepsilon_s}{\varepsilon_m + \varepsilon_s}} = \frac{2\pi}{\lambda}\sqrt{\frac{\varepsilon_m n_s^2}{\varepsilon_m + n_s^2}}$ is the propagation constant of the surface plasmon wave and *c* is the speed of light in vacuum. The left hand side of Eq. (4.5) denotes the propagation constant of the light incident at an angle θ and the right hand side shows the real part of the propagation constant of the surface plasmon wave.

4.2.4 Transmitted Power

The expression for the reflection coefficient (reflectance) of p-polarized incident light is obtained by using the matrix method for N-layer model as mentioned in appendix A. Considering that all the guided rays are launched in the fiber using a collimated source and a microscope objective, the angular power distribution of rays guided in the fiber is given as [18],

$$dP \propto \frac{n_1^2 \sin\theta\cos\theta}{(1-n_1^2\cos^2\theta)^2}\,d\theta \tag{4.6}$$

Where, θ is the angle of the ray with the normal to the core-cladding interface. Also, n_1 is the refractive index of the core of the fiber. To calculate the effective transmitted power, the reflectance (R_p) for a single reflection is raised to the power of the number of reflections the specific propagating angle undergoes with the sensor interface. Hence, for p-polarized light, the generalized expression for the normalized transmitted power in an optical fiber based SPR sensor will be given as,

$$P_{trans} = \frac{\int_{\theta_{cr}}^{\pi/2} R_p^{N_{ref}(\theta)} \dfrac{n_1^2 \sin\theta\cos\theta}{(1-n_1^2\cos^2\theta)^2}\,d\theta}{\int_{\theta_{cr}}^{\pi/2} \dfrac{n_1^2 \sin\theta\cos\theta}{(1-n_1^2\cos^2\theta)^2}\,d\theta} \tag{4.7}$$

Where, $N_{ref}(\theta) = \dfrac{L}{D\tan\theta}$ (4.8)

And, $\theta_{cr} = \sin^{-1}\left(\dfrac{n_{cl}}{n_1}\right)$ (4.9)

Here, $N_{ref}(\theta)$ is the total number of reflections performed by a ray making an angle θ with the normal to the core-metal layer interface in the sensing region. L and D are the length of

the exposed sensing region and the fiber core diameter respectively. Also, θ_{cr} is the critical angle of the fiber and n_{cl} is the refractive index of the cladding of the fiber.

4.2.5 Sensitivity

Resonance wavelength (λ_{res}) is determined corresponding to the refractive index of the sensing medium (n_s) in the LSPR sensor based on wavelength interrogation. If the refractive index of the sensing medium is altered by δn_s, the resonance wavelength shifts by $\delta\lambda_{res}$. The sensitivity (S_n) of the sensor with wavelength interrogation is defined as [64],

$$S_n = \frac{\delta\lambda_{res}}{\delta n_s} \tag{4.10}$$

4.3 Results and discussion

For theoretical calculations, the refractive index of the sensing medium is changed from 1.30 to 1.38 in steps of 0.02 and following values of the parameters have been used:
Numerical aperture of the fiber = 0.24, fiber core diameter D = 600 μm, length of the exposed sensing region L = 15 mm.

To optimize the thickness of nanoparticles layer, the transmitted output power of LSPR based fiber optic sensor have been calculated for 40 nm, 50 nm and 60 nm thick nanoparticles layer of all four materials: ITO, Au, Ag and Cu individually. It is to be mentioned here that the calculations of transmitted output power of LSPR sensor have also been made for higher thicknesses i.e. 70 nm and 80 nm thick nanoparticles layer of all four materials individually. However, the higher thickness values i.e. 70 nm and 80 nm thick nanoparticles layer (of four materials individually) have not been considered in the present discussion because the proper SPR transmittance curves (i.e. clear resonance dips) have not been found for 70 nm and 80 nm thick nanoparticles layer. Hence, the higher thickness values i.e. 70 nm and 80 nm thick nanoparticles layer (of all four materials individually) only deteriorate the sensing behaviour of LSPR based fiber optic sensor. The particle sizes for each nanoparticles layer have been considered to be 5 nm, 10 nm, 15 nm, 20 nm, 25 nm and 30 nm. The variations of LSPR resonance wavelength with refractive index of sensing medium for 40 nm, 50 nm and 60 nm

thick nanoparticles layers (of ITO, Au, Ag and Cu materials) with 5 nm, 10 nm, 15 nm, 20 nm, 25 nm and 30 nm particle sizes have been plotted in Figs. 4.2-4.19.

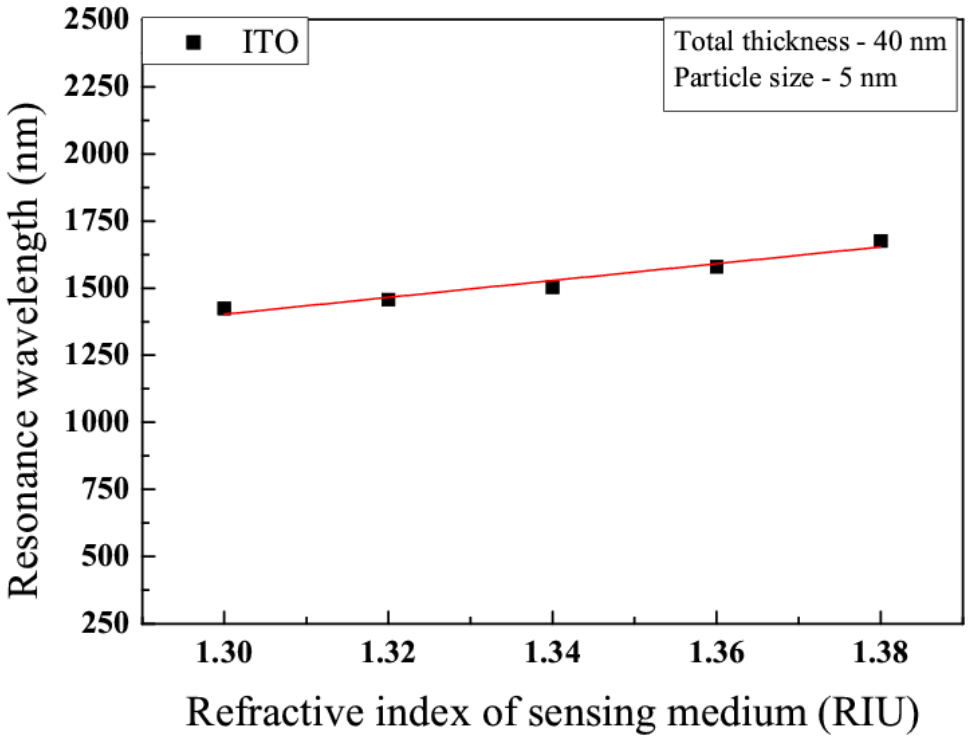

Figure 4.2: Variation of resonance wavelength with refractive index of sensing medium for 40 nm thick ITO nanoparticles layer with 5 nm particle size

Fig. 4.2 shows the plot of LSPR resonance wavelength for 40 nm thick ITO nanoparticles layer of 5 nm particle size with refractive index of sensing medium. The resonance wavelength increases linearly with increase in refractive index of the sensing medium.

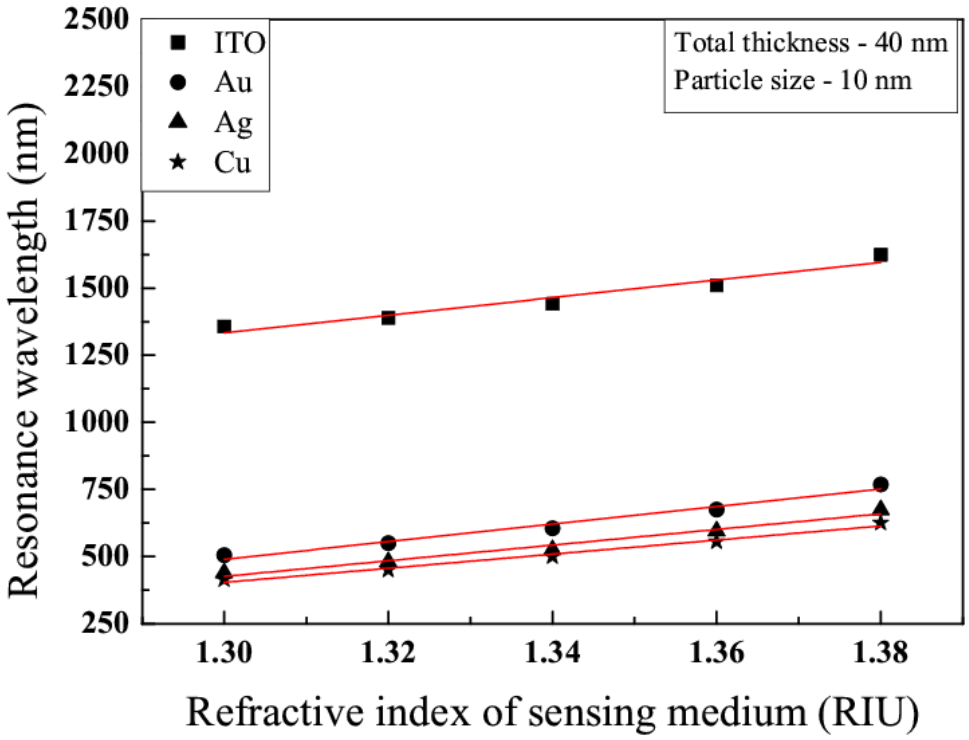

Figure 4.3: Variations of resonance wavelength with refractive index of sensing medium for 40 nm thick ITO, Au, Ag and Cu nanoparticles layer with 10 nm particle size

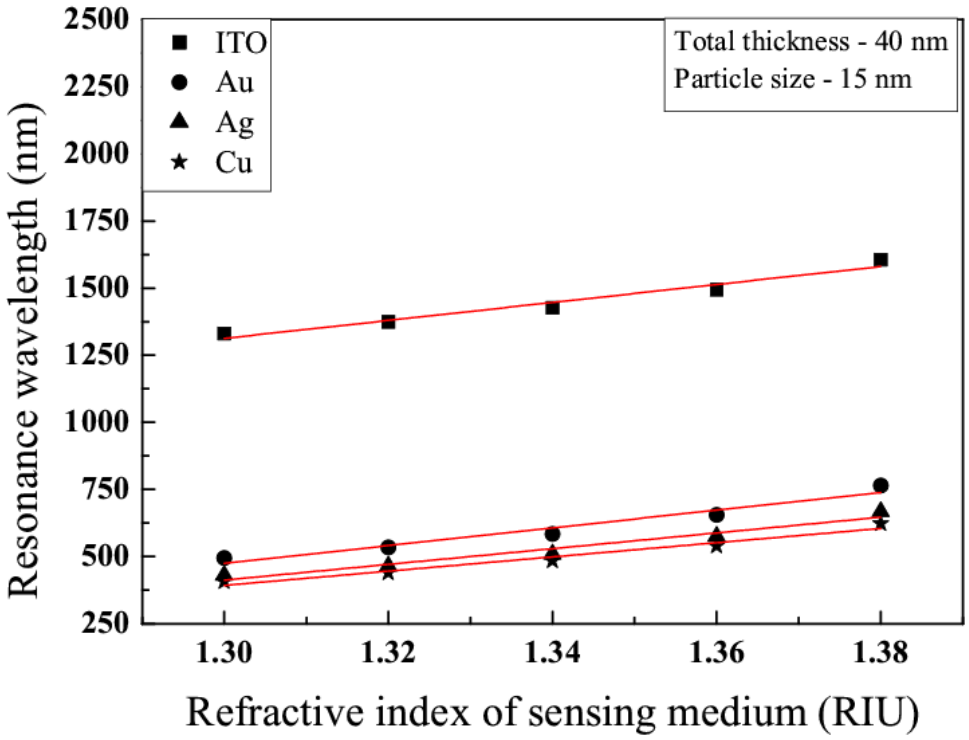

Figure 4.4: Variations of resonance wavelength with refractive index of sensing medium for 40 nm thick ITO, Au, Ag and Cu nanoparticles layer with 15 nm particle size

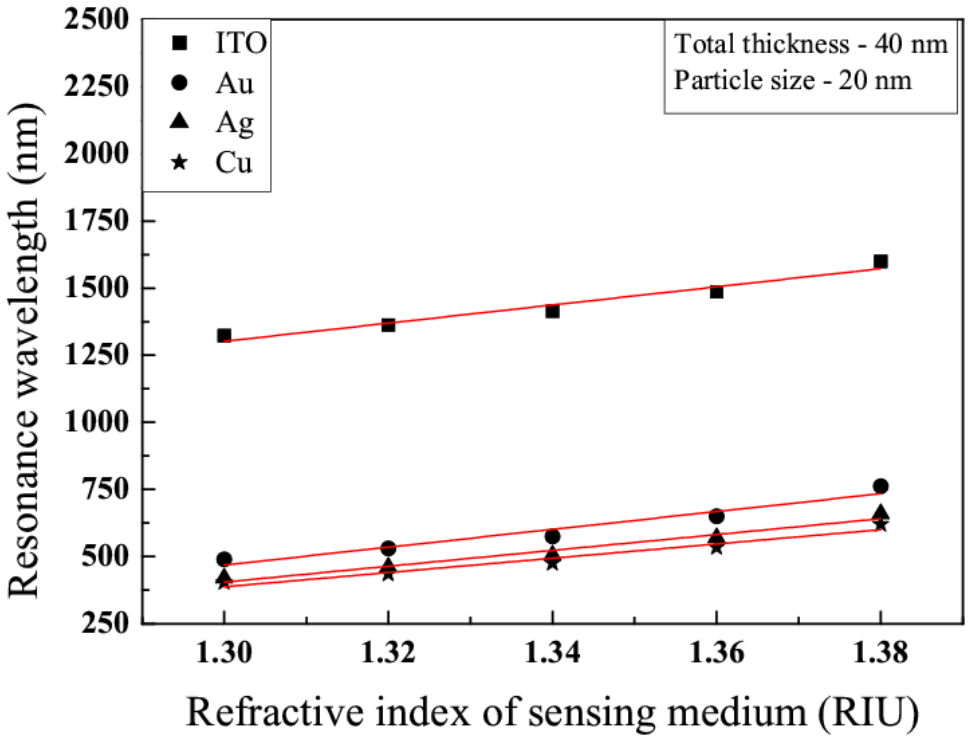

Figure 4.5: Variations of resonance wavelength with refractive index of sensing medium for 40 nm thick ITO, Au, Ag and Cu nanoparticles layer with 20 nm particle size

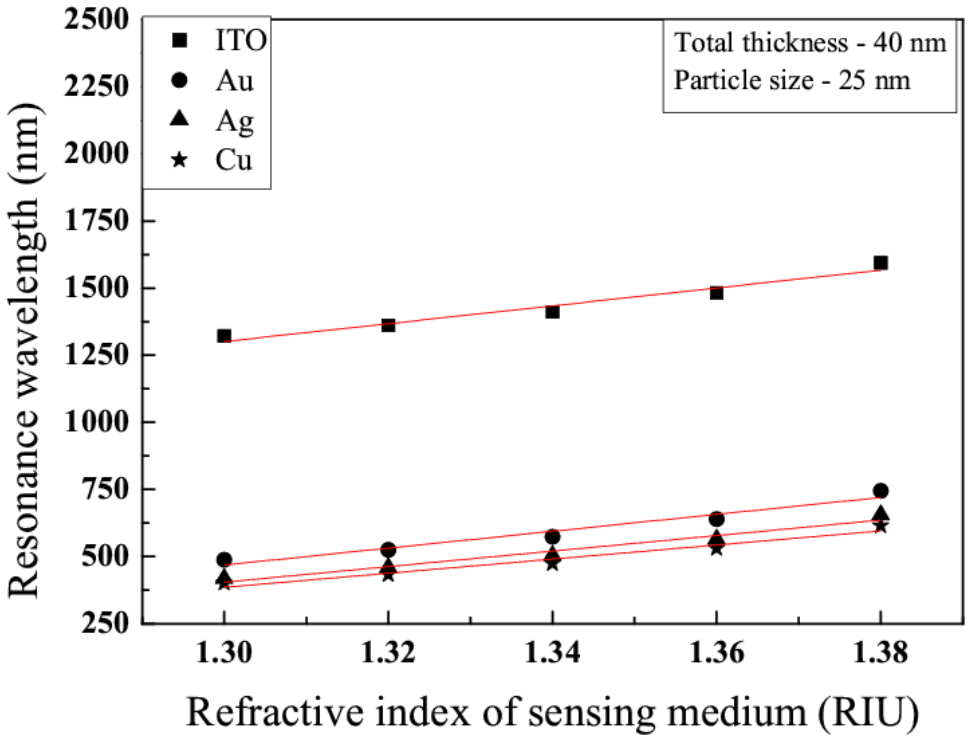

Figure 4.6: Variations of resonance wavelength with refractive index of sensing medium for 40 nm thick ITO, Au, Ag and Cu nanoparticles layer with 25 nm particle size

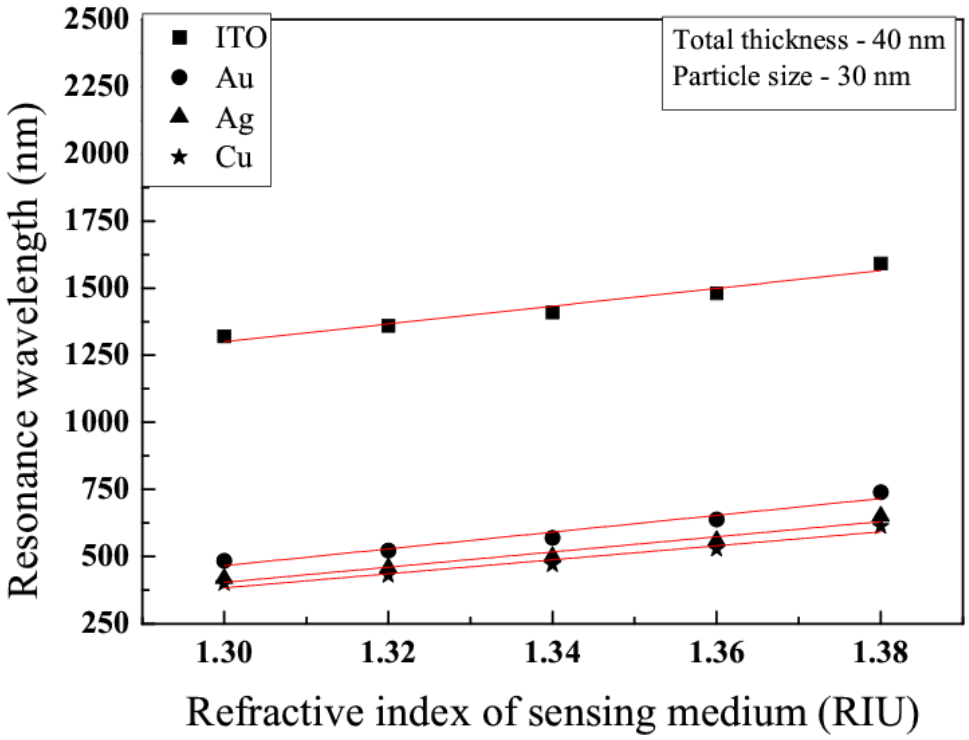

Figure 4.7: Variations of resonance wavelength with refractive index of sensing medium for 40 nm thick ITO, Au, Ag and Cu nanoparticles layer with 30 nm particle size

Similarly, Figs. 4.3-4.7 illustrate the variations of LSPR resonance wavelength for 40 nm thick ITO, Au, Ag and Cu nanoparticles layers with refractive index of sensing medium for 10 nm, 15 nm, 20 nm, 25 nm and 30 nm particle sizes respectively. In addition, the variations for 40 nm thick ITO, Au, Ag and Cu nanoparticles layers shown in Figs. 4.3; 4.4; 4.5; 4.6 and 4.7 have correlation coefficients (1, 0.99618, 0.99527, 0.99334); (1, 0.99983, 0.99959, 0.99949); (1, 0.99981, 0.99915, 0.99980); (1, 0.99996, 0.99914, 0.99983) and (1, 0.97768, 0.97954, 0.98365) respectively. The variations of resonance wavelength with refractive index of the sensing medium for all these cases follow the same pattern. For fixed 40 nm thick nanoparticles layer and fixed 10 nm particle size, the slope of resonance wavelength over the refractive index is highest for ITO nanoparticles, while it is least for Cu nanoparticles. However, the slope of resonance wavelength over the refractive index for Au and Ag nanoparticles is larger than Cu nanoparticles but still smaller than ITO nanoparticles. Similarly, for fixed 40 nm thick nanoparticles layer and fixed 15 nm particle size, the slope of

resonance wavelength over the refractive index is maximum for ITO nanoparticles and minimum for Cu nanoparticles. In the same way, the slopes of resonance wavelength over the refractive index are again greatest for ITO nanoparticles and smallest for Cu nanoparticles for fixed 40 nm thick nanoparticles layer and fixed 20 nm, 25 nm and 30 nm particle sizes each. Nevertheless, the shifts in resonance wavelength for all these cases are almost linear over the whole range of refractive indices i.e. 1.30 to 1.38 of the sensing medium. Hence, for fixed 40 nm thick nanoparticles layer, the slope of resonance wavelength over the refractive index is maximum for ITO nanoparticles than those of Au, Ag and Cu nanoparticles for 10 nm, 15 nm, 20 nm, 25 nm and 30 nm particle sizes.

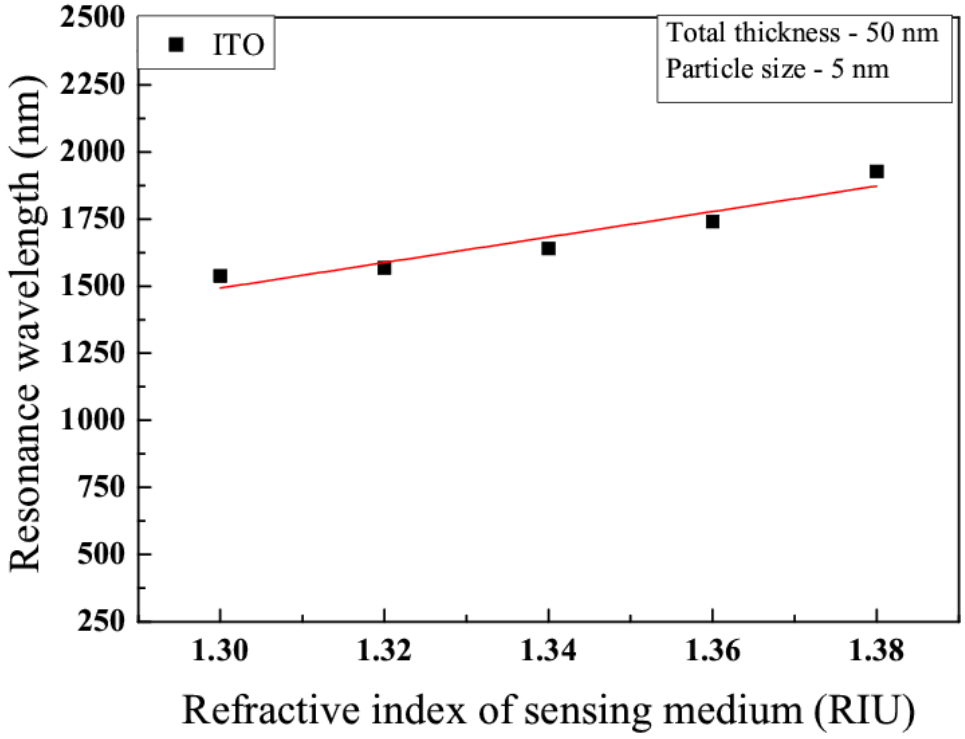

Figure 4.8: Variation of resonance wavelength with refractive index of sensing medium for 50 nm thick ITO nanoparticles layer with 5 nm particle size

Similarly, Fig. 4.8 reveals the plot of LSPR resonance wavelength for 50 nm thick ITO nanoparticles layer of 5 nm particle size with refractive index of sensing medium. The resonance wavelength increases linearly with increase in refractive index of the sensing medium.

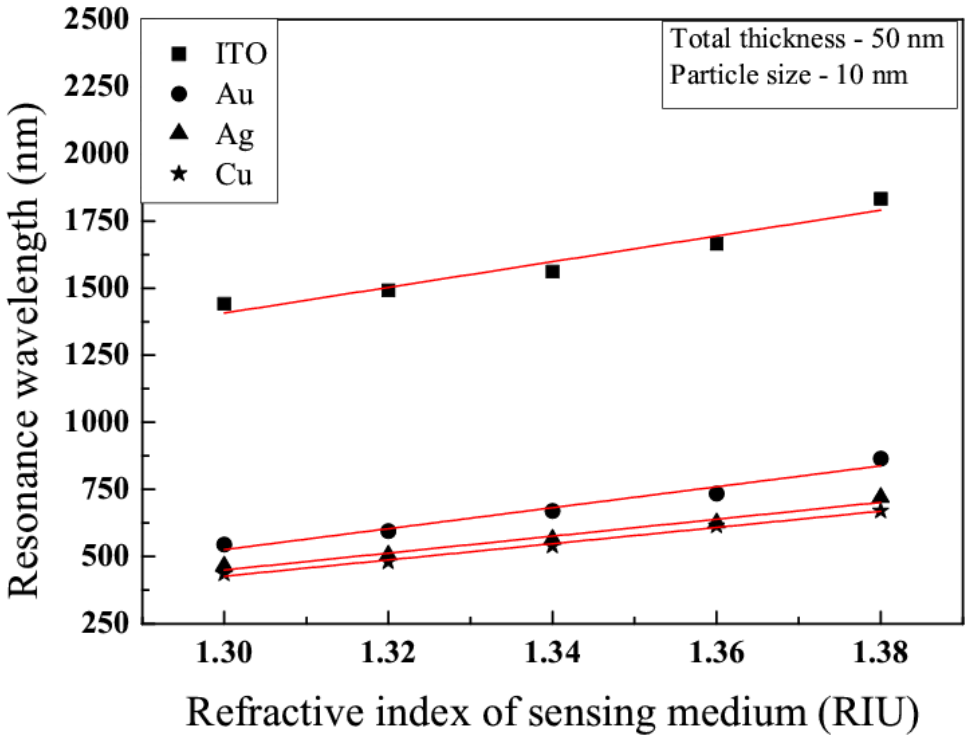

Figure 4.9: Variations of resonance wavelength with refractive index of sensing medium for 50 nm thick ITO, Au, Ag and Cu nanoparticles layer with 10 nm particle size

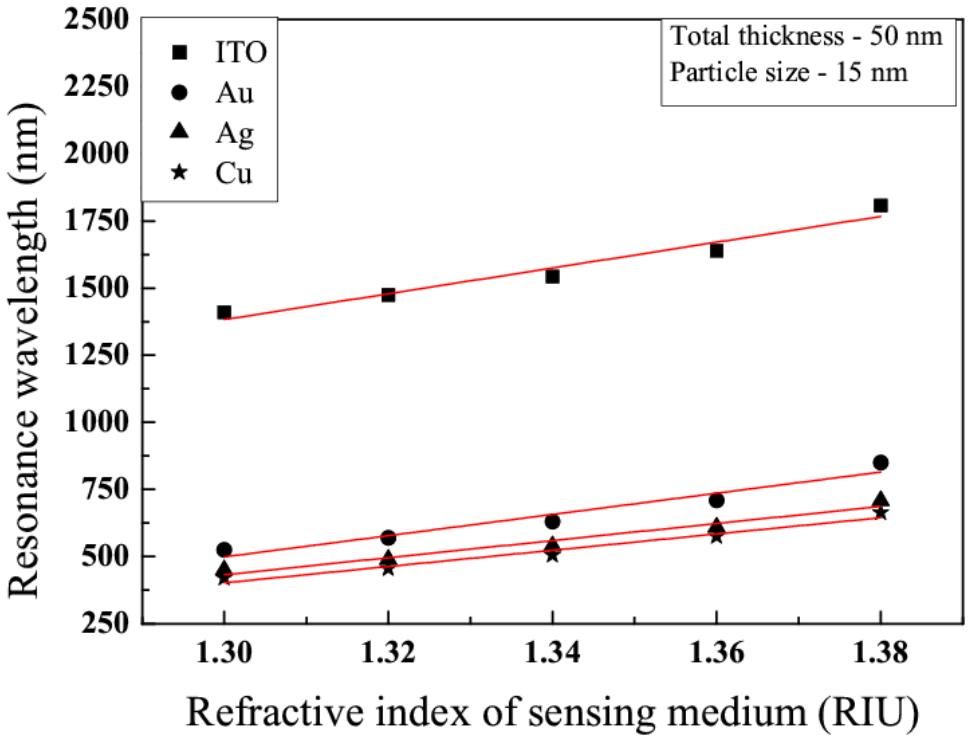

Figure 4.10: Variations of resonance wavelength with refractive index of sensing medium for 50 nm thick ITO, Au, Ag and Cu nanoparticles layer with 15 nm particle size

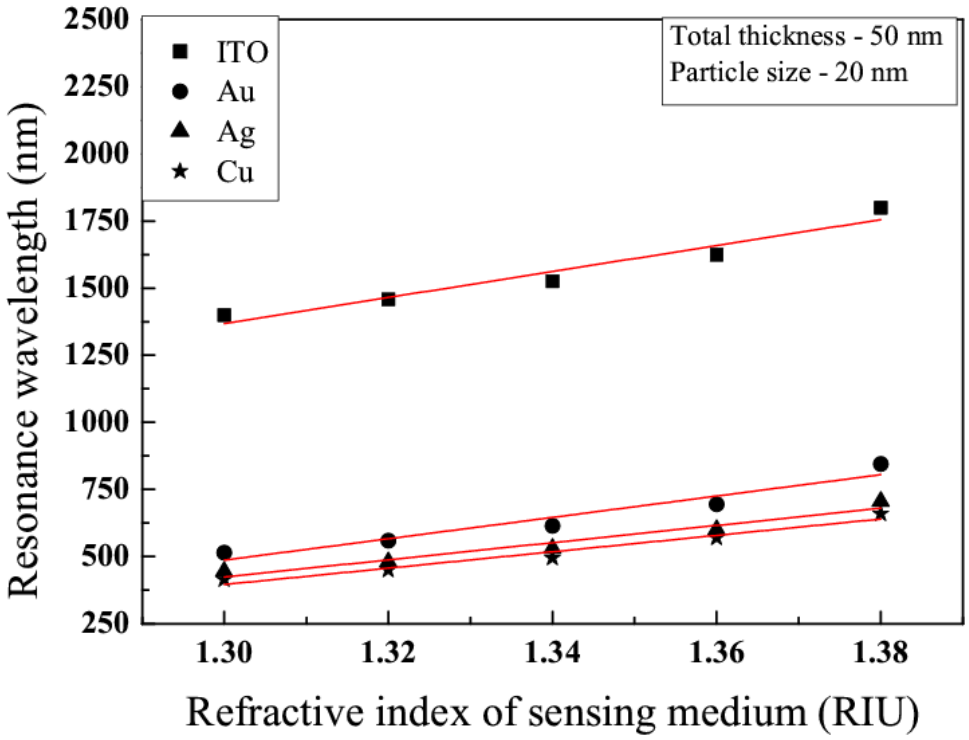

Figure 4.11: Variations of resonance wavelength with refractive index of sensing medium for 50 nm thick ITO, Au, Ag and Cu nanoparticles layer with 20 nm particle size

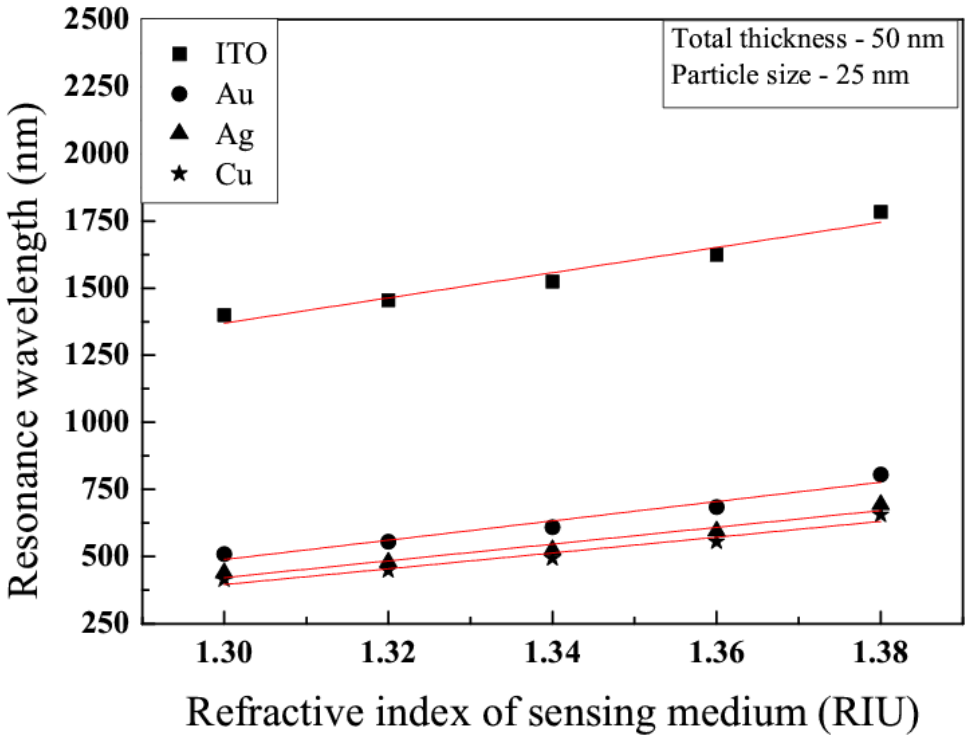

Figure 4.12: Variations of resonance wavelength with refractive index of sensing medium for 50 nm thick ITO, Au, Ag and Cu nanoparticles layer with 25 nm particle size

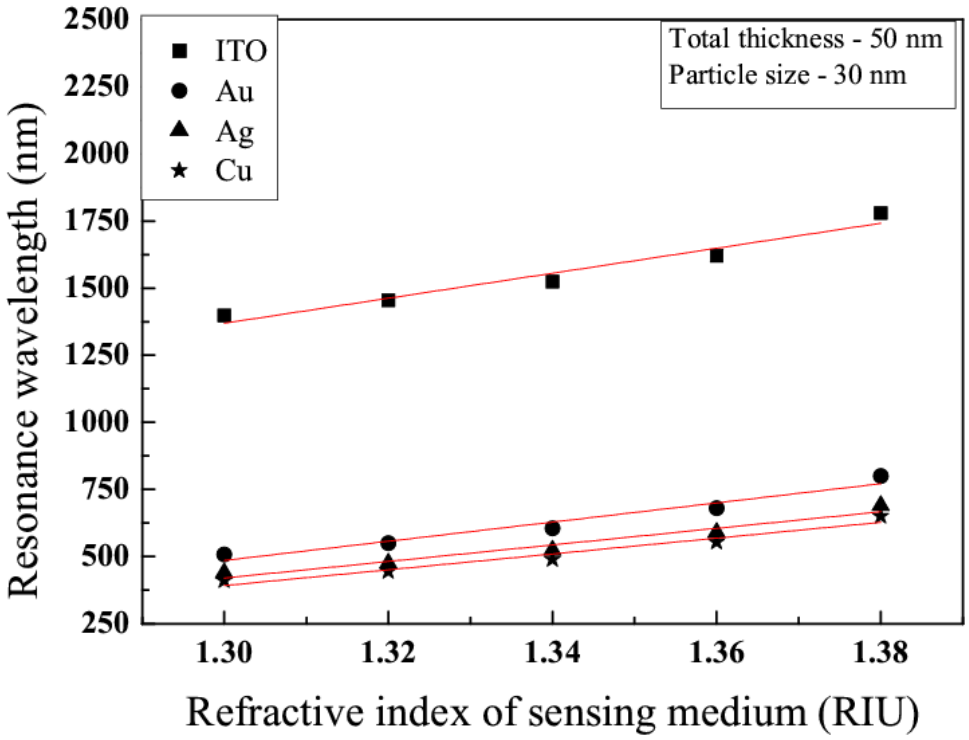

Figure 4.13: Variations of resonance wavelength with refractive index of sensing medium for 50 nm thick ITO, Au, Ag and Cu nanoparticles layer with 30 nm particle size

Likewise, Figs. 4.9-4.13 demonstrate the variations of LSPR resonance wavelength for 50 nm thick ITO, Au, Ag and Cu nanoparticles layers with refractive index of sensing medium for 10 nm, 15 nm, 20 nm, 25 nm and 30 nm particle sizes respectively. Furthermore, the variations for 50 nm thick ITO, Au, Ag and Cu nanoparticles layers exposed in Figs. 4.9; 4.10; 4.11; 4.12 and 4.13 have correlation coefficients (1, 0.99625, 0.99558, 0.97730); (1, 0.99970, 0.99867, 0.99724); (1, 0.99987, 0.99876, 0.99589); (1, 0.99991, 0.99964, 0.99998) and (1, 0.99997, 0.99977, 0.99984) respectively. Again, the variations of resonance wavelength elevate linearly in the same fashion with refractive index of the sensing medium for all these cases. Once more, for fixed 50 nm thick nanoparticles layer, the slope of resonance wavelength over the refractive index is greater for ITO nanoparticles than those of Au, Ag and Cu nanoparticles for 10 nm, 15 nm, 20 nm, 25 nm and 30 nm particle sizes.

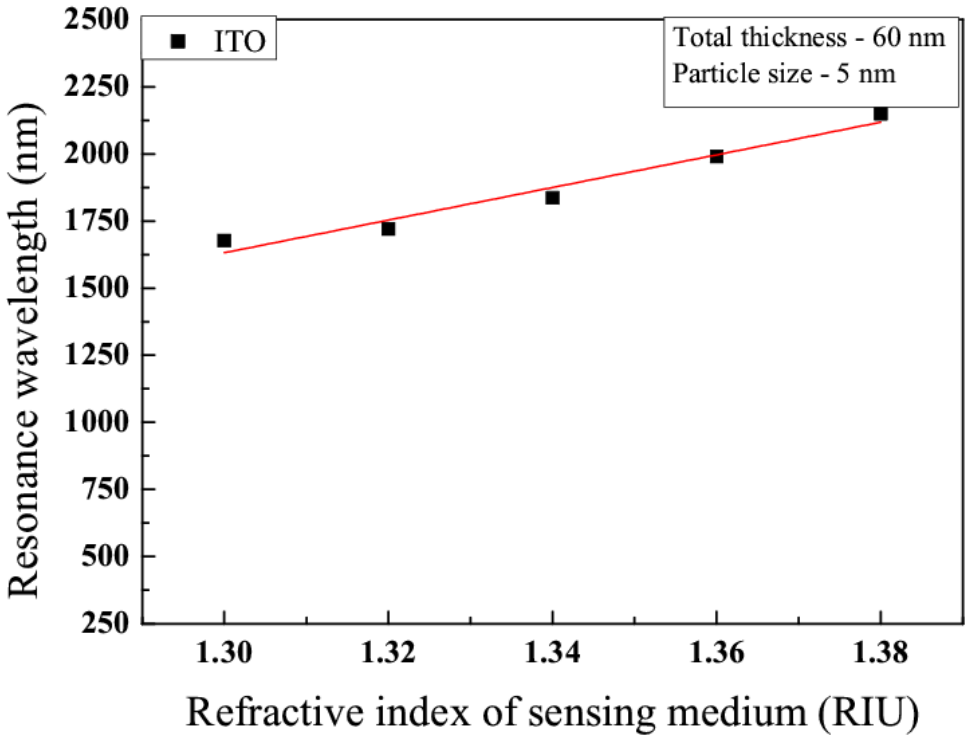

Figure 4.14: Variation of resonance wavelength with refractive index of sensing medium for 60 nm thick ITO nanoparticles layer with 5 nm particle size

In the same way, Fig. 4.14 depicts the plot of LSPR resonance wavelength for 60 nm thick ITO nanoparticles layer of 5 nm particle size with refractive index of sensing medium. The resonance wavelength boosts linearly with increase in refractive index of the sensing medium.

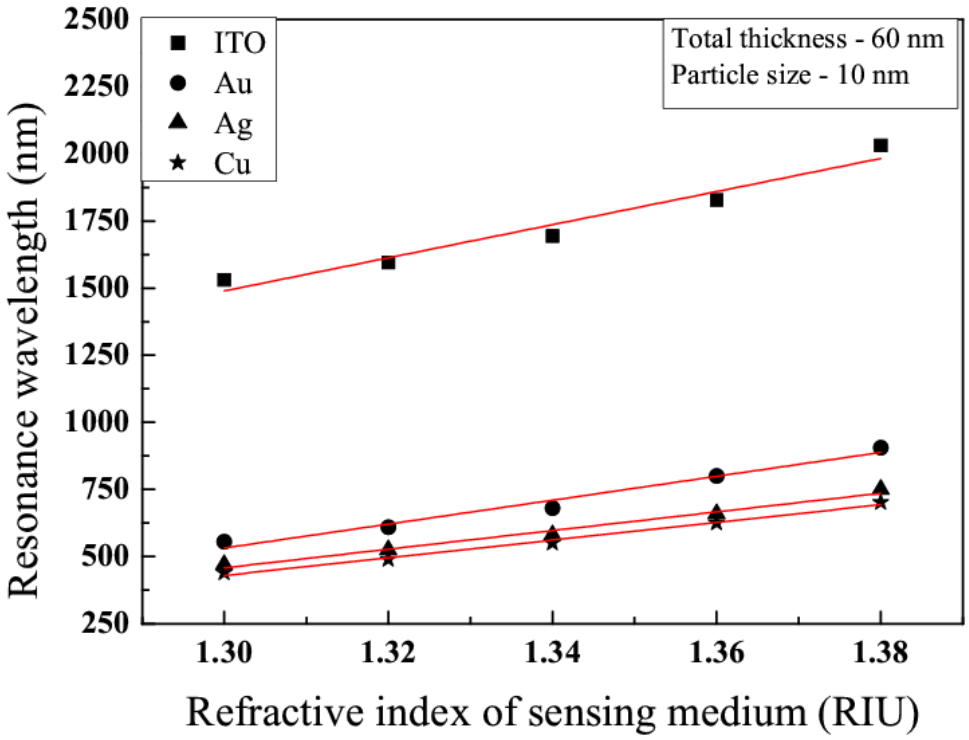

Figure 4.15: Variations of resonance wavelength with refractive index of sensing medium for 60 nm thick ITO, Au, Ag and Cu nanoparticles layer with 10 nm particle size

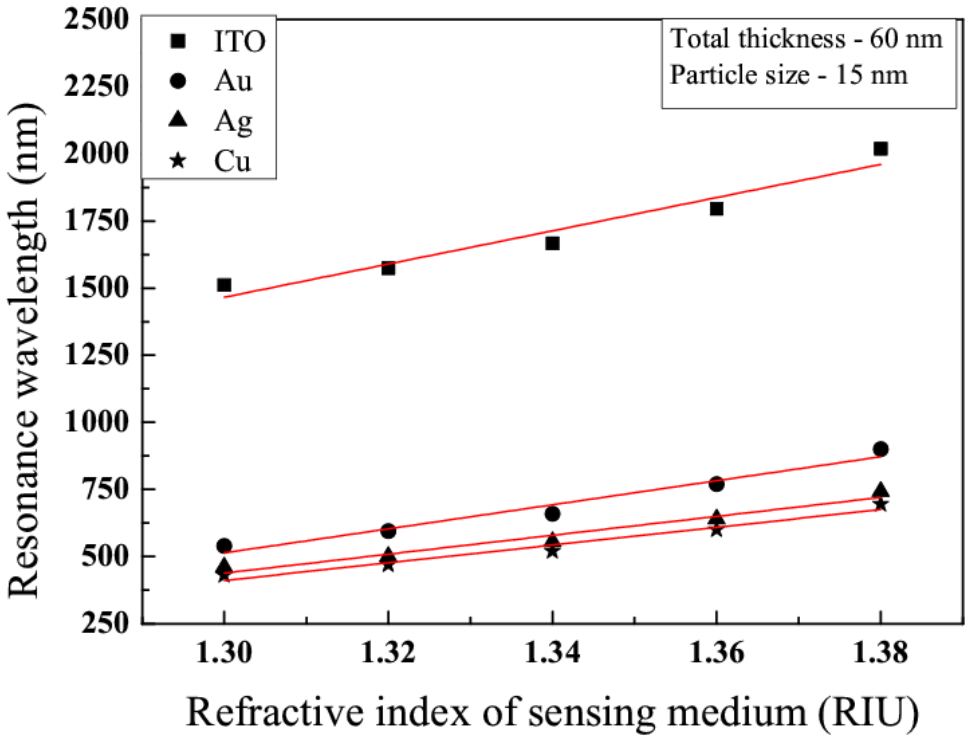

Figure 4.16: Variations of resonance wavelength with refractive index of sensing medium for 60 nm thick ITO, Au, Ag and Cu nanoparticles layer with 15 nm particle size

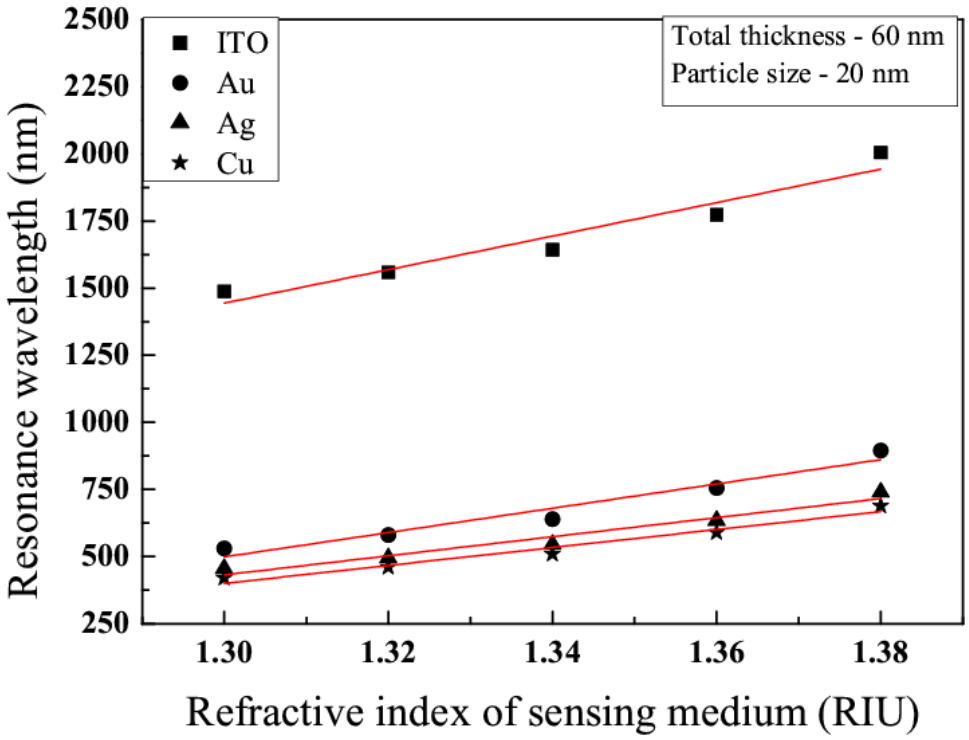

Figure 4.17: Variations of resonance wavelength with refractive index of sensing medium for 60 nm thick ITO, Au, Ag and Cu nanoparticles layer with 20 nm particle size

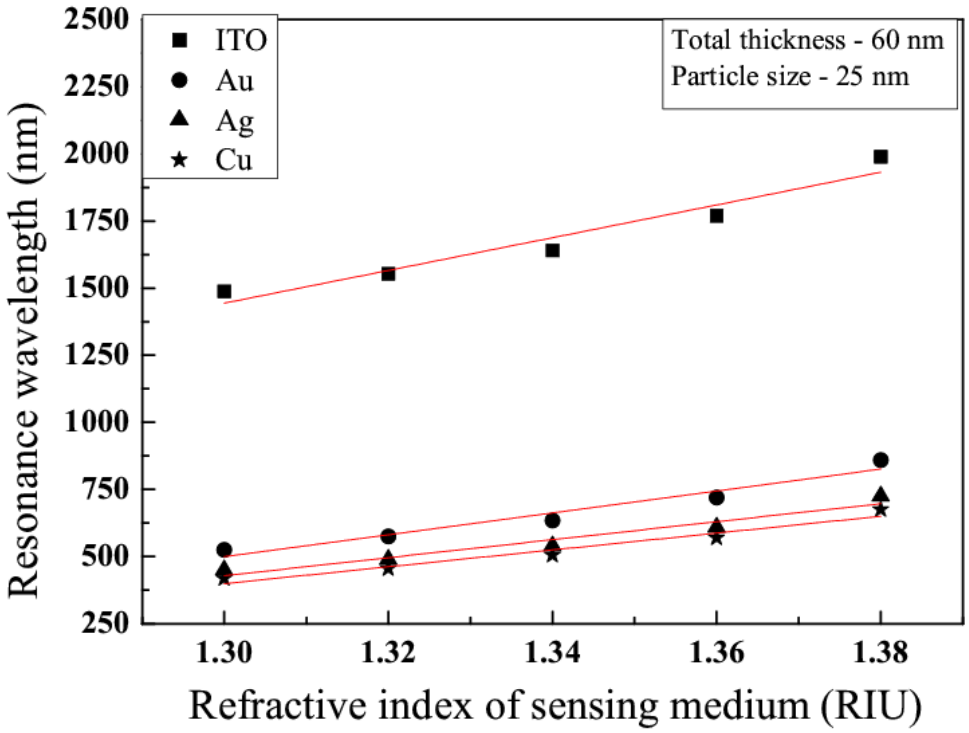

Figure 4.18: Variations of resonance wavelength with refractive index of sensing medium for 60 nm thick ITO, Au, Ag and Cu nanoparticles layer with 25 nm particle size

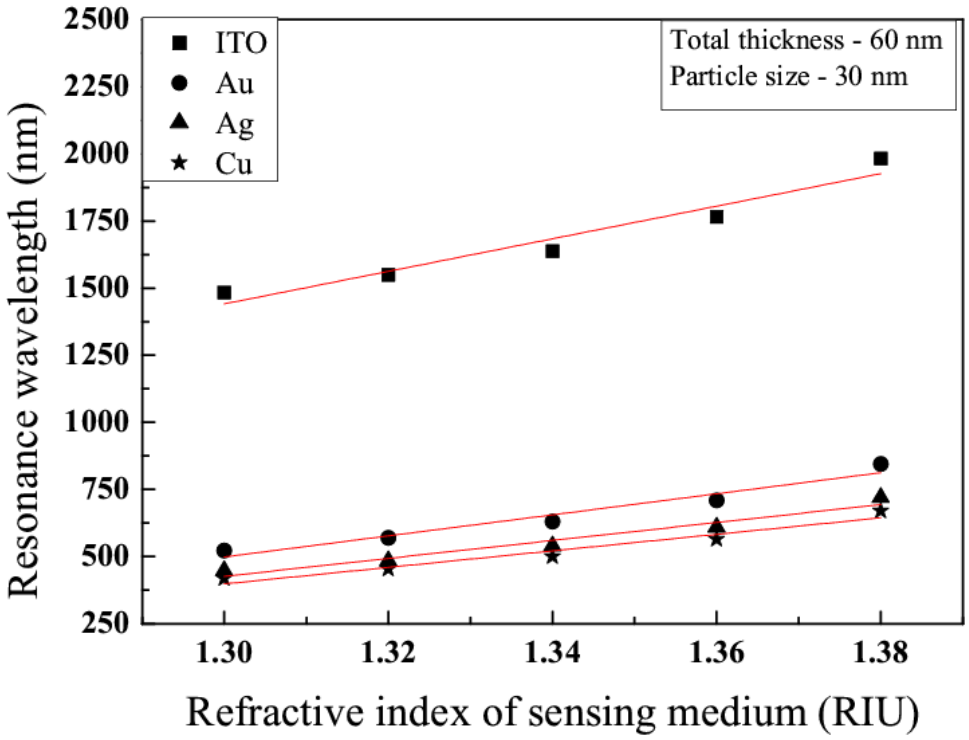

Figure 4.19: Variations of resonance wavelength with refractive index of sensing medium for 60 nm thick ITO, Au, Ag and Cu nanoparticles layer with 30 nm particle size

In the same way, Figs. 4.15-4.19 display the variations of LSPR resonance wavelength for 60 nm thick ITO, Au, Ag and Cu nanoparticles layers with refractive index of sensing medium for 10 nm, 15 nm, 20 nm, 25 nm and 30 nm particle sizes respectively. Moreover, the variations for 60 nm thick ITO, Au, Ag and Cu nanoparticles layers revealed in Figs. 4.15; 4.16; 4.17; 4.18 and 4.19 have correlation coefficients (1, 0.99460, 0.99498, 0.99167); (1, 0.99685, 0.99684, 0.99659); (1, 0.99750, 0.99644, 0.99641); (1, 0.99960, 0.99963, 0.99925) and (1, 0.99968, 0.99945, 0.99977) respectively. The variations of resonance wavelength increase linearly in the same manner with refractive index of the sensing medium for all these cases. Further, for fixed 60 nm thick nanoparticles layer, the slope of resonance wavelength over the refractive index is larger for ITO nanoparticles than those of Au, Ag and Cu nanoparticles for 10 nm, 15 nm, 20 nm, 25 nm and 30 nm particle sizes.

To obtain the maximum value of sensitivity (i.e. shift in resonance wavelength per unit change in refractive index of sensing medium) of LSPR sensor, it will be necessary to

recognize the appropriate thickness of nanoparticles layer of all four materials. The sensitivity of LSPR sensor for 40 nm, 50 nm and 60 nm thick nanoparticles layers (of ITO, Au, Ag and Cu materials) with 5 nm, 10 nm, 15 nm, 20 nm, 25 nm and 30 nm particle sizes is compared in table 4.2.

Table 4.2: Comparison of sensitivity of LSPR based fiber optic sensor for various thickness values of nanoparticles layer of ITO, Au, Ag and Cu nanoparticles with 5, 10, 15, 20, 25 and 30 nm particle sizes

Nanoparticle size (nm)	Sensitivity S_n (nm/RIU)											
	Nanoparticles layer thickness = 40 nm				Nanoparticles layer thickness = 50 nm				Nanoparticles layer thickness = 60 nm			
	ITO	Au	Ag	Cu	ITO	Au	Ag	Cu	ITO	Au	Ag	Cu
5	3135	Small	Small	Small	4750	Small	Small	Small	6075	Small	Small	Small
10	3285	3265	2915	2625	4785	3900	3150	3025	6165	4450	3475	3295
15	3345	3300	2930	2650	4800	3950	3180	3030	6185	4475	3520	3300
20	3385	3320	2950	2660	4835	3975	3200	3050	6240	4525	3550	3340
25	3325	3145	2890	2625	4695	3600	3120	2960	6095	4075	3350	3135
30	3315	3125	2830	2610	4655	3570	3085	2945	6065	3920	3340	3075

It can be seen from table 4.2, that for fixed 40 nm thick nanoparticles layer with fixed 5 nm particle size, the sensitivity of LSPR sensor is maximum (3135 nm/RIU) for ITO nanoparticles, whereas it is small for Au, Ag and Cu nanoparticles. Besides it, for fixed 40 nm thick nanoparticles layer, the sensitivity of ITO nanoparticles based LSPR sensor increases from 3135 nm/RIU to 3385 nm/RIU as the particle size of ITO nanoparticles increases from 5 nm to 20 nm gradually and then it starts decreasing from 3385 nm/RIU to 3315 nm/RIU as the particle size of ITO nanoparticles increases from 20 nm to 30 nm. On the other hand, the sensitivity of LSPR sensor increases to 3320 nm/RIU, 2950 nm/RIU and 2660 nm/RIU for Au, Ag and Cu nanoparticles respectively as the particle sizes of these nanoparticles increase from 10 nm to 20 nm for fixed 40 nm thick nanoparticles layer. In the same way, for fixed 50 nm thick nanoparticles layer with fixed 5 nm particle size, the sensitivity of LSPR sensor is maximum (4750 nm/RIU) for ITO nanoparticles, while it is least for Au, Ag and Cu nanoparticles. Moreover, for fixed 50 nm thick nanoparticles layer, the sensitivity of ITO nanoparticles based LSPR sensor enlarges from 4750 nm/RIU to 4835 nm/RIU as the particle size of ITO nanoparticles raises from 5 nm to 20 nm and then it

decreases from 4835 nm/RIU to 4655 nm/RIU as the particle size of ITO nanoparticles increases from 20 nm to 30 nm. Further, the sensitivity of LSPR sensor increases to 3975 nm/RIU, 3200 nm/RIU and 3050 nm/RIU for Au, Ag and Cu nanoparticles respectively as the particle sizes of these nanoparticles increase from 10 nm to 20 nm for fixed 50 nm thick nanoparticles layer. Also, for fixed 60 nm thick nanoparticles layer with fixed 5 nm particle size, the sensitivity of LSPR sensor is highest (6075 nm/RIU) for ITO nanoparticles, whereas it is smallest for Au, Ag and Cu nanoparticles. In addition, for fixed 60 nm thick nanoparticles layer, the sensitivity of ITO nanoparticles based LSPR sensor enhances from 6075 nm/RIU to 6240 nm/RIU as the particle size of ITO nanoparticles boosts from 5 nm to 20 nm steadily and then it reduces from 6240 nm/RIU to 6065 nm/RIU as the particle size of ITO nanoparticles increases from 20 nm to 30 nm. However, the sensitivity of LSPR sensor increases to 4525 nm/RIU, 3550 nm/RIU and 3340 nm/RIU for Au, Ag and Cu nanoparticles respectively as the particle sizes of these nanoparticles increase from 10 nm to 20 nm for fixed 60 nm thick nanoparticles layer. It is also noticeable that the average sensitivities of ITO, Au, Ag and Cu nanoparticles based LSPR sensor are 3298 nm/RIU, 2693 nm/RIU, 2419 nm/RIU, 2195 nm/RIU respectively for 40 nm thick nanoparticles layer; 4753 nm/RIU, 3166 nm/RIU, 2623 nm/RIU, 2502 nm/RIU respectively for 50 nm thick nanoparticles layer and 6138 nm/RIU, 3574 nm/RIU, 2873 nm/RIU, 2691 nm/RIU respectively for 60 nm thick nanoparticles layer. The variations of sensitivity of LSPR based fiber optic sensor with particle size of nanoparticles for 40 nm, 50 nm and 60 nm thick nanoparticles layer (of ITO, Au, Ag and Cu materials) have been plotted in Figs 4.20-4.22 respectively.

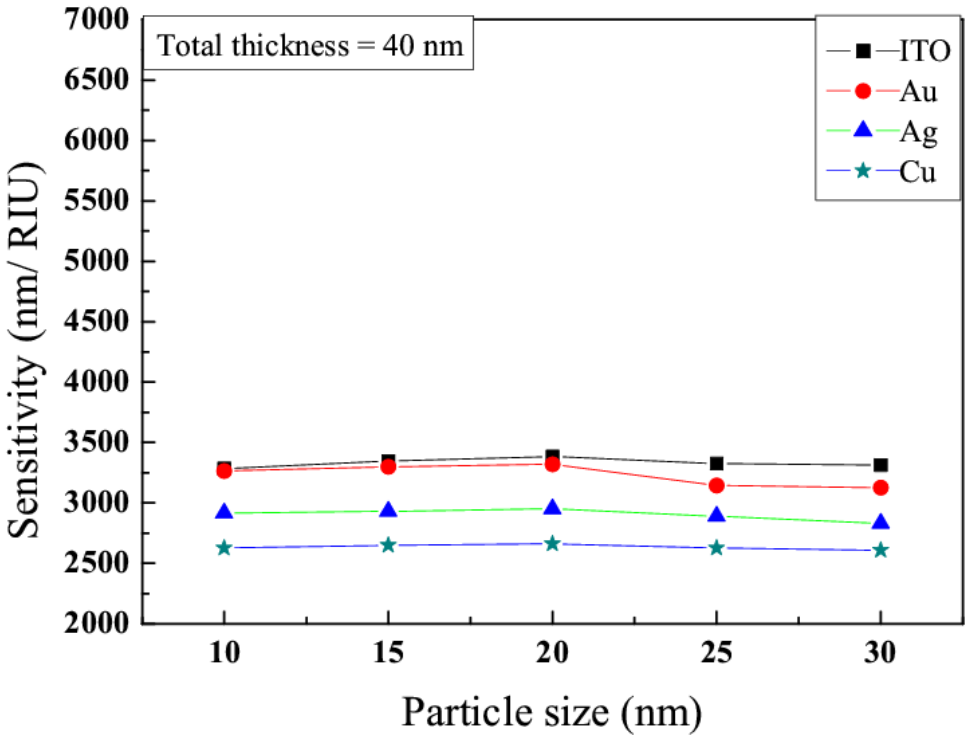

Figure 4.20: Variations of sensitivity with particle size of nanoparticles for 40 nm thick ITO, Au, Ag and Cu nanoparticles layer

Fig. 4.20 interprets the variation of sensitivity of LSPR sensor with particle size of nanoparticles for fixed 40 nm thick nanoparticles layer for all four materials: ITO, Au, Ag and Cu individually. The sensitivity of LSPR sensor increases as the particle size of nanoparticles increases from 10 nm to 20 nm and then it starts decreasing as the particle size of nanoparticles further increases from 20 nm to 30 nm. The sensitivity of ITO nanoparticles layer based LSPR sensor is better than that of Au, Ag and Cu nanoparticles layers.

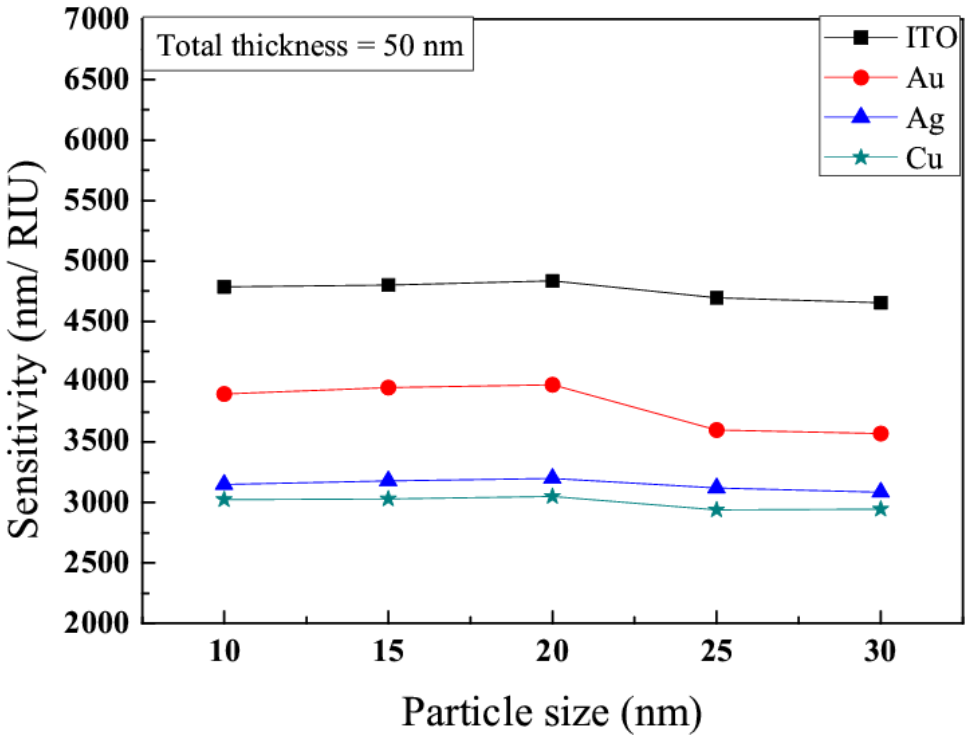

Figure 4.21: Variations of sensitivity with particle size of nanoparticles for 50 nm thick ITO, Au, Ag and Cu nanoparticles layer

Fig. 4.21 explains the variation of sensitivity of LSPR sensor with particle size of nanoparticles for fixed 50 nm thick nanoparticles layer for all four materials: ITO, Au, Ag and Cu individually. Again, the sensitivity of LSPR sensor enhances as the particle size of nanoparticles increases from 10 nm to 20 nm and then it begins reducing as the particle size of nanoparticles further increases from 20 nm to 30 nm. The sensitivity of ITO nanoparticles layer based LSPR sensor is superior to that of Au, Ag and Cu nanoparticles layers.

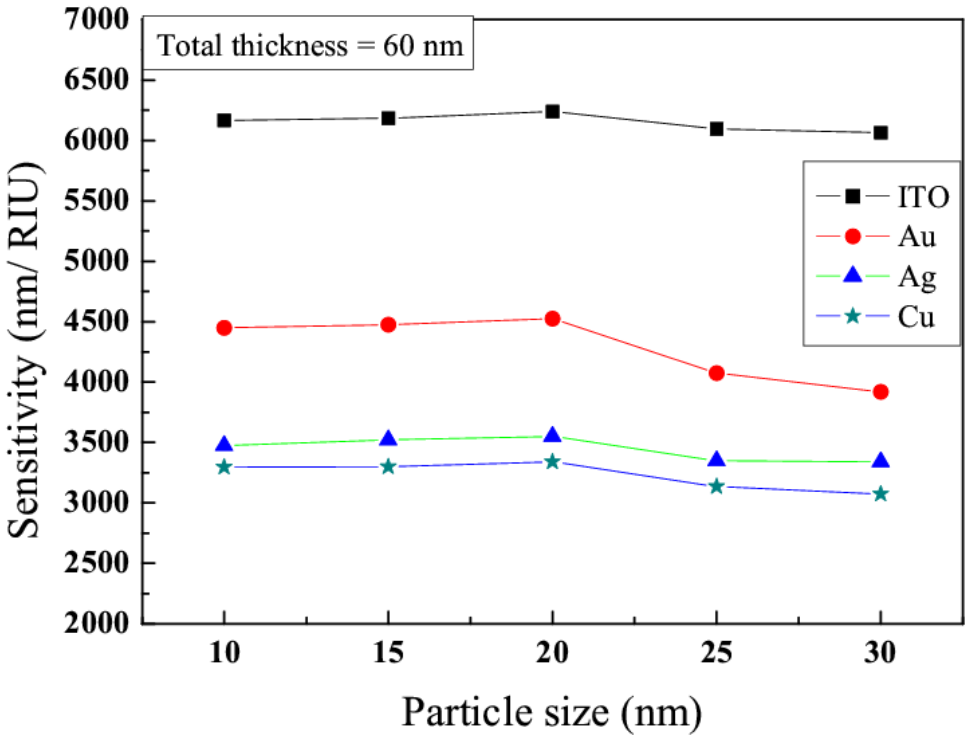

Figure 4.22: Variations of sensitivity with particle size of nanoparticles for 60 nm thick ITO, Au, Ag and Cu nanoparticles layer

Fig. 4.22 displays the variation of sensitivity of LSPR sensor with particle size of nanoparticles for fixed 60 nm thick nanoparticles layer for all four materials: ITO, Au, Ag and Cu individually. The sensitivity of LSPR sensor rises as the particle size of nanoparticles increases from 10 nm to 20 nm and then it starts falling as the particle size of nanoparticles further increases from 20 nm to 30 nm. The sensitivity of ITO nanoparticles layer based LSPR sensor is greater than that of Au, Ag and Cu nanoparticles layers.

Thus, the sensitivity of LSPR based fiber optic sensor increases with increase in thickness of nanoparticles layer for all four materials. In addition, for a fixed thickness of nanoparticles layer, the sensitivity of LSPR sensor further increases as the particle size of nanoparticles increases up to 20 nm. This effect can be explained in terms of the variation in absorption of light due to the change in particle size of the nanoparticles [133]. It is clearly observed from Eq. (4.3) that the decrease in particle size results in decrease in collision wavelength (λ_c), that in turn increases the imaginary part of the dielectric function of metallic nanoparticles as

per Eq. (4.4) and hence the imaginary part of propagation constant of surface plasmon wave (K_{sp}). As the imaginary part of K_{sp} corresponds to the optical absorption of incident light, it is obvious that more absorption of light intensity takes place for nanoparticles of smaller particle size. It outcomes the transmitted light intensity through the optical fiber to decrease and the SPR curve shifts downward. Therefore, the smaller the particle size of nanoparticles, the larger will be the downward shifting i.e. broadening of the SPR curve. Also, the real part of the dielectric function of metallic nanoparticles and hence the real part of K_{sp} is responsible for the shifting of resonance condition/wavelength. Moreover, the position of SPR dip is not altered much by the change in particle size of nanoparticles because the real part of K_{sp} does not change much with the variation in size-dependent collision wavelength i.e. with the particle size of the nanoparticles. Thus, the shift in SPR curve remains nearly independent of particle size of the nanoparticles. Therefore, it can be understood that the variation of sensitivity of LSPR based fiber optic sensor with the particle size of nanoparticles is much influenced by the broadening/FWHM of SPR curve rather than its shifting. Further, the resonance wavelengths for Au, Ag and Cu nanoparticles happen in the visible region of the spectrum, whereas for ITO nanoparticles, the resonance condition is fulfilled at a higher value of wavelength i.e. in IR region.

Hence, for fixed 40 nm, 50 nm and 60 nm thick nanoparticles layer with fixed 5 nm particle size, the sensitivities of LSPR based fiber optic sensor are 3135 nm/RIU, 4750 nm/RIU and 6075 nm/RIU respectively for ITO nanoparticles, whereas it is smaller for Au, Ag and Cu nanoparticles. Further, the sensitivities of ITO, Au, Ag and Cu nanoparticles based LSPR sensor reach as high as 3385 nm/RIU, 3320 nm/RIU, 2950 nm/RIU, 2660 nm/RIU respectively for fixed 40 nm thick nanoparticles layer with fixed 20 nm particle size; 4835 nm/RIU, 3975 nm/RIU, 3200 nm/RIU, 3050 nm/RIU respectively for fixed 50 nm thick nanoparticles layer with fixed 20 nm particle size and 6240 nm/RIU, 4525 nm/RIU, 3550 nm/RIU, 3340 nm/RIU respectively for fixed 60 nm thick nanoparticles layer with fixed 20 nm particle size. Therefore, it is obvious that the sensitivity of LSPR sensor increases with increase of particle size of nanoparticles (from 5 nm to 20 nm) for 40 nm, 50 nm and 60 nm thick nanoparticles layer (of ITO, Au, Ag and Cu materials). The sensitivity of LSPR sensor for various thicknesses of nanoparticles layer is found in the order of ITO > Au > Ag > Cu. Therefore, keeping all the above discussion about LSPR based fiber optic sensor in to consideration, it can be concluded that the optimized thickness of ITO, Au, Ag and Cu nanoparticles layers is 60 nm and the optimized particle size of ITO, Au, Ag and Cu nanoparticles is 20 nm. Further, the maximum values of sensitivity of LSPR sensor have been

observed as 6240 nm/RIU, 4525 nm/RIU, 3550 nm/RIU and 3340 nm/RIU for fixed 60 nm thick nanoparticles layer with fixed 20 nm particle size of ITO, Au, Ag and Cu nanoparticles respectively. As a result, ITO nanoparticles based LSPR sensor exhibits better sensing performance than those of other three material's nanoparticles.

4.4 Conclusions

Theoretical analysis of a LSPR based fiber optic sensor with nanoparticles layer has been presented. Nanoparticles of four materials: ITO, Au, Ag and Cu have been considered. The nanoparticles are assumed to be spherical in shape with various radii. The sensitivity of LSPR sensor with each nanoparticles layer individually for various thickness values (40 nm, 50 nm and 60 nm) with 5 nm, 10 nm, 15 nm, 20 nm, 25 nm and 30 nm particle size is studied. The sensitivity of LSPR sensor increases with increase in thickness of nanoparticles layer for all four materials. In addition, for a fixed thickness of nanoparticles layer, the sensitivity of LSPR sensor further increases as the particle size of nanoparticles increases (up to 20 nm). The optimized values of thickness and particle size of nanoparticles layers for all four materials are found to be 60 nm and 20 nm respectively. The proposed LSPR sensor based on 60 nm thick nanoparticles layer with 20 nm particle size possesses high sensitivity. The sensitivity of LSPR based fiber optic sensor has been found to be 6240 nm/RIU, 4525 nm/RIU, 3550 nm/RIU and 3340 nm/RIU for 60 nm thick nanoparticles layer with fixed 20 nm particle size of ITO, Au, Ag and Cu nanoparticles respectively. Hence, containing sensitivity as high as 6240 nm/RIU, 60 nm thick ITO nanoparticles layer (with 20 nm particle size) based LSPR sensor shows better performance than Au, Ag and Cu nanoparticles based LSPR sensors. Therefore, it is concluded that ITO nanoparticles represent a better sensing behavior than Au, Ag and Cu nanoparticles.

CHAPTER 5

NANOCOMPOSITES BASED FIBER OPTIC SPR SENSOR

5.1 Introduction

For sensing of samples having low refractive indices (such as gases), noble metals (Au and Ag) are not appropriate because the SPR sensors based on noble metals offer small sensitivity. Besides, their SPR resonance dips appear in UV region. Recently, a nanocomposite based fiber optic SPR sensor has been shown theoretically to sense small concentrations of gases in visible region [160]. In the present chapter, we shall theoretically analyze SPR based fiber optic sensor utilizing nanocomposites. Nanocomposites are the solid structures with nanometer scale dimensional repeat distances between various phases that constitute the structure. These materials typically comprise an inorganic (host) solid containing an organic component or vice versa. They can also consist of two or more inorganic/organic phases in some combinatorial form with the constraint that at least one of the phases is in nanosize. Nanocomposites exhibit different optical, electrical, mechanical, structural, catalytic and electrochemical properties than those of each individual component. Nanocomposite films comprising of metal nanoparticles dispersed in a dielectric matrix have received significant attention due to their attractive optical properties originating from surface plasmons [161,162] i.e. quantized collective oscillation of free electrons dielectrically confined in a metal nanoparticle. Near the surface plasmon resonance wavelength, the local field around the metal nanoparticle and the effective optical nonlinearity of the nanocomposite films are highly increased [163].

In this chapter, numerous innovative nanocomposites comprising nanoparticles of gold (Au), silver (Ag) and copper (Cu) with their varying volume fractions embedded in host dielectric matrices of titanium oxide (TiO_2) and indium nitride (InN) are considered and a SPR based fiber optic sensor with each nanocomposite layer (one at a time) has been theoretically investigated. The surface plasmon resonance produced by coupling of evanescent light to surface plasmons is utilized as the sensing scheme. The wavelength

interrogation method is employed for the analysis of SPR based fiber optic sensor. The performance analysis of the SPR sensor is done in terms of its sensitivity. The sensitivity of the SPR sensor with each nanocomposite layer (individually) has been evaluated numerically and compared. Further, the influences of thickness of each nancomposite layer and volume fraction of metal nanoparticles on the sensitivity of the sensor have been observed. The current study reveals that the sensitivity of Au/Ag/Cu-InN nanocomposites based SPR sensor for all thicknesses of nanocomposites with any volume fraction of nanoparticles is higher than that of Au/Ag/Cu-TiO_2 nanocomposites. Further, the sensitivity of proposed SPR sensor enhances with increase in both thickness of nanocomposites and volume fraction of metal nanoparticles. Moreover, for a fixed nanocomposite thickness and fixed volume fraction of metal nanoparticles, the sensitivity of SPR sensor is superior for Au nanoparticles based nanocomposites to that of Ag and Cu nanoparticles. Besides, the SPR sensor with 70 nm thick Au-InN nanocomposite containing volume fraction of 0.85 illustrates high sensitivity of 2875 nm/RIU.

5.2 Theory

The SPR sensing is based on the principle of attenuated total reflection (ATR) with Kretschmann configuration. In the proposed SPR based fiber optic sensor, the sensing system consisting of a fiber core-nanocomposite layer-sensing medium is considered as shown in Fig. 5.1.

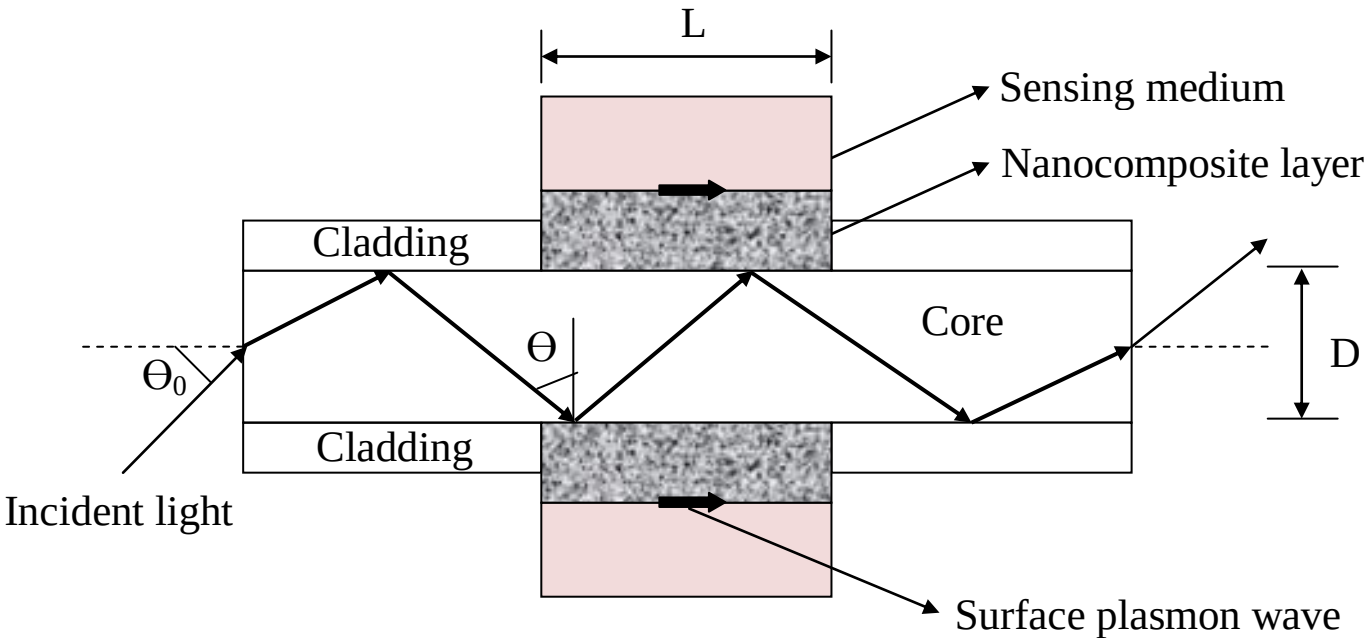

Figure 5.1: Schematic diagram of SPR based fiber optic sensor with nanocomposite layer

The plastic cladding around the core from the middle portion of a step index multimode plastic clad silica (PCS) fiber (Numerical aperture = 0.24 and fiber core diameter = 600 μm) is removed and is then coated with a thin nanocomposite layer, which is finally surrounded by the sensing medium. The light from a broadband (polychromatic) source is launched into one of the ends of the optical fiber with proper optics and the transmitted light is detected at the other end of the optical fiber.

5.2.1 Layer I (Fiber core)

Layer I is made of core of optical fiber. The core of the optical fiber is assumed to be made of fused silica. The refractive index of fused silica varies with wavelength according to Sellmeier dispersion relation as,

$$n_1(\lambda) = \sqrt{1 + \frac{a_1\lambda^2}{\lambda^2 - b_1^2} + \frac{a_2\lambda^2}{\lambda^2 - b_2^2} + \frac{a_3\lambda^2}{\lambda^2 - b_3^2}} \tag{5.1}$$

Where, λ is the wavelength in μm and a_1, a_2, a_3, b_1, b_2 and b_3 are Sellmeier coefficients. The values of these coefficients are given as, a_1 = 0.6961663, a_2 = 0.4079426, a_3 = 0.8974794, b_1 = 0.0684043 μm, b_2 = 0.1162414 μm and b_3 = 9.896161 μm [141].

5.2.2 Layer II (Nanocomposite layer)

Layer II is made of nanocomposite. In a nanocomposite material, nanoparticles of one component material are embedded in a continuous host dielectric matrix of other component [160]. If the particle sizes of nanoparticles are much smaller than the wavelength of the incident radiation, then without the violation of Rayleigh's scattering theory, the effective dielectric constant of nanocomposite can be determined by using Maxwell-Garnett Model [164]. If ε_1 is the dielectric constant of metal/metal oxide nanoparticles of component 1 and ε_2 is the dielectric constant of host dielectric matrix of component 2, the effective dielectric constant of nanocomposite is given as,

$$\varepsilon_{eff} = \varepsilon_2 \left[\frac{\varepsilon_1 + 2\varepsilon_2 + 2f(\varepsilon_1 - \varepsilon_2)}{\varepsilon_1 + 2\varepsilon_2 - f(\varepsilon_1 - \varepsilon_2)} \right] \tag{5.2}$$

Where, f is the volume filling factor (volume fraction) of nanoparticles of component 1. In Eq. (5.2), the effective dielectric constant of nanocomposite is assumed to be independent of particle size and shape of the nanoparticles. In the present investigation, Au, Ag and Cu are considered as component 1 while TiO_2 and InN are regarded as component 2.

The dielectric constants of Au, Ag and Cu metals are written according to Drude model as,

$$\varepsilon_1 = 1 - \frac{\lambda^2 \lambda_c}{\lambda_p^2 (\lambda_c + i\lambda)} \tag{5.3}$$

Here, λ_p and λ_c are the plasma wavelength and the collision wavelength of Au, Ag and Cu. Where, λ_p = 1.6826 x 10^{-7} m, 1.4541 x 10^{-7} m, 1.3617 x 10^{-7} m and λ_c = 8.9342 x 10^{-6} m, 1.7614 x 10^{-5} m, 4.0852 x 10^{-5} m for Au, Ag and Cu respectively [142].

For host dielectric matrix TiO_2, the variation of refractive index with wavelength is given by the empirical formula as [165],

$$n_{TiO_2} = \sqrt{5.913 + \frac{0.2441}{\lambda^2 - 0.0843}} \tag{5.4}$$

The dielectric constant of host dielectric matrix InN is written according to Drude model as [166],

$$\varepsilon_2 = \varepsilon_\infty \left[1 + \frac{(\omega_{LO}^2 - \omega_{TO}^2)}{(\omega_{LO}^2 - \omega^2 - i\omega\gamma)} - \frac{\omega_p^2}{(\omega^2 + i\omega\Gamma)} \right] \tag{5.5}$$

Here, ε_∞ is the high frequency dielectric constant, ω_{LO} and ω_{TO} are LO and TO frequencies of phonon mode, ω_p is the plasma frequency, γ and Γ are the two corresponding damping constants. For InN, ε_∞ = 7.5, ω_p = 4100 cm^{-1}, Γ = 1382 cm^{-1}, ω_{LO} = 590 cm^{-1}, ω_{TO} = 450 cm^{-1} and γ = 120 cm^{-1}.

5.2.3 Layer III (Sensing medium)

Layer III is made of sensing medium. The dielectric constant of the sensing medium is ε_s. If n_s is the refractive index of the sensing medium, then $\varepsilon_s = n_s^2$. The resonance condition for excitation of surface plasmon wave is given as,

$$\frac{2\pi}{\lambda} n_1 \sin\theta = \mathrm{Re}\{K_{sp}\} \tag{5.6}$$

Where, $K_{sp} = \frac{\omega}{c}\sqrt{\frac{\varepsilon_m \varepsilon_s}{\varepsilon_m + \varepsilon_s}} = \frac{2\pi}{\lambda}\sqrt{\frac{\varepsilon_m n_s^2}{\varepsilon_m + n_s^2}}$ is the propagation constant of the surface plasmon wave and *c* is the speed of light in vacuum. The left hand side of Eq. (5.6) denotes the

propagation constant of the light incident at an angle θ and the right hand side shows the real part of the propagation constant of the surface plasmon wave.

5.2.4 Transmitted Power

The expression for the reflection coefficient (reflectance) of p-polarized incident light is obtained by using the matrix method for N-layer model as mentioned in appendix A. Considering that all the guided rays are launched in the fiber using a collimated source and a microscope objective, the angular power distribution of rays guided in the fiber is given as [18],

$$dP \propto \frac{n_1^2 \sin\theta\cos\theta}{(1-n_1^2\cos^2\theta)^2}\,d\theta \tag{5.7}$$

Where, θ is the angle of the ray with the normal to the core-cladding interface. Also, n_1 is the refractive index of the core of the fiber. To calculate the effective transmitted power, the reflectance (R_p) for a single reflection is raised to the power of the number of reflections the specific propagating angle undergoes with the sensor interface. Hence, for p-polarized light, the generalized expression for the normalized transmitted power in an optical fiber based SPR sensor will be given as,

$$P_{trans} = \frac{\int_{\theta_{cr}}^{\pi/2} R_p^{N_{ref}(\theta)} \frac{n_1^2 \sin\theta\cos\theta}{(1-n_1^2\cos^2\theta)^2}\,d\theta}{\int_{\theta_{cr}}^{\pi/2} \frac{n_1^2 \sin\theta\cos\theta}{(1-n_1^2\cos^2\theta)^2}\,d\theta} \tag{5.8}$$

Where, $N_{ref}(\theta) = \frac{L}{D\tan\theta}$ (5.9)

And, $\theta_{cr} = \sin^{-1}\left(\frac{n_{cl}}{n_1}\right)$ (5. 10)

Here, $N_{ref}(\theta)$ is the total number of reflections performed by a ray making an angle θ with the normal to the core-metal layer interface in the sensing region. *L* and *D* are the length of the exposed sensing region and the fiber core diameter respectively. Also, θ_{cr} is the critical angle of the fiber and n_{cl} is the refractive index of the cladding of the fiber.

5.2.5. Sensitivity

Resonance wavelength (λ_{res}) is determined corresponding to the refractive index of the sensing medium (n_s) in the SPR sensor based on wavelength interrogation. If the refractive index of the sensing medium is altered by δn_s, the resonance wavelength shifts by $\delta\lambda_{res}$. The sensitivity (S_n) of a SPR sensor with wavelength interrogation is defined as [64],

$$S_n = \frac{\delta\lambda_{res}}{\delta n_s} \tag{5.11}$$

5.3 Results and discussion

For numerical calculations, the refractive index of the sensing medium is changed from 1.30 to 1.37 in steps of 0.01 and following values of the parameters have been used:
Numerical aperture of the fiber = 0.24, fiber core diameter D = 600 μm, length of the exposed sensing region L = 15 mm. In addition, several nanocomposites consisting of Au/Ag/Cu nanoparticles with their varying volume fractions embedded in host dielectric matrices of TiO_2 and InN are considered in the present study.

For optimizing thicknesses of various nanocomposite layers and volume fractions of nanoparticles, the transmitted output power of SPR based fiber optic sensor have been calculated for 10 nm, 30 nm, 50 nm and 70 nm thick nanocomposite layers with fixed volume fractions of 0.55, 0.65, 0.75 and 0.85. The variations of SPR resonance wavelength with refractive index of sensing medium for a range of thicknesses of Au-TiO_2, Ag-TiO_2, Cu-TiO_2, Au-InN, Ag-InN and Cu-InN nanocomposite layers with various volume fractions have been plotted in Figs. 5.2-5.9 respectively.

Figs. 5.2-5.5 show the plots of resonance wavelength of SPR sensor with refractive index of sensing medium for 10 nm, 30 nm, 50 nm and 70 nm thick Au-TiO_2, Ag-TiO_2 and Cu-TiO_2 nanocomposite layers with fixed volume fractions of 0.55, 0.65, 0.75 and 0.85 respectively.

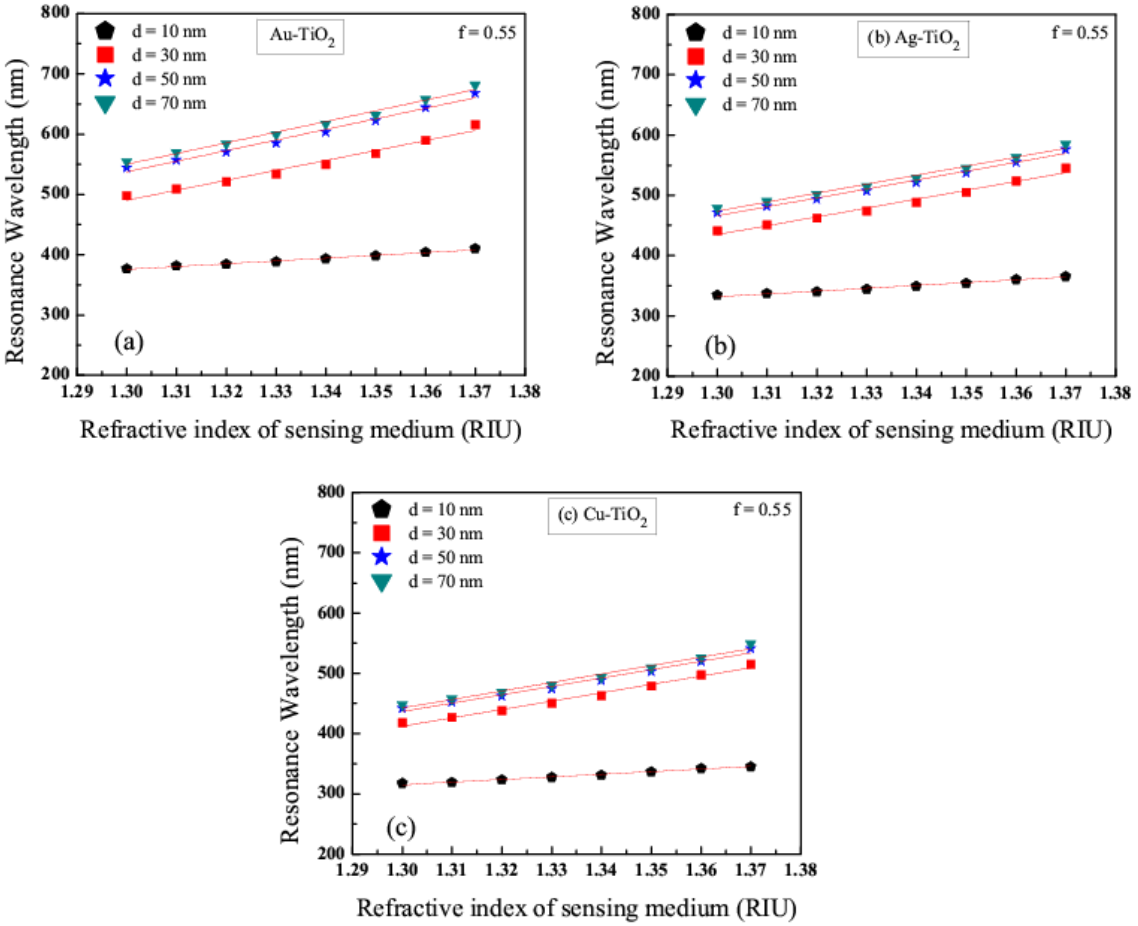

Figure 5.2: Variations of resonance wavelength with refractive index of sensing medium for 10-70 nm thick (a) Au-TiO_2 (b) Ag-TiO_2 and (c) Cu-TiO_2 nanocomposite layers with fixed volume fraction of 0.55

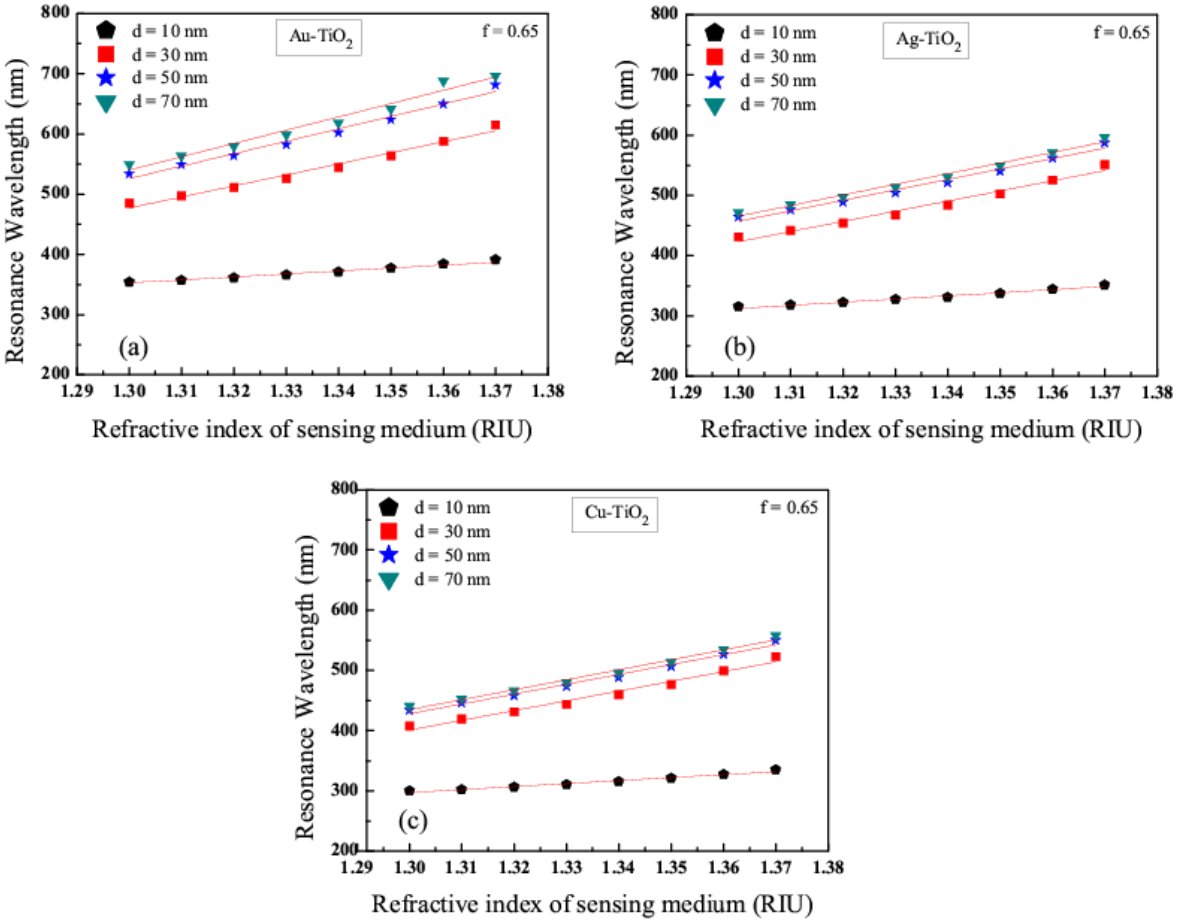

Figure 5.3: Variations of resonance wavelength with refractive index of sensing medium for 10-70 nm thick (a) Au-TiO_2 (b) Ag-TiO_2 and (c) Cu-TiO_2 nanocomposite layers with fixed volume fraction of 0.65

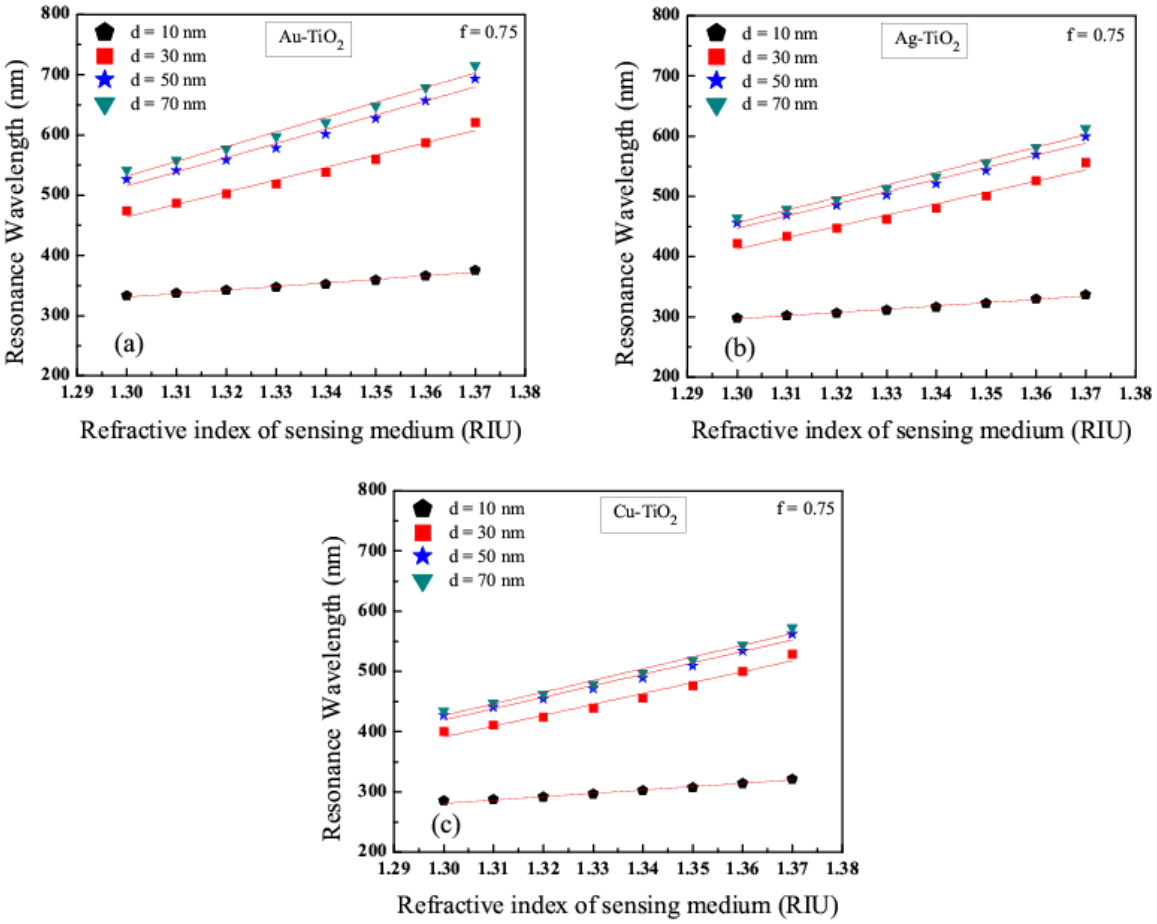

Figure 5.4: Variations of resonance wavelength with refractive index of sensing medium for 10-70 nm thick (a) Au-TiO_2 (b) Ag-TiO_2 and (c) Cu-TiO_2 nanocomposite layers with fixed volume fraction of 0.75

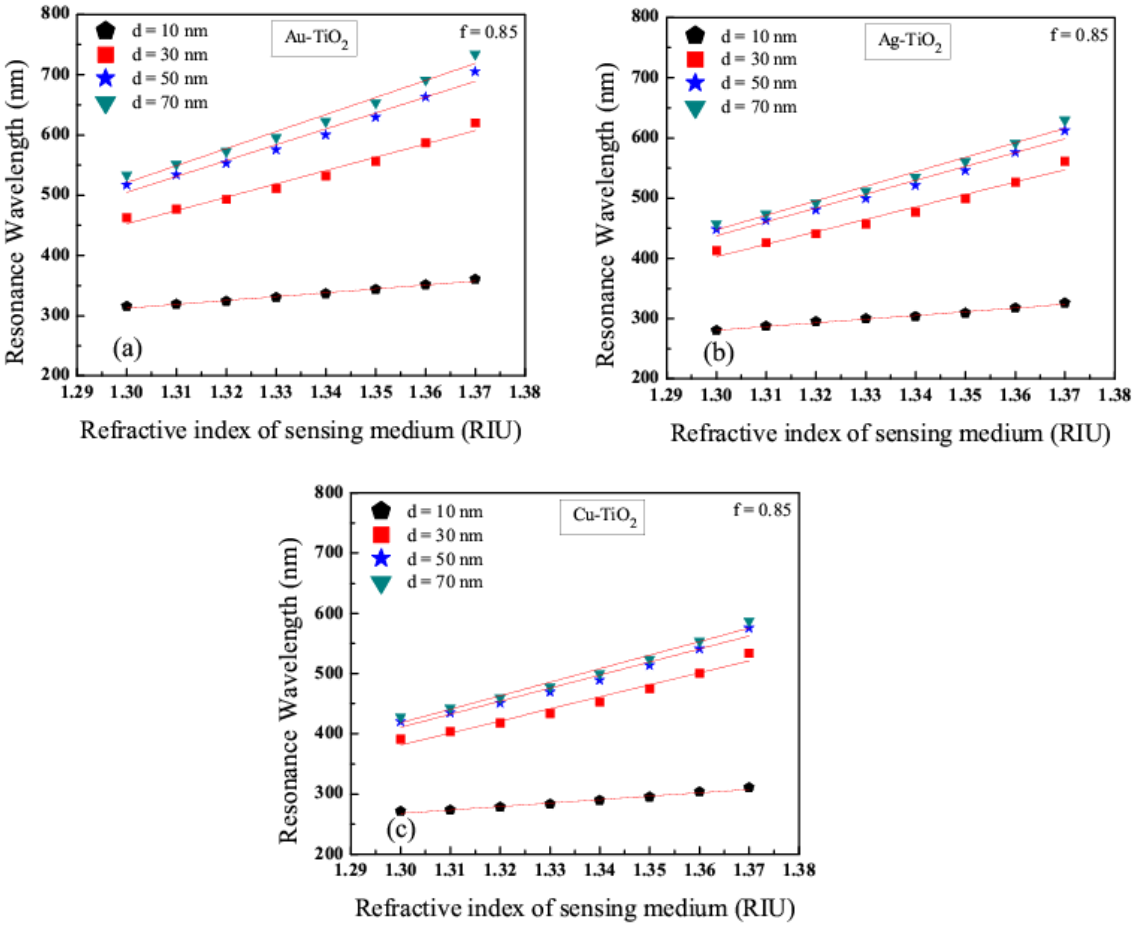

Figure 5.5: Variations of resonance wavelength with refractive index of sensing medium for 10-70 nm thick (a) Au-TiO_2 (b) Ag-TiO_2 and (c) Cu-TiO_2 nanocomposite layers with fixed volume fraction of 0.85

Similarly, Figs. 5.6-5.9 illustrate the variations of resonance wavelength of SPR sensor with refractive index of sensing medium for 10 nm, 30 nm, 50 nm and 70 nm thick Au-InN, Ag-InN and Cu-InN nanocomposite layers with fixed volume fractions of 0.55, 0.65, 0.75 and 0.85 respectively.

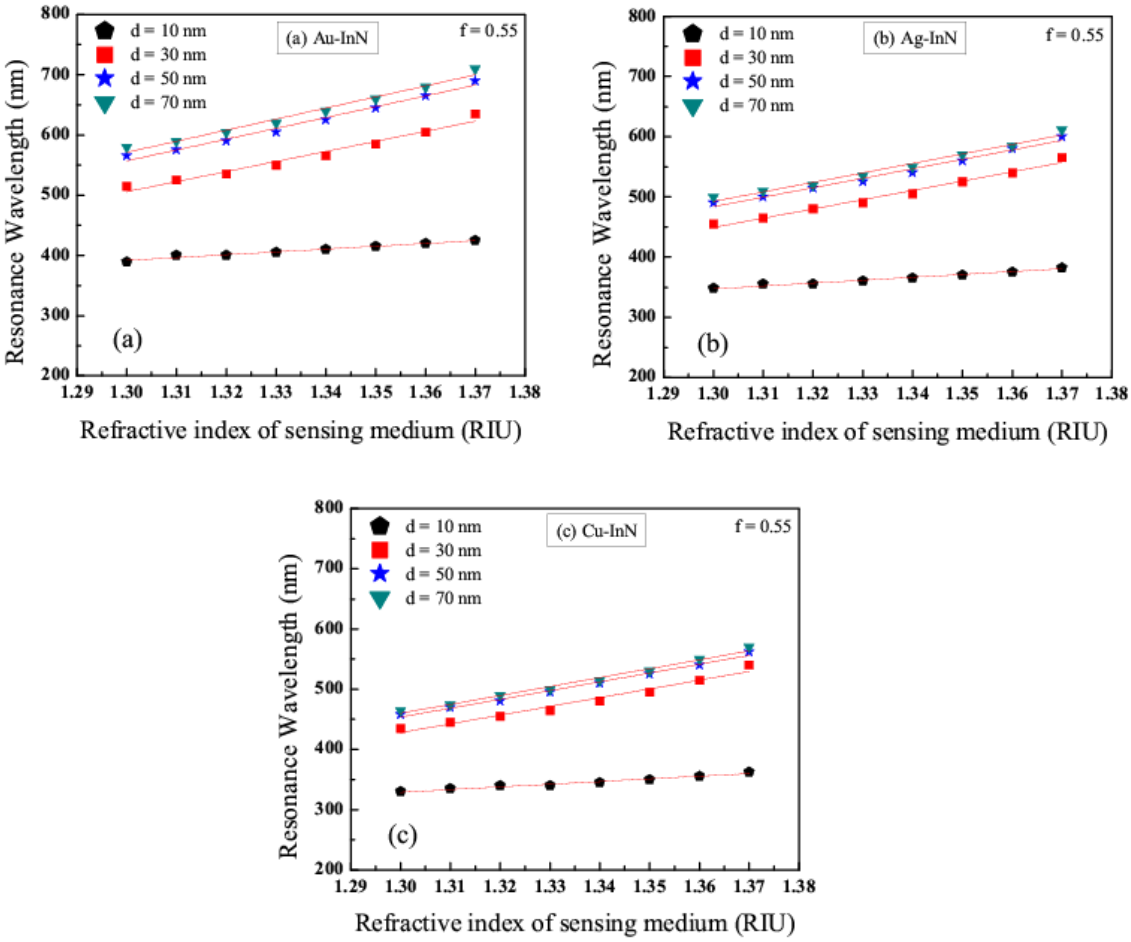

Figure 5.6: Variations of resonance wavelength with refractive index of sensing medium for 10-70 nm thick (a) Au-InN (b) Ag-InN and (c) Cu-InN nanocomposite layers with fixed volume fraction of 0.55

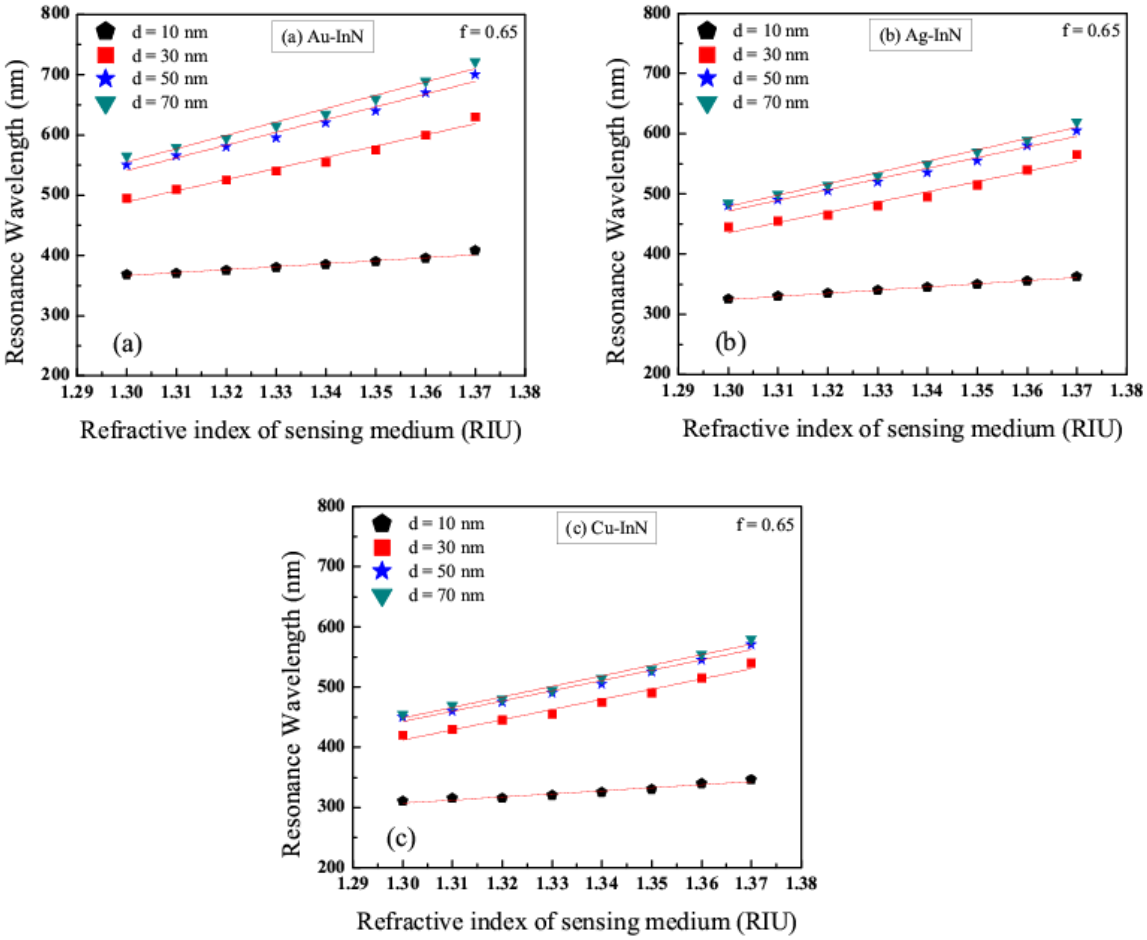

Figure 5.7: Variations of resonance wavelength with refractive index of sensing medium for 10-70 nm thick (a) Au-InN (b) Ag-InN and (c) Cu-InN nanocomposite layers with fixed volume fraction of 0.65

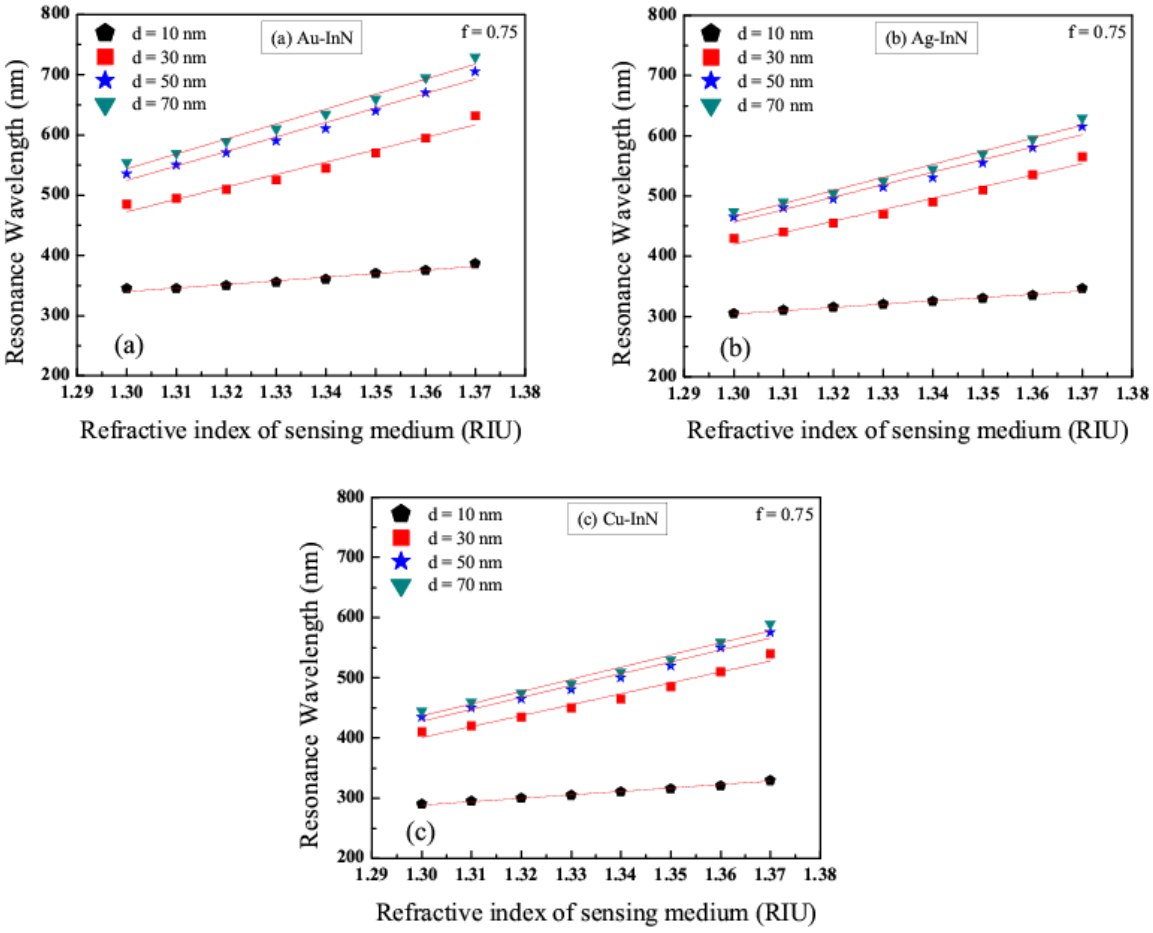

Figure 5.8: Variations of resonance wavelength with refractive index of sensing medium for 10-70 nm thick (a) Au-InN (b) Ag-InN and (c) Cu-InN nanocomposite layers with fixed volume fraction of 0.75

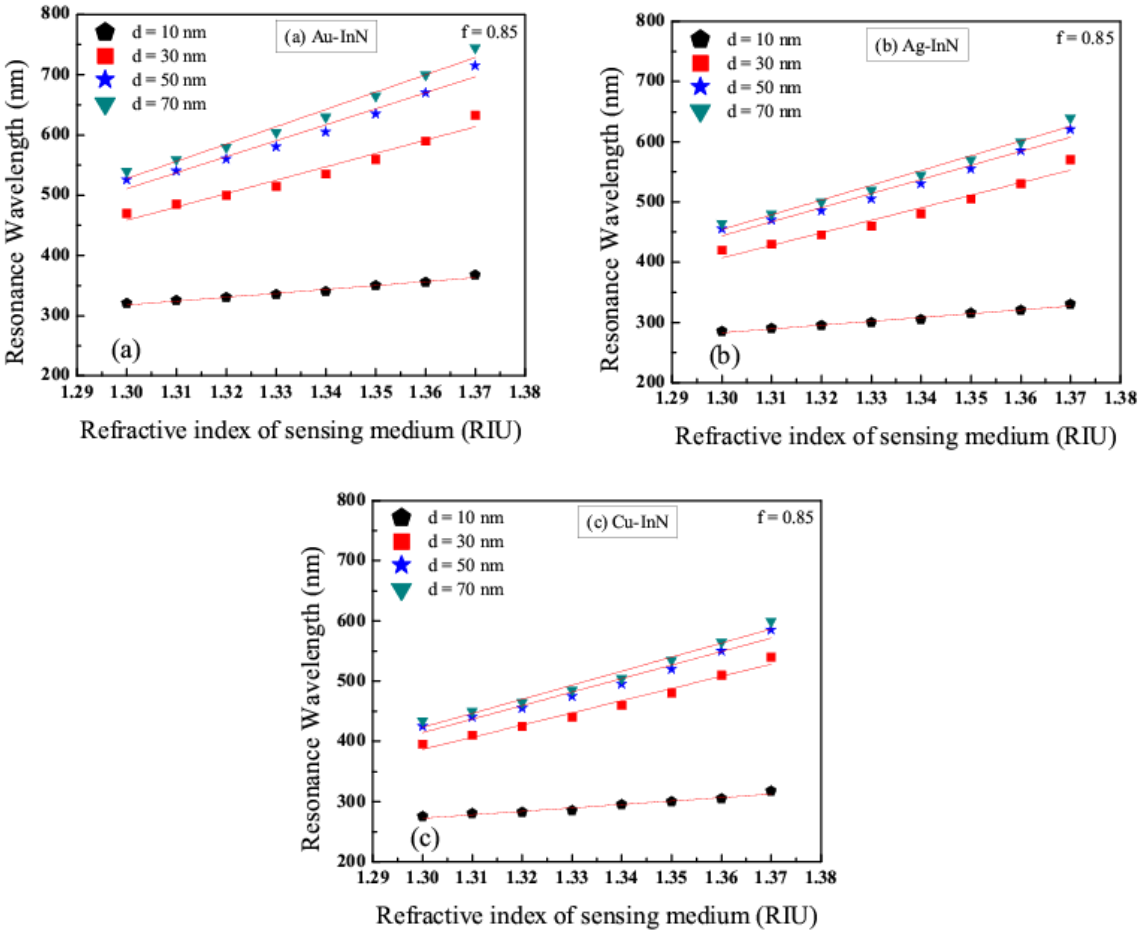

Figure 5.9: Variations of resonance wavelength with refractive index of sensing medium for 10-70 nm thick (a) Au-InN (b) Ag-InN and (c) Cu-InN nanocomposite layers with fixed volume fraction of 0.85

It can be seen from these figures that the resonance wavelengths for a variety of thicknesses (10 nm to 70 nm) of any nanocomposite layer with fixed volume fraction (0.55 to 0.85) of metal nanoparticles increase linearly with increase in refractive index of the sensing medium. These variations of resonance wavelength with refractive index of sensing medium for all the cases chase the same pattern. Further, the shifts in resonance wavelength for all the cases are linear over the complete range of refractive indices i.e. 1.30 to 1.37 of the sensing medium. This linear escalation in resonance wavelengths for all thicknesses of each nanocomposite layer with any volume fraction of metal nanoparticles with increase in refractive index of sensing medium can be understood by the variation of real part of propagation constant (K_{sp}) of surface plasmon wave. According to Eq. (5.6), the real part of

K_{sp} is accountable for the resonance condition. The real part of K_{sp} will be smaller for small value of refractive index of sensing medium and hence its resonance condition is satisfied at smaller wavelength [103]. Likewise, for the larger value of refractive index of sensing medium, the resonance condition is satisfied at longer wavelength due to the largest real part of K_{sp}. The SPR transmittance curves for 50 nm and 70 nm thick Au-TiO_2 as well as Au-InN nancomposite layers with different values of volume fraction have been plotted in Figs. 5.10-5.13.

Figs. 5.10 and 5.11 show the SPR transmittance curves for Au-TiO_2 nanocomposite layers having thicknesses 50 nm with volume fraction of 0.85 and 70 nm with volume fractions of 0.75, 0.85 respectively for refractive index of sensing medium = 1.37.

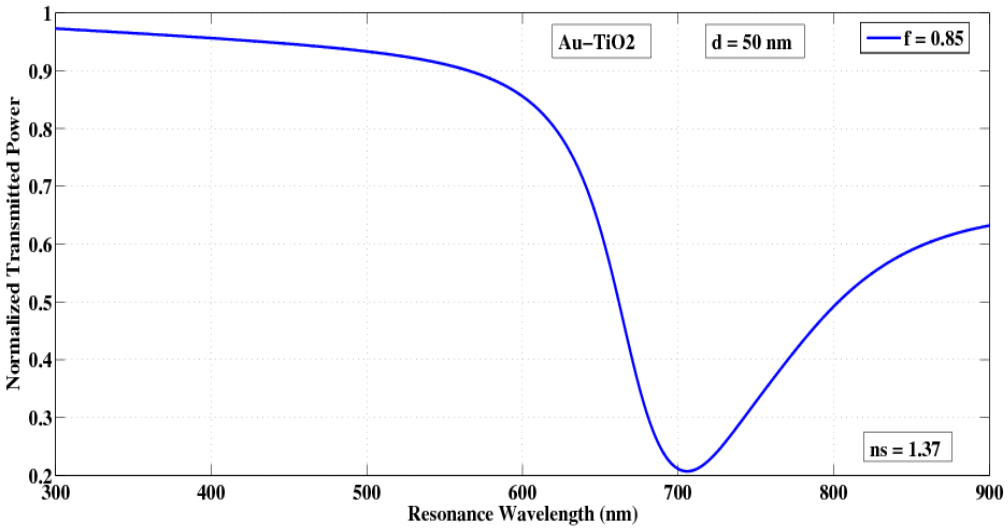

Figure 5.10: Transmittance curve of SPR based fiber optic sensor for 50 nm thick Au-TiO_2 nanocomposite layer with fixed volume fraction of 0.85 for refractive index of sensing medium = 1.37

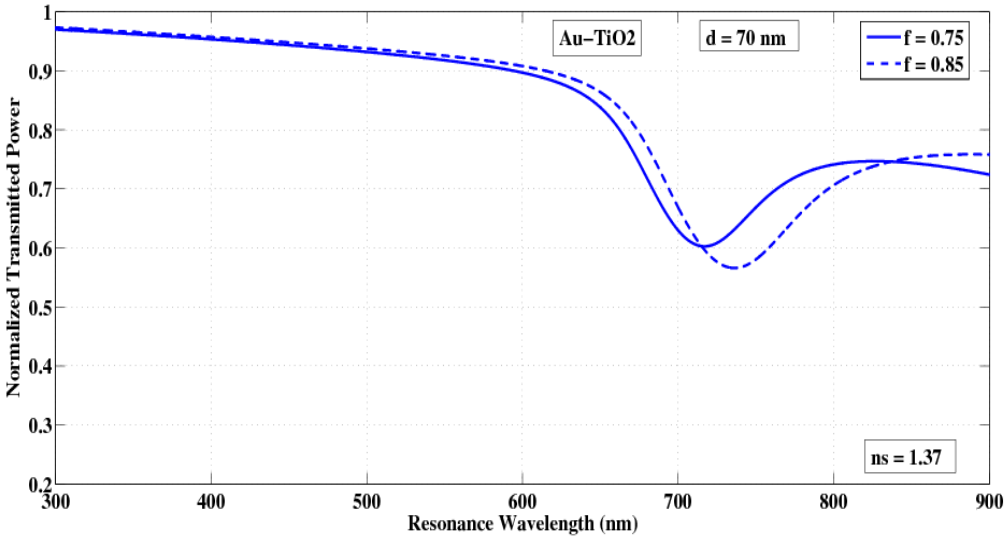

Figure 5.11: Transmittance curves of SPR based fiber optic sensor for 70 nm thick Au-TiO_2 nanocomposite layer with fixed volume fractions of 0.75 and 0.85 for refractive index of sensing medium = 1.37

Likewise, Figs. 5.12 and 5.13 depict the SPR transmittance curves for Au-InN nanocomposite layers holding thicknesses 50 nm with volume fractions of 0.65, 0.75, 0.85 and 70 nm with volume fractions of 0.55, 0.65, 0.75, 0.85 respectively for refractive index of sensing medium = 1.37.

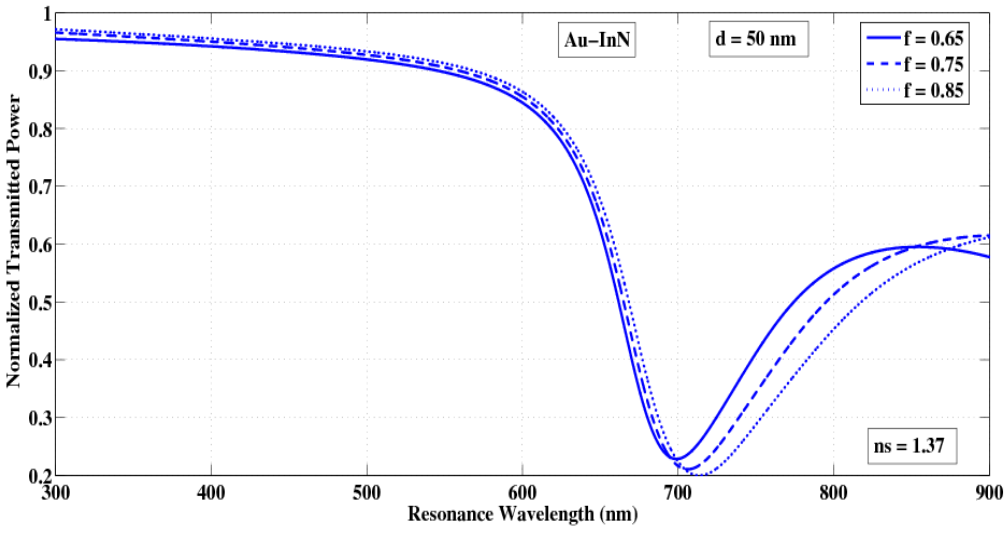

Figure 5.12: Transmittance curves of SPR based fiber optic sensor for 50 nm thick Au-InN nanocomposite layer with fixed volume fractions of 0.65, 0.75 and 0.85 for refractive index of sensing medium = 1.37

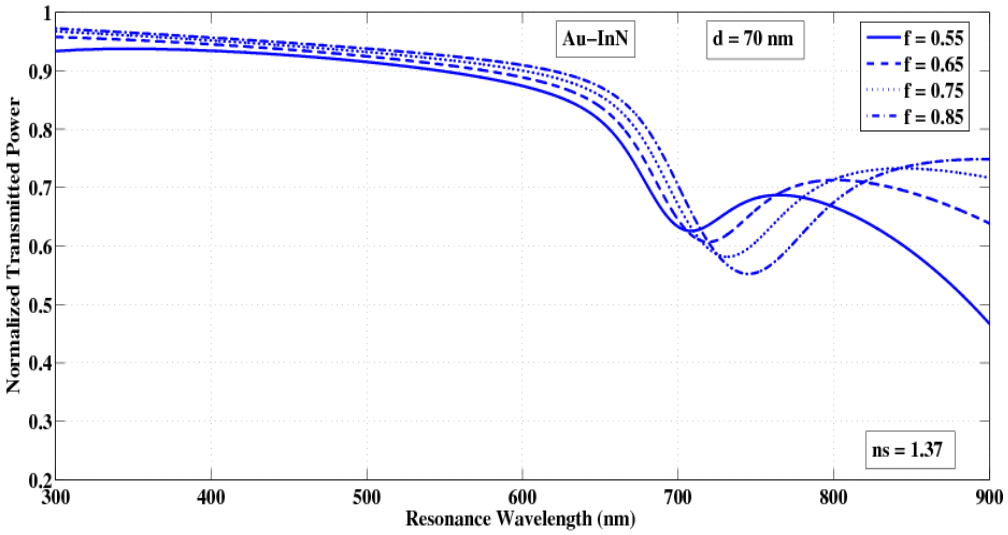

Figure 5.13: Transmittance curves of SPR based fiber optic sensor for 70 nm thick Au-InN nanocomposite layer with fixed volume fractions of 0.55, 0.65, 0.75 and 0.85 for refractive index of sensing medium = 1.37

Furthermore, the optimized thickness of nanocomposite layer as well as optimized volume fraction of nanoparticles needs to be identified in order to achieve the maximum sensitivity from the SPR based fiber optic sensor. The sensitivities of SPR sensor for a number of thicknesses of Au/Ag/Cu-TiO_2 and Au/Ag/Cu-InN nanocomposite layers with various volume fractions are compared in tables 5.1 and 5.2 respectively.

Table 5.1: Comparison of sensitivity of SPR sensor for different thickness values of TiO_2 based various nanocomposite layers

Thickness of nanocomposite layer (nm)	Sensitivity (nm/RIU)											
	Volume fraction of metal nanoparticles = 0.55			Volume fraction of metal nanoparticles = 0.65			Volume fraction of metal nanoparticles = 0.75			Volume fraction of metal nanoparticles = 0.85		
	Nanocomposites			Nanocomposites			Nanocomposites			Nanocomposites		
	Au-TiO_2	Ag-TiO_2	Cu-TiO_2	Au-TiO_2	Ag-TiO_2	Cu-TiO_2	Au-TiO_2	Ag-TiO_2	Cu-TiO_2	Au-TiO_2	Ag-TiO_2	Cu-TiO_2
10	476	451	421	532	513	500	589	540	525	640	615	571
30	1652	1471	1387	1836	1688	1618	2051	1879	1811	2213	2065	1995
50	1758	1480	1393	2064	1739	1638	2356	2017	1902	2636	2301	2168
70	1774	1488	1405	2208	1765	1654	2451	2088	1944	2830	2410	2249

Table 5.2: Comparison of sensitivity of SPR sensor for different thickness values of InN based various nanocomposite layers

Thickness of nanocomposite layer (nm)	Sensitivity (nm/RIU)											
	Volume fraction of metal nanoparticles = 0.55			Volume fraction of metal nanoparticles = 0.65			Volume fraction of metal nanoparticles = 0.75			Volume fraction of metal nanoparticles = 0.85		
	Nanocomposites			Nanocomposites			Nanocomposites			Nanocomposites		
	Au-InN	Ag-InN	Cu-InN	Au-InN	Ag-InN	Cu-InN	Au-InN	Ag-InN	Cu-InN	Au-InN	Ag-InN	Cu-InN
10	479	462	427	542	517	508	598	550	533	648	631	575
30	1673	1542	1452	1857	1702	1690	2058	1911	1815	2221	2083	2024
50	1798	1571	1462	2119	1774	1702	2405	2077	1982	2655	2339	2244
70	1839	1576	1482	2219	1881	1750	2482	2173	2024	2875	2452	2333

It can be noticed from tables 5.1 and 5.2, that the sensitivity of Au/Ag/Cu-InN nanocomposites based SPR sensor for all thicknesses of nanocomposite layer with any volume fraction of nanoparticles is larger than that of Au/Ag/Cu-TiO_2 nanocomposites. Further, table 5.1 clearly reveals that the sensitivity of SPR sensor is maximum (2830 nm/RIU) for 70 nm thick Au-TiO_2 nanocomposite having volume fraction of 0.85 and is minimum (421 nm/RIU) for 10 nm thick Cu-TiO_2 nanocomposite containing volume fraction of 0.55. Similarly, from table 5.2 it is obvious that 70 nm thick Au-InN nanocomposite with volume fraction of 0.85 based SPR sensor demonstrates highest sensitivity (2875 nm/RIU) while, 10 nm thick Cu-InN nanocomposite with volume fraction of 0.55 based SPR sensor displays lowest sensitivity (427 nm/RIU). The variations of sensitivity of Au/Ag/Cu-TiO_2 and Au/Ag/Cu-InN nanocomposite layers based SPR sensor with volume fraction of metal nanoparticles for fixed 10 nm, 30 nm, 50 nm and 70 nm thick nanocomposite layers have been plotted in Figs. 5.14 and 5.15 respectively.

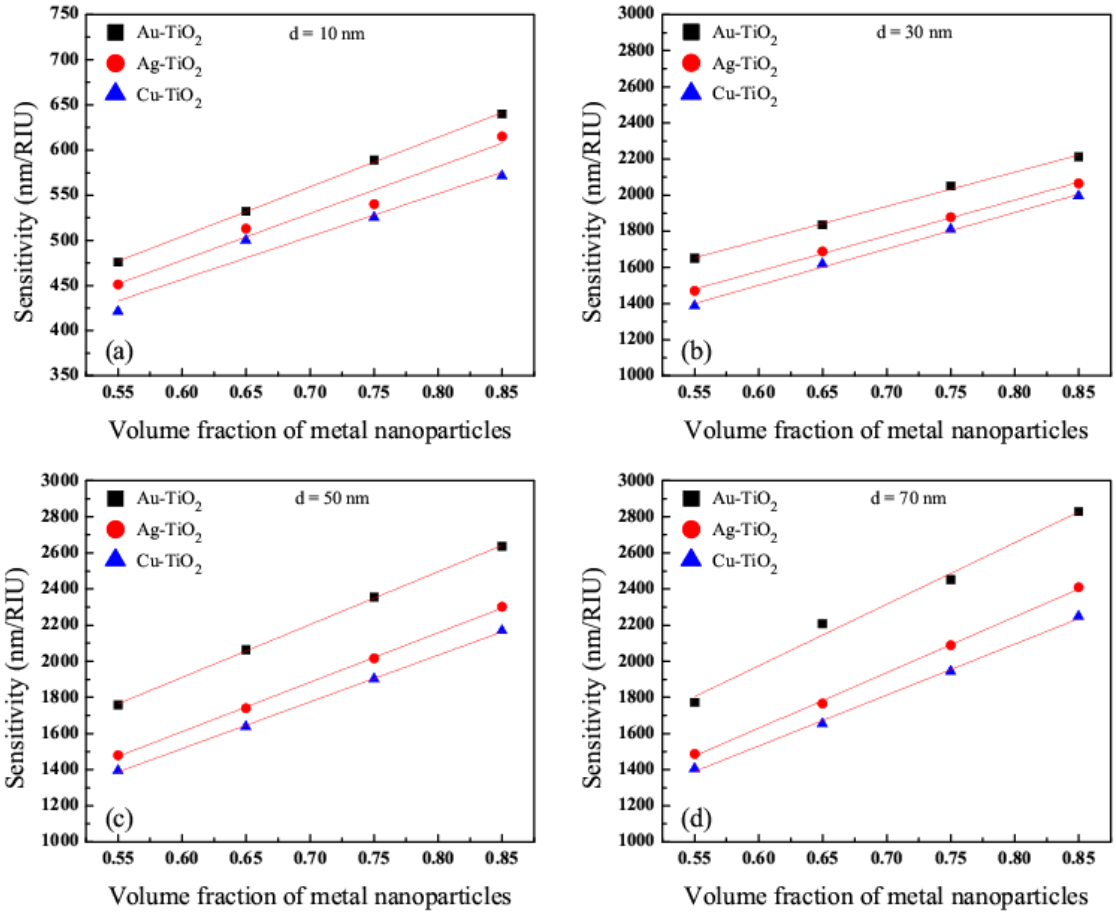

Figure 5.14: Variation of sensitivity with volume fraction of metal nanoparticles in Au-TiO_2, Ag-TiO_2 and Cu-TiO_2 nanocomposites for fixed nanocomposite thickness of (a) 10 nm (b) 30 nm (c) 50 nm and (d) 70 nm

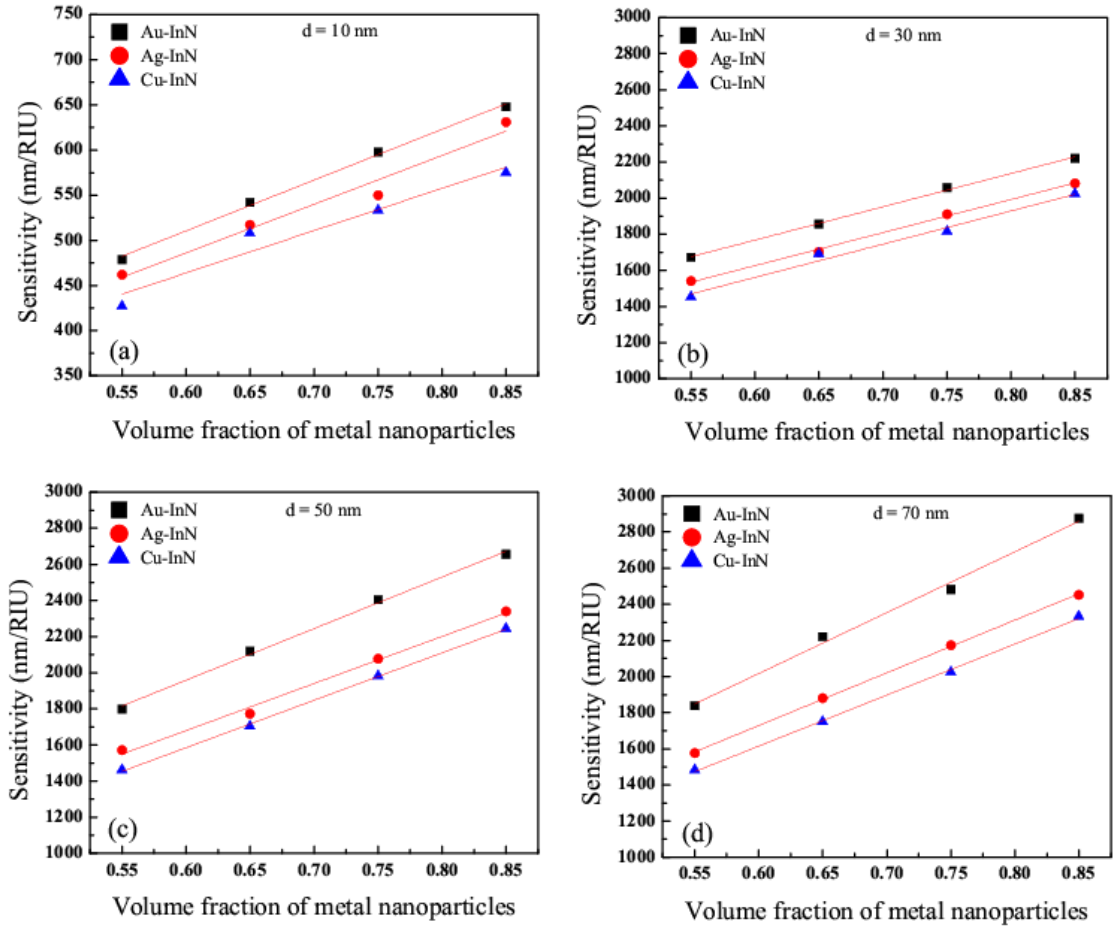

Figure 5.15: Variation of sensitivity with volume fraction of metal nanoparticles in Au-InN, Ag-InN and Cu-InN nanocomposites for fixed nanocomposite thickness of (a) 10 nm (b) 30 nm (c) 50 nm and (d) 70 nm

Figs. 5.14 and 5.15 display the variations of sensitivity of SPR sensor with volume fraction of metal nanoparticles for fixed 10 nm, 30 nm, 50 nm and 70 nm thick Au/Ag/Cu-TiO_2 and Au/Ag/Cu-InN nanocomposite layers respectively. It is clear from both figures that sensitivity of SPR sensor increases linearly with increase in volume fraction of metal nanoparticles for all thicknesses of nanocomposite layers. In addition, the sensitivity of SPR sensor also enhances with increase in thickness of nanocomposite layers for all volume fractions of metal nanoparticles. Further, for a fixed volume fraction of metal nanoparticles and fixed nanocomposite thickness, the sensitivity of sensor is greater for Au nanoparticles based nanocomposites than that of Ag as well as Cu nanoparticles and found to be in the order of Au nanoparticles > Ag nanoparticles > Cu nanoparticles. The reason for this fact can

be ascribed to the real part of K_{sp} as it is responsible for the shifting of resonance condition/wavelength. The Au nanoparticles show higher sensitivity than Ag/Cu nanoparticles because Au illustrates large value of real part of its dielectric function at all wavelengths [103]. Thus, Au nanoparticles in any nanocomposite enhance the shift between resonance wavelengths for a given change of refractive index of the sensing medium and therefore the sensitivity of the sensor increases. Also, the variations of sensitivity of Au/Ag/Cu-TiO_2 and Au/Ag/Cu-InN nanocomposite layers based SPR sensor with thickness of nanocomposite layer for fixed 0.55, 0.65, 0.75 and 0.85 volume fractions of metal nanoparticles have been shown in Figs. 5.16 and 5.17 respectively.

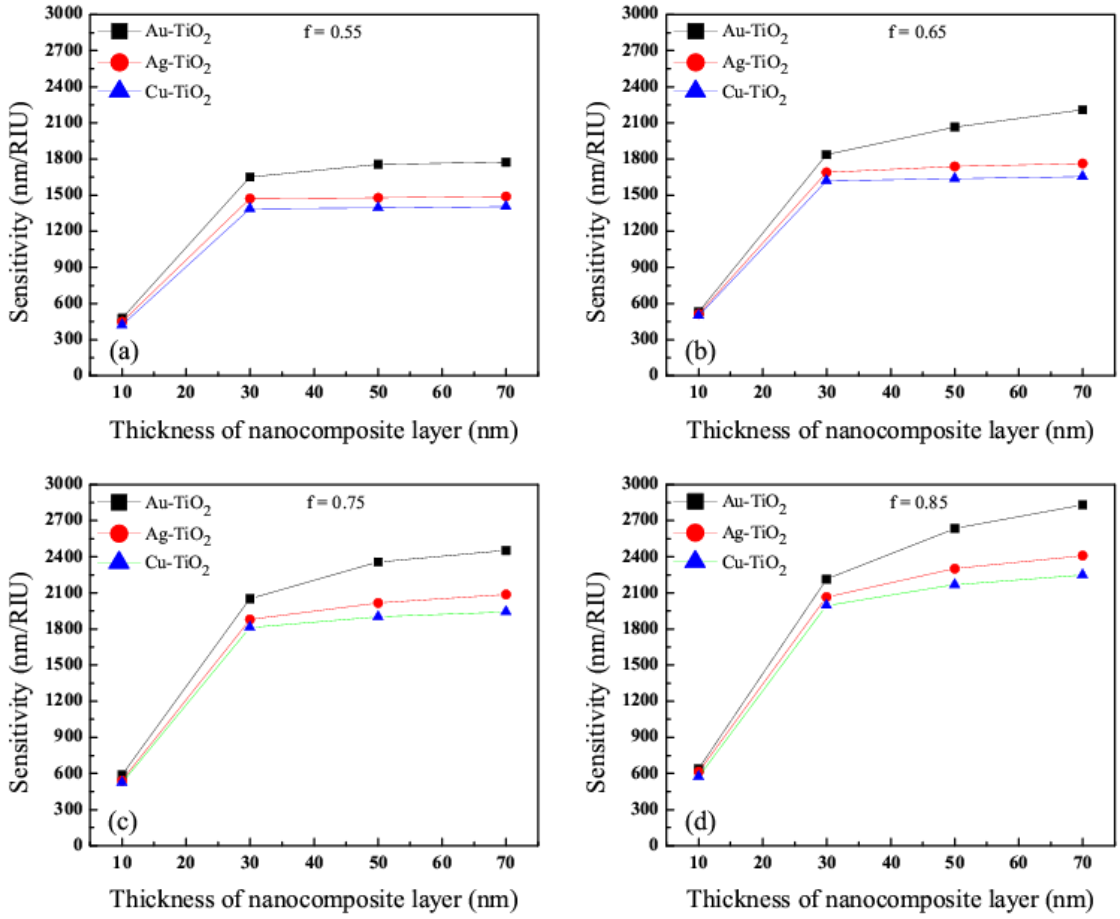

Figure 5.16: Variation of sensitivity with thickness of Au-TiO_2, Ag-TiO_2 and Cu-TiO_2 nanocomposites for fixed (a) 0.55 (b) 0.65 (c) 0.75 and (d) 0.85 volume fraction of metal nanoparticles

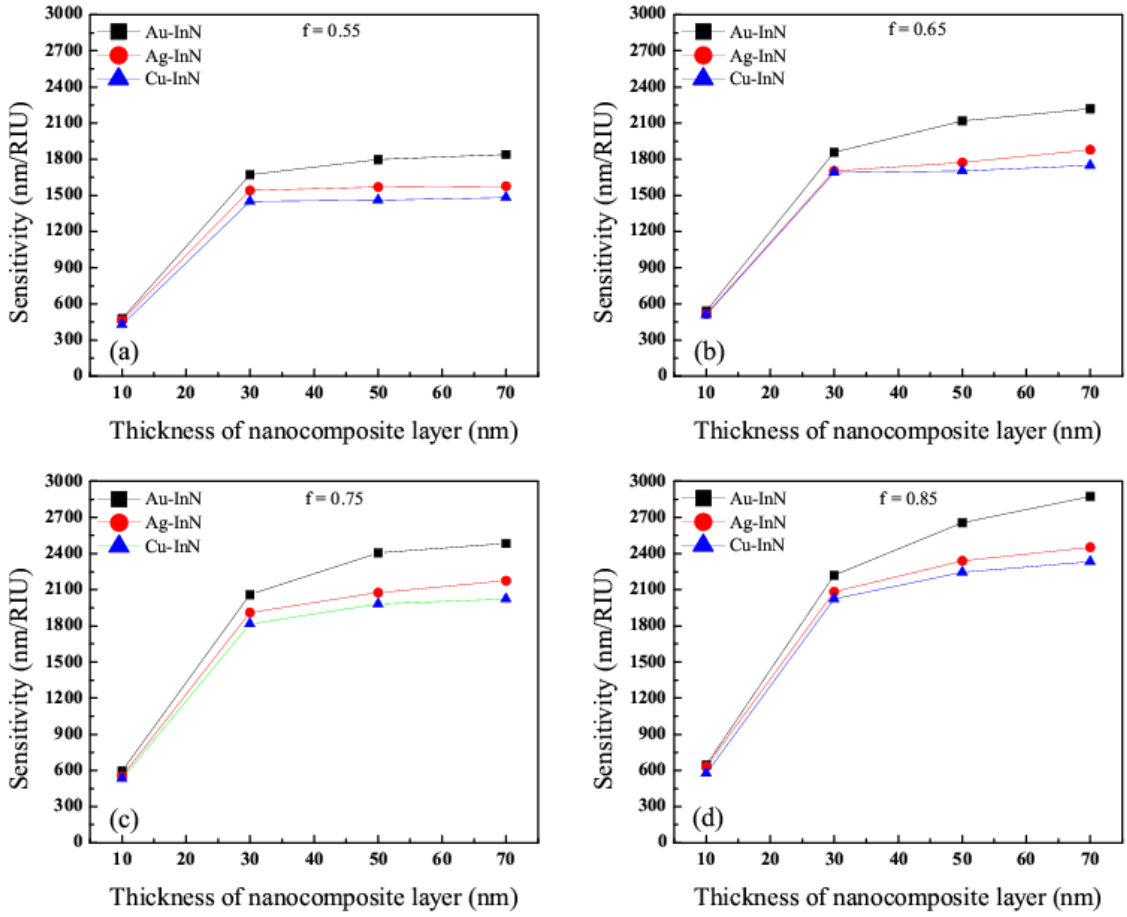

Figure 5.17: Variation of sensitivity with thickness of Au-InN, Ag-InN and Cu-InN nanocomposites for fixed (a) 0.55 (b) 0.65 (c) 0.75 and (d) 0.85 volume fraction of metal nanoparticles

Figs. 5.16 and 5.17 show the variations of sensitivity of SPR sensor with thickness of Au/Ag/Cu-TiO_2 and Au/Ag/Cu-InN nanocomposite layers for fixed 0.55, 0.65, 0.75 and 0.85 volume fractions of metal nanoparticles respectively. It is again evident from both figures that increase in thickness of nanocomposite layer increases the sensitivity of SPR sensor for all volume fractions of metal nanoparticles. Once again, the sensitivity of sensor enhances with increase in volume fractions of metal nanoparticles for all thicknesses of nanocomposites layers. Furthermore, for a fixed nanocomposite thickness and fixed volume fraction of metal nanoparticles, the sensitivity of sensor is larger for Au nanoparticles based nanocomposites

than that of Ag as well as Cu nanoparticles and originated to be in the order of Au nanoparticles > Ag nanoparticles > Cu nanoparticles.

Thus from table 5.1, it is clear that SPR based fiber optic sensor exhibits larger sensitivity of 2830 nm/RIU for 70 nm thick Au-TiO_2 nanocomposite with volume fraction of 0.85 and smaller sensitivity of 421 nm/RIU for 10 nm thick Cu-TiO_2 nanocomposite with volume fraction of 0.55. On the other hand table 2 discloses that 70 nm thick Au-InN nanocomposite with volume fraction of 0.85 based SPR sensor provides the highest sensitivity of 2875 nm/RIU whereas, 10 nm thick Cu-InN nanocomposite with volume fraction of 0.55 based SPR sensor shows lowest sensitivity of 427 nm/RIU. Consequently, among all the nanocomposites used, the sensor based on 70 nm thick Au-InN nanocomposite with volume fraction of 0.85 presents the highest sensitivity of 2875 nm/RIU. Therefore, it is concluded that the optimized thickness and optimized volume fraction (of metal nanoparticles) for Au-InN nanocomposite are 70 nm and 0.85 respectively as 70 nm thick Au-InN nanocomposite with volume fraction of 0.85 based SPR sensor possesses maximum sensitivity (2875 nm/RIU).

5.4 Conclusions

A SPR based fiber optic sensor with nanocomposite layer has been theoretically studied. Nanocomposites consisting of Au, Ag and Cu nanoparticles with their varying volume fractions embedded in host dielectric matrices of TiO_2 and InN are considered. The sensitivity of Au/Ag/Cu-InN nanocomposites based SPR sensor for all thicknesses of nanocomposites with any volume fraction of metal nanoparticles has been observed to be greater than that of Au/Ag/Cu-TiO_2 nanocomposites. Also, the sensitivity of SPR sensor increases with increase in both thickness of nanocomposites and volume fraction of metal nanoparticles. In addition, for a fixed nanocomposite thickness and fixed volume fraction of metal nanoparticles, the sensitivity of sensor is larger for Au nanoparticles based nanocomposites than that of Ag and Cu nanoparticles. The SPR based fiber optic sensor with 70 nm thick Au-InN nanocomposite having volume fraction of 0.85 reveals maximum sensitivity of 2875 nm/RIU.

CHAPTER 6

SURFACE PLASMON RESONANCE BASED FIBER OPTIC SENSOR USING INDIUM NITRIDE

6.1 Introduction

In recent times, research on plasmonics has been extended to IR spectral region beyond the visible region. This leads to explore some new materials which could satisfy the surface plasmon resonance condition at lower plasma frequencies. Group III-nitrides are usually wide band gap semiconducting materials, which are suitable for the applications in optical devices and high power electronics [167]. Among these nitrides, only indium nitride (InN) is observed to be a capable material for optoelectronics and other devices [168,169]. This chapter deals with the theoretical study of a SPR based fiber optic sensor using InN. InN (band gap ~ 0.7-1.1 eV) has been found to be an attention-grabbing material because of its numerous advanced properties over other group-III nitrides, metals and transparent conducting oxides. Since, InN has a smaller electron effective mass than those of other III-nitrides, it shows a higher mobility and higher saturation velocity, which makes it attractive and useful for a number of electronic applications. In addition, InN is shown to have vast remarkable applications in various research fields like high speed transistor devices [170], solar cell industries [171] and optoelectronic devices for optical fiber communications [169]. Qian et al. showed that InN thin films are suitable for application of plasma filters with different carrier concentration, mobility and film thickness [172]. InN shows good performance as a plasma filter material for widely employed GaSb or GaInAsSb photovoltaic cells. InN is a potential candidate for plasmonics based sensing applications not only in IR but also in THz regimes because of its smaller magnitudes of real permittivity than those of metals [135]. InN possesses lower value of plasma frequency compared to that of metals, displaying greater confinement of surface plasmon waves to the interface and greater field enhancement in IR and THz regimes. Recently, Lu et al. reported the utilization of InN as an appropriate material for biosensing, owing to its high superficial electron concentration [136].

Besides, InN dielectric overlay has been used to demonstrate Al-InN bilayers based SPR sensor experimentally [173].

In the present chapter, a SPR based fiber optic sensor with InN layer has been proposed and theoretically analyzed. The surface plasmon resonance formed by coupling of evanescent light to surface plasmons is used as the sensing method. The wavelength interrogation scheme is used for the analysis of SPR sensor. SPR sensor with InN layer is shown to possess high sensitivity in the near infrared region of spectrum. For the best sensing performance of SPR sensor, the thickness of InN layer has also been optimized. The optimized thickness of InN layer of SPR sensor is unveiled to be 70 nm. 70 nm thick InN layer based fiber optic SPR sensor exhibits high sensitivity of 4493 nm/RIU.

6.2 Theory

The SPR sensing is based on the principle of attenuated total reflection (ATR) with Kretschmann configuration. In the proposed SPR based fiber optic sensor, the sensing system consisting of a fiber core-InN layer-sensing medium is considered as shown in Fig. 6.1.

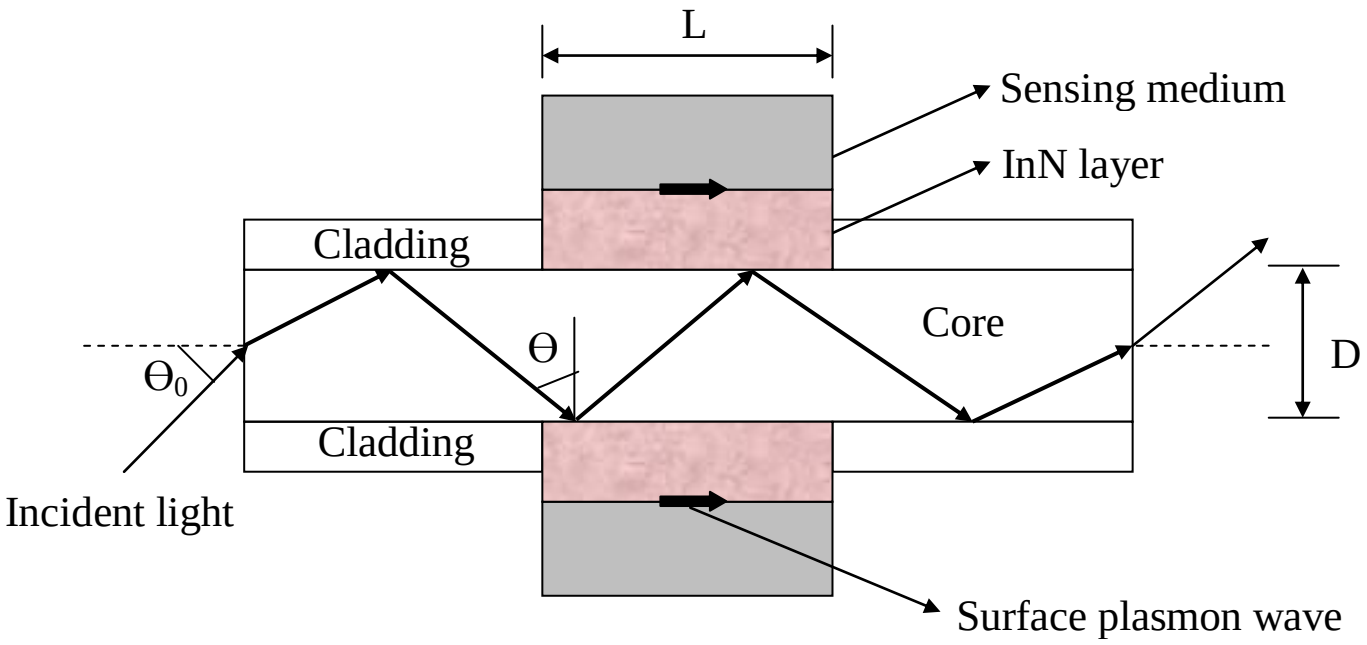

Figure 6.1: Schematic diagram of SPR based fiber optic sensor with InN layer

The plastic cladding around the core from the middle portion of a step index multimode plastic clad silica (PCS) fiber (Numerical aperture = 0.24 and fiber core diameter = 600 μm) is removed and is then coated with a thin InN layer. This InN layer is finally surrounded by the sensing medium. The light from a broadband (polychromatic) source is launched into one of the ends of the optical fiber with proper optics and the transmitted light is detected at the other end of the optical fiber.

6.2.1 Layer I (Fiber core)

This layer is made of core of optical fiber. The core of the optical fiber is assumed to be made of fused silica. The refractive index of fused silica varies with wavelength according to Sellmeier dispersion relation as,

$$n_1(\lambda) = \sqrt{1 + \frac{a_1\lambda^2}{\lambda^2 - b_1^2} + \frac{a_2\lambda^2}{\lambda^2 - b_2^2} + \frac{a_3\lambda^2}{\lambda^2 - b_3^2}} \tag{6.1}$$

Where, λ is the wavelength in μm and a_1, a_2, a_3, b_1, b_2 and b_3 are Sellmeier coefficients. The values of these coefficients are given as, a_1 = 0.6961663, a_2 = 0.4079426, a_3 = 0.8974794, b_1 = 0.0684043 μm, b_2 = 0.1162414 μm and b_3 = 9.896161 μm [141].

6.2.2 Layer II (InN layer)

This layer is made of InN. The dielectric constant of InN is written according to Drude model as [166],

$$\varepsilon(\omega) = \varepsilon_\infty \left[1 + \frac{(\omega_{LO}^2 - \omega_{TO}^2)}{(\omega_{LO}^2 - \omega^2 - i\omega\gamma)} - \frac{\omega_p^2}{(\omega^2 + i\omega\Gamma)} \right] \tag{6.2}$$

Here, ε_∞ is the high frequency dielectric constant, ω_{LO} and ω_{TO} are LO (Longitudinal Optical) and TO (Transverse Optical) frequencies of phonon mode, ω_p is the plasma frequency, γ and Γ are the two corresponding damping constants. Five sets of values of

various parameters used for InN are: ε_∞ = 6.7, ω_p = 845 cm^{-1}, Γ = 117 cm^{-1}; ε_∞ = 6.7, ω_p = 1170 cm^{-1}, Γ = 64 cm^{-1}; ε_∞ = 6.7, ω_p = 1940 cm^{-1}, Γ = 260 cm^{-1}; ε_∞ = 7.5, ω_p = 4100 cm^{-1}, Γ = 1382 cm^{-1} and ε_∞ = 7.5, ω_p = 5480 cm^{-1}, Γ = 1054 cm^{-1} [166]. Further for each set, the values of LO, TO frequencies and damping constants considered are: ω_{LO} = 590 cm^{-1}, ω_{TO} = 450 cm^{-1} and γ = 120 cm^{-1}.

6.2.3 Layer III (Sensing medium)

This layer is made of sensing medium. The dielectric constant of the sensing medium is ε_s. If n_s is the refractive index of the sensing medium, then $\varepsilon_s = n_s^2$. The resonance condition for excitation of surface plasmon wave is given as,

$$\frac{2\pi}{\lambda} n_1 \sin\theta = \mathrm{Re}\{K_{sp}\} \tag{6.3}$$

Where, $K_{sp} = \frac{\omega}{c}\sqrt{\frac{\varepsilon_m \varepsilon_s}{\varepsilon_m + \varepsilon_s}} = \frac{2\pi}{\lambda}\sqrt{\frac{\varepsilon_m n_s^2}{\varepsilon_m + n_s^2}}$ is the propagation constant of the surface plasmon wave and *c* is the speed of light in vacuum. The left hand side of Eq. (6.3) denotes the propagation constant of the light incident at an angle θ and the right hand side shows the real part of the propagation constant of the surface plasmon wave.

6.2.4 Transmitted Power

The expression for the reflection coefficient (reflectance) of p-polarized incident light is obtained by using the matrix method for N-layer model as mentioned in appendix A. Considering that all the guided rays are launched in the fiber using a collimated source and a microscope objective, the angular power distribution of rays guided in the fiber is given as [18],

$$dP \propto \frac{n_1^2 \sin\theta\cos\theta}{(1 - n_1^2\cos^2\theta)^2} d\theta \tag{6.4}$$

Where, θ is the angle of the ray with the normal to the core-cladding interface. Also, n_1 is the refractive index of the core of the fiber. To calculate the effective transmitted power, the reflectance (R_p) for a single reflection is raised to the power of the number of reflections the specific propagating angle undergoes with the sensor interface. Hence, for p-polarized light, the generalized expression for the normalized transmitted power in an optical fiber based SPR sensor will be given as,

$$P_{trans} = \frac{\int_{\theta_{cr}}^{\pi/2} R_p^{N_{ref}(\theta)} \frac{n_1^2 \sin\theta\cos\theta}{(1-n_1^2\cos^2\theta)^2} d\theta}{\int_{\theta_{cr}}^{\pi/2} \frac{n_1^2 \sin\theta\cos\theta}{(1-n_1^2\cos^2\theta)^2} d\theta} \tag{6.5}$$

Where, $N_{ref}(\theta) = \frac{L}{D\tan\theta}$ (6.6)

And, $\theta_{cr} = \sin^{-1}\left(\frac{n_{cl}}{n_1}\right)$ (6.7)

Here, $N_{ref}(\theta)$ is the total number of reflections performed by a ray making an angle θ with the normal to the core-metal layer interface in the sensing region. L and D are the length of the exposed sensing region and the fiber core diameter respectively. Also, θ_{cr} is the critical angle of the fiber and n_{cl} is the refractive index of the cladding of the fiber.

6.2.5 Sensitivity

Resonance wavelength (λ_{res}) is determined corresponding to the refractive index of the sensing medium (n_s) in the SPR sensor based on wavelength interrogation. If the refractive index of the sensing medium is altered by δn_s, the resonance wavelength shifts by $\delta\lambda_{res}$. The sensitivity (S_n) of a SPR sensor with wavelength interrogation is defined as [64],

$$S_n = \frac{\delta\lambda_{res}}{\delta n_s} \tag{6.8}$$

6.3 Results and discussion

For numerical calculations, the refractive index of the sensing medium is changed from 1.30 to 1.40 in steps of 0.02 and following values of the parameters have been used:
Numerical aperture of the fiber = 0.24, fiber core diameter D = 600 μm, length of the exposed sensing region L = 15 mm.

To optimize the thickness of InN layer, the transmitted output power of SPR based fiber optic sensor has been calculated for various thicknesses (40 nm to 100 nm) of InN layer. It is to be noted here that the transmitted output power of SPR sensor has also been calculated for lower thicknesses i.e. 5-35 nm of InN layer. However, the SPR sensor based on lower thicknesses (5-35 nm) of InN layer has not been discussed in the present study because the proper SPR transmittance curves (i.e. clear resonance dips) have not been observed for these thicknesses of InN layers. Further, for first three sets of values of different parameters i.e. ε_∞ = 6.7, ω_p = 845 cm^{-1}, Γ = 117 cm^{-1}; ε_∞ = 6.7, ω_p = 1170 cm^{-1}, Γ = 64 cm^{-1}; ε_∞ = 6.7, ω_p = 1940 cm^{-1}, Γ = 260 cm^{-1} [166], the appropriate resonance dips have not been obtained for large number of thicknesses (40-100 nm) of InN layer. As a result, these three sets of values of various parameters for InN have not been taken in to account in the current discussion. Therefore, two sets of values of parameters i.e. ε_∞ = 7.5, ω_p = 4100 cm^{-1}, Γ = 1382 cm^{-1} (say "Sensor A") and ε_∞ = 7.5, ω_p = 5480 cm^{-1}, Γ = 1054 cm^{-1} (say "Sensor B") [166] have been used to calculate the transmitted output power of SPR sensor for various thicknesses i.e. 40 nm to 100 nm of InN layer. The resonance wavelengths of SPR based sensors A and B for various thicknesses of InN layer are determined and are mentioned in tables 6.1 and 6.2 respectively.

Table 6.1: Resonance wavelength of SPR based Sensor A for different values of thickness of InN layer

Thickness of InN layer (nm)	Resonance wavelength (nm) for various refractive indices of sensing medium					
	1.30	1.32	1.34	1.36	1.38	1.40
40	625	655	700	755	835	960
45	700	735	780	845	930	1065
50	770	810	860	930	1025	1165
55	840	885	935	1010	1110	1260
60	905	950	1010	1085	1190	1345
65	970	1020	1080	1155	1265	1420
70	1030	1080	1145	1225	1335	1490
75	1090	1140	1205	1285	1395	1550
80	1145	1200	1265	1345	1455	1600
85	1200	1255	1320	1400	1505	1650
90	1250	1305	1370	1450	1555	1690
95	1295	1350	1415	1495	1600	1725
100	1340	1395	1460	1540	1635	1760

Table 6.2: Resonance wavelength of SPR based Sensor B for different values of thickness of InN layer

Thickness of InN layer (nm)	Resonance wavelength (nm) for various refractive indices of sensing medium					
	1.30	1.32	1.34	1.36	1.38	1.40
40	605	635	675	725	795	895
45	675	705	745	800	875	975
50	735	770	815	870	945	1050
55	795	830	875	935	1010	1110
60	850	890	935	990	1065	1160
65	905	940	985	1045	1115	1205
70	950	990	1035	1090	1155	1240
75	995	1030	1075	1130	1195	1275
80	1035	1070	1115	1165	1230	1300
85	1070	1110	1150	1200	1255	1325
90	1105	1140	1180	1230	1280	1340
95	1135	1170	1210	1255	1300	1360
100	1165	1200	1235	1275	1320	1375

From table 6.1, it is obvious that the shift in resonance wavelength of sensor A is highest for 70 nm thick InN layer and lowest for 40 nm thick InN layer as the refractive index of sensing medium varies from 1.30 to 1.40. Similarly, it can be seen from table 6.2 that the sensor B exhibits maximum shift in resonance wavelength for 55 nm thick InN layer and minimum shift in resonance wavelength for 100 nm thick InN layer as the refractive index of sensing medium changes from 1.30 to 1.40. Thus, the shifts in resonance wavelength of both sensors A and B are different for different thicknesses of InN layer. The variations of resonance wavelength of sensors A and B with refractive index of sensing medium for various thicknesses of InN layer have been shown in Figs. 6.2-6.5.

Fig. 6.2 shows the plots of resonance wavelength of sensor A with refractive index of sensing medium for different thicknesses i.e. 40 nm, 45 nm, 50 nm, 55 nm, 60 nm, 65 nm and 70 nm of InN layer.

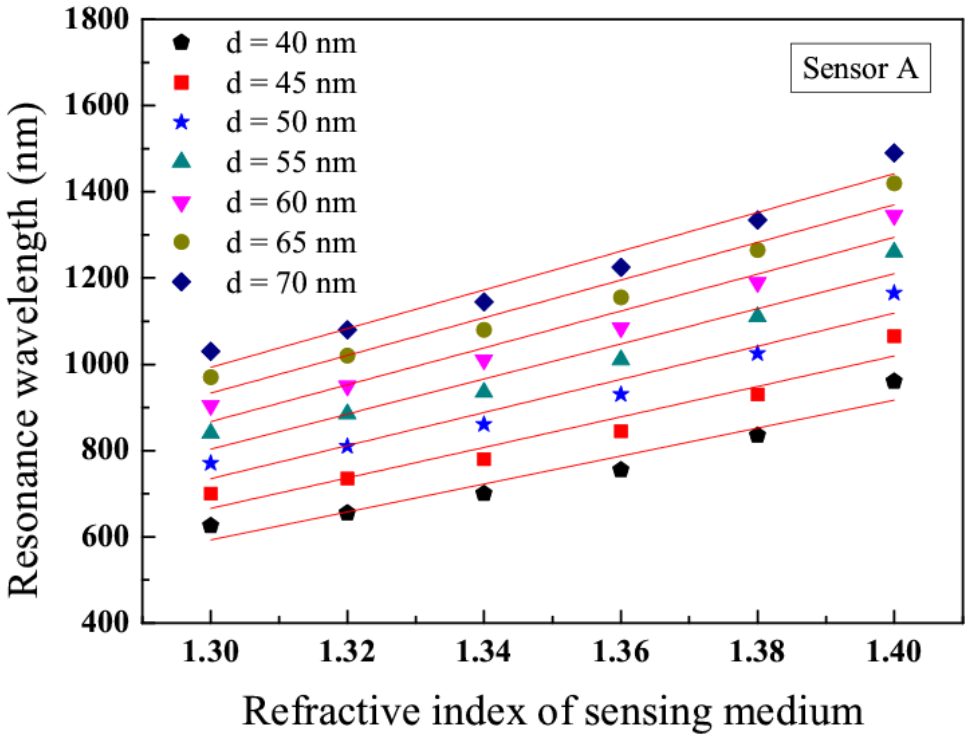

Figure 6.2: Variations of resonance wavelength of the SPR based sensor A with refractive index of sensing medium for different thickness values (40 nm to 70 nm) of InN layer

Similarly, Fig. 6.3 displays the variations of resonance wavelength of sensor A with refractive index of sensing medium for various thicknesses i.e. 75 nm, 80 nm, 85 nm, 90 nm, 95 nm and 100 nm of InN layer.

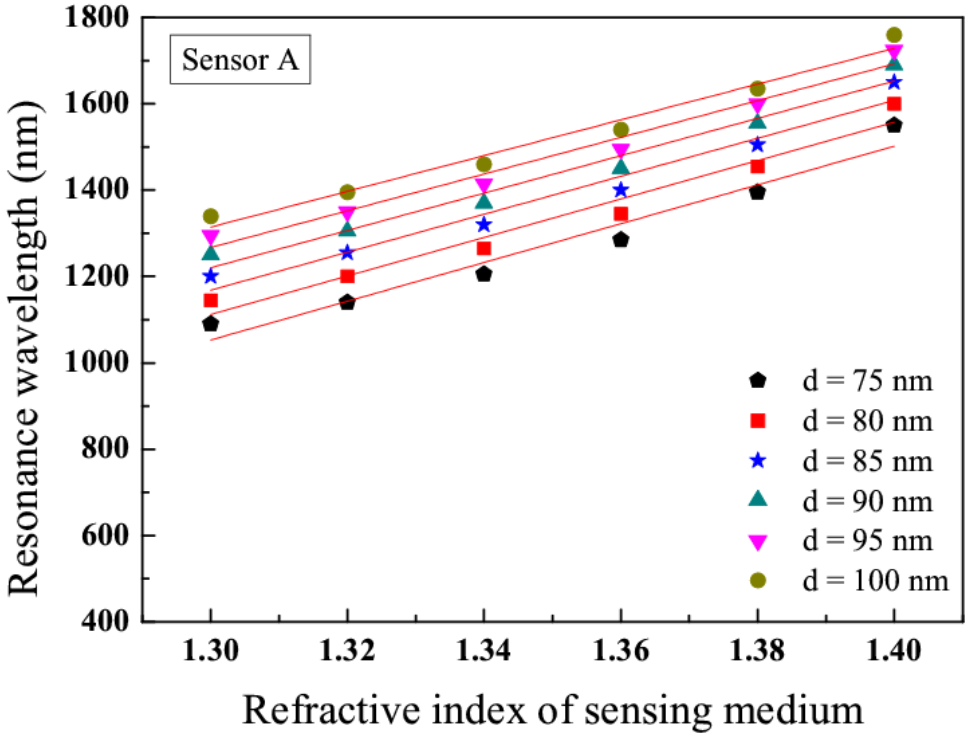

Figure 6.3: Variations of resonance wavelength of the SPR based sensor A with refractive index of sensing medium for different thickness values (75 nm to 100 nm) of InN layer

Likewise, Fig. 6.4 illustrates the variations of resonance wavelength of sensor B with refractive index of sensing medium for a range of thicknesses i.e. 40 nm, 45 nm, 50 nm, 55 nm, 60 nm, 65 nm and 70 nm of InN layer.

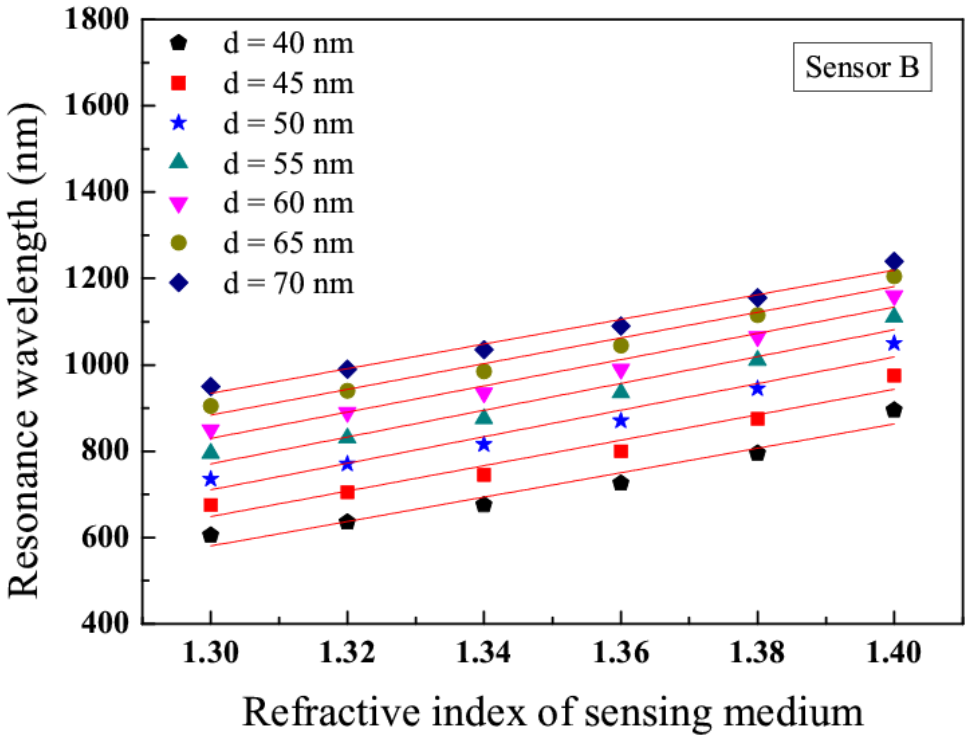

Figure 6.4: Variations of resonance wavelength of the SPR based sensor B with refractive index of sensing medium for different thickness values (40 nm to 70 nm) of InN layer

In the same way, Fig. 6.5 reveals the plots of resonance wavelength of sensor B with refractive index of sensing medium for different thicknesses i.e. 75 nm, 80 nm, 85 nm, 90 nm, 95 nm and 100 nm of InN layer.

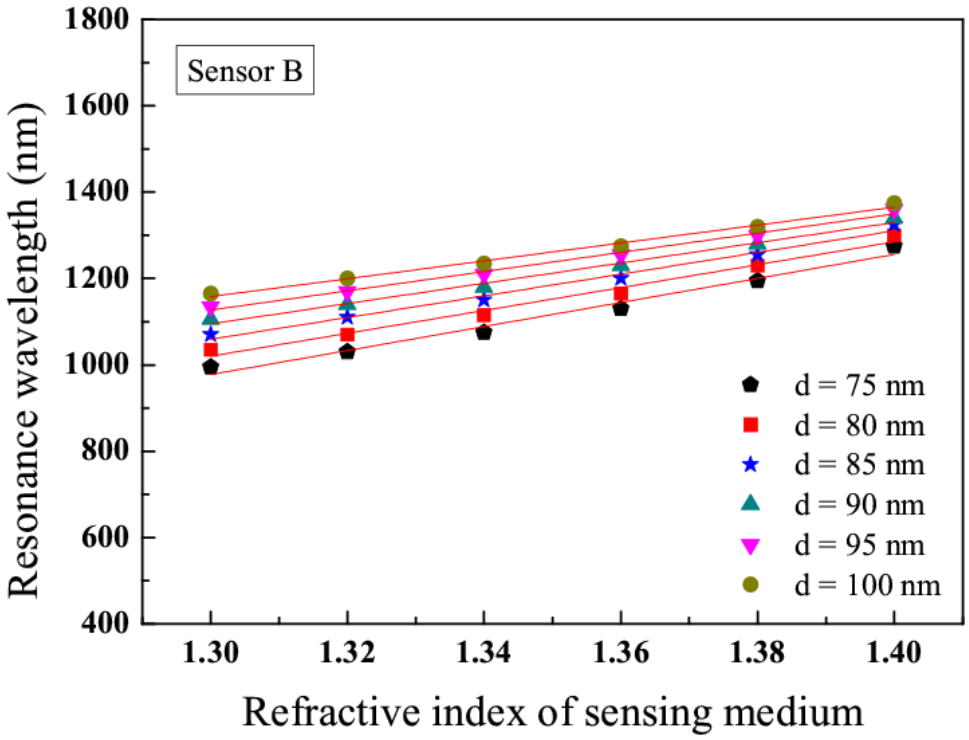

Figure 6.5: Variations of resonance wavelength of the SPR based sensor B with refractive index of sensing medium for different thickness values (75 nm to 100 nm) of InN layer

It can be seen from these figures that the resonance wavelengths of both sensors A and B for different thicknesses (40 nm to 100 nm) of InN layer increases linearly with increase in refractive index of the sensing medium. The variations of resonance wavelength with refractive index of sensing medium for all thicknesses of InN layer pursue the similar outfit for both sensors A and B. Further, the shifts in resonance wavelength for all these cases are almost linear over the entire range of refractive indices (1.30 to 1.40) of the sensing medium for each sensor. To find the maximum value of sensitivity of both sensors, it will be essential to find the appropriate thickness of InN layer. The sensitivities of both sensors A and B for a range of thicknesses of InN layer are compared in table 6.3.

Table 6.3: Comparison of sensitivities of SPR based Sensors A and B for different values of thickness of InN layer

Thickness of InN layer (nm)	Sensitivity (nm/RIU)	
	Sensor A	Sensor B
40	3243	2829
45	3536	2950
50	3843	3079
55	4071	3107
60	4279	3043
65	4371	2979
70	4493	2857
75	4492	2786
80	4457	2650
85	4400	2514
90	4329	2350
95	4257	2229
100	4143	2071

It can be observed from table 6.3, that the sensitivity of sensor A is greatest (4493 nm/RIU) for 70 nm thick InN layer and is least (3243 nm/RIU) for 40 nm thick InN layer. In the same way, the sensitivity of sensor B is maximum (3107 nm/RIU) for 55 nm thick InN layer and is minimum (2071 nm/RIU) for 100 nm thick InN layer. The variations of sensitivity of both sensors A and B with thickness of InN layer have been shown in Fig. 6.6.

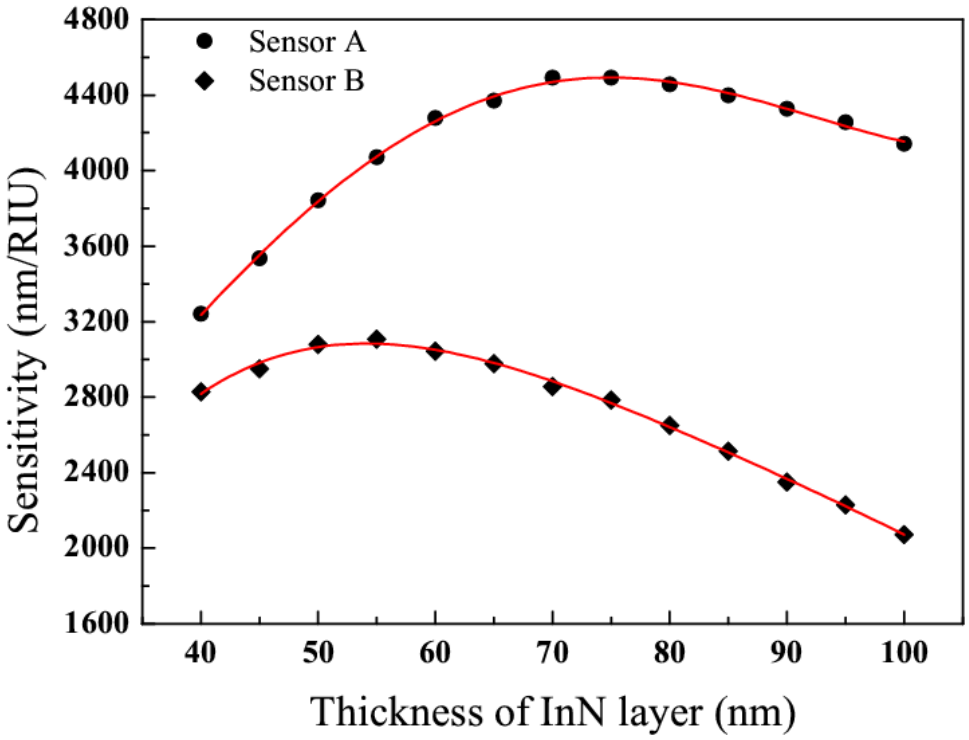

Figure 6.6: Variations of sensitivity of the SPR based sensors A and B with thickness of InN layer

Fig. 6.6 depicts the variations of sensitivity of SPR based sensors A and B with thickness of InN layer. It is evident that the sensitivity of sensor A enhances initially as the thickness of InN layer increases from 40 nm to 70 nm and finally it starts reducing as the thickness of InN layer is further increased from 70 nm to 100 nm. Similarly, the sensitivity of sensor B increases in the beginning as the thickness of InN layer increases from 40 nm to 55 nm and later it starts falling as the thickness of InN layer is again increased from 55 nm to 100 nm. The sensitivities of both sensors enhance initially with increase in thickness of InN layer because the thin layer of InN allows huge interaction between surface plasmon mode and the fiber mode, resulting in large absorption of light power by the sensing medium around resonance wavelength. This results in decrease in the normalized transmitted power and hence increases the sensitivities of the sensors. Additionally, it can be viewed from Fig. 6.6 and table 6.3 that sensors A and B exhibit maximum sensitivities of 4493 nm/RIU and 3107 nm/RIU for 70 nm and 55 nm thick InN layers respectively. Thus, the optimized thicknesses of InN layer for sensors A and B are found to be 70 nm and 55 nm respectively. Furthermore,

sensor A displays good sensing behavior than sensor B for all thicknesses of InN layer. Apart from this, the operating range of InN coated both SPR sensors A and B are in the near infrared region of spectrum, which is an additional advantage of using InN. Therefore, in devising a SPR based fiber optic sensor with high sensitivity, one should prefer Sensor A parameters values (i.e. ε_∞ = 7.5, ω_p = 4100 cm^{-1}, Γ = 1382 cm^{-1}) [166] together with appropriate thickness of InN layer. Hence, taking all these facts in to consideration, it is concluded that 70 nm thick InN layer based fiber optic SPR sensor with various parameter values (ε_∞ = 7.5, ω_p = 4100 cm^{-1}, Γ = 1382 cm^{-1}) exhibits good sensing performance with high sensitivity of 4493 nm/RIU. The SPR transmittance curves of sensor A for different thicknesses of InN layer have also been plotted in Figs. 6.7-6.10 for various refractive indices of the sensing medium.

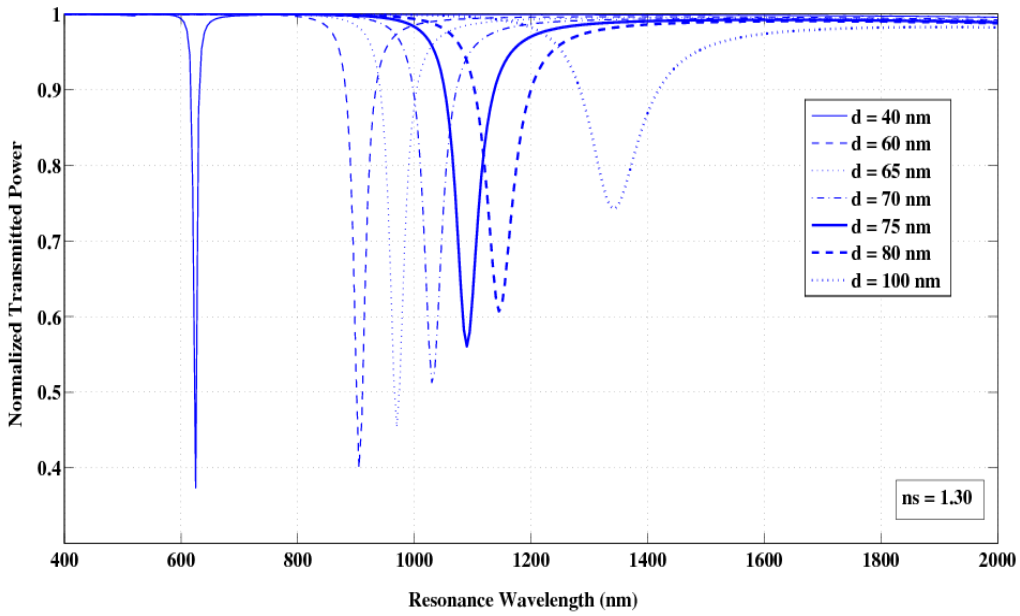

Figure 6.7: Transmittance curves of SPR based sensor A for different thickness values of InN layer for refractive index of sensing medium = 1.30

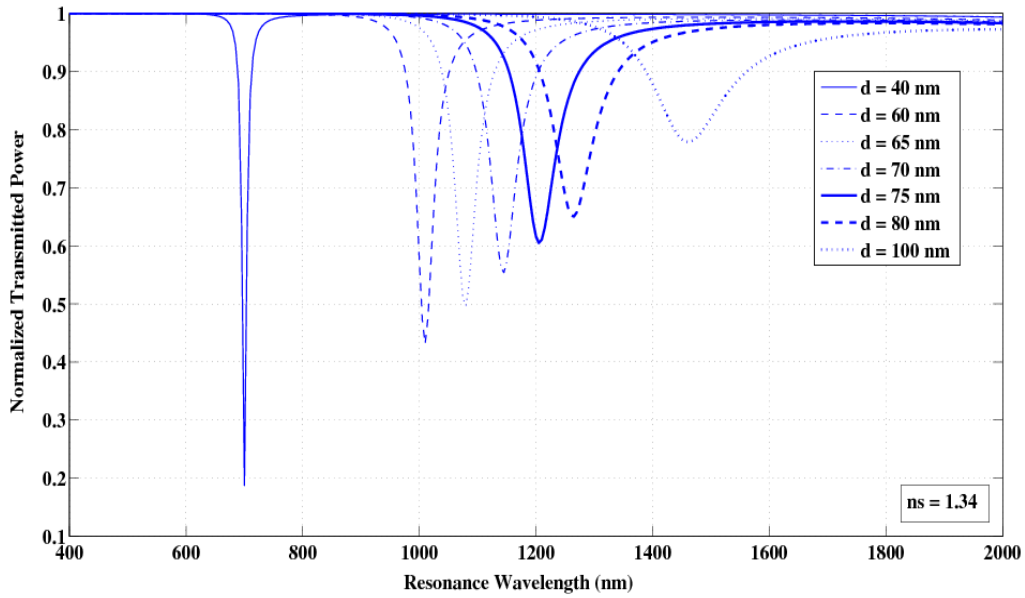

Figure 6.8: Transmittance curves of SPR based sensor A for different thickness values of InN layer for refractive index of sensing medium = 1.34

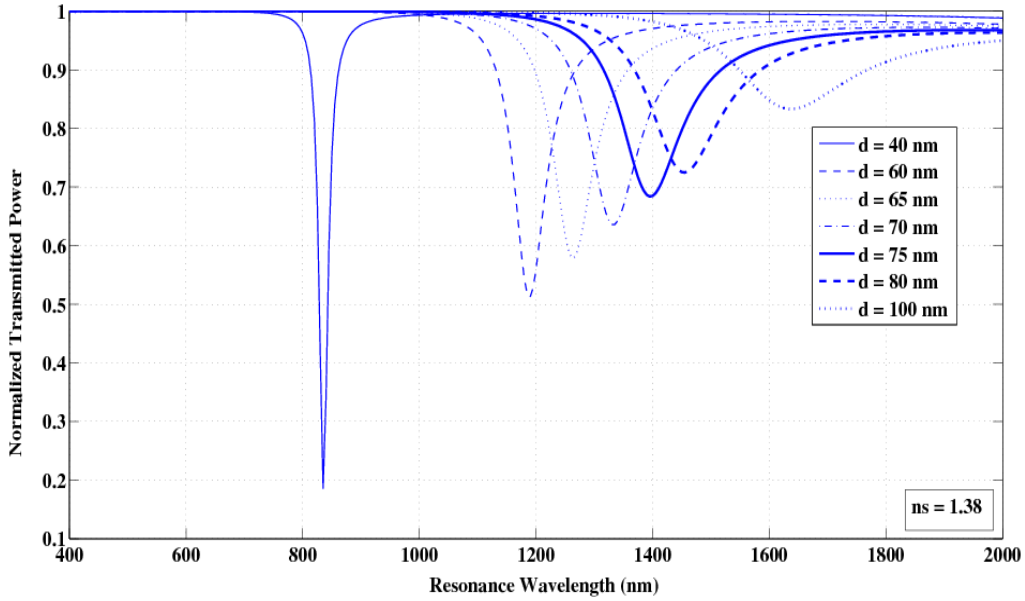

Figure 6.9: Transmittance curves of SPR based sensor A for different thickness values of InN layer for refractive index of sensing medium = 1.38

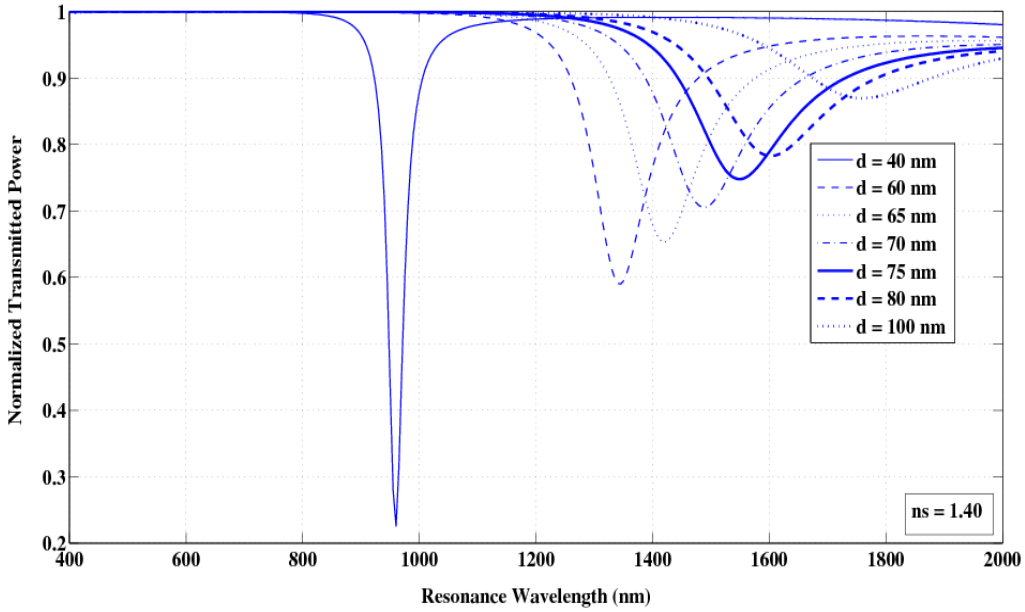

Figure 6.10: Transmittance curves of SPR based sensor A for different thickness values of InN layer for refractive index of sensing medium = 1.40

Figs. 6.7-6.10 show the SPR transmittance curves of sensor A for seven different thicknesses i.e. 40 nm, 60 nm, 65 nm, 70 nm, 75 nm, 80 nm and 100 nm of InN layer for refractive index of sensing medium 1.30, 1.34, 1.38 and 1.40 respectively.

6.4 Conclusions

The theoretical analysis of a SPR based fiber optic sensor with InN layer has been presented. Depending upon various parameter values for InN; $\varepsilon_\infty = 7.5$, $\omega_p = 4100$ cm^{-1}, $\Gamma = 1382$ cm^{-1} and $\varepsilon_\infty = 7.5$, $\omega_p = 5480$ cm^{-1}, $\Gamma = 1054$ cm^{-1}, two SPR sensors say "Sensor A" and "Sensor B" have been considered. The sensitivity of sensor A increases initially as the thickness of InN layer increases from 40 nm to 70 nm and finally it starts reducing as the thickness of InN layer is further increased from 70 nm to 100 nm. In the same way, the sensitivity of sensor B increases in the beginning with increase in thickness of InN layer from 40 nm to 55 nm and at last it starts falling as the thickness of InN layer is again increased from 55 nm to 100 nm. Sensors A and B display maximum sensitivities of 4493 nm/RIU and 3107 nm/RIU for 70 nm and 55 nm thick InN layers respectively. Both sensors A and B demonstrate their SPR resonance dips in near infrared region of spectrum. 70 nm thick InN layer based fiber optic

SPR sensor with various parameter values (ε_∞ = 7.5, ω_p = 4100 cm^{-1}, Γ = 1382 cm^{-1}) possesses high sensitivity of 4493 nm/RIU.

CHAPTER 7

SUMMARY

The present thesis focuses on the theoretical studies of SPR based fiber optic sensors using different materials. This chapter summarizes all the results reported in the previous chapters.

7.1 Surface plasmon resonance based fiber optic sensor with double resonance dips

(i) In this study, a SPR based fiber optic sensor with bi layers of metal oxide-metal i.e. bi layers of ITO-Au is theoretically analyzed.
(ii) The SPR sensor possesses high sensitivity with two resonance dips, one in the visible and other in the near infrared region of spectrum. In addition, two differentiated SPR dips have been obtained from the same device within 510 nm to 870 nm spectrum.
(iii) Increase in ITO layer thickness decreases the sensitivity of both left and right resonance dips for all thicknesses of Au layer.
(iv) Furthermore, for a fixed thickness of ITO layer, the sensitivity of left resonance dip increases with increase in Au layer thickness while that of right resonance dip decreases with increase in Au layer thickness.
(v) The optimized thicknesses of ITO and Au layers of SPR sensor are revealed to be 100 nm and 35 nm respectively.
(vi) 100 nm ITO-35 nm Au layers based fiber optic SPR sensor displays sensitivities of 1929 nm/RIU and 929 nm/RIU for left and right resonance dips respectively.

7.2 Surface plasmon resonance based fiber optic sensor utilizing indium oxide

(i) This study reports the simulation of a SPR based fiber optic sensor using indium oxide (In_2O_3).
(ii) The SPR sensor possesses high sensitivity with resonance dip in near infrared region of spectrum permitting the sensing in the infrared spectral region, which needs attention to many environmental and security applications.
(iii) In addition, the sensitivity of SPR sensor decreases with increase in thickness of In_2O_3 layer.
(iv) 170 nm thick In_2O_3 layer based fiber optic SPR sensor displays high sensitivity of 4600 nm/RIU.

7.3 Localized surface plasmon resonance based fiber optic sensor using nanoparticles

(i) This study presents the theoretical analysis of a LSPR based fiber optic sensor using nanoparticles.
(ii) Nanoparticles of four materials: ITO, Au, Ag and Cu have been considered and are assumed to be spherical in shape with various radii.
(iii) The sensitivity of LSPR sensor increases with increase in thickness of nanoparticles layer for all four materials.
(iv) In addition, for a fixed thickness of nanoparticles layer, the sensitivity of LSPR sensor further increases as the particle size of nanoparticles increases.
(v) The optimized values of thickness and particle size of nanoparticles for all four materials (individually) are found to be 60 nm and 20 nm respectively.
(vi) The sensitivity of LSPR sensor has been found to be 6240 nm/RIU, 4525 nm/RIU, 3550 nm/RIU and 3340 nm/RIU for 60 nm thick nanoparticles layer with fixed 20 nm particle size of ITO, Au, Ag and Cu nanoparticles respectively.
(vii) 60 nm thick ITO nanoparticles layer (with 20 nm particle size) based LSPR sensor shows maximum sensitivity of 6240 nm/RIU.

7.4 Nanocomposites based fiber optic SPR sensor

(i) This study deals with the theoretical analysis of a SPR based fiber optic sensor using nanocomposites.

(ii) Nanocomposites consisting of Au, Ag and Cu nanoparticles with their varying volume fractions embedded in host dielectric matrices of TiO_2 and InN are considered.

(iii) The sensitivity of Au/Ag/Cu-InN nanocomposites based SPR sensor for all thicknesses of nanocomposites with any volume fraction of metal nanoparticles has been observed to be greater than that of Au/Ag/Cu-TiO_2 nanocomposites.

(iv) The sensitivity of SPR sensor increases with increase in both thickness of nanocomposites and volume fraction of metal nanoparticles. In addition, for a fixed nanocomposite thickness and fixed volume fraction of metal nanoparticles, the sensitivity of sensor is larger for Au nanoparticles based nanocomposites than that of Ag and Cu nanoparticles.

(v) SPR based fiber optic sensor with 70 nm thick Au-InN nanocomposite having volume fraction of 0.85 reveals maximum sensitivity of 2875 nm/RIU.

7.5 Surface plasmon resonance based fiber optic sensor using indium nitride

(i) In this study, a SPR based fiber optic sensor with indium nitride (InN) layer is theoretically investigated.

(ii) Depending upon various parameter values for InN; ε_∞ = 7.5, ω_p = 4100 cm^{-1}, Γ = 1382 cm^{-1} and ε_∞ = 7.5, ω_p = 5480 cm^{-1}, Γ = 1054 cm^{-1}, two SPR sensors i.e. “Sensor A” and “Sensor B” have been considered.

(iii) Sensors A and B display maximum sensitivities of 4493 nm/RIU and 3107 nm/RIU for 70 nm and 55 nm thick InN layers respectively. Both sensors A and B demonstrate their SPR resonance dips in near infrared region of spectrum.

(iv) 70 nm thick InN layer based fiber optic SPR sensor with Sensor A parameters values possesses high sensitivity of 4493 nm/RIU.

****

APPENDIX A

Matrix method for the determination of reflection coefficient

Various layers are assumed to be stacked along z-axis.

The tangential fields at the first boundary are related to the final boundary by:

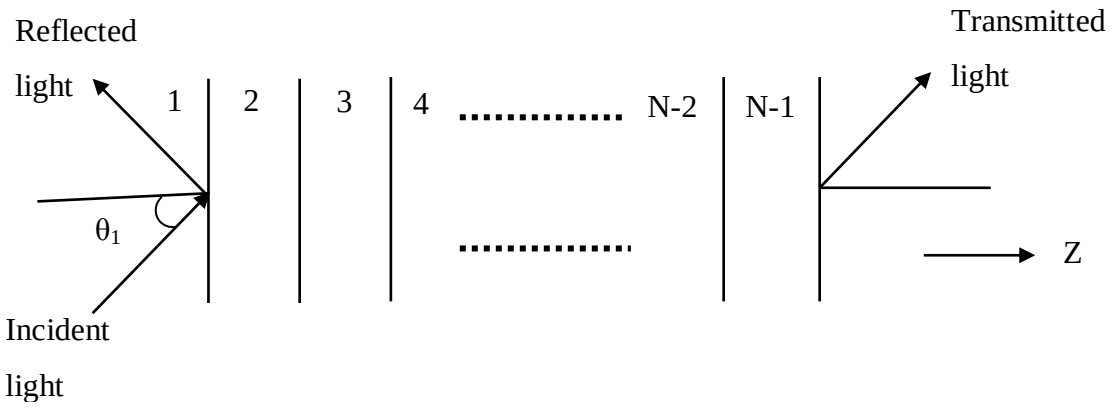

$$\begin{bmatrix} U_1 \\ V_1 \end{bmatrix} = M \begin{bmatrix} U_{N-1} \\ V_{N-1} \end{bmatrix}$$

Where U_1 and V_1, respectively are tangential components of electric and magnetic field at the boundary of first layer. U_{N-1} and V_{N-1} are the corresponding fields at the boundary of N^{th} layer. M is characteristics matrix of the combined structure and is given as,

$$M = \begin{bmatrix} M_{11} & M_{12} \\ M_{21} & M_{22} \end{bmatrix}$$

$$M_k = \begin{bmatrix} \cos\beta_k & (-i\sin\beta_k)/q_k \\ -iq_k in\beta_k & \cos\beta_k \end{bmatrix}$$

Where,

$$q_k = \left(\frac{\mu_k}{\varepsilon_k}\right)^{1/2}, \ \cos\theta_k = \frac{\left(\varepsilon_k - n_1^2 \sin^2\theta_1\right)^{1/2}}{\varepsilon_k}$$

$$\beta_k = \frac{2\pi}{\lambda} n_k \cos\theta_k \left(z_k - z_{k-1}\right) = \frac{2\pi d_k}{\lambda}\left(\varepsilon_k - n_1^2 \sin^2\theta_1\right)^{1/2}$$

The amplitude reflection coefficient for p-polarized incident wave is:

$$r_p = \frac{\left(M_{11} + M_{12} q_N\right) q_1 - \left(M_{21} + M_{22} q_N\right)}{\left(M_{11} + M_{12} q_N\right) q_1 + \left(M_{21} + M_{22} q_N\right)}$$

Finally the intensity reflection coefficient for p-polarized light is:

$$R_p = \left|r_p^2\right|$$

REFERENCES

1. Yu F.T.S., Yin S., ed., "*Fiber Optic Sensors*", Marcel Dekker, Inc., New York, 2002.
2. Krohn D.A., "*Fiber Optic Sensors: Fundamentals and Applications*", Instrument Society of America, Research Triangle Park, NC, 1988.
3. Dakin J., Culshaw B., "*Optical Fiber Sensors: Principles and Components*", vol. 1, Artech, Boston, 1988.
4. Culshaw B., Dakin J., "*Optical Fiber Sensors: Systems and Applications*", vol. 2, Artech, Norwood, 1989.
5. Udd E., ed., "*Fiber Optic Sensors: An Introduction for Engineers and Scientists*", Wiley, New York, 1991.
6. Goss W.C., Goldstein R., Nelson M.D., Fearnehaugh H.T., Ramer O.G., "*Fiber optic rotation sensor technology*", Applied Optics, vol. 19, pp. 852-858, 1980.
7. Tai S., kyuma K., Nunoshita M., "*Fiber optic acceleration sensor based on the photoelastic effect*", Applied Optics, vol. 22, pp. 1771-1774, 1983.
8. Ura S., Sunagawa H., Suhara T., Nishihara H., "*Focusing grating couplers for polarization detection*", Journal of Lightwave Technology, vol. 6, pp. 1028-1033, 1988.
9. Vohra S.T., Bucholtz F., Kersey A.D., "*Fiber optic dc and low frequency electric field sensor*", Optics Letters, vol. 16, pp. 1445-1447, 1991.
10. Willson J.P., Jones R.E., "*Magnetostrictive fiber optic sensor system for detecting dc magnetic fields*", Optics Letters, vol. 8, pp. 333-335, 1983.
11. Sedlar M., Paulica I, Sayer M., "*Optical fiber magnetic field sensor with ceramic magnetostrictive jackets*", Applied Optics, vol. 35, pp. 5340-5344, 1996.
12. Gupta B.D., Sharma A., Goyal R., "*Optical fiber temperature sensor based on liquid crystals*", International Journal of Optoelectronics, vol. 8, pp. 13-19, 1993.
13. Choi H.Y., Park K.S., Park S.J., Peak U.C., Lee B.H., Choi E.S., "*Miniature fiber-optic high temperature sensor based on a hybrid structured fabry Perot interferometer*", Optics Letters, vol. 33, pp. 2455-2457, 2008.
14. Apelsmeier A., Schmauss B., Shamonin M., "*Compensation of parasitic losses in an extrinsic fiber optic temperature sensor based on intensity measurement*", Sensors and Actuators A, vol. 173, pp. 49-54, 2012.
15. Volkov P.V., Goryunov A.V., Lukyanov A.Y., "*Fiber optic temperature sensor based on low-coherence interferometry without scanning*", Optik, vol. 124, pp. 1982-1985, 2013.

16. Wu D., Zhao Y., Hu H., "*Experimental research on FLM temperature sensor with an ethanol-filled photonic crystal fiber*", Sensors and Actuators A, vol. 209, pp. 62-67, 2014.
17. Wang S.F., Chiu M.H., Chang R.S., "*New idea for a D-type optical fiber sensor based on Kretschmann's configuration*", Optical Engineering, vol. 44, pp. 030502, 2005.
18. Gupta B.D., Sharma A., Singh C.D., "*Evanescent wave absorption sensor based on uniform and tapered fibers*", International Journal of Optoelectronics, vol. 8, pp. 409-418, 1993.
19. Gupta B.D., Sharma A., Singh C.D., "*Fiber optic evanescent field absorption sensor: effect of launching condition and the geometry of the sensing region*", Optical Engineering, vol. 33, pp. 1864-1868, 1994.
20. Gupta B.D., Tomar A.K., Sharma A., "*A novel probe for an evanescent wave fiber-optic absorption sensor*", Optical Quantum Electronics, vol. 27, pp. 747-753, 1995
21. Fabiny L., Kersay D., "*Interferometrically decoded fiber optic laser Doppler Velocimeter*", Optical Fiber Sensors, (Optical Society of America), paper Th 54, Sapporo, Japan, May 21, 1996.
22. Xiong F.B., Sisler D., "*Determination of low-level water content in ethanol by fiber optic evanescent absorption sensor*", Optics Communications, vol. 283, pp. 1326-1330, 2010.
23. Armin A., Soltanolkotabi M., Feizollah P., "*On the pH and concentration response of an evanescent field absorption sensor using a coiled-shape plastic optical fiber*", Sensors and Actuators A, vol. 165, pp. 181-184, 2011.
24. Zhan Y., Luo J., Wu H., Yu M., "*An all fiber high resolution fiber grating concentration sensor*", Optik, vol. 123, pp. 637-640, 2012.
25. Khan Md., Ho Kang B., Yeom S., Kwon D., "*Fiber optic pulse width modulation sensor for low concentration VOC gas*", Sensors and Actuators B, vol. 188, pp. 689-696, 2013.
26. Zhao Y., Deng Z., Wang Q., "*Fiber optic SPR sensor for liquid concentration measurement*", Sensors and Actuators B, vol. 192, pp. 229-233, 2014.
27. Donlegic D., Cibula E., "*All fiber high sensitivity pressure sensor with O_2 diaphram*", Optics Letters, vol. 30, pp. 2071-2073, 2005.
28. Chen H., "*Fiber optic pressure sensor based on a single mode fiber F–P cavity*", Measurement, vol. 43, pp. 370-374, 2010.
29. Bremer K., Lewis E., Leen G., Moss B., Lochmann S., Mueller I., "*Fabrication of a miniature all-glass fibre optic pressure and temperature sensor*", Procedia Engineering, vol. 25, pp. 503-506, 2011.

30. Chen R., Hahn C.E.W., Farmery A.D., "*A flowing liquid test system for assessing the linearity and time response of rapid fiber optic oxygen partial pressure sensors*", Respiratory Physicology and Neurobiology, vol. 183, pp. 100-107, 2012.
31. Cho S., Lee K., Kim J., Kim D., "*Rugate-structured free standing porous silicon based fiber optic sensor for the simultaneous detection of pressure and organic gases*", Sensors and Actuators B, vol. 183, pp. 428-433, 2013.
32. Wang Y., Bartelt H., Brueckner S., Kobelke J., Rothhardt M., Morl K., Ecke W., Willsch R., "*Slicing Ge-doped photonic crystal fibers using commercial fashion splicer with default discharge parameters*", Optics Express, vol. 16, pp. 7258-7263, 2008.
33. Martin A., Badcock R., Nightingale C., Fernando G.F., "*A novel optical fiber based strain sensor*", IEEE Photonic Technology Letters, vol. 9, pp. 982-984, 1997.
34. Schmidt m., Werther B., Fuerstenau n., Matthias M., Melz T., "*Fiber-optic extrinsic Febry-perot interferometer strain sensor with <50 pm displacement resolution using three wavelength digital phase modulation*", Optics Express, vol. 8, pp. 475-480, 2001.
35. Gupta B.D., Ratnanjali, "*A novel probe for a fiber optic humidity sensor*", Sensors and Actuators B, vol. 80, pp. 132-135, 2001.
36. Kronenberg P., Rastogi P.K., Giaccari P., Limberger H.G., "*Relative humidity sensor with optical fiber Bragg gratings*", Optics Letters, vol. 27, pp. 1385-1387, 2002.
37. Estella J., Vicente P., Echeverria J., Garrido J., "*A fibre optic humidity sensor based on a porous silica xerogel film as the sensing element*", Sensors and Actuators B, vol. 6, pp. 122-128, 2010.
38. Consales M., Buosciolo A., Cutola A., Breglio G., Irace A., Buontempo S., Petagna P., Giordano M., Cusano A., "*Fiber optic humidity sensors for high energy physics applications at CERN*", Sensors and Actuators B, vol. 159, pp. 66-74, 2011.
39. Chen L.H., Li T., Chan C.C, Menon R., Balamurali M., Shaillender M., Neu B., Ang X.M., Zu P., Wong W.C., Leong K.C., "*Chitosan based fiber optic Fabry Perot humidity sensor*", Sensors and Actuators B, vol. 169, pp. 167-172, 2012.
40. Xu W., Huang W., Huang X., Yu C., "*A simple fiber optic humidity sensor based on extrinsic Fabry-Perot cavity constructed by cellulose acetate butyrate film*", Optical Fiber Technology, vol. 19, pp. 583-586, 2013.
41. Hu P., Dong X., Ni K., Chen L.H., Wong W.C., Chan C.C., "*Sensitivity enhanced Michelson interferometric humidity sensor with waist-enlarged fiber bitaper*", Sensors and Actuators B , vol. 194, pp. 180-184, 2014.

42. Haidekkar M.A., Akers W.J., Fischer D., Theodoreakis E.A., "*Optical fiber based fluorescent viscosity sensor*", Optics Letters, vol. 31, pp. 2529-2531, 2006.
43. Gupta B.D., Sharma D.K., "*Evanescent wave absorption based fiber optic pH sensor prepared by dye doped sol-gel immobilization technique*", Optics Communication, vol. 140, pp. 32-35, 1997.
44. Gupta B.D., Sharma N.K., "*Fabrication and characterization of U-shaped fiber optic pH probes*", Sensors and Actuators B, vol. 82, pp. 89-93, 2002.
45. Sharma N.K., Gupta B.D., "*Fabrication and characterization of pH sensor based on side polished single mode optical fiber*", Optics Communication, vol. 216, pp. 299-303, 2003.
46. Sharma N.K., Gupta B.D., "*Fabrication and characterization of a fiber optic pH sensor for the pH range 2 to 13*", Fiber and Integrated Optics, vol. 23, pp. 327-335, 2004.
47. Gu B., Yin M.J., Zhang A.P., Qian J.W., He S., "*Low cost high performance fiber optic pH sensor based on thin core modal interferometer*", Optics Express, vol. 17, pp. 22296-22302, 2009.
48. Wu S., Cheng W., Qiu Y., Li Z., Shuang S., Dong C., "*Fiber optic pH sensor based on mode-filtered light detection*", Sensors and Actuators B, vol. 144, pp. 255-259, 2010.
49. Zamarreno C.R., Hernaez M., Villar I.D., Matias I.R., Arregui F.J., "*Optical fiber pH sensor based on lossy-mode resonances by means of thin polymeric coatings*", Sensors and Actuators B, vol. 155, pp. 290-297, 2011.
50. Singh S., Gupta B.D., "*Fabrication and characterization of a highly sensitive surface plasmon resonance based fiber optic pH sensor utilizing high index layer and smart hydrogel*", Sensors and Actuators B, vol. 173, pp. 268-273, 2012.
51. Li W., Cheng H., Xia M., Yang K., "*An experimental study of pH optical sensor using a section of no-core fiber*", Sensors and Actuators A, vol. 199, pp. 260-264, 2013.
52. Nguyen T. H., Venugopala T., Chen S., Sun T., Grattan K.T.V., Taylor S., Muhammed Basheer P.A., Long A.E., "*Fluorescence based fiber optic pH sensor for the pH 10-13 range suitable for corrosion monitoring in concrete structures*", Sensors and Actuators B, vol. 191, pp. 498-507, 2014.
53. Nylander C., Liedberg B., Lind T., "*Gas detection by means of surface plasmon resonance*", Sensors and Actuators, vol. 3, pp.79-88, 1982.
54. Liedberg B., Nylander C., Sundstrom L., "*Surface plasmon resonance for gas detection and biosensing*", Sensors and Actuators, vol. 4, pp. 299-304, 1983.
55. Jorgenson R.C., Yee S.S., "*A fiber optic chemical sensor based on surface plasmon resonance*", Sensors and Actuators B, vol. 12, pp. 213-220, 1993.

56. Homola J., Yee S.S., Gauglitz G., "*Surface plasmon resonance sensors: review*", Sensors and Actuators B, vol. 54, pp. 3-15, 1999.
57. Homola J., Koudela I., Yee S.S., "*Surface plasmon resonance sensors based on diffraction gratings and prism couplers: sensitivity comparison*", Sensors and Actuators B, vol. 54, pp. 16-24, 1999.
58. Lin W.B., Jaffrezic-Renault N., Agnaire H., "*The effects of polarization of the incident light-modeling and analysis of a SPR multimode optical fiber sensor*", Sensors and Actuators A, vol. 84, pp. 198-204, 2000.
59. Lin W.B., Lacroix M., Chovelon J.M., Jaffrezic-Renault N., Gagnaire H., "*Development of a fiber optic sensor based on surface plasmon resonance on silver film for monitoring aqueous media*", Sensors and Actuators B, vol. 75, pp. 203-209, 2001.
60. Cheng S.F., Chau L.K., "*Colloidal gold-modified optical fiber for chemical and biochemical sensing*", Analytical Chemistry, vol. 75, pp. 16-21, 2003.
61. Lin W.W., "*Fiber-optic current sensor*", Optical Engineering, vol. 42, pp. 896-899, 2003.
62. Sharma A.K., Gupta B.D., "*Absorption based fiber optic surface plasmon resonance sensor: A theoretical evaluation*", Sensors and Actuators B, vol.100, pp. 423-431, 2004.
63. Homola J., Vaisocherova H., Dostalek J., Pilliarik M., "*Multi-analyte surface plasmon resonance biosensing*", Methods, vol. 37, pp. 26-36, 2005.
64. Sharma A.K., Gupta B.D., "*On the sensitivity and signal to noise ratio of a step-index fiber optic surface plasmon resonance sensor with bimetallic layers*", Optics Communications, vol. 245, pp. 159-169, 2005.
65. Sharma A.K., Gupta B.D., "*Fiber optic sensor based on surface plasmon resonance with nanoparticles films*", Photonics and Nanostructures-Fundamentals and Applications, vol. 3, pp. 30-37, 2005.
66. Sharma A.K., Gupta B.D., "*Fiber optic sensor based on surface plasmon resonance with Ag-Au alloy nanoparticles films*", Nanotechnology, vol. 17, pp. 124-131, 2006.
67. Sharma A.K., Gupta B.D., "*Influence of temperature on sensitivity and signal to noise ratio of a fiber optic surface plasmon resonance sensor*", Applied Optics, vol. 45, pp. 151-161, 2006.
68. Brantzen S., Volklein F., Knoll W., Menges B., "*A new sensor for the thermo-optical detection of surface plasmon resonance*", Sensors and Actuators A, vol. 135, pp.492-501, 2007.

69. Jeenanong A., Kawaguchi H., "*SPR response of stimuli-sensitive microgel on sensor chip*", Colloids and Surfaces A: Physicochemical and Engineering Aspect, vol. 302, pp. 403-410, 2007.
70. Shen X.W., Huang C.Z., Li Y.F., "*Localized surface plasmon resonance sensing detection of glucose in the serum samples of diabetes sufferers based on the redox reaction of chlorauric acid*", Talanta, vol. 72, pp. 1432-1437, 2007.
71. Rhodes C., Cerruti M., Efremenko A., Losego M., Aspnes D.E., Maria J.P., Franzen S., "*Dependence of plasmon polaritons on the thickness of indium tin oxide thin films*", Journal of Applied Physics, vol. 103, pp. 093108, 2008.
72. Kabashin A.V., Evans P., Pastkovsky S., Hendren W., Wurtz G.A., Atkinson R., Polard R., Podolskiy V.A., Zayats A.V., "*Plasmonic nanorod metamaterials for biosensing*", Nature Materials, vol. 8, pp. 867-871, 2009.
73. Jha R., Badenes G., "*Effect of fiber core dopant concentration on the performance of surface plasmon resonance based fiber optic sensor*", Sensors and Actuators A, vol. 150, pp. 212-217, 2009.
74. Mitsushioa M., Watanabeb K., Abeb Y., Higoa M., "*Sensor properties and surface characterization of aluminium deposited SPR optical fibers*", Sensors and Actuators A, vol. 163, pp. 1-8, 2010.
75. Verma R.K., Gupta B.D., "*Surface plasmon resonance based fiber optic sensor for the IR region using a conducting metal oxide film*", Journal of the Optical Society of America A, vol. 27, pp. 846-851, 2010.
76. Srivastava S.K., Verma R.K., Gupta B.D., "*Surface plasmon resonance based fiber optic sensor for the detection of low water content in ethanol*", Sensors and Actuators B, vol. 153, pp. 194-198, 2011.
77. Yuan Y., Ding L., Guo Z., "*Numerical investigation for SPR based optical fiber sensor*", Sensors and Actuators B, vol. 157, pp. 240-245, 2011.
78. Srivastava S.K., Gupta B.D., "*Influence of ions on the surface plasmon resonance spectrum of a fiber optic refractive index sensor*", Sensors and Actuators B, vol. 156, pp. 559-562, 2011.
79. Bhatia P., Gupta B.D., "*Fabrication and characterization of a surface plasmon resonance based fiber optic urea sensor for biomedical applications*", Sensors and Actuators B, vol. 161, pp. 434-438, 2012.

80. Cao J., Galbraith E.K., Sun T., Grattan K.T.V., "*Cross comparison of surface plasmon resonance based optical fiber sensors with different coating structures*", IEEE Sensors Journal, vol. 12, pp. 2355-2361, 2012.
81. Srivastava S.K., Arora V., Sapra S., Gupta B.D., "*Localized surface plasmon resonance based fiber optic U-shaped biosensor for the detection of blood glucose*", Plasmonics, vol. 7, 261-268, 2012.
82. Salari M., Askari H.R., "*Theoretical investigation of absorption and sensitivity of nano-plasmonic fiber optic sensors*", Optics and Laser Technology, vol. 48, pp. 315-325, 2013.
83. Yuan Y., Hu D., Hua L., Li M., "*Theoretical investigations for surface plasmon resonance based optical fiber tip sensor*", Sensors and Actuators B, vol. 188, pp. 757-760, 2013.
84. Cao J., Tu M.H., Sun T., Grattan K.T.V., "*Wavelength based localized surface plasmon resonance optical fiber biosensor*", Sensors and Actuators B, vol. 181, pp. 611-619, 2013.
85. Bharadwaj R., Mukherji S., "*Gold nanoparticle coated U-bend fiber optic probe for localized surface plasmon resonance based detection of explosive vapors*", Sensors and Actuators B, vol. 192, pp. 804-811, 2014.
86. Gao D., Guan C., Wen Y., Zhong X., Yuan L., "*Multi-hole fiber based surface plasmon resonance sensor operated at near-infrared wavelengths*", Optics Communications, vol. 313, pp. 94-98, 2014.
87. Navarrete M.C., Herrera N.D., Cano A.G., Esteban O., "*Surface plasmon resonance in the visible region in sensors based on tapered optical fibers*", Sensors and Actuators B, vol. 190, pp. 881-885, 2014.
88. Kik P.G., Maier S.A., Atwater H.A., "*Image resolution of surface plasmon mediated near field focusing with planar metal films in three dimensions using finite line width dipole sources*", Physical Review B, vol. 69, pp. 045418, 2004.
89. Bozhevolnyi S.I., "*Effective index modeling of channel plasmon polariton waveguides*", Optics Express, vol. 14, pp. 9467-9476, 2006.
90. Thyagarajan K., Diggavi S., Ghatak A.K., Johnstone W., Stewart G., Culshaw B., "*Thin metal clad waveguide polarizers: analysis and comparison with experiment*", Optics Letters, vol. 15, pp.1041-1043, 1990.
91. Campion A., Kambhampati P., "*Surface-enhanced Raman scattering*", Chemical Society Reviews, vol. 27, pp. 241-250, 1998.
92. Wood R.W., "*On a remarkable case of uneven distribution of light in a diffraction grating spectrum*", Philosophical Magazine, vol. 4, pp. 396-402, 1902.

93. Zenneck J., "*Uber die Fortpflanztmg ebner elektro-magnetischer Wellen langs einer ebenen Leiterflache and ihre Beziehung zur drahtlosen Telegraphie*", Annalen der Physik, vol. 328, pp. 846-866, 1907.
94. Sommerfeld A., "*Propagation of waves in wireless telegraphy*", Anals der Physik, vol. 28, pp. 665-736, 1909.
95. Fano R.M., "*The theory of anomalous diffraction grating of quasi stationary wave on metallic surfaces*", Journal of Optical Society America, vol. 31, pp. 213-222, 1941.
96. Ritchie R.H., "*Plasma losses by fast electrons in thin films*", Physical Review, vol. 106, pp. 874-881, 1957.
97. Thurbadar T., "*Complete absorption of light by thin metal films*", Proceedings of the Physical Society, vol. 73, pp. 40-44, 1959.
98. Powell C.J., Swan J.B., "*Effect of oxidation on characteristic loss spectra of aluminum and magnesium*", Physical Review, vol. 118, pp. 640-643, 1960.
99. Stern E.A., Ferrell, R.A., "*Surface plasma oscillation of degenerate electron gas*", Physical Review, vol. 120, pp. 130-136, 1960.
100. Otto A., "*Excitations of nonradiative surface plasma waves in silver by the method of frustrated total reflection*", Zeitschrift fur Physik, vol. 216, pp. 398-410, 1968.
101. Kretschmann E., "*Die Bestimmung optischer Konstanten von Metallen durch Anregung von Oberflachenplasmashwingungen*", Zeitschrift fur Physik, vol. 241, pp. 313-324, 1971.
102. Zynio S.A., Samoylov A.V., Surovtseva E. R., Mirsky V. M., Shirshov Y. M., "*Bimetallic layers increase sensitivity of affinity sensors based on surface plasmon resonance*", Sensors, vol. 2, pp. 62-70, 2002.
103. Sharma A.K., Gupta B.D., "*On the performance of different bimetallic combinations in surface plasmon resonance based fiber optic sensors*", Journal of Applied Physics, vol. 101, pp. 093111, 2007.
104. Villatoro J., Hernandez D.M., Mejia E., "*Fabrication and modeling of uniform waist single mode tapered optical fiber sensor*", Applied Optics, vol. 42, pp. 2278-2283, 2003.
105. Diez A., Andres M.V., Cruz J.L., "*In line fiber optic sensors based on excitation of surface plasmon modes in metal-coated tapered fibers*", Sensors and Actuators B, vol. 73, pp. 95-99, 2001.
106. Kim Y.C., Banerji S., Masson J.F., Peng W, Booksh K.S., "*Fiber optic surface plasmon resonance for vapor phase analysis*", Analyst, vol. 130, pp. 838-843, 2005.

107. Bueno F.J., Esteban O., Herrera N.D., Navarrete M.C., Cano A.G., "*Sensing properties of asymmetric double layer covered tapered fibers*", Applied Optics, vol. 43, pp. 1615-1620, 2004.

108. Grunwald B., Holst G., "*Fiber optic refractive index microsensor based on white light SPR excitation*", Sensors and Actuators A., vol. 113, pp. 174-180, 2004.

109. Lang N.D., "*Surface dipole barriers in simple metals*", Physical Review B., vol. 8, pp. 6010-6012, 1973.

110. Raether H., "*Surface plasmons on smooth and rough surfaces and on gratings*", Springer, Verlag, 1988.

111. Bouchelier A., Wiederrecht G.P., "*Surface plasmon rainbow jets*", Optics Letters, vol. 30, pp. 884-886, 2005.

112. Hecht B., Bielefeld H., Novotny L., Inouye Y., Paul D.W., "*Local excitation, scattering and interference of surface plasmon*", Physical Review Letters, vol. 77, pp. 1889-1892, 1996.

113. Kretschmann E., Raether H., "*Radiative decay of non radiative surface plasmons excited by light*", Z. Naturforsch A, vol. 23, pp. 2135-2136, 1968.

114. Harris R.D., Wilkinson J.S., "*Waveguide surface plasmon resonance* sensors", Sensors and Actuators B, vol. 29, pp. 261-267, 1995.

115. Homola J., "*Optical fiber sensor based on surface plasmon excitation*", Sensors and Actuators B, vol. 29, pp. 401-405, 1995.

116. Homola J., "*On the sensitivity of surface plasmon resonance* sensors *with spectral interrogation*", Sensors and Actuators B, vol. 41, pp. 207-211, 1997.

117. Salamon Z., Macleod H.A., Tollin G., "*Surface plasmon resonance spectroscopy as a tool for investigating the biochemical and biophysical properties of membrane protein systems. II: Applications to biological systems*", Biochimica et Biophysica Acta, vol. 1331, pp. 117-129, 1997.

118. Slavik R., Homola J., Ctyroky J., "*Miniaturization of fiber optic surface plasmon resonance sensor*", Sensors and Actuators B, vol. 51, pp. 311-315, 1998.

119. Slavik R., Homola J., Ctyroky J., "*Single mode optical fiber surface plasmon resonance sensor*", Sensors and Actuators B, vol. 54, pp. 74-79, 1999.

120. Bardin F., Kasik I., Trouillet A., Matejec V., Gagnaire H., Chomat M., "*Surface plasmon resonance sensor using an optical fiber with an inverted graded index profile*", Applied Optics, vol. 41, pp. 2514-2520, 2002.

121. Kurihara S., Ohkawa H., Iwasaki Y., Niwa O., Tobita T., Suzuki K., "*Fiber optic conical microsensors for surface plasmon resonance using chemically etched single mode fiber*", Analytica Chimica Acta, vol. 523, pp. 165-170, 2004.

122. Chau L.K., Lin Y.F., Cheng S.F., Lin T.J., "*Fiber optic chemical and biochemical probes based on localized surface plasmon resonance*", Sensors and Actuators B, vol. 113, pp. 100-105, 2006.

123. Suzuki H., Sugimoto M., Matsui Y., Kondoh J., "*Effects of gold film thickness on spectrum profile and sensitivity of a multimode optical fiber SPR sensor*", Sensors and Actuators B, vol. 132, pp. 26-33, 2008.

124. Brewer S.H., Franzen S., "*Calculation of the electronic and optical properties of indium tin oxide by density functional theory*", Chemical Physics, vol. 300, pp. 285-293, 2004.

125. Rhodes C., Franzen S., Maria J.P., Losego M., Leonard D.N., Laughlin B., Duscher G., Weibel S., "*Surface plasmon resonance in conducting metal oxides*", Journal of Applied Physics, vol. 100, pp. 054905, 2006.

126. Villar I.D., Zamarreno C.R., Hernaez M., Arregui F.J., Matias I.R., "*Lossy mode resonance generation with indium tin oxide coated optical fibers for sensing applications*", Journal of Lightwave Technology, vol. 28, pp. 111-117, 2010.

127. Solieman A., "*Effect of sintering temperature on the structural, optical and electrical properties of sol-gel derived indium oxide thin films*", Journal of sol-gel Science and Technology, vol. 60, pp. 48-57, 2011.

128. Villar I.D., Zamarreno C.R., Sanchez P., Hernaez M., Valdivielso C.F., Arregui F.J., Matias I.R., "*Generation of lossy mode resonances by deposition of high refractive index coatings on uncladded multimode optical fibers*", Journal of Optics, vol. 12, pp. 095503, 2010.

129. Lal S., Link S., Halas N.J., "*Nano-optics from sensing to waveguiding*", Nature Photonics, vol. 1, pp. 641-648, 2007.

130. Bohren C.F., Huffman D.R., "*Absorption and scattering of light by small particles*", Wiley-VCH, New York, 1983.

131. Noguez C., "*Surface plasmons on metal nanoparticles: The influence of shape and physical environment*", Journal of Physical Chemistry C, vol. 111, pp. 3806-3819, 2007.

132. Lee K., El-Sayed M.A., "*Gold and silver nanoparticles in sensing and imaging: sensitivity of plasmon response to size, shape and metal composition*", Journal of Physical Chemistry B, vol. 110, pp. 19220-19225, 2006.

133. Jha R., Sharma A.K., "*Chalcogenide glass prism based SPR sensor with Ag-Au bimetallic nanoparticle alloy in infrared wavelength region*", Journal of Optics A: Pure and Applied Optics, vol. 11, pp. 045502, 2009.

134. Sharma A.K., Jha R., Gupta B.D., "*Influence of dopants on the performance of a fiber optic surface plasmon resonance sensor*", Optics Communications, vol. 274, pp. 320-326, 2007.

135. Naik G.V., Kim J., Boltasseva A., "*Oxides and nitrides as alternative plasmonic materials in the optical range*", Optical Materials Express, vol. 1, pp.1090-1099, 2011.

136. Lu H., Schaff W.J., Eastman L.F., "*Surface chemical modification of InN for sensor applications*", Journal of Applied Physics, vol. 96, pp. 3577-3579, 2004.

137. Hamberg I., Granqvist C.G., "*Evaporated Sn-doped In_2O_3 films: Basic optical properties and applications to energy-efficient windows*", Journal of Applied Physics, vol. 60, pp. R123-R160, 1986.

138. Liu C.S., Kumar G., Tripathi V.K., "*Laser mode conversion into a surface plasma wave in a metal coated optical fiber*", Journal of Applied Physics, vol. 100, pp. 013304, 2006.

139. Kumar G., Singh D.B., Tripathi V.K., "*Surface enhanced Raman scattering of a surface plasma wave*", Journal of Physics D, vol. 39, pp. 4436-4439, 2006.

140. Zayats A.V., Smolyaninov I.I., Maradudin A.A., "*Nano-optics of surface plasmon polaritons*", Physics Reports, vol. 408, pp. 131-314, 2005.

141. Ghatak A.K., Thyagarajan K., "*An introduction to Fiber optics*", ed. 1, Cambridge University Press, Cambridge, 1999.

142. Ordal M.A., Long L.L., Bell R.J., Bell S.E., Bell R.R., Alexander Jr. R.W., Ward C.A., "*Optical properties of metals Al, Co, Cu, Au, Fe, Pb, Ni, Pd, Pt, Ag, Ti, and W in the infrared and far infrared*", Applied Optics, vol. 22, pp. 1099-1119, 1983.

143. Dwivedi Y.S., Sharma A.K., Gupta B.D., "*Influence of skew rays on the sensitivity and signal to noise ratio of a fiber optic surface plasmon resonance sensor: a theoretical study*", Applied Optics, vol. 46, pp. 4563-4569, 2007.

144. Kim H., Horwitz J.S., Kushto G.P., Qadri S.B., Kafafi Z.H., Chrisey D.B. "*Transparent conducting Zr-doped In_2O_3 thin films for organic light-emitting diodes*", Applied Physics Letters, vol. 78, pp. 1050-1052, 2001.

145. Granqvist C.G., Hultaker A., "*Transparent and conducting ITO films: new developments and applications*", Thin Solid Films, vol. 411, pp.1-5, 2002.

146. Mammana A.P., Braga E.S., Torriani I., Anderson R.L., "*Structural characterization of transparent semiconducting thin films of SnO_2 and In_2O_3*", Thin Solid Films, vol. 85, pp. 355-359, 1981.

147. Awschalom D.D., McCord M.A., Grinstein G., "*Observation of macroscopic spin phenomena in nanometer-scale magnets*", Physical Review Letters, vol. 65, pp. 783-786, 1990.

148. Hewakuruppu Y.L., Dombrovsky L.A., Chen C., Timchenko V., Jiang X., Baek S., Taylor R.A., "*Plasmonic pump–probe method to study semi-transparent nanofluids*", Applied Optics, vol. 52, pp. 6041–6050, 2013.

149. Bohren C.F., Huffman D.R., "*Absorption and scattering of light by small particles*", Wiley-VCH, New York, 1983.

150. Yu C., Irudayaraj J., "*Multiplex biosensor using gold nanorods*", Analytical Chemistry, vol. 79, pp. 572-579, 2007.

151. Willets K.A., Duyne R.P.V., "*Localized surface plasmon resonance spectroscopy and sensing*", Annual Review of Physical Chemistry, vol. 58, pp. 267-297, 2007.

152. Cao J., Galbraith E.K., Sun T., Grattan K.T.V., "*Comparison of surface plasmon resonance and localized surface plasmon resonance-based optical fibre sensors*", Journal of Physics: Conference Series, vol. 307, pp. 012050, 2011.

153. Klar T., Perner M., Grosse S., Plessen G.V., Spirkl W., Feldman J., "*Surface plasmon resonance in single metallic nanoparticles*" Physical Review Letters, vol. **80**, pp. 4249-4952, 1998.

154. Krenn J.R., Dereux A., Weeber J.C., Bourillot E., Lacroute Y., Goudonnet J.P., Schider B., Gotschy W., Leitner A., Aussenegg F.R., "*Squeezing the optical near-field zone by plasmon coupling of metallic nanoparticles*", Physical Review Letters, vol. 82, pp. 2590-2593, 1999.

155. Krenn J.R., Weeber J.C., Dereux A., Bourillot E., Goudonnet J.P., Schider B., Leitner A., Aussenegg F.R., Girard C., "*Direct observation of localized surface plasmon coupling*", Physical Review B, vol. 60, pp. 5029-5033, 1999.

156. Lamprecht B., Krenn J.R., Leitner A., Aussenegg F.R., "*Metal nanoparticle gratings: influence of dipolar particle interaction on the plasmon resonance*", Physical Review Letters, vol. 84, pp. 4721-4724, 2000.

157. Ditlbacher H., Krenn J.R., Lamprecht B., Leitner A., Aussenegg F.R., "*Spectrally coded optical data storage by metal nanoparticles*", Optics Letters, vol. 25, pp. 563-565, 2000.

158. Stockle R.M., Suh Y.D., Deckert V., Zenobi R., "*Nanoscale chemical analysis by tip enhanced Raman spectroscopy*", Chemical Physics Letters, vol. 318, pp. 131-136, 2000.

159. Gilliot M., En Naciri A., Johann L., Stoquert J.P., Grob J.J., Muller D., "*Optical properties of isolated cobalt clusters synthesized by ion implantation***",** Journal of Applied Physics, vol. 101, pp. 014319, 2007.

160. Singh S., Gupta B.D., "*Simulation of a surface plasmon resonance based fiber optic sensor for gas sensing in visible range using films of nanocomposites*", Measurement Science and Technology, vol. 21, pp. 115202, 2010.

161. Kelly K.L., Coronado E., Zhao L.L., Schatz G.C., "*The Optical Properties of Metal Nanoparticles: The Influence of Size, Shape, and Dielectric Environment*", Journal of Physical Chemistry B, vol. 107, pp. 668-677, 2003.

162. Medda S.K., De S., De G., "*Synthesis of Au-nanoparticle doped SiO_2-TiO_2 films: tuning of Au-surface plasmon band position through controlling the refractive index*", Journal of Materials Chemistry, vol. 15, pp. 3278-3284, 2005.

163. Ma G., Sun W., Tang S.H., Zhang H., Shen Z., "*Size and dielectric dependence of the third-order nonlinear optical response of Au nanocrystals embedded in matrices*", Optics Letters, vol. 27, pp. 1043-1045, 2002.

164. Niklasson G.A., Granqvist C.G., Hunderi O., "*Effective medium models for the optical properties of inhomogeneous materials*", Applied Optics, vol. 20, pp. 26-30, 1981.

165. Devore J.R., "*Refractive indices of rutile and sphalerite*", Journal of Optical Society of America, vol. 41, pp. 416-417, 1951.

166. Thakur J.S., Auner G.W., Haddad D.B., Naik R., Naik V.M., "*Disorder effects on infrared reflection spectra of InN films*", Journal of Applied Physics, vol. 95, pp. 4795-4801, 2004.

167. Dixit A., Sudakar C., Naik R., Lawes G., Thakur J.S., MaCullen E.F., Auner G.W., Naik V.M., "*Phase separation and optical properties in oxygen-rich InN films*", Applied Physics Letters, vol. 93, pp. 142103, 2008.

168. Bhuiyan A.G., Hashimoto A., Yamamoto A., "*Indium nitride (InN): A review on growth, characterization, and properties*", Journal of Applied Physics, vol. 94, pp. 2779-2808, 2003.

169. Jain S.C., Willander M., Narayan J., Overstraeten R.V., "*III-nitrides: Growth, characterization and properties*", Journal of Applied Physics, vol. **87**, pp. 965-1006, 2000.

170. Chao C.K., Chang H.S., Hsu T.M., Hsiao C.N., Kei C.C., Kuo S.Y., Chyi J.I., "*Optical properties of indium nitride nanorods prepared by chemical-beam epitaxy*", Nanotechnology, vol. 17, pp. 3930-3932, 2006.

171. Yamamoto A., Tsujino M., Ohkubo M., Hashimoto A., "*Metalorganic chemical vapor deposition growth of InN for InN/Si tandem solar cell*", Solar Energy Materials and Solar Cells, vol. 35, pp. 53-60, 1994.

172. Qian Z.G., Shen W.Z., Ogawa H., Guo Q.X., "*Infrared reflection characteristics in InN thin films grown by magnetron sputtering for the application of plasma filters*", Journal of Applied Physics, vol. 92, pp. 3683-3687, 2002.

173. Esteban O., Naranjo F.B., Herrera N.D., Felip S.V., Navarrete M.C., Cano A.G., "*High-sensitive SPR sensing with indium nitride as a dielectric overlay of optical fibers*", Sensors and Actuators B, vol. 158, pp. 372-376, 2011.

LIST OF PUBLICATIONS

Journals

[1] Sharma N.K., **Rani M.**, Sajal V., "*Surface plasmon resonance based fiber optic sensor with double resonance dips*", Sensors and Actuators B, vol. 188, pp. 326-333, 2013.

[2] **Rani M.**, Sharma N.K., Sajal V., "*Surface plasmon resonance based fiber optic sensor utilizing Indium oxide*", Optik, vol. 124, pp. 5034-5038, 2013.

[3] **Rani M.**, Sharma N.K., Sajal V., "*Localized surface plasmon resonance based fiber optic sensor with nanoparticles*", Optics Communications, vol. 292, pp. 92-100, 2013.

[4] **Rani M.**, Shukla S., Sharma N.K., Sajal V., "*Theoretical study of nanocomposites based fiber optic SPR sensor*", Optics Communications, vol. 313, pp. 303-314, 2014.

[5] **Rani M.**, Shukla S., Sharma N.K., Sajal V., "*Theoretical analysis of surface plasmon resonance based fiber optic sensor using indium nitride*", (accepted in Optik).

Conference Proceedings

[1] **Rani M.**, Sharma N.K., "*ITO based fiber optic SPR sensor*", AIP Conf. Proc., vol. 1536, pp. 1117-1118, 2013.

Conferences

[1] **Rani M.**, Sharma N.K., "*Simulation of Cobalt based fiber optic surface plasmon resonance sensor*", International Conference on Optics & Optoelectronics ICOL-2014, Dehradun, March 05-08, 2014.

SYNOPSIS

The main application of optical fibers has been in telecommunication industries. However, there is rising application of optical fibers in sensing of different physical and chemical parameters such as temperature, pressure, magnetic field, current, rotation, acceleration, displacement, refractive index, chemical concentration, humidity, viscosity and pH etc. These kinds of fiber optic sensors are finding applications in electrical power industry, industrial process control, medical sciences, automobiles, defense sector and many more. This is because fiber optic sensors present various advantages over other types of sensors like optical fibers are purely dielectric, so these can be easily used in hazardous areas, where conventional electrically powered sensors would not be safe to use. Moreover, fiber optic sensors are safer for *in vivo* use because the signal is optical and these are immune to electromagnetic interference. Further, fiber optic sensors possess greater geometric versatility and have very short response time. In addition, remote sensing can be attained by using fiber optic sensors because the signal can be carried over a long distance. Besides it, optical fibers avoid cross talk, therefore a small and compact multi-sensing fiber optic probe is feasible. Optical fiber sensing is remarkably proficient and fast growing technology.

The basic requirement for the sensor is light source, detection system, referencing scheme and sensor geometry. In a typical fiber optic sensor, light from the source is launched in to one of the ends of optical fiber, which is guided inside the fiber by the phenomenon of total internal reflection. The sensing action takes place either within the fiber or external to the fiber. The measurand (the sample) is placed in contact of the fiber core, which modulates some property such as intensity, phase, polarization, wavelength etc. of the guided light. By measuring the change in the property of the light at the output end of the fiber, the information about the change in the measurand can be found out. For sensing, various techniques such as evanescent wave absorption spectroscopy, interferometry, Doppler Effect, photolumnisense and surface plasmon resonance (SPR) are used. In addition to all other sensing techniques, SPR based sensing has achieved much attention during last thirty years. Collective resonating oscillation of free electrons may exist on the plasma surface (like, metal), giving rise to a charge density wave propagating along the plasma surface. This transverse electromagnetic wave, propagating parallel to the metal-dielectric interface is known as the surface plasmon wave. Since surface

plasmon wave is transverse in nature, it can be excited by exponentially decaying evanescent field of the incident *p*-polarized light (electric field vector parallel to the incident plane). When the wave vector and the frequency of the incident *p*-polarized light coincide with those of the surface plasmon wave, this light resonantly excites the surface plasmon wave, propagating along the metal-dielectric interface. The resonance condition depends on the incident angle, wavelength of the light and the dielectric constants of both the metal as well as the dielectric. A sharp dip appears in the spectrum of output signal at the resonance angle or at the resonance wavelength. The angle or the wavelength at which the resonant excitation of surface plasmon occurs is very sensitive to variations in the refractive index of the dielectric adjacent to the metal. Hence, the variations in the refractive index of the sensing medium (dielectric) can be detected by measuring the resonance angle or resonance wavelength.

For observing SPR, Kretschmann's configuration is most widely used. In Kretschmann's configuration, a high refractive index prism is coated with a thin metal film touching the sample (sensing medium). Surface plasmon waves are excited by evanescent wave from the prism at the total reflection condition. The SPR phenomenon using Kretschmann's configuration was first time demonstrated for biosensing by Liedberg et al. in 1983 [1]. Their experiment released numerous opportunities in the area of SPR based sensors for chemical and biological applications. However, in the fiber optic SPR sensor the prism is replaced by depositing the metal film directly on the core of the optical fiber. For SPR sensing, the method of fixed angle of incidence and modulated wavelength i.e. wavelength interrogation method is chosen. The utilization of optical fiber along with surface plasmon resonance for sensing applications was first time done by Jorgenson and Yee [2]. Since then fiber optic SPR sensor has been an interesting research subject and a number of devices have been reported on fiber optic SPR sensors [3-6]. However with time, a large number of theoretical and experimental research investigations have been carried out to improve the performance of the fiber optic SPR sensor [7-29]. Now a days, some new types of fiber optic sensors such as micro and nano structured fiber sensors are attracting a number of researchers due to outstanding progress in the fields of surface plasmon resonance and photonic crystal fiber technology. In continuation to this, we have carried out the theoretical analysis of different materials based fiber optic SPR sensors to enhance the sensitivity of the fiber optic sensor.

Chapter 1 of the thesis gives general introduction about fiber optic sensors. As the surface plasmon resonance (SPR) forms the subject of the thesis, this chapter covers SPR based fiber optic sensors in greater detail. It reviews various fiber optic sensors for the measurement of different physical and chemical parameters as well as discusses the phenomenon of surface plasmon resonance. A section of this chapter is also dedicated to the recent SPR based fiber optic sensors for various sensing applications.

Gold (Au) and silver (Ag) metals are mainly utilized for SPR sensor. However, Ag based SPR sensor is not chemically much stable because Ag is very prone to oxidation. The problem of oxidation of Ag is automatically eliminated by coating another metal on it. Zynio et al. reported a SPR sensor based on resonant bimetallic layers of Ag-Au (Ag as an inner layer and Au as an outer layer) [30]. In addition of protecting Ag against oxidation by the outer Au layer, this SPR sensor based on bimetallic layers showed high values of both sensitivity and detection accuracy. However, both of these metals have various significant disadvantages like occurrence of band to band transitions in the visible spectral region for Au films and very thin films of deposited Au and Ag are not continuous but agglomerate as islands [31]. Apart from this, the SPR sensors with a single metallic layer/ bimetallic layers have their SPR wavelength in the visible range and therefore not permitting the sensing in the infrared spectral region, which needs attention to many environmental and security applications. It has been possible to obtain the surface plasmon resonance with transparent conducting metal oxide thin films. Recently, Indium tin oxide (ITO) has been reported to be a better substitute of noble metals (Au and Ag) for producing surface plasmons [32,33]. Highest available transmissivity for visible light combined with the lowest electrical resistivity, reflection spectra in IR region and wide band gap semiconductor makes ITO as most widely used transparent conducting metal oxide. In addition to this, ITO thin films are continuous (i.e. no agglomeration as islands) and no involvement of band to band transitions. Villar et al. have shown that surface plasmon resonances can be produced with ITO coated optical fibers [34]. In order to enhance the sensitivity of ITO based SPR sensor further, **Chapter 2** presents the theoretical analysis of SPR based fiber optic sensor with bi layers of ITO (as an inner layer)-Au (as an outer layer). In the SPR based fiber optic sensor, the sensing system consisting of a fiber core-ITO-Au-sensing medium is considered. The plastic cladding around the core from the middle portion of a step index multimode plastic clad silica (PCS) fiber is removed and is then coated with a thin ITO layer, which is then further coated with Au layer. These bi

layers of ITO-Au are finally surrounded by the sensing medium. Liquids of different refractive indices are assumed as the sensing mediums. The light from a broadband source is launched into one of the ends of the optical fiber with proper optics and the transmitted light is detected at the other end of the optical fiber. The surface plasmon resonance produced by coupling of evanescent light to surface plasmons is used as the sensing mechanism. The wavelength interrogation method is used for the analysis of SPR based fiber optic sensor. In this method, the wavelength of the light from the broadband source is varied and the corresponding transmitted power through the optical fiber is measured. The proposed SPR based fiber optic sensor with bi layers of ITO-Au is shown to possess high sensitivity with two resonance dips, one in the visible and other in the near infrared region of spectrum, opposite to the single metal layer based SPR sensor with one and only resonance dip. The reason of occurrence of two resonance dips can be understood by the double character of ITO. In the region of high reflectance (wavelengths higher than 1500 nm), the imaginary part of refractive index of ITO is higher while it is lower for the low reflectance region (wavelengths lower than 1500 nm) [34]. This low reflectance region i.e. low imaginary part of refractive index of ITO is responsible for the generation of double resonance dips. Moreover, these two differentiated SPR dips have been obtained from the same device within 510 nm to 870 nm spectrum. Besides it, increase in ITO layer thickness decreases the sensitivity of both left and right resonance dips for all values of thickness of Au layer. This happens because the thick ITO layer permits less interaction between surface plasmon mode and fiber mode, resulting in little absorption of light power by the sensing medium around resonance wavelength. This forms the ground of increase in normalized transmitted power and as a result decreases the sensitivity of the sensor. Furthermore, for a fixed thickness value of ITO layer, the sensitivity of left resonance dip increases with the increase in Au layer thickness while that of right resonance dip decreases with the increase in Au layer thickness. The optimized values of thicknesses of ITO and Au layers of SPR based fiber optic sensor are found to be 100 nm and 35 nm respectively. The 100 nm ITO-35 nm Au layers based SPR sensor has been shown to possess 1929 nm/RIU and 929 nm/RIU sensitivities for left and right resonance dips respectively.

Among various transparent conducting oxides, Indium oxide (In_2O_3) is a potential material for sensing applications due to its highest available transmissivity for visible light combined with the lowest electrical resistivity, reflection spectra in IR region and wide band gap semiconductor, making it one of the most widely used transparent conducting oxides [35]. Recently, In_2O_3 has

been reported to be a better replacement of noble metals for producing surface plasmons [36]. **Chapter 3** describes the SPR based fiber optic sensor with Indium oxide (In_2O_3) theoretically. In the sensor, the sensing system comprising of a fiber core-In_2O_3-sensing medium is considered. The sensitivity of the sensor is studied for various thickness values of In_2O_3 layer. The In_2O_3 layer based sensor possesses high sensitivity with resonance dip in the near infrared region of spectrum allowing the sensing in the infrared spectral region, which needs attention to many environmental and security related applications. The sensitivity of the sensor decreases with the increase in the thickness of In_2O_3 layer. The 170 nm thick In_2O_3 layer based fiber optic SPR sensor comprises high sensitivity of 4600 nm/RIU.

The metal nanoparticles (much smaller than the wavelength of light) are supposed to have better sensing performances than materials in the micro or larger scales and reveal tremendous optical properties because of the collective excitation of conduction electrons [37]. A metal-dielectric interface on the nanoparticles produce significant changes in the optical properties, which make them size and shape dependent. Localized surface plasmon resonance (LSPR) refers to metallic nanoparticles and takes place when the wave vector and the frequency of the incident light are resonant with the collective oscillation of conduction electrons in metallic nanoparticles [38]. The LSPR wavelength is reliant on nanoparticle material, size, shape and surrounding medium refractive index [39,40]. Therefore, the sensitivity of LSPR sensor is controlled/ optimized by the change of the sizes and shapes of nanoparticles. **Chapter 4** discusses the theoretical investigations of LSPR based fiber optic sensor with nanoparticles. Nanoparticles of four materials: Indiums tin oxide (ITO), gold (Au), silver (Ag) and copper (Cu) have been considered individually and the nanoparticles are assumed to be spherical in shape with various radii. In the LSPR based fiber optic sensor, the sensing system consisting of fiber core-nanoparticles (of one material at a time)-sensing medium is assumed. The sensitivity of LSPR based fiber optic sensor with each nanoparticle layer individually for various thickness values and with different particle sizes is studied. The sensitivity of LSPR based fiber optic sensor increases with the increase in the thickness of nanoparticles layer for all four materials. Also, for a fixed value of thickness of nanoparticles layer, the sensitivity of LSPR based fiber optic sensor further increases as the particle size of nanoparticles increases. This can be explained in terms of the variation in absorption of light due to the change in particle size of the nanoparticles [41]. The decrease in particle size results in decrease in collision wavelength, that in turn increases the

imaginary part of the dielectric function of metallic nanoparticles and hence the imaginary part of propagation constant of surface plasmon wave. The optimized values of thickness and particle size of nanoparticles layers for all four materials individually are found to be 60 nm and 20 nm respectively. The sensitivity of LSPR based fiber optic sensor is obtained to be 6240 nm/RIU, 4525 nm/RIU, 3550 nm/RIU and 3340 nm/RIU for 60 nm thick nanoparticles layer with fixed 20 nm particle size of ITO, Au, Ag and Cu nanoparticles respectively. Containing sensitivity of 6240 nm/RIU, the 60 nm thick ITO nanoparticles layer (with 20 nm particle size) based LSPR sensor has been shown to comprise better sensing performance than Au, Ag and Cu nanoparticles based LSPR sensors.

The noble metals are not appropriate for sensing of samples having low refractive indices (such as gases) as the SPR sensors based on these metals offer small sensitivity. Besides, their SPR resonance dips arise in UV region. **Chapter 5** elaborates the theoretical analysis of SPR based fiber optic sensor with nanocomposite. Numerous nanocomposites comprising nanoparticles of gold (Au), silver (Ag) and copper (Cu) with their varying volume fractions embedded in host dielectric matrices of titanium oxide (TiO_2) and indium nitride (InN) are considered for the study. The sensitivity of Au/Ag/Cu-InN nanocomposites based SPR sensor for all thickness values of nanocomposites with any volume fraction of nanoparticles is higher than that of Au/Ag/Cu-TiO_2 nanocomposites. Further, the sensitivity of the sensor increases with increase in both thickness of nanocomposites and volume fraction of metal nanoparticles. Moreover, for a fixed nanocomposite thickness and fixed volume fraction of metal nanoparticles, the sensitivity of sensor is superior for Au nanoparticles based nanocomposites to that of Ag and Cu nanoparticles. The rationale that Au nanoparticles show higher sensitivity than Ag/Cu nanoparticles is attributed to the large value of real part of dielectric function of Au at all wavelengths [42]. Thus, Au nanoparticles in any nanocomposite enhance the shift between resonance wavelengths for a given change of refractive index of the sensing medium and therefore the sensitivity of the sensor increases. The SPR based fiber optic sensor with 70 nm thick Au-InN nanocomposite containing volume fraction of 0.85 illustrates high sensitivity of 2875 nm/RIU.

In recent times, research on plasmonics has been extended to infrared (IR) spectral region beyond the visible region. This leads to explore some new materials which could satisfy the SPR condition at lower plasma frequencies. Recently, Indium nitride (InN) has been found to be a

fascinating semiconducting material having band gap around 0.7-1.1 eV because of its numerous advanced properties over other group-III nitrides, metals and transparent conducting oxides. InN is a potential candidate for plasmonics based sensing applications not only in IR but also in THz regimes because of its smaller magnitudes of real permittivity than metals [43]. Further, InN possesses lower value of plasma frequency compared to that of metals, displaying greater confinement of surface plasmon waves to the interface and greater field enhancement in IR and THz regions. In addition, Lu et al. reported the utilization of InN as a suitable material for biosensing due to its high superficial electron concentration [44]. **Chapter 6** of the thesis reports the theoretical study of surface plasmon resonance based fiber optic sensor with InN. Depending upon various parameters values of InN, two SPR sensors viz "Sensor A" and "Sensor B" have been analyzed theoretically. Sensors A and B are found to display maximum sensitivities of 4493 nm/RIU and 3107 nm/RIU for 70 nm and 55 nm thick InN layers respectively. Both sensors A and B reveal their SPR resonance dips in the near IR region of spectrum permitting the sensing in IR spectral region. The 70 nm thick InN layer based fiber optic SPR sensor with Sensor A parameters values has been shown to acquire high sensitivity of 4493 nm/RIU.

Chapter 7 summarizes all the results reported in the thesis.

The above work has resulted in the following **publications**:

Journals

[1] Sharma N.K., **Rani M.**, Sajal V., "*Surface plasmon resonance based fiber optic sensor with double resonance dips*", Sensors and Actuators B, vol. 188, pp. 326-333, 2013.

[2] **Rani M.**, Sharma N.K., Sajal V., "*Surface plasmon resonance based fiber optic sensor utilizing Indium oxide*", Optik, vol. 124, pp. 5034-5038, 2013.

[3] **Rani M.**, Sharma N.K., Sajal V., "*Localized surface plasmon resonance based fiber optic sensor with nanoparticles*", Optics Communications, vol. 292, pp. 92-100, 2013.

[4] **Rani M.**, Shukla S., Sharma N.K., Sajal V., "*Theoretical study of nanocomposites based fiber optic SPR sensor*", Optics Communications, vol. 313, pp. 303-314, 2014.

[5] **Rani M.**, Shukla S., Sharma N.K., Sajal V., "*Theoretical analysis of surface plasmon resonance based fiber optic sensor using indium nitride*", (communicated, 2014).

Conference Proceedings

[1] **Rani M.**, Sharma N.K., "*ITO based fiber optic SPR sensor*", AIP Conf. Proc., vol. 1536, pp. 1117-1118, 2013.

Conferences

[1] **Rani M.**, Sharma N.K., "*Simulation of Cobalt based fiber optic surface plasmon resonance sensor*", International Conference on Optics & Optoelectronics ICOL-2014, Dehradun, March 05-08, 2014.

REFERENCES

[1] Liedberg B., Nylander C., Sundstrom L., "Surface plasmon resonance for gas detection and biosensing", Sensors and Actuators, vol. 4, pp. 299-304, 1983.

[2] Jorgenson R.C., Yee S.S., "A fiber optic chemical sensor based on surface plasmon resonance", Sensors and Actuators B, vol. 12, pp. 213-220, 1993.

[3] Harris R.D., Wilkinson J.S., "Waveguide surface plasmon resonance sensors", Sensors and Actuators B, vol. 29, pp. 261-267, 1995.

[4] Homola J., "Optical fiber sensor based on surface plasmon excitation", Sensors and Actuators B, vol. 29, pp. 401-405, 1995.

[5] Homola J., "On the sensitivity of surface plasmon resonance sensors with spectral interrogation", Sensors and Actuators B, vol. 41, pp. 207-211, 1997.

[6] Salamon Z., Macleod H.A., Tollin G., "Surface plasmon resonance spectroscopy as a tool for investigating the biochemical and biophysical properties of membrane protein systems. II: Applications to biological systems", Biochimica et Biophysica Acta, vol. 1331, pp. 117-129, 1997.

[7] Slavik R., Homola J., Ctyroky J., "Miniaturization of fiber optic surface plasmon resonance sensor", Sensors and Actuators B, vol. 51, pp. 311-315, 1998.

[8] Slavik R., Homola J., Ctyroky J., "Single mode optical fiber surface plasmon resonance sensor", Sensors and Actuators B, vol. 54, pp. 74-79, 1999.

[9] Lin W.B., Jaffrezic-Renault N., Gagnaire A., Gagnaire H., "The effects of polarization of the incident light-modeling and analysis of a SPR multimode optical fiber sensor", Sensors and Actuators A, vol. 84, pp. 198-204, 2000.

[10] Bardin F., Kasik I., Trouillet A., Matejec V., Gagnaire H., Chomat M., "Surface plasmon resonance sensor using an optical fiber with an inverted graded index profile", Applied Optics, vol. 41, pp. 2514-2520, 2002.

[11] Kurihara S., Ohkawa H., Iwasaki Y., Niwa O., Tobita T., Suzuki K., "Fiber optic conical microsensors for surface plasmon resonance using chemically etched single mode fiber", Analytica Chimica Acta, vol. 523, pp. 165-170, 2004.

[12] Sharma A.K., Gupta B.D., "Absorption based fiber optic surface plasmon resonance sensor: a theoretical evaluation", Sensors and Actuators B, vol. 100, pp. 423-431, 2004.

[13] Chau L.K., Lin Y.F., Cheng S.F., Lin T.J., "Fiber optic chemical and biochemical probes based on localized surface plasmon resonance", Sensors and Actuators B, vol. 113, pp. 100-105, 2006.

[14] Suzuki H., Sugimoto M., Matsui Y., Kondoh J., "Effects of gold film thickness on spectrum profile and sensitivity of a multimode optical fiber SPR sensor", Sensors and Actuators B, vol. 132, pp. 26-33, 2008.

[15] Jha R., Badenes G., "Effect of fiber core dopant concentration on the performance of surface plasmon resonance based fiber optic sensor", Sensors and Actuators A, vol. 150, pp. 212-217, 2009.

[16] Mitsushioa M., Watanabeb K., Abeb Y., Higoa M., "Sensor properties and surface characterization of aluminium deposited SPR optical fibers", Sensors and Actuators A, vol. 163, pp. 1-8, 2010.

[17] Verma R.K., Gupta B.D., "Surface plasmon resonance based fiber optic sensor for the IR region using a conducting metal oxide film", Journal of the Optical Society of America A, vol. 27, pp. 846-851, 2010.

[18] Srivastava S.K., Verma R.K., Gupta B.D., "Surface plasmon resonance based fiber optic sensor for the detection of low water content in ethanol", Sensors and Actuators B, vol. 153, pp. 194-198, 2011.

[19] Yuan Y., Ding L., Guo Z., "Numerical investigation for SPR based optical fiber sensor", Sensors and Actuators B, vol. 157, pp. 240-245, 2011.

[20] Srivastava S.K., Gupta B.D., "Influence of ions on the surface plasmon resonance spectrum of a fiber optic refractive index sensor", Sensors and Actuators B, vol. 156, pp. 559-562, 2011.

[21] Bhatia P., Gupta B.D., "Fabrication and characterization of a surface plasmon resonance based fiber optic urea sensor for biomedical applications", Sensors and Actuators B, vol. 161, pp. 434-438, 2012.

[22] Cao J., Galbraith E.K., Sun T., Grattan K.T.V., "Cross comparison of surface plasmon resonance based optical fiber sensors with different coating structures", IEEE Sensors Journal, vol. 12, pp. 2355-2361, 2012.

[23] Srivastava S.K., Arora V., Sapra S., Gupta B.D., "Localized surface plasmon resonance based fiber optic U-shaped biosensor for the detection of blood glucose", Plasmonics, vol. 7, 261-268, 2012.

[24] Salari M., Askari H.R., "Theoretical investigation of absorption and sensitivity of nano-plasmonic fiber optic sensors", Optics and Laser Technology, vol. 48, pp. 315-325, 2013.

[25] Yuan Y., Hu D., Hua L., Li M., "Theoretical investigations for surface plasmon resonance based optical fiber tip sensor", Sensors and Actuators B, vol. 188, pp. 757-760, 2013.

[26] Cao J., Tu M.H., Sun T., Grattan K.T.V., "Wavelength based localized surface plasmon resonance optical fiber biosensor", Sensors and Actuators B, vol. 181, pp. 611-619, 2013.

[27] Bharadwaj R., Mukherji S., "Gold nanoparticle coated U-bend fiber optic probe for localized surface plasmon resonance based detection of explosive vapors", Sensors and Actuators B, vol. 192, pp. 804-811, 2014.

[28] Gao D., Guan C., Wen Y., Zhong X., Yuan L., "Multi-hole fiber based surface plasmon resonance sensor operated at near-infrared wavelengths", Optics Communications, vol. 313, pp. 94-98, 2014.

[29] Navarrete M.C., Herrera N.D., Cano A.G., Esteban O., "Surface plasmon resonance in the visible region in sensors based on tapered optical fibers", Sensors and Actuators B, vol. 190, pp. 881-885, 2014.

[30] Zynio S.A., Samoylov A.V., Surovtseva E.R., Mirsky V.M., Shirshov Y.M., "Bimetallic layers increase sensitivity of affinity sensors based on surface plasmon resonance", Sensors, vol. 2, pp. 62-70, 2002.

[31] Rhodes C., Cerruti M., Efremenko A., Losego M., Aspnes D.E., Maria J.P., Franzen S., "Dependence of plasmon polaritons on the thickness of indium tin oxide thin films", Journal of Applied Physics, vol. 103, pp. 093108, 2008.

[32] Brewer S.H., Franzen S., "Calculation of the electronic and optical properties of indium tin oxide by density functional theory", Chemical Physics, vol. 300, pp. 285-293, 2004.

[33] Rhodes C., Franzen S., Maria J.P., Losego M., Leonard D.N., Laughlin B., Duscher G., Weibel S., "Surface plasmon resonance in conducting metal oxides", Journal of Applied Physics, vol. 100, pp. 054905, 2006.

[34] Villar I.D., Zamarreno C.R., Hernaez M., Arregui F.J., Matias I.R., "Lossy mode resonance generation with indium tin oxide coated optical fibers for sensing applications", Journal of Lightwave Technology, vol. 28, pp. 111-117, 2010.

[35] Solieman A., "Effect of sintering temperature on the structural, optical and electrical properties of sol-gel derived indium oxide thin films", Journal of sol-gel Science and Technology, vol. 60, pp. 48-57, 2011.

[36] Villar I.D., Zamarreno C.R., Sanchez P., Hernaez M., Valdivielso C.F., Arregui F.J., Matias I.R., "Generation of lossy mode resonances by deposition of high refractive index coatings on uncladded multimode optical fibers", Journal of optics, vol. 12, pp. 095503, 2010.

[37] Lal S., Link S., Halas N.J., "Nano-optics from sensing to waveguiding", Nature Photonics, vol. 1, pp. 641-648, 2007.

[38] Bohren C.F., Huffman D.R., "Absorption and scattering of light by small particles", New York: Wiley-VCH (1983).

[39] Noguez C., "Surface plasmons on metal nanoparticles: The influence of shape and physical environment", Journal of Physical Chemistry C, vol. 111, pp. 3806-3819, 2007.

[40] Lee K., El-Sayed M.A., "Gold and silver nanoparticles in sensing and imaging: sensitivity of plasmon response to size, shape and metal composition", Journal of Physical Chemistry B, vol. 110, pp. 19220-19225, 2006.

[41] Jha R., Sharma A.K., "Chalcogenide glass prism based SPR sensor with Ag-Au bimetallic nanoparticle alloy in infrared wavelength region", Journal of Optics A: Pure and Applied Optics, vol. 11, pp. 045502, 2009.

[42] Sharma A.K., Gupta B.D., "On the performance of different bimetallic combinations in surface plasmon resonance based fiber optic sensors", Journal of Applied Physics, vol. 101, pp. 093111, 2007.

[43] Naik G.V., Kim J., Boltasseva A., "Oxides and nitrides as alternative plasmonic materials in the optical range", Optical Materials Express, vol. 1, pp.1090-1099, 2011.

[44] Lu H., Schaff W.J., Eastman L.F., "Surface chemical modification of InN for sensor applications", Journal of Applied Physics, vol. 96, pp. 3577-3579, 2004.